# Towards a novel and safe EVA71 VLP vaccine: Enhancing capsid stability with thermal selection

**Mona Abdulhadi Shegdar**

**Submitted in accordance with the requirements for the degree of Doctor of Philosophy**

**The University of Leeds**

**School of Molecular and Cellular Biology**

**April 2022**

This candidate confirms that the work submitted is her own, except where work which has formed part of jointly authored publications has been included. The contribution of the candidate and the other authors to this work has been explicitly indicated below. The candidate confirms that appropriate credit has been given within the thesis where reference has been made to the work of others.

The work in Chapter 3 of the thesis has appeared in publication as follows:

Thermal stabilisation of enterovirus A 71 and production of antigenically stabilised empty capsids.

Natalie J Kingston#1, Mona Shegdar#1, Joseph S Snowden1, Helen Fox2, Elisabetta Groppelli1,3, Andrew Macadam2, David J Rowlands1*, Nicola J Stonehouse1*.

MS carried out all thermal stressing experiments and generated the stabilised virus, supervised by EG. NJS, DJR and NJK conceived and planned experiments. Funding was sourced by AM, NJS and DJR. HF performed NGS on virus samples. JSS generated renderings of mutation localisation. NJK generated the reverse genetics system, purified virus, and carried out all antigenicity experiments. NJK prepared the initial manuscript, and all authors were involved in review of the data and the final manuscript.

# Table of Contents

## List of figures

## List of tables

## Appendices

## Table of Abbreviations

| | |
|---|---|
| An | Mutant #9.3. |
| CDC | Centre for Disease control |
| CL | Cloverleaf |
| CsCl | Caesium chloride |
| CSF | Cerebrospinal fluid |
| CV | Coxsackievirus |
| DEPC | Diethylpyrocarbonate [C6H10O5] |
| DMEM | Dulbecco's Modified Eagles Medium |
| DNA | Deoxynucleic acid |
| dNTP | Deoxynucleoside triphosphate |
| DTT | Dithiothreitol |
| EC | Empty capsid |
| EDTA | Diaminoethanetetra-acetic acid |
| ELISA | Enzyme-linked immunosorbent assay |
| EV | Enterovirus |
| EVA71 | Enterovirus A 71 |
| FCS | Foetal calf serum |
| h.p.i | Hours post-infection |
| HBc | Hepatitis B virus core |
| HCl | Hydrochloric acid |
| HeLa | Henrietta Lax |
| HAg/CAg | VLPs/virus particles with non-native or expanded antigenic conformation |
| HPV | Human Papillomavirus |
| ICTV | International Committee on the Taxonomy of viruses |
| IgG | Immunoglobulin G |

| | |
|---|---|
| IRES | Internal ribosome entry site |
| iVDPV | Immunodeficient vaccine-derived poliovirus |
| mAb | Monoclonal antibodies |
| MOPS | 3-morpholinopropane-1-sulfonic acid |
| NaCl | Sodium Chloride |
| NaOH | Sodium Chloride Sodium hydroxide |
| NIBSC | National Institute of Biological Standards and Control |
| NAg/DAg | VLPs/virus particles with native antigenic confirmation |
| OD | Optical density |
| OPV | Oral polio vaccine |
| ORF | Open reading frame |
| PBS | Phosphate buffered saline |
| PCR | Polymerase chain reaction |
| PFU/ml | Plaque forming units per millilitre |
| PV | Poliovirus |
| pNwt | NAg wt |
| pHwt | HAg wt |
| pNn | NAg #9.3 |
| pHn | HAg #9.3 |
| RdRp | RNA-dependent RNA-polymerase |
| RT | Reverse Transcription |
| SDM | Site-directed mutagenesis |
| SDS-PAGE | Sodium dodecyl-sulfate polyacrylamide gel electrophoresis |
| ssRNA | Single-stranded RNA |
| TAE | Tris Acetic Acid EDTA |
| TB | Tris-buffer |
| TBE | Tris Borate EDTA |
| TBST | Tris-Buffered Saline and Tween 20 |
| TEMED | Tetramethylethylenediamine |
| Tm | Melting temperature |

| | |
|---|---|
| UTR | Untranslated region |
| VLPs | Virus-like particles |
| WHO | World Health Organisation |
| Wt | Wild-type |

## Acknowledgement

First and foremost, I am extremely grateful to my supervisor, Prof Stonehouse, for always being there when I needed support, reviewing my progress constantly, and guiding me through my PhD studies. Her immense knowledge and plentiful experience have always encouraged me in my academic research. Then, I would like to say that I was honoured by having the chance to be supervised by Prof Rowlands, who was my second supervisor. I am greatly appreciating his mentoring and support during my study.

During this project, I worked closely with Dr Kingston, to whom I would like to express a special thanks for all the guidance, support, and outstanding feedback. I would like to also thank Dr Sherry for his kindness and the technical help he offered me during the past years. My sincere thanks go out to everyone in the Stonehouse group for enriching my working experience.

I am so grateful to my beloved country Saudi Arabia for giving me this precious chance to go through a lifetime experience that reflects positively on my personality and allows me to grow in many aspects. I would also like to deeply appreciate my family, especially my sister Majdah, and my friends in Saudi Arabia, Egypt, and the United Kingdom, for their continuous love and support. Finally, I want to say thank you to myself for not giving up when it would have been an easier choice.

## Abstract

Enterovirus A71 (EVA71) is an important etiological agent of hand, foot, and mouth disease (HFMD), especially among infants and young children. HFMD caused by EVA71 can vary from mild and self-limited disease to severe and complicated illness. Severe symptoms or neurological complications such as brainstem encephalitis or acute flaccid paralysis can be fatal. Currently, none of the antiviral therapies against EVA71 has reached clinical trials. Therefore, preventive vaccines are crucial to tackling this disease. Different types of vaccines have been developed against EVA71, such as inactivated vaccines, subunit vaccines, recombinant vaccines, or virus-like particles (VLPs). However, except the inactivated vaccines, all of them are in the early stages of development. The inactivated vaccines, based on formaldehyde-inactivated viruses, were licensed and used effectively in China, the country that suffers the most from cyclic outbreaks of HFMD caused by EVA71. However, these vaccines have not been approved internationally yet due to some issues in safety and quality of production.

The production of an inactivated virus is hazardous as there is the risk of an escape of the live virus into the environment. In contrast, the VLP vaccine would produce a cost-effective virus-free vaccine. Empty capsids (ECs) that are produced during the lifecycle of EVA71, along with mature infectious particles, offer the potential to be developed as a safe and effective VLP vaccine. The reasons are that these particles are antigenically indistinguishable from virus particles, and unable to replicate as they are devoid of the RNA genome. Indeed, it was shown that VLPs based on ECs are alternative virus-free vaccine candidates for poliovirus, which is a related picornavirus. However, our studies with poliovirus have shown that native ECs are

antigenically unstable and can be easily converted to an expanded conformation (HAg) at moderate temperatures. This instability results in the loss of native antigenic conformation (NAg) or the appropriate display of epitopes essential to elicit a long-lived protective immune response. Thus, it was essential to stabilise VLPs to maintain the native form of antigenicity. Whether this is true for EVA71 or not is yet to be confirmed.

**Objective:** This study with EVA71 aimed to enhance the antigenic stability of EVA71 VLPs using a thermal selection approach to understand the impact of this stability on the virus antigenicity.

**Results:** Here, a thermally stable EVA71 B2 genogroup population were selected through cycles of thermal stressing at 52.5°C. The assessment of antigenic conversion at increased temperatures of both virions and ECs of the selected population showed that the selected ECs were thermally stable. The possible capsid-stabilising mutations were found in the structural protein coding region and were dispersed across the capsid. These mutations were successfully introduced into heterologous systems to generate stable VLPs. The antigenicity assessment of the stabilised *P. pastoris* VLPs has shown that these VLPs have retained a native virion-like conformation compared to the wild-type, with #9.3 being primarily NAg (60%) and stable to >44°C. However, whether gaining a NAg conformation may influence the eliciting long-term protective immunity over the HAg is yet to be confirmed.

**Conclusion:** This study has proven the success of applying thermal stressing to obtain EVA71 thermal-resistant mutations that can stabilise both the virus capsid and recombinantly expressed VLPs. However, more antigenic mapping and structural studies might elucidate how stabilisation mutation functions.

# Chapter 1
# Introduction

## 1.1. Hand, foot, and mouth disease (HFMD)

HFMD is a highly contagious acute febrile viral disease that commonly affects children especially infants under five years (reviewed in Zhang et al., 2020), though maternal antibodies protect infants who are less than six months (reviewed in Lou et al., 2009). On the other hand, adults rarely get affected by this virus as they are primarily immunogenic (reviewed in Yin et al., 2014). This disease is primarily triggered by environmental conditions of elevated temperatures and in humid and warm regions, which may explain why EVA71 infection is more effective in Asia in general (reviewed in Nayak et al., 2022). The symptoms of HFMD can be mild and the disease is self-limited, and in some cases patients can be asymptomatic (reviewed in Mcminn, 2002). Symptoms include fever, malaise, difficulty swallowing, and maculopapular rash or blisters on the hand, feet, buttocks, and genitalia, with herpangina (reviewed in Mcminn, 2002). The herpangina is a painful oral ulcerative lesion, usually less than 5 mm in size. These lesions may appear on the buccal wall and posterior tongue and may persist for about a one week (reviewed in Corsino, Ali and Linklater, 2022).

Still, HFMD caused by EVA71 may progress into a severe illness with neurological and cardiopulmonary complications that can be fatal (reviewed in Liu et al., 2015). Complicated cases can lead to a long-term sequelae such as cognitive and motor disorders or death from pulmonary oedema or brainstem encephalitis (reviewed in Change et al., 2019). While complications are rare, the substantial death toll among children in countries with high incidences, such as China, is concerning. In 2014, China witnessed the deaths of 384 children out of almost 2.7 million cases (reviewed in Koh et al., 2016).

Many enteroviruses can cause HFMD, but the primary etiological agents are Enterovirus A71 (EVA71) and Coxsackievirus A16 (CVA16) (reviewed in Liu et al., 2015). While both share a close genetic relationship, EVA71 tends to cause neurological disease and can be fatal (reviewed in Man-Li et al., 2012). In contrast, CVA16 present milder symptoms and neurological complications in CVA16 infection are probably infrequent (reviewed in Man-Li et al., 2012). Indeed, the CAV16 virus was not previously isolated from Cerebrospinal fluid (CSF) or tissue of Central Nervous System (CSF) (reviewed in Ong and Wong, 2015). The co-circulation of both viruses, besides other enteroviruses, is not unusual in some large HFMD outbreaks when neurological complications are more likely to occur (reviewed in Ong and Wong, 2015). It is, therefore, more challenging to identify the causative neurotropic virus without isolation from a clinically relevant site (reviewed in Ong and Wong, 2015).

## 1.2. EVA71 related HFMD

EVA71 could be considered as the most prevalent neurotropic enterovirus with the expected polio eradication (reviewed in Ong and Wong, 2015). EVA71 infection has proven to be complicated by aseptic meningitis, acute flaccid paralysis (AFP), cardiopulmonary dysfunction, and encephalomyelitis (reviewed in Ong and Wong, 2015). The EVA71 was isolated for the first time in 1969 in California, USA (reviewed in Wang, Hu and Zheng, 2022). Since then, many outbreaks with significant neurological complications and mortality were reported worldwide in Europe, Australia, the USA, but the most significant episodes were in Asia-Pacific region (reviewed in Lee 2016).

Understanding how EVA71 gains access to the nervous system is essential to understand its pathogenesis that was described as ‘ a complex pathogenesis’ (reviewed in Zhang et al., 2011). This virus can transmit directly from person to person through oral-oral and oral-faecal routes (reviewed in Ong and Wong, 2015). It also can transmit through vesicular fluid, oropharyngeal secretion, and direct contact with contaminated fomite and surfaces (reviewed by Zhang et al., 2020). The oral-oral route might be the main route of viral entry, as Mong et al (2007) found that the viral load isolated from throat swabs seems remarkably higher than that isolated from rectal swabs or faeces. Moreover, EVA71 shedding in the throat and faeces could originate from the tonsil and oral mucosa, as the viral antigens and RNA were detected only in tonsillar crypts squamous epithelium (He et al., 2014). A study by Song et al (2020) could also emphasise this speculation. They showed that the clinical severities of EVA71-associated HFMD have a positive correlation with the viral genomic loads of in throat swabs.

The proliferation of EVA71 in tissue or specific organs is followed by viremia or virus dissemination or circulating into blood, which is a clinical pathological indictor of EVA71 infectious process (reviewed in Zhao et al., 2017). Viremia spreads the infection to the skin and perhaps other organs and positively correlated to the clinical severities of EVA71 associated HFMD. It occurred more frequently in children under one year old and if persist three days after the onset of disease it might cause a severe disease in EVA71 patients. (Cheng et al., 2014).

EVA71 neuroinvasion and CNS infection occur by direct pathway through which the blood-brain barrier (BBB) that protects CNS from harmful pathogens in the blood is invaded. In this pathway, EVA71 infects the brain microvascular endothelial cells (BMECs) that comprise BBB, and the integrity of the barrier is moculated by cytokines that is produced during viral infection (Jin et

al., 2021). The second pathway is known as the “Trojan horse route’’ through which the EVA71 hijack CD14+ cells, leukocytes, dendritic cells, and other peripheral immune cells, to intrude CNS (reviewed in Yang et al 2022). In the third pathway, EVA71 hijack the retrograde axonal transport to enter the CNS to retrogradely transported together with hSCARB2 to the cell body within the CNS, motor and other neural pathways (Ohka et al., 2022).

### 1.2.1. Clinical symptoms

The EVA71 incubation period is between 3–7 days, and it is frequently associated with high fever (≥39°C) that can last for 3–4 days. The most observed symptoms in patients infected with EVA71 are pyrexia with a skin rash (smaller than the ones related to CAV16), insomnia, vomiting, lethargy, myoclonus, and ataxia (Nayak et al., 2022). As mentioned previously, neurological complications can occur, and if severity of the disease increased, the damage to the CNS may lead to functional cardiopulmonary failure and neurogenic pulmonary oedema associated with high mortality (reviewed in McMinn, 2014). The EVA71 infection could be summarised into four clinical stages of the disease. Stage one, in most cases, is self-limited mild HFMD and localised herpangina. Some cases from stage one progress to stage two, where CNS is involved. At stage three, a few cases (less than 1%) advanced from stage two to severe neurological complications such as cardiopulmonary collapse. In stage four, surviving patients may develop significant neurological sequelae, including severe respiratory and motor damage, cerebellar dysfunction, delayed neurodevelopment and affected cognitive function (Lee and Chang, 2014).

### 1.2.2. Laboratory Diagnosis

Rapid identification of the causative agent of HFMD, mainly whether there is EVA71 infection, can help clinical management by focusing attention on the possible complications. It also helps in disease surveillance to detect outbreaks and predict their severity, thus initiating appropriate public health responses (reviewed in Sabanathan et al., 2014; Wang et al., 2019). Enteroviruses clinical specimens include throat swabs, stool samples, and cerebrospinal fluid (reviewed in Ong and Wong, 2015; Lee 2016; Wang et al., 2019). EVA71 infections can be detected via several diagnostic methods including virus isolation and cell culture, molecular methods, and serology. The gold standard for diagnosis of EVA71 is virus isolation in mammalian cell lines such as Vero cells (African green monkey kidney cells) or Rbdomyosarcoma (RD), which is carried out in biosafety level 2 virus. Isolated viruses can be detected by neutralisation tests using pools of EVA71 antisera, or by via indirect-immunofluorescence assay with EVA71 monoclonal antibodies (reviewed in Ooi et al., 2010; Ong and Wong, 2015).

Molecular diagnosis based on polymerase chain reaction (PCR) and sequencing of the VP1 gene has proven practical in diagnosing hospitalised patients as it saves time and is more sensitive (reviewed in Lee 2016). However, the possible disadvantage of applying molecular methods is that they require a skilled workforce and are unsuitable for clinics and community hospitals. On the other hand, neutralisation assay and enzyme-linked immunosorbent assay (ELISA) are serological methods for laboratory diagnosing of recent EVA71 infections that are considered cost-effective (reviewed in Lee 2016).

## 1.3. Enterovirus A 71 (EVA71)

### 1.3.1. *Picornaviridae*

The positive sense single-stranded RNA (+) ssRNA of picornaviruses ranges between 7.1 and 8.9kb, comprises of a single open reading frame (ORF) and flanked with two untranslated regions (UTR) 5'UTR and 3'UTR. They are enclosed within non-enveloped icosahedral viral capsids that display 5-, 3-, and 2- fold axes, which consist of 60 densely-packed protomers. Each one of these protomers comprises of four polypproteins, VP1, VP3, VP2 on the outer surface of the capsid, and VP4 located internally (reviewed in Tuthill et al., 2010; Racaniello, 2013; Rowlands, 2015).

### 1.3.2. EVA71 genome

EVA71 is a non-enveloped RNA virus that belongs to the genus Enterovirus within the family *Picornaviridae* (see section 2.3.1). The EVA71 genome is (+) ssRNA of approximately 7.5 kb. It consists of a single open reading frame (ORF) that encodes structural proteins and nonstructural proteins flanked with two UTR: 5'UTR and 3'UTR (reviewed in Tuthill et al., 2010; Yuan et al., 2018) (Figure 1.1 A).

The 5'UTR end of the picornaviruses genome is approximately 750 nucleotides and comprises a number of essential replication and translation control elements (reviewed in Paul and Wimmer, 2015). It is covalently attached to a non-capsid short peptide containing 21 to 23 amino acids known as virion protein genome linked (VPg) instead of a of a methylated nucleotide cap structure (m7GpppN) as in cellular mRNA (reviewed in Paul and Wimmer, 2015). Moreover, it consists of six domains or stem-loop structures of RNA secondary structures (domains I-VI). The first domain (I) of these six is the cloverleaf structure (I), and the other five domains II-VI are an

internal ribosomal entry site (IRES). The VPg protein is involved in initiating both minus and plus-strand RNA synthesis as it is used by RNA-dependent RNA polymerase 3Dpol to serve as a protein-primer (reviewed in Paul and Wimmer, 2015). The VPg attachment is believed to occur by uridylylation of VPg to generate VPg-pUpU (Lin et al., 2009). This step involves the transfer of one or two uridylate residues to VPg and requires 3D polymerase, UTP and the *cre* motif from the viral genome as the template. For EVA71 it was found that the site 311 on EVA71 3D is potentially the binding site of VPg (Sun et al., 2012). 3AB protein is regarded as the precursor of VPg (3B) in the RNA replication complex, although this is controversial. VPg-pUpU is transferred to the 3' end of plus or minus strand RNA and used as a primer for full-length RNA synthesis (Pathak et al., 2007; Steil and Barton, 2009). Upon initiating the replication cycle of picornaviruses, the VPg is cleaved and removed from the genome by unlinkase (Rozovics et al., 2011). The reason behind that is still an unresolved issue. However, it was suggested that the unlinkase activity might help distinguish translation templates from replication templates or those encapsidated in virions (Rozovics et al., 2011).

The cloverleaf is a cis-acting RNA replication element required for initiating negative and positive-strand RNA synthesis and interacting with viral and cellular proteins to form a ribonucleoprotein complex (reviewed in Paul and Wimmer, 2015. It is found within the first 84 - 86 nucleotides of 5' UTR in the genome of the enteroviruses (Barton et al., 2001). This structure facilitates viral replication of polio as it functions as a binding site for viral 3CD and the host cellular protein poly (rC) binding protein 2 (PCBP2), which forms a bridge between the 5' end and 3'ends (Martinez-Salas, 2015).

Most picornaviral IRES can be one of four types depending on the location of the IRES in relation to the AUG start codon. Type I IRES reside between 30 to 150 nucleotides upstream of the start

codon, while type II and type III IRESs comprise the start site AUG codon. The enteroviruses such as polio and EVA71, and human rhinoviruses include type I IRES, encephalomyocarditis virus (EMCV), and aphthoviruses (FMDV) contain type II IRESs. Hepatitis A virus (HAV) has Type III, and the newly characterized teschoviruses contain type IV I (Lin et al., 2009). EVA71 translation into viral protein is cap-independent and initiated by a type I IRES since the EVA71 RNA lacks the 5' cap structure m7GpppN recognised by the initiation factor eIF4F. Hence, the EVA71 type I IRES initiate mRNA translation by recruiting the cellular ribosomes to an internal AUG codon with the help of cellular proteins (Lai et al., 2020). The translation of IRES of EVA71 requires binding the initiation factors eIF4G, eIF1, eIF1A, eIF2, eIF3, eIF4A, and eIF4B.

The 3' UTR end is 100–300 nucleotides long, highly conserved, contains a pseudoknot involved in regulating replication, and ends with a poly A tail (reviewed in Tuthill et al., 2010; Raciniello, 2007; Rowlands, 2015). The secondary structures within the 3' UTR play an essential role in picornavirus replication. For example, the binding of host proteins to the 3' UTR is crucial for circularising the PV viral genome and replication (reviewed in Kloc et al., 2018).

The EVA71 polyprotein encodes three regions P1, P2, and P3. Region P1 encodes structural proteins and comprises VP1 (32 kDa), VP3 (27 kDa), and VP0 (36 kDa) that cleaves into VP2 (28 kDa) and VP4 (8 kDa). The P2 and P3 regions encode the non-structural proteins responsible for virus replication and virulence, such as proteases 2A, $3C^{pro}$, its precursor $3CD^{pro}$ and the viral polymerase $3D^{pol}$ (reviewed in Lin et al., 2009) (Figure 1.2 A). The P2 region comprises three functional proteins: 2A, 2B, and 2C. 2A is a proteinase responsible for cleaving the P1 region from the P2 and P3 regions and can also cleave 3CD to release 3C and the 3D cleaving eIF4g. The 2A protein is essential in replication, apoptosis, escaping innate immunity, and hijacking cellular machineries (reviewed by Yuan et al., 2018). The 2B protein is an ion channel protein that

induces apoptosis but, more importantly, is required to release the virus from infected cells. The 2C is encoded in the P2 regions with the proteins involved in generating viral replication complex and reorganising the host cell membrane proteins. It also contributes to innate immune evasion (reviewed by Yuan et al., 2018). The P3 region encodes three functional proteins also: 3A, 3B, and 3C. The 3A protein is a membrane-bound protein that can form a large complex with host proteins to facilitate virus replication. It also may have a role in escaping innate immunity. 3B protein is also the VPg, and 3D is essential for VPg uridylylation and RNA synthesis. The 3C and its precursor 3CD are involved in virus genome processing and capsid assembly. (reviewed in Yuan et al., 2021).

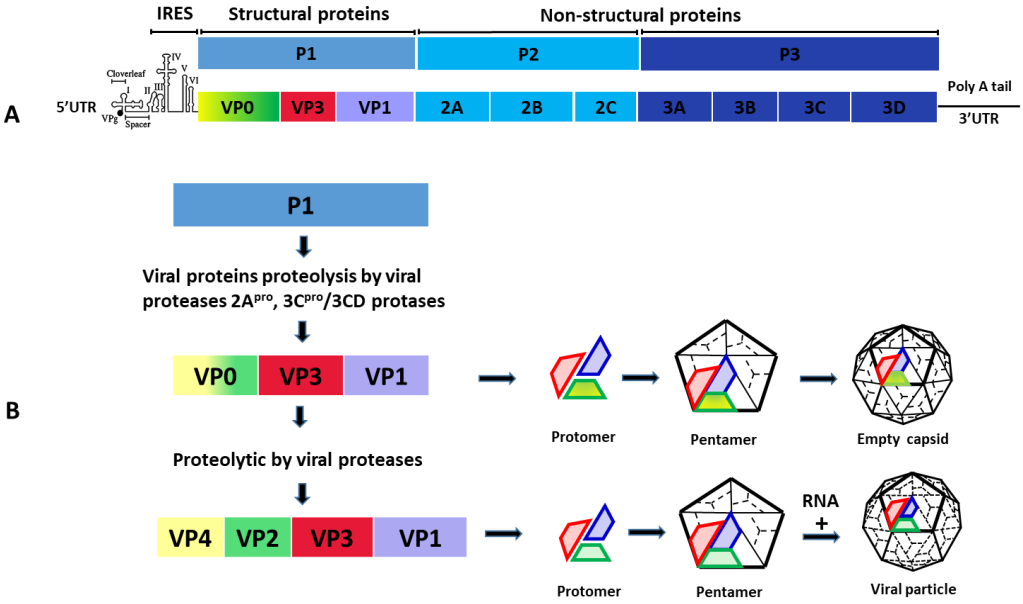


**Figure 1.1 EVA71 genome structure and capsid assembly:** (A) The is EVA71 genome comprised of one open reading frame flanked by two untranslated regions 5'prime UTR and 3'prime UTR. The genome translation results in three polyproteins that encode structural and non-structural precursors and proteins: P1 encode structural proteins, P2 and P3 encode non-structural and functional proteins. (B)The P1 proteolysis at first will result in cleavage of three capsid proteins VP1, VP3, and VP0, which is a precursor of VP2 and VP4. The figure shows the two pathways that either lead to the assembly of empty capsid or mature virions, which that requires cleavage of the VP0 and RNA packaging (Adapted from Adeyemi, 2017).

### 1.3.3. Capsid structure

The EVA71 RNA genome is enclosed within non-enveloped icosahedral viral capsids that display 5-, 3-, and 2- fold axes, which consist of 60 densely packed protomers shell with T=1 (quasi-T=3) symmetry. Each one of these protomers (sediment at 14 sedimentation coefficients (S)) comprises four pentamers (sediment at 5S), VP1, VP3, VP2 on the outer surface of the capsid and VP4 located internally (Figure 1.1 B) (reviewed in Tuthill et al., 2010; Racaniello, 2013; Rowlands, 2015). Similar to other picornaviruses, the mature capsids of EVA71 have the structural proteins of VP1, VP2, and VP3 exposed on the surface and comprise a wedge-shaped eight-stranded antiparallel β-barrel that facilitates packing. The form looks like β-sandwich "jelly-roll" folds (Figure 1.2 B) (Plevka, et al., 2012).

To form the provirion that sediments at 150S due to uncleaved VP0 (Guttman and Baltimore, 1977), the pentamers, which sediment at 4S, assemble around the viral RNA and then the cleavage of the VP0 into VP2 and VP4 occurs to form the mature capsid. However, there is another possible model of provirion assembly suggesting in which an empty capsid is formed first, and then the viral RNA is inserted into it. The autocatalytic cleavage of VP0 into VP2 and VP4, which depends on the RNA encapsidation, triggers the capsid protein rearrangement, and stabilises the icosahedral viral particles to finally form mature viral particles that sediment by 160S (reviewed by Cifuente and Moratorio, 2019; Cifuente et al., 2013). As a picornavirus, EVA71 produces ECs along with mature virions. Compared to the mature virion, the EVA71 ECs are expanded and are larger than the virion, and VP1 pockets are collapsed (Wang et al., 2012). Like other picornaviral ECs,

these particles are less stable than viral particles, and can readily be transformed into antigenic form.

However, compared to polio, the EVA71 HAg can still elicit an immune response (Liu et al., 2011; Cifuente et al., 2012). VP4 lies inside the viral capsid and confers stability to the capsid is highly conserved compared to other capsid viral proteins. (Chow et al., 1987). (De Colibus et al., 2014) (Fig 3.1). The five-fold axes of the capsid surface are dominated by mesas or star-shaped five-fold vertexes formed from a cluster of five copies of VP1 with the narrow edges of the β barrels. Likewise, the three-fold axes are surrounded by alternating three copies each of the VP2 and VP3 to form "Three-bladed propeller-like features" (Figure 1.2) and (Figure 1.3) (reviewed in Strauss et al., 2015).

In many picornaviruses, including EVA71, a deep cleft surrounds the fivefold mesas and around each of the 12 vertices of the icosahedron, known as the canyon. The canyon is lined by the C-termini of VP1 and VP3 molecules and contains the virus attachment sites for cellular receptors or antiviral drugs and plays a role in stabilising the virus by locking the capsid in a stable configuration and preventing conformational changes (reviewed by Tuthill et al., 2010; Racaniello. 2007). Just beneath the canyon floor there is a hydrophobic pocket, which is occupied by lipids (pocket factors).

The canyon of the EVA71 is shallower than other picornaviruses such as polio (Figure 4.1). The pocket factor is composed of a mixture of lipids that consist of palmitic acid and myristic acid molecules (reviewed in Plevka et al., 2012). Once a receptor binds to a virion, this pocket factor is dislodged as the first step of the capsid destabilisation process that aims to release the viral genome.

The β strands are named for the letters (B to I), whereas two letters were used to name each loop, referring to β strands connected to it (reviewed in Strauss et al., 2015). The VP1 of EVA71 has six surface loops (BC, DE, BE/aB, GF, GH, and HI). The topology of the capsid surface is influenced by the connecting loops and the C-termini (Kiener et al., 2012). In VP2, the "puff" is the largest surface loop, while the "knob" of VP3 is the largest protrusion on the surface (Plevka, et al., 2012). Cifuente and Moratorio (2019) described the topography of capsid surface as a "rugged topography". This uneven surface results from the arrangement of different protein structures and the differences in loops and C-terminus, which form a distinctive surface between different members of picornaviruses (reviewed by Cifuente and Moratorio, 2019). The surface topology of the capsid, specificities of receptor binding and antigenic characteristics are determined by how the β barrel is tilted and the length and structure of attached loops (reviewed by Tuthill et al., 2010). The most variable regions of EVA71 are the loops exposed on the virion surface, which are essential in determining the site of antibody binding sites.

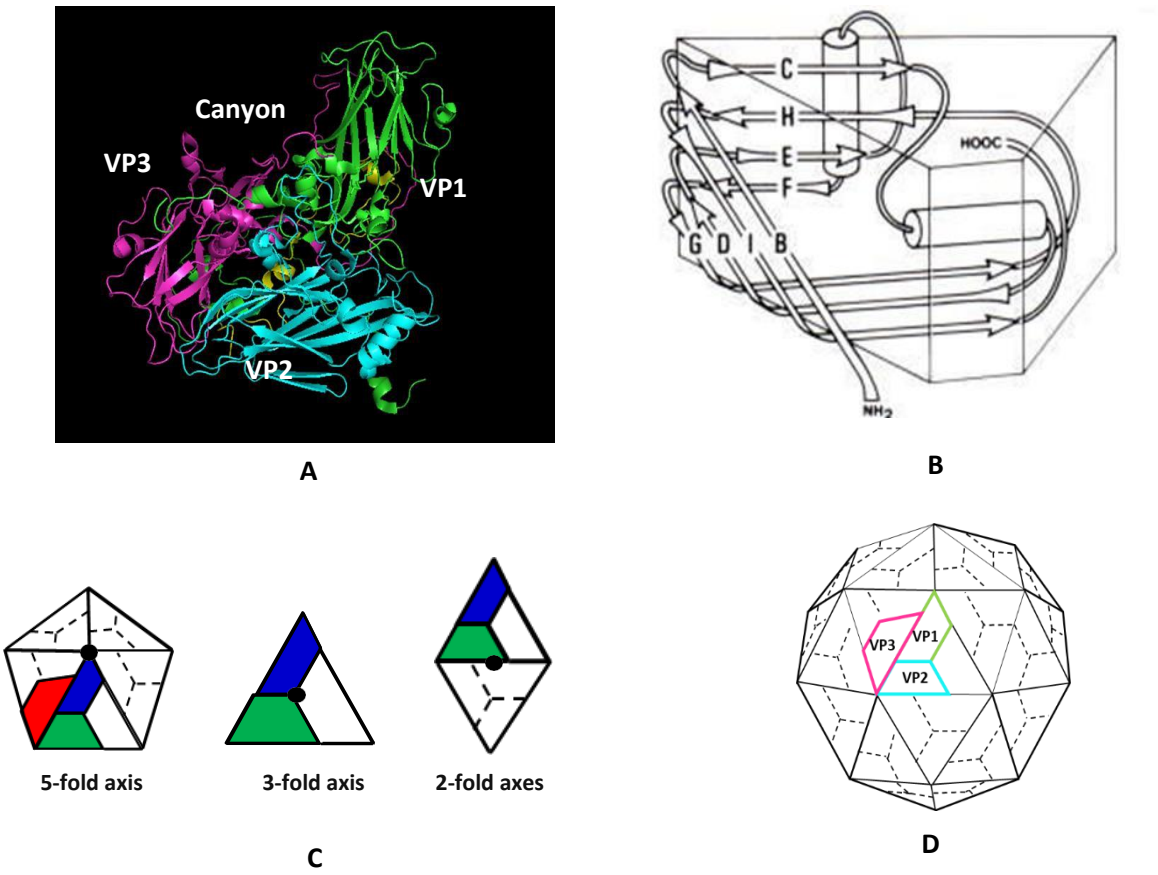


**Figure 1.2 Schematic representations of EVA71 particle:** (A) the structure of capsid proteins VP1 (green), VP2 (blue), VP3 (magenta), and VP4 (yellow). It also shows the location of the canyon (dark green). (B) A cartoon represents an eight stranded antiparallel beta barrel of poliovirus. Each of the major capsid proteins: VP1, VP2, and VP3 has the "jelly-roll" topology of a wedge-shaped eight-stranded Beta strands and are named by the letters (B to I). Loops are named using two letters designating the beta strands that the loop connect. This shape of the capsid proteins is shared by a number of other icosahedral viruses (Adapted from Adeyemi, 2017) (C) Cartoon are showing the different symmetry axes (D) The capsid shell comprised of 60 protomers consisting of the surface proteins VP1, VP2, VP3 and the internal VP4.

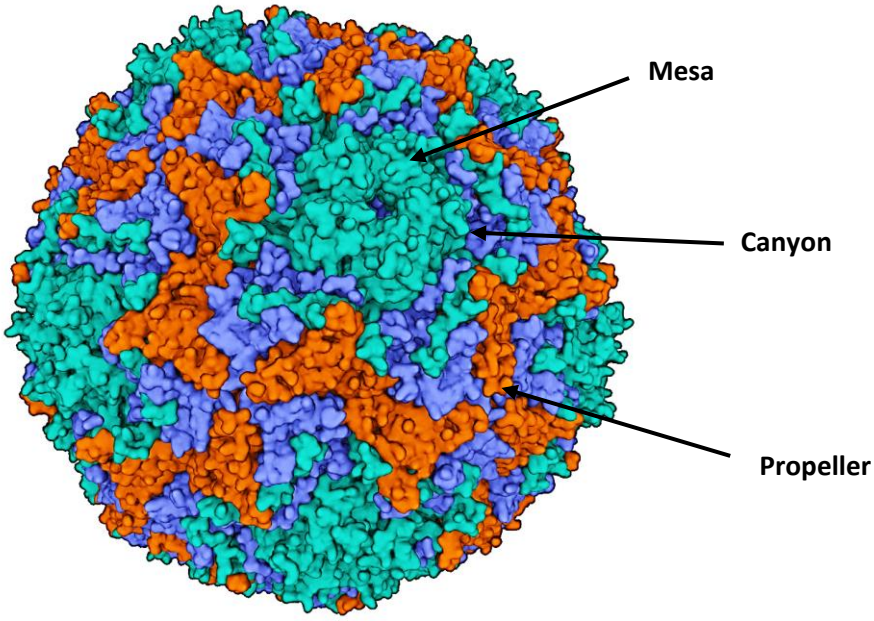


**Figure 1.3 The crystal structure of EVA71 viral particle:** VP1 (green) is forming the mesa around the 5-fold axes. The cleft around the mesa representing the canyon. VP2 (purple) and VP3 (dark orange) are alternating and forming the three bladed propeller. The crystal structure is of EVA71 strain C4 (PDB 3VBS).

### 1.3.4. EVA71 life cycle

#### 1.3.4.1. EVA71 receptors

Similar to other picornaviruses, the first event of EVA71 infection or life cycle is initiated by the binding of infectious virus to virus receptors on the surface of targeted cells by the help of the attachment factors. There are two functional EVA71 receptors: Scavenger receptor B2 (SCARB2) and p-selectin glycoprotein ligand-1 (PSGL-1) (reviewed in Kobayashi and Koike, 2020). Attachment factors such as heparan sulfate and sialylated glycan help in allowing the binding of the virus to entry receptors (reviewed in Yi et al., 2017). These factors are essential in aiding virus attachment to targeted cells as the SCARB2 is an endosomal protein and not expressed in large quantities on the cell surface. Attachment factors include sialylated glycan, annexin II, vimentin, fibronectin, and prohibitin (reviewed in Kobayashi and Koike, 2020)

The SCARB2 contributes to the early stages of EVA71 infection. This receptor is widely expressed on various cell types, including neurons, and is utilised by most EVA71 strains as it is essential for uncoating (reviewed in Yuan et al., 2018b; Kobayashi and Koike, 2020). The SCARB2 attaches to the virus at the southern rim of the canyon to the VP1 GH-loop and VP2 EH-loop (Zhou et al., 2019). This attachment causes conformational changes to the capsid and converts 160S to 135S particles. The uncoating efficacy is significantly increased when the pH is 5.6 (Chen et al., 2012). The conformational changes due to low pH inside SCARB2 may change the VP1 GH-loop, an adaptor-sensor for cell receptors, to release the pocket factor (Wang et al., 2012).

PSGL-1 is another functional EVA71 receptor that was found to be expressed on leukocytes,

thus, may facilitate virus entry and replication of EVA71 in these cells (Nishimura et al., 2009). However, the role of PSGL-1 as EVA71 is controversial. First, not all EVA71 strains bind to PSGL-l. It was found that the PSGL-1 expressing cells can be infected with EVA71, the effective infection required a long exposure time to the virus and a rather high multiplicity of infection (MOI) (Nishimura et al., 2009; Liu and Rossmann, 2014). EVA71 complexed with PSGL-1 showed no uncoating activity, indicating that the PSGL-1 might function as an attachment receptor (Yamayoshi et al., 2014). A schematic figure was constructed in order to describe EVA71 infectious cycle (Figure 1.4).

The EVA71 can invade the central nervous system (CNS) by crossing the blood-brain barrier by infected leukocytes or neural cells. EVA71 tropism for PSGL-1-expressing leukocytes is determined by residue 1145 in VP1. It was found that viruses binding to PSGL-1 had either a G1145 or a Q1145 in VP1, whereas the viruses that do not bind to PSGL-1 had E1145 in VP1. The 1145 residue in VP1 was found to control positively charged residue lysine in K1244E in VP1 (Yamayoshi et al., 2013; Yamayoshi et al., 2014; M. Yuan et al., 2018). The mutation in 1145 in VP1 changes the orientation of the L1244. Q1145 turn the residue outward, while the E1145 turn the residue upward to the surface of the capsid. This change in position alters the accessibility of the negatively charged tyrosine sulfated N terminus of PSGL-1 to a positively charged lysine side chain of K1244. Mutation in K1244 prevents PSGL-1 from binding to the virus capsid. Interestingly, K1244E in the B5 strain or Q1145E in C4, were found to contribute to mouse adaptation and virulence (Zaini and McMinn, 2012). Both receptors undergo endocytosis by a clathrin-dependent mechanism. Clathrin-mediated endocytosis is employed to facilitate the entry of EVA71 into host cells (Yamayoshi et al., 2013). The acidification of endosomes controls the uncoating as conformational

changes are induced by low pH. The uncoating might occur in coordination with membrane permeabilisation to protect the RNA from endosomal ribonuclease (Groppelli et al., 2017).

#### 1.3.4.2. Capsid expansion, uncoating, and antigenic states (DAg/ANg and ACg/AHg).

The uncoating of picornaviruses is a complex process, which exposes the viral positive sense RNA ((+) RNA)) for translation. However, the details of the uncoating process are not fully understood (reviwed at Smyth, 2002; Groppelli et al., 2017). Early studies on polio determined three particles found during the entry process according to the difference in two factors; differences in their sedimentation coefficients (S) and antigenic properties. These particles are the 160S particle which is the native and infectious form of the virion. The 135S particle (A-particle) is a destabilised, infectious particle. The 80S particle is the empty virion, which has released its genome and is a non-infectious end product of the uncoating process.

Dislodging the pocket factor due to receptor binding at physiological temperature or by exposing virus particles to a high temperature or very low pH changes the capsid structure (Bouvier, 1955; Wang et al., 2012). the protomeric units within the capsid are rearranged to expand the capsid and release RNA. The expansion externalises the VP1 N terminus and VP4 protein, thus converting the mature 160S capsid into 135S. The RNA is expelled through a subsequent uncoating process, and the capsid is converted from 135S into 80S. The RNA is released through a pore formed at the two and three axes (Shingler et al., 2013). The pocket factor competes with canyon-binding receptors for binding to the virion. The 80S are unstable and readily converted to the expanded antigenic form. These two distinct antigenic forms were described by Mayer et al (1957) and Le Bouvoir (1955). They called

polio infectious and native antigenic form (DAg) or (NAg), and the non-infectious expanded antigenic form was called (CAg) or (HAg).

During their life cycle, picornaviruses generate, alongside mature virions, particles known as “empty capsids” (ECs), which resemble the viral capsid but lack the viral genome. Each EC contains 60 copies of VP0, VP1, and VP3, as VP0 has not been cleaved due to the absence of RNA during the phase of encapsidation (Plevka, et al., 2012). Picornaviral ECs are less stable than viral particles. Binding to receptors will depress the canyon floor, but the binding of lipid or antiviral to the pocket will expand its roof. The role of the pocket factor in stabilising the virion structure could be evidenced by an experiment aimed to test the effect of an antiviral (Plevka, et al., 2012). In this experiment, the pocket factor was replaced with a capsid-binding inhibitor called WIN 51711. The replacement maintained the stability of the capsid structure, similar to the pocket factor. It restricted its infectivity, perhaps by preventing the capsid from expanding, which is necessary to release the viral genome.

The expansion of the empty particles includes a major conformational shift in external loops: the residues in the C terminus of VP2, the GH-loop of VP1, and the VP3 GH-loop become less ordered. Likewise, inside the particle, residues in the internal VP1 N-termini and VP0 are disordered (Wang et al., 2012). The capsid expansion for pore formation occurs in a screw-like motion or by counter-clockwise rotation of the five-fold proximal region of the VP1 β-barrel in a jackknife extension, and the rotation of protomers about the threefold axis (Wang et al., 2012; Ross et al., 2018). This motion results in moving the VP2 from the 2-fold-axis. The central regions of the pentamers are expanded, while the pentamer edges collapse inwards at the pentamer-pentamer interface (Ross et al., 2018). It also leads to 5-fold-axis expansion outward from the centre of the capsid. In addition, there is a shift in

residue at the pentameric interface similar to PV. This shift is vital for releasing RNA by releasing the VP1 N terminus through a 'junction channel' at the 3-fold-axis. They also suggested that the EVA71 capsid can breathe similar to the PV capsid. The breathing is like the expansion, but here it is reversible, as the externalised VP1 N terminus and VP4 on the capsid surface can be pulled back into the capsid.

The uncoating process may not be exclusively dependent on receptor binding, but also the RNA contributes to virus capsid assembly and stabilisation. Through a hotspot mapping, Ross et al., (2018) were able to identify spot "a hot spot" in VP1 around the 5-fold-axis and extended toward the pocket. These residues were also located at the interface between VP1 and VP3 and above VP4 residues. Finding this hotspot in the capsid assembly region indicates that the interaction of RNA with this region provides a scaffold for the assembled capsid (Ross et al., 2018).

#### 1.3.4.3. RNA translation and replication

Once in the cytoplasm, the viral genome is translated via an IRES into a single polyprotein, co- and post-translationally processed. Cleavage by the virus-encoded proteases 2Apro and 3Cpro results in a number of capsid proteins (VP0, VP1 and VP3) and replication proteins (2A–2 C and 3A–3D) and some stable and functional cleavage intermediates. (Yuan et al., 2018b). The translation is mediated by an internal ribosome entry site (IRES) and requires a subset of the canonical translation machinery and several IRES trans-acting factors (ITAFs). To initiate viral mRNA translation into a primary polyprotein, picornaviruses, including EVA71, tend to hijack the eukaryotic initiation factor mechanism to shut down the host cap-dependent translation (Avanzino et al., 2017). This inactivation aims to direct the ribosomes into the IRES structure to initiate cap-independent translation, which is initiated by cleaving

eIF4g by 2Apro. The eIF4g can still form a complex with eIF3 and eIF4A, and IRES to recruit ribosomes. Ribosomes bind to the genome of EVA71 internally and scan the genome downstream to determine the start site AUG codon (reviewed in Thompson and Sarnow, 2003).

To release functional and structural proteins required for genome replication and the generation of new virus particles, the P2 and P3 proteins undergo proteolytic cleavage by viral proteinases 2A and $3C^{pro}$ and the 3CD precursor (Jiang et al., 2014). $3C^{pro}$ is responsible for almost all secondary cleavages to form polyprotein precursors, which exhibit a different activity than the individual proteins (Sun et al., 2016). $3CD^{pro}$ cleaves the P1 capsid precursor to release three capsid proteins VP0, VP3, and VP1, to generate the capsid protomer, and help in RNA binding protein during RNA replication (reviewed in Steil and Barton, 2009). Whereas the 2A protein mediates primary cleavage at the junction between the precursors of capsid polyproteins and the non-structural polyproteins. 2CATPase, and its precursor 2BC contribute to the different viral RNA replication activities. This protein helps rearrange the host membrane originating from the endoplasmic reticulum (ER) and/or Golgi apparatus membranes to form RNA replication complexes, in addition to the conversion of VPg into VPgpUpU and polyprotein proteolysis (reviewed in Steil and Barton, 2009).

The replication of RNA is mediated by genome circularisation, which is a prerequisite of Enterovirus replication. This mechanism requires the formation of ribonucleoprotein complex (RNP complex) around a 5’ UTR 5 cloverleaf structure from the host and viral proteins (cellular poly(rC)-binding protein (PCBP)) the viral polymerase precursor, and 3CD

(Zoll et al., 2009; Shih et al., 2011). This complex is formed during viral RNA replication and translation. The synthesis of negative and positive strand RNisA initiated by the interaction

of RNP with poly (A) binding protein in the 3’ UTR tail. Picornavirus RNA acts as a messenger (mRNA) to synthesise viral proteins. The RNA replicates in replication organelles (RO) contain viral RNA and polymerase in addition to cellular proteins, and all are tightly associated with a cytoplasmic membrane structure. The replication occurs using two double-stranded RNAs as templates known as the “replicative intermediates”; one is a positive sense (+) RNA, while the other is the antisense RNA strand (-) RNA) (reviewed in Racaniello, 2013). Using the uncoated (+) RNA, the synthesis of a (-) RNsAtr is initiated at the 3’ UTR and uses VPg as a primer. The newly synthesised (-) RNA is used to generate (+) RNA that in turn is used either as a template for generating more (-) RNA or is used as a precursor for viral capsid generation, or to assemble with capsid pentamers to form virus particles (reviewed in Steil and Barton, 2009). Encapsidation begins when a sufficient number of capsid proteins are present (reviewed in Jiang et al., 2014). These newly formed viral nucleic acids and structural proteins are assembled to form the nucleocapsid of the virus. EV71 may primarily release its progeny via cell lysis (Yuan et al.,2018).

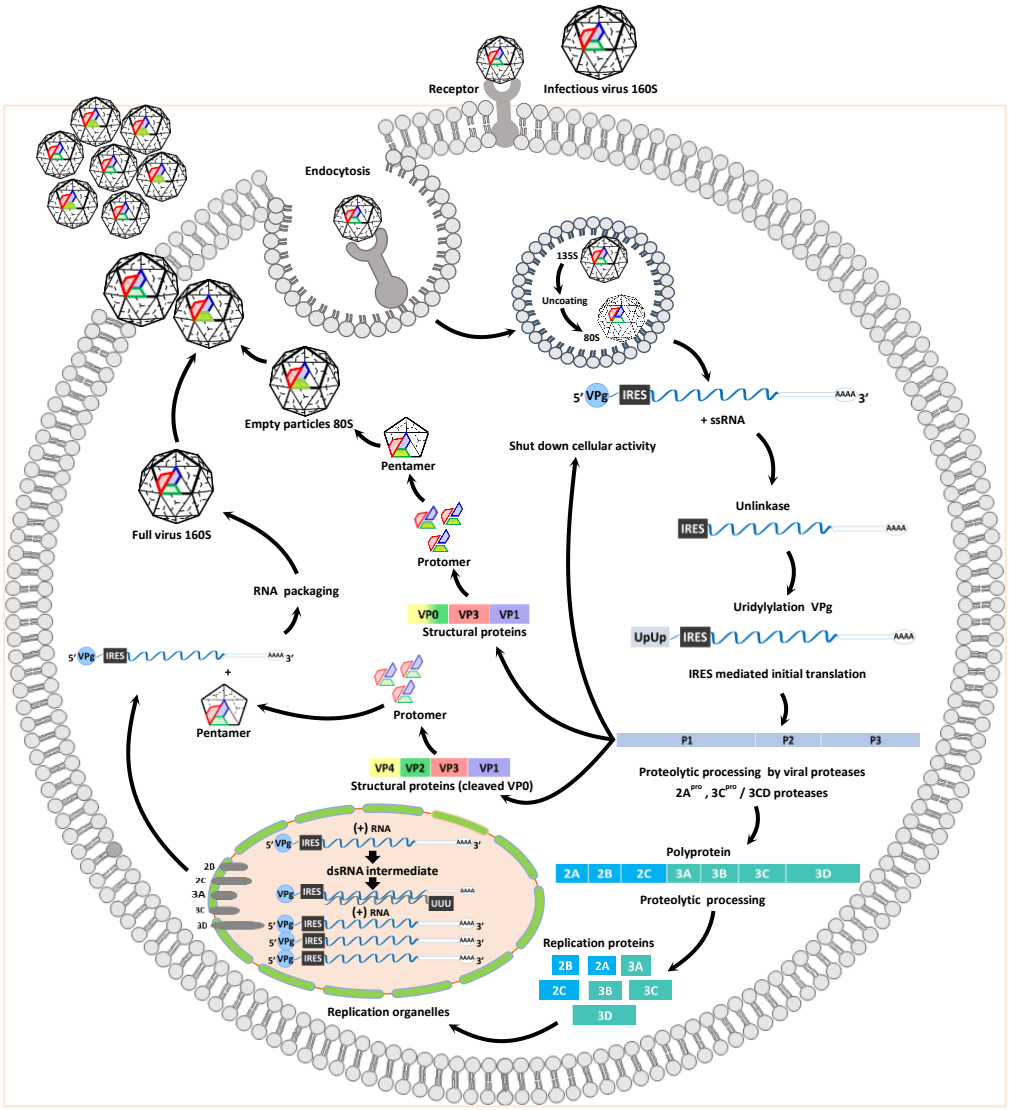


**Figure 1.4 Schematic overview of the EVA71 life cycle:** When the virus binds to its specific receptor, it will be uptaken into the cell by endocytosis. Inside the endocytosis vesicle, the virus undergoes conformational changes that lead to the uncoat of the virus to release the viral genome across the membrane into the cytoplasm. Once inside the cytoplasm, the genome is translated into +ssRNA, which then undergoes autoproteolytic cleavage to release the capsid proteins and replication proteins required for synthesising new viruses and shutting cellular activities. The viral genome replication occurs within membranous replication organelles generated by replication proteins and host proteins. Rreplication starts with synthesising (-) 3' strand RNA used as a template to generate (+) 5' strand RNA through dsRNA intermediate. The newly synthesised +ssRNA will be either used as a template for new replication rounds or packaged in newly assembled provirions to produce full virions. In parallel, capsid proteins are assembled into two different particles, either as full virion or as empty particles. Finally, mature viral viruses are released by cell lysis. Adapted from Cifuent et al (2019).

### 1.3.5. EVA71 classification

EVA71 is a non-enveloped RNA virus that belongs to the genus *Enterovirus* within the family *Picornaviridae*. The enterovirus genus is historically subdivided into five groups: Polioviruses, Coxsackie A viruses, Coxsackie B viruses, echoviruses and newly identified enteroviruses. A genome-based classification has replaced this (reviewed in Korsman et al., 2012). Virus serotypes use their original names given before the current reclassification was adopted so that, although it appears strange at first glance, Coxsackievirus A9, Coxsackievirus B4, echovirus 6, and EV-69 are all members of the species "Enterovirus B" (WHO, 2015).

The genus Enterovirus consist of 15 species; 7 of them are human enteroviruses (ICTV, 2021). In Enterovirus species A there are six EVA71 genotypes based on genetic variation in capsid protein VP1 (A-D). They include genotype A that consist of one subgenotype (BrCr). Genotype B is subdivided into five subgenotypes (B1 to B5) as well genotype C (C1 to C5). Genotype C4 is further subdivide into two subgenotype C4a and C4b (reviewed in Sun et al., 2020). The D strain was found in India, while F and E were found in Africa (reviewed in Chong et al., 2015).

### 1.3.6. EVA71 antigenicity

The surface of the EVA71 capsid is decorated with the loops and C terminus of the viral capsid proteins: VP1, VP2, and VP3 (Kiener et al., 2012). One of the linear neutralising epitopes of VP1 was found to comprise residues 215–220 of the VP1 GH-loop (Huang et al., 2017). The VP2 epitope was found in the EF-loop and comprised residues 141–155 (Xu et al., 2014), while for VP3 the conformational epitope was found in the knob region (Kiener et al., 2012). Gao et al (2012) aimed to characterise the human humoral immune repose

against EVA71 infection and map human epitopes on the viral capsid proteins. They found that IgM epitopes were mainly located in VP2 and VP3, with the occurrence of multi epitope responses during acute infection. They also found only one IgM epitope in VP1, and one IgG epitope that activated in recovery phase sera. These variations of the humoral immune response at different stages of infection may help in the evaluation of EVA71 vaccines immunogenicity and the development of diagnostic reagents. (Gao et al., 2012). As an alternative approach to cope with the high genetic variation of EVA71, Zaho et al (2013) have investigated VP4 to identify neutralisation epitopes. The first 20 N-terminal amino acid residues in VP4 were highly conserved among various EVA71 genotypes. Immunisation of chimeric particles carrying the peptide VP4N20 has elicited a specific neutralising antibody response in mice, exhibiting broad neutralising activity against different genotypes of EVA71 in vitro. Despite that, VP1, VP2, and VP3 exhibit variations in antigenic activity.

VP1 is considered the main EVA71 capsid protein as many neutralising epitopes identified on its surface correspond to virus serotyping and receptor binding (reviewed in Ma et al., 2009). Indeed, VP1 plays an essential role in characterising antigenicity as the EVA71 genotyping, phylogenetic analysis, and classification into six genotypes were built upon sequencing of VP1. As well considered an indicator of eliciting a protective immune response after EVA71 infection (reviewed in Bessaud, et al., 2014). The two neutralising linear epitopes SP70 and SP55, located on the VP1, were found to induce EVA71-specific CD4+ T-cell proliferation and were capable of eliciting neutralising antibodies against it (Foo et al., 2007). Residue 145 in the DE-loop on the surface of VP1 has been identified as a critical antigenic determinant of strain-specific murine mAbs (Fujii et al., 2018). It can also alter the binding efficacy of surface receptors such as Heparan Sulphate (Ke et al., 2020;

Huang et al., 2015) found that VP1–98, VP1−145, and VP1−164 co-operatively function as antigenic determinants for B4 and B5 strains.

### 1.3.7. Origin of diversity: molecular epidemiology, evolution and recombination of EVA71

RNA viruses present within the infected host as quasispecies that are genetically diverse and moves through fitness landscapes where distinct variants of the viral community will be selected depending on the selective pressure they encounter (Domingo et al., 2012). Antigenic drift and antigenic shift are the two types of genetic changes that can occur to the members of RNA viruses. This phenomenon is important for determining a suitable vaccine strain (reviewed in Tee et al., 2010; Kim et al., 2018).

The influenza virus is the best example of antigenic shift and drift, and it imposes a critical challenge to the development of an effective vaccine that can elicit protective neutralising antibody responses (reviewed in Kim et al., 2018). Influenza vaccine strains are selected primarily based on genetic and antigenic characterisation of circulating influenza strains, their global prevalence, and virus inhibition activity by candidate vaccine (reviewed in Kim et al., 2018; WHO 2022). The target of the current influenza vaccine is the two A virus subtypes A(H1N1) and A(H3N2), and the influenza B viruses lineage B/Victoria/2/87-like and B/Yamagata/16/88-like viruses (reviewed in Kim et al., 2018; WHO 2022). These vaccines are redesigned regularly due to rapid genetic changes in the virus population through the genetic processes of antigenic drift and shift (reviewed in Kim et al., 2018; WHO 2022).

Antigenic drift can be defined as the process by which minor genetic changes are introduced into critical viral epitopes such as surface glycoprotein, either hemagglutinin

(HA) or neuraminidase (NA) is caused by a point mutation or deletion in the viral gene. This results in replacement of older viruses by new variant that requires a yearly reformulation of the seasonal influenza vaccine (reviewed in Carrat and Flahault, 2007). Thus, any vaccination approach that targets the classic neutralising responses to HA and/or NA must manage antigenic drift effectively. In contrast, the antigenic shift among influenza A viruses due to their extensive animal reservoirs is due to genetic segment reassortments resulting in novel viruses. Reassortment occurs by exchanging the RNA segments within a respiratory cell infected by two virus strains. Because avian, swine and human viruses are similar, they can share RNA segments if they have infected the same cell (reviewed in Carrat and Flahault, 2007; Kim et al., 2018). For example, in 1968 the A (H3N2) pandemic virus was derived from an A(H2N2) virus that had acquired HA and PB1 genes from an avian virus.

Natural recombination in picornaviruses is a frequently documented phenomenon related to their evolutionary diversity. This phenomenon facilitates the acquisition of new phenotypic traits through a novel combination of structural and non-structural genes and (5’ UTR) sequences (Simmonds and Welch, 2006). This was first seen between serotypes of poliovirus in vaccine recipients (Martín et al., 2002).

EVA71 may impose a risk for vaccine development as it has shown antigenic drift and shift similar to the influenza virus (Karlsson Hedestam et al., 2008; Tee et al., 2010). As an RNA virus, EVA71 has extremely high mutation rates due to the lack of proof-reading ability in RNA polymerases compared to DNA viruses and has high error rates due to misincorporation during chain elongation (reviewed in Domingo et al., 1996). The mutation rate of EVA71 was estimated to be $3.1 \times 10^{-3}$ nucleotide substitutions per site per year (reviewed in Wang, Hu and Zheng, 2022). Thus, virus populations exist as quasispecies or

mixtures of many different genome sequences, which is believed to be essential for their survival under selective pressure (Domingo et al., 2012).

The EVA71 continuous evolution and, thus antigenic drift has an implication on vaccine development, and diagnostic test development aims to monitor EV7A1 antigenic variation that may appear even in strains from the same genotype (Chia et al., 2014). This implication emphasises the importance of closely monitoring the virus antigenic status.

EVA71 VP1 gene is usually tested for phylogenetic analysis as it shows a high degree of genetic diversity, and no recombination has been detected in this protein. Based on the VP1 nucleotide sequence, EVA71 can be classified as six separate genotypes A, B, C, and D the Indian strain, while F and E are African strains (reviewed in Chong et al., 2015). Each genotype can be subdivided further into subgenotypes on the same basis (reviewed in Yip et al., 2013; Chong et al., 2015).

Genotype A contained the prototype EVA71 strain (BrCr-CA-70) and was first detected in the USA in 1969, and it remained undetected until 2008 when it reemerged in China (reviewed in Yip et al., 2013). Genotype B has been categorised into sub-genotypes B1, B2, B3, B4, and B5. Genotype C is also classified into sub-genotypes C1, C2, C3, C4, and C5. Furthermore, the C4 sub-genotypes have two lineages, C4a and C4b. EVA71 strain genotype B subgenotype B1 - B2 have been circulating globally. B1 is the major type in America, Europe, Asia and Australia. While B2 is more prevalent in USA, Netherlands, and Japan. China has been affected mainly by C4 (reviewed in Yip et al., 2013). The D genotype that was detected in India might be divergent from the C4 sequence by 18.2% (reviewed in Yip et al., 2013; Chong et al., 2015). Genotypes E and F phylogenetic analysis showed a shared ancestor among the genogroup D isolates and members of genogroup E. Similarly, the

isolates of genogroup F descended from a recent common ancestor shared with members of genogroup B (Bessaud et al., 2014).

Sometimes recombinant strains can occur such as the intertypic recombination that occur between C2 CAV16 strain G-10 and EVA71 genotype A and the CAV16 strain G-10 C4 (reviewed in Yip et al., 2013; Woodman et al., 2019). Another recombination occurred in 2000-2001 caused by EVA71 subgenotype B4 evolved between B2 and B1. Two recombinations have been detected between genotype B and genotype C at 2A-2Bjunciton, and intertypic recombination between the B and CAV16 strain G-10 in the 3C region. Another genetic drift witnessed was the emergence of genotype D, which is believed to be an 18.2% divergence of C4 (reviewed in Yip et al., 2013; Woodman et al., 2019). A single genotype or subgenotype can cause cyclic EVA71 epidemics every 2-4 years, such as continuously circulating C4 in China (reviewed in Chong et al., 2015). Although, it is not uncommon to observe the co-circulation of divergent isolates and the occurrence of unpredictable genetic changes in genotypes and sub-genotypes. Malaysia has observed B3 intra-genotype shifts to B4 between 1997 and 2008 and B4 to B5 between 2000 to 2003. In Taiwan, shifts occurred from C2 to B4 and C4 to B5. An interatypic genetic recombination also appeared in Taiwan between B and C genotypes due to the co-circulating of CAV16 with several types of EVA71. This co-circulation has led to recombination between subgenotype C2 and CVA16 in China (reviewed in Chong et al., 2015).

EVA71 infections are associated with high morbidity and mortality rate in children (Chang et al., 2016). As previously mentioned, EVA71 was first identified in California in 1969 and described in 1974. After this event, two epidemic outbreaks associated with high mortality rates occurred in Europe in the 1970, first in Bulgaria in 1975 and then Hungary in 1978

(reviewed in Yip et al., 2017). Since then, many outbreaks have affected many countries around the globe, but the significant outbreaks of EVA71-related HFMD were centralised across the Asia-Pacific region (Mao et al., 2010). The impact of the spread of disease on public health is profound in Asian countries, including Japan, Malaysia, and China, due to the increase in laboratory-confirmed cases. Since 1990 many recurrent epidemics of fluctuating scale have hit the Asia Pacific region, including China, Malaysia, Singapore and Taiwan. Analysing the phylogenetic tree has shown two significant epidemics named after the affected cities: Malaysia in 1997 and Taiwan in 1998. These major outbreaks were caused by different prevalent strains belonging to genogroups B3 and C2 (reviewed in Bible et al., 2008; Tee et al., 2010). However, the most affected countries were China, with 78 deaths; Taiwan, with 78 in 1998 and 41 deaths in 2000; and Malaysia, with 29 deaths. China, since 2008, has to include HFMD as a notifiable disease in the surveillance system (reviewed in Yip et al., 2013). From 2008 until 2011, this country was hit by many outbreaks, and the number of cases increased from 488-955 with 126 deaths to 1619706 with 509 deaths. Both EVA71 and CAV16 were co-circulating (reviewed in Yip et al., 2013).

In Europe, EVA71 is considered mild, and the risk is unrecognised despite occasional cases of severe disease and two severe outbreaks in Eastern Europe: Bulgaria in 1975 and Hungary in 1978 (reviewed in McMinn 2002; Yip et al., 2013). In Norway, asymptomatic children were detected, which could be related to the host, e.g., the status of the immune system, genetic, nutrition, and hygiene status, or it could be related to the viral factor (reviewed in Yip et al., 2013). Kamu et al (2021) suggested that the severity of the symptoms associated with CVA6 infections and the recent increase of EVA71-related HFMD cases and CVA6 in Europe might be due to two reasons. First, the evolution of recombinant or changes in the

pathogenicity of emerging strains could be due to the increase in infections in large unexposed and susceptible populations. Accordingly, this hypothesis was tested by conducting a seroprevalence study in the UK to understand the population susceptibility, the emergence of serotypes, and possible changes in pathogenicity related to serotypes as well the transmissibility (Kamu et el., 2021). The number of EVA71 and CVA6 was estimated using cross-sectional age-stratified samples collected in 2006, 2011, and 2017 (Kamu et al., 2021). The results have shown that EVA71 and CVA6 infections were highly prevalent among children and adults in the UK. Seroprevalences of both EVA71 and CVA6 increased from 32% and 54% at 6–11 months to >75% by ten years. The decline of antibody titers after 20 years may indicate infrequent re-exposure in older populations. The CVA6 seroprevalence was higher than that of EVA71 in younger children (1–10 years) in each study year, and there was an increase in CAV6 incidence since 2010. However, in Europe, there is no established surveillance for EV infection. Most data are obtained from voluntary data collection of hospitalised patients who suffer from severe HFMD disease (reviewed in Esposito and Principi, 2022).

EVA71 HFMD imposes a global threat that substantially burdens healthcare services, families, and societies. Failing to halt the spread of the disease will intensify the impact on public health. EVA71 might be considered the main acute Flaccid Paralysis (AFP) case in the post-polio eradication era. Consequently, it is necessary to establish a global HFMD surveillance network to evaluate EVA71 vaccines in controlling antigenic shifts, virus fitness, and the emergence of new viruses. It is also essential to coordinate the global effort of standardised immunoassays and animal models to evaluate the potency of vaccine candidates and determine the most potent and affordable products (reviewed in Chong et al., 2015).

### 1.3.8. Treatment and prevention

EVA71 is the most neurotropic virus associated with severe neurological complications. Beyond the polio eradication era, it imposes a new threat to children, especially in the absence of specific treatments or vaccines. At the main time, supportive therapy and symptomatic treatment are still the primary management for severe cases.

#### 1.3.8.1. Immune therapy

- **Neutralising antibodies**

Passive immunisation could be a valuable tool to treat HFMD caused by EV7A1. Neutralising antibodies could be used clinically to neutralise the virus and suppress inflammation non-specifically (Jia et al., 2017). In their study, Jia et al (2017) have identified and characterised an EVA71-specific IgG2a antibody designated 5H7, which was able to efficiently neutralises several EVA71 genogroups (A, B4, C2, C4) by efficiently interrupting viral attachment. Moreover, generated human single-chain antibodies (HuscFvs) specific to the EVA71-internal capsid protein (VP4) inhibit virus replication by interfering with the VP4-N-terminus, which is essential for membrane pore formation and virus genome release. Another example is the EVA71-specific IgG2a antibody designated 5H7, a cross-neutralising IgG monoclonal antibody (Phanthong et al., 2020). However, despite reporting the promising generation and application of neutralising antibodies against EVA71, none has yet reached clinical trials.

- **Intravenous immunoglobulin (IVIg)**

Treating severe cases of HFMD in general with Intravenous immunoglobulin (IVIg) has been recommended by the World Health Organisation (WHO) and the Centre for disease control (CDC) and has been adopted by some countries (reviewed in Jiao et al., 2019; WHO 2011). Despite the potential of immune therapies to treat severe cases of HFMD, the application seems to have some disadvantages. These advantages include variations related to the availability of donors and variations between batches. Another significant disadvantage is the risk of transmitting human pathogens with the serum, necessitating screening and treatment before using pooled human sera (reviewed in Jiao et al., 2019; WHO 2011). In 2014 infectious Disease Clinical Research Network (SEAICRN) in Bangkok, Thailand, Southeast Asia, held a workshop to discuss the use of Intravenous Immunoglobulin to treat cases of HFMD in Southeast Asia (Chea et al., 2015). They agreed on the importance of studying the efficacy of IVIg in treating severe cases and safety concerns surrounding the use of this treatment. They also agreed on the need to conduct a multinational trial randomised, placebo-controlled trial. This committee discussed a potential hurdle for carrying out a multinational trial. However, that would be a challenge due to the variance of guidelines, IVIg brands and financial issues.

### 1.3.8.2. Antiviral drugs

The current researched antiviral drugs utilise identified viral proteins and host factors as potential drug targets to prevent EVA71 infection. However, no antiviral medications are available to treat affected patients with EVA71 (reviewed in Lin, Kung and Shih, 2019). None of them has reached clinical trial despite the considerable progress that has been made in discovering candidates that are effective in both in vitro and in vivo. Moving drugs from the

stage of lab testing and animal testing to human clinical is hindered by several issues. One of these issues is the need to generate a broad-spectrum antiviral that targets EVA71 in addition to other HFMD virus strains, such as CVA16 (reviewed in Wang, Hu and Zheng, 2022). Requiring a high safety profile is the second issue. The side effect, such as headaches and drug-drug interactions of capsid inhibitors vapendavir, ceased the clinical trial. Also, using broad-spectrum antiviral drug targets host could be effective against enteroviruses with a high genetic barrier but toxic at the same time as was found when conducting in vivo mouse model study with PI4KB inhibitors (reviewed in Wang, Hu and Zheng 2022). Third, resistance against EVA71 antiviral drugs should be addressed when generating new drugs by selecting or developing a compound with a high genetic barrier to drug resistance. This drug can continue working even as more changes occur and require a more significant number of critical mutations to render treatment ineffective. In addition, the fitness and transmission of mutant viruses, which are the consequences of resistance, should also be addressed. For example, the application of 2C inhibitors successfully compromised the mutant fitness of replication (reviewed in Wang, Hu and Zheng, 2022).

Due to the lack of antiviral therapy, most healthcare providers rely on infection prevention and control measures. These measures include setting up surveillance systems, education and sharing public health surveillance data between decision-makers and those concerned. The WHO published guidelines to prevent and control HFMD and has recommended establishing a surveillance system that helps to monitor the disease (WHO, 2015).

### 1.3.8.3. EVA71 vaccines

- **Brief history of vaccines**

Vaccines could be defined as a 'pharmacologic compound' containing antigens derived from a disease-causing agent and capable of inducing an immune response (Galiza and Heath, 2017). The antigen could be a protein fragment of the invading pathogen, inactivated toxins, or the killed or attenuated form of the pathogen itself. Vaccines could be therapeutic or prophylactic (Galiza and Heath, 2017).

Since the discovery of cowpox inoculum that protects against human smallpox infection by vaccination by the English physician Edward Jenner (1749 - 1823), immunisation by vaccines came to prominence and became a vital part of public health. This approach helped in eradicating smallpox worldwide in 1979 (Riedel, 2005). Perhaps the first well known modern vaccine was the inactivated poliovirus vaccine developed in 1955 by Jonas Salk (Tan and Ponstein, 2019), and attenuated oral polio developed by Albert Sabin in 1960. Both vaccines remain effective until today (Sabin and Boulger, 1973). Despite the advancement in vaccine technology, the continuous threat imposed by emerging and re-emerging infectious pathogens necessitate exploring new vaccine technologies and approval as a rapid response to confront such a threat (reviewed in Excler et al., 2021). These vaccines need to be safe, effective, inexpensive, and easy to produce, with long lasting immunity, stable for convenient storage and delivery.

Live attenuated and inactive vaccines have been employed effectively for a very long time to prevent and control diseases. However, each of them has inherent risks associated with manipulating living viruses. Risks include incomplete attenuation, instability and the

possible reversion to the wild-type form, toxicity and risk of mutation (reviewd in Fox et al., 2017). In contrast, genetically engineered vaccines such as subunit vaccines, synthetic peptide vaccines, DNA/RNA vaccines and virus like particle VLP vaccines, offer a safe, stable, and can be robust immunogenic alternatives (Brisse et al., 2020).

- **Inactivated vaccine**

The inactivation process involves treating propagated and purified pathogen with heat, radiation, or chemicals, including formalin (Budowsky et al., 1981) and heat (reviewd in Nims and Plavsic, 2013). These treatments aim to inactivate any biological materials that allow the pathogen to replicate, leaving only the virion shell or capsid with necessary antigens.

Most of the licensed human viral vaccines are inactivated using formaldehyde. However, there are some concerns regarding this chemical method of inactivation. In certain cases, formaldehyde inactivation was insufficient to inactivate virus particles entirely and led to outbreaks of virus infections due to contaminated vaccines. This was observed in Cutter incident. in April 1955, when 40,000 children fell ill after receiving the polio vaccine manufactured by Cutter Laboratories. In this incident, 70,000 had muscle weakness, 220 were 35infected with the live poliovirus, 164 were permanently paralysed, and ten children died (Offit, 2017). The WHO has recommended the inactivation of the poliovirus to be carried out before and after the purification to avoid such an incident. However, that might lead to over- inactivation of the viruses, resulting in less effective vaccines. Also, the FMDV outbreak reported in Western Europe in the 1980 due to ineffective inactivated virus vaccines. Indeed, inactivation might affect the neutralising

epitopes of the virus, which may be destroyed during inactivation, resulting in weak neutralising antibody hence inadequate immune response (reviewd in Paton et al., 2021). Currently, there are three commercially available inactivated vaccines against HFMD that were developed in China using C4 strains as it is the most prevalent strain there (reviewed in Li et al., 2021). They have developed by three Chinese companies: Sinovac Biotech, Neijing Vigoo, and the Chines Academy of Medical Science (CAMS). All vaccines were licensed by China's FDA between 2015 and 2016 (Mao et al., 2016; Zhou et al., 2016). At the laboratory testing and development stage, two doses were found to be needed to induce a potent through *in vivo* study aimed to test the immunogenicity and safety of the inactivated vaccines (reviewed in Li et al., 2021). Following phase, I and phase II, the immunogenicity and safety of inactivated vaccines were proven through further in large phase III clinical trials. 12,000 infants and children (between 6-71 months) were recruited for phase III clinical trials of CAMS vaccines. They were randomly vaccinated with two doses of 100 U (EVA71 antigen unit) or were giving placebo. After two years of following the vaccine efficacy against EVA71-related HFMD was 97.4% (reviewed in Li et al., 2021). In the Vigoo phase III clinical trial 10,245 infants and children (6-35 months) were randomly given 320 U vaccine or placebo and followed for two years. The efficacy of the vaccine against was 100% at the second year. The vaccine did not cause any serious adverse effects (reviewed in Li et al., 2021). The phase III trial of the Sinovac (Beijing, China) has recruited 10,077 children (6 to 35 months) and were given 400 U of Sinovac vaccine or placebo. After two years of following the vaccine efficacy against EVA71-related HFMD was 95.1%. Several other new inactivated vaccines using B4 and B5 genogroups are currently under development but still far from approval (reviewed in Li et al., 2021).

None of these vaccines was approved by the US FDA due to many concerns regarding the effectiveness of the vaccine against other HFMD causing strains and the safety and quality control during the manufacturing (reviewed in Li et al., 2021). The 67th meeting of the WHO Expert Committee on Biological Standardization in 2016 reviewed the current status of EVA71 vaccine development and regulations to standardise the vaccine and assure the development of safe and efficient vaccines (WHO, 2021). However, these recommendations have not covered the other type of vaccines such as virus- like particle vaccines (VLPs) vaccines, or subunit vaccines or production of bivalent vaccines against both EVA71 and CA16.

- **Attenuated vaccines**

Attenuated vaccines are created by reducing pathogen virulence, yet they can replicate similar to wild-type viruses. Exposing the host immune system to attenuated viruses, a genetically weakened version of their wild-type, will induce a host immune response like natural wild-type infection. However, produced infections are milder than the illnesses produced by the virulent wild-type. Several approaches could be followed to achieve attenuation (reviewed in Yadav et al., 2013). For example, select a naturally attenuated virus from a different tropism than the wild-type. That means that the replication capacity of attenuated viruses with a host range is high in selected cell culture systems but much lower *in vivo*. Select live attenuated virus for oral polio attenuated vaccine (OPV) exhibits a different pattern of tropism than wild-type. The wild-type replicates robustly in the gastrointestinal tract and the central nervous system (CNS), while the attenuated virus can only replicate well in the gastrointestinal tract (Morrison and Plotkin 2016).

The attempt to attenuate EVA71 was based on the successful experience with attenuated Sabin OPV vaccines that have been used to eradicate polio globally. Several approaches have been used to attenuate EVA71. One of these approaches was by passaging the virus in one cell line and then changing that cell culture. EVA71 was grown in Vero cells and then passaged in RD cells to select mutant viruses adapted to RD cells. This attenuation changes three amino acids: c G, V146 I, and S241 L, in VP1 and a single nucleotide mutation at nt 494 of the 5’ UTR of the selected mutant virus (Chang et al., 2018).

Moreover, modifying the targeted virus by genetic engineering is another approach for attenuation, e.g., altered fidelity of RNA-dependent RNA polymerase (RNAP) replication in

RNA viruses, genome rearrangements, and gene deletions. The highly structured 5' UTR plays a vital role in viral translation and virulence. Changing cytosine to uridine at position 158 in stem-loop II of the 5' UTR reduced EVA71 viral translation and virulence in a mouse model (Yeh et al., 2011).

Although engineer attenuation has become more accessible and new methods have been developed to suppress viral growth in the short term, the molecular basis of attenuation remains poorly understood.

EVA71 attenuated vaccines can provide long-lasting immunity and cost-effective production. However, the pathogenic molecular mechanism of EVA71 still needs more study despite the progress in developing attenuated EVA7 vaccines, e.g., EVA71 virulence determinants have not been completely elucidated. Despite their reduced pathogenicity, there is still concern about reversion to virulent wild-type that can cause disease in immunocompromised individuals (reviewed in Li et al., 2021).

- **Recombinant VP1 and synthetic peptide vaccines**

Recombinant protein vaccines are not based on using the entire organism but on the expression of protective protein antigens in bacterial, yeast, plant or animal cells. The recombinant EVA71 proteins were expressed to be used as recombinant vaccine candidates. For example, the EVA71 VP1 protein, a capsid protein that contains neutralisation epitopes, has been expressed in different expression systems, such as *Escherichia coli* (*E. coli*) and baculovirus. The protective effect of recombinant VP1 protein against EVA71 infection was positive in mice. However, the protection was lower than that of inactivated vaccine (reviewed in Li et al., 2021).

In contrast*, Pichia pastoris* expressed P1 protein might be a promising EVA71 vaccine candidate. The EVA71 P1 vaccine candidate was evaluated in rabbits and showed high cross-neutralisation and persistence antibodies for different EVA71 subtypes. Using the same candidate to vaccinate pregnant mice resulted in a cross-protection of neonatal mice against different subtypes of EVA71. The level and duration of EVA71 antibody production were more substantial than that of inactivated EVA71 virus, which was related to antigen glycosylation (Han et al., 2014).

Synthetic peptides vaccine can be considered safe and effective, especially as a multivalent vaccine. Antigen epitopes were mapped by a synthetic and overlapping peptide spanning VP1 had identified two epitopes SP55 and SP70 amino acids 163–177 and 208–222 in VP1, respectively. Both peptides were able to elicit protective antibodies in mice against EVA71 infection. In addition, it was found that anti-SP70 antisera passively protected suckling mice against various EVA71 strains (Foo et al., 2007).

Recombinant VP1 and synthetic peptide vaccines are promising vaccine candidates as they are safer and more cost-effective. Moreover, the application of these vaccines will reduce the risk of unwanted antibody-dependent enhancement to prevent possible infection amplification or triggering of harmful immune responses (reviewed in Li et al., 2021).

### 1.3.9. VLPs as vaccine platforms

Virus-like particles (VLPs) are generated by the expression and self-assembly of viral structural proteins that can take place in many cell expression systems. VLPs mimic the morphology of their authentic viruses but are non-infectious as they lack genomic material (reviewed in Frietze et al., 2016). The advantage of VLPs of resembling the parent viruses is that they can display antigenic epitopes in a highly repetitive manner and the correct conformation to stimulate a humoral and cellular response like a real virus. Highly repetitive manner of antigenic epitopes increases the ability of phagocytosis to activate complement and recruit other molecules of the innate humoral immune system. Also, the antigens with repetitive surface organisation facilitate the activation of B cells by cross-linking the B cell receptor (BCR) and activation of complement (Tagliamonte et al., 2017; Bachmann and Jennings, 2010). Therefore, VLP vaccines are considered highly immunogenic and have been considered safe, which made them a favourable alternative to traditional vaccines such as inactivated or attenuated vaccines.

VLPs size are about 20-100 nm in size, and as the shape of the VLPs is critical, the size also is essential to determine the antigen-presenting cells (APCs) uptake pathways and antigen retention in lymph nodes. VLPs larger than 5 nm VLPs are attached to myeloid immune cells, smaller than transported by small antigen conduits. While VLPs are larger than 200nm APCs actively transport them (reviewed in Donaldson et al., 2018). Some VLPs can utilise Similar

immune processing pathways to their parent viruses and retention of intracellular processing mechanisms. However, it is not clear if VLPs mimic the intracellular processing of their native viruses (reviewed in Donaldson et al., 2018).

In general, cells can absorb VLPs through phagocytosis or macropinocytosis. To activate the adaptive immune response, and in the absence of infection or intracellular replication, VLPs are recognised by APCs and dendritic cells (DCs) and transported to the lymph nodes.

The VLPs are processed within the phagolysosome to present antigenic peptides on major histocompatibility complex (MHC) class I and II molecules. That, in turn, leads to stimulating CD4 and cytotoxic T lymphocytes. Due to the repetitive epitope, VLPs can activate B-cells sufficiently to activate T follicular helper cell development in the absence of DCs (Cervantes et al., 2020).

The VLP structural proteins can be derived from viral capsid, envelope, or core viral proteins either of a single virus or from different types of viruses to form chimeric VLPs (reviewed in Nooraei et al., 2021; Tariq et al., 2022). VLPs can be assembled from one or more structural proteins and adopt different structures. The capsid proteins can self-assemble to form one or two layers up to three layers, and some single layer VLPs may be formed from a multi-protein structure. For example, the VLPs of the human papillomavirus (HPV) are made of a single structural protein. While more complex VLPs comprise several structural proteins such as triple-layered rotavirus VLP (RLP), consisting of three viral proteins (VP2, VP6, VP7) (Vieira et al., 2005).

#### 1.3.9.1. The structural classification of VLPs

The VLP structural proteins can be derived from viral capsid, envelope, or core viral proteins

either of a single virus or from different types of viruses to form chimeric VLPs (reviewed in Nooraei et al., 2021; Tariq et al., 2022). VLPs can be assembled from one or more structural proteins and adopt different structures. The capsid proteins can self-assemble to form one or two layers up to three layers, and some single layer VLPs may be formed from a multi-protein structure. For example, the VLPs of the human papillomavirus (HPV) are made of a single structural protein. While more complex VLPs comprise several structural proteins such as triple-layered rotavirus VLP (RLP), consisting of three viral proteins (VP2, VP6, VP7) (Vieira et al., 2005).

#### 1.3.9.2. Modification of VLPs

VLPs can be modified to carry antigenic epitopes either from their native or foreign viruses. In the case of the non-enveloped VLPs, the modification can be carried out by chemically conjugating the targeted antigen to the surface of the VLPs. For example, chimeric vaccine for foot and mouth disease virus (FMDV) was synthesised by inserting a short peptide mimicking the GH-loop epitope of VP1 protein into the e1 loop of the core of hepatitis B virus (HBc) particles (Bittle et al., 1982; Chambers et al., 1996). This vaccine levels were able to elicit high level of virus neutralising antibodies and provide protection to laboratory animals, but the protection was less in pigs and cattle.

#### 1.3.9.3. EVA71 VLP vaccines

EVA71 VLPs have been expressed in many cell expression systems. The successful expression of polio VLPs has led to the first attempt to generate EVA71 VLPs in insect cells (reviewed in Li et al., 2021). EVA71 VLPs were expressed using two recombinant baculoviruses encoding P1 polyprotein and 3CD protease in insect cells *Spodoptera*

*frugiperda* (Sf-9) and RD cells (Chung et al., 2006). The expressed 3CD successfully cleaved the P1 *in vitro* and *in vivo*. However, the yield obtained by co-infection of Bac-P1 and Bac-3CD was low. The low yield issue was attributed to the non-optimised vector MOI ratio that needs to be addressed in a future study. To increase the yield, it was also suggested to use a single baculovirus that carries both P1 and 3CD or expresses the whole ORF. Similarly, the EVA71 VLPs were generated successfully in Sf-9 again in another study using three recombinant vectors, Bac-P1 and Bac-3CD and a single baculovirus vector that carries both P1 and 3CD (Chung et al., 2008).

The results suggested that the assembly and processing pathways of the EVA71 VLPs in insect cells might be similar to poliovirus assembly in mammalian cells. These VLPs have been evaluated further for their immunogenicity by immunising BALB/c mice with different VLP preparations, including purified VLPs, 2- mercaptoethanol denatured VLPs, heat-inactivated, and EVA71 virus RD cell lysate or Sf-9 cell lysate (Chung et al., 2008). All the preparations were responsible for inducing a high titer of both IgG and neutralisation antibodies as evidence of potent, long-lasting humoral and cellular immune responses (Chung et al., 2008). They also protected mice against lethal EVA71 infection. Both denatured EVA71 VLPs and heat inactivated EVA71 have elicited lower neutralisation titers and confer less protection against lethal EVA71 infection in new-born mice, which may be a clear indication that the VLP integrity is essential to produce a potent immune response (Chung et al., 2008). The potential of EVA71 VLP vaccines expressed in Sf-9 with the recombinant Bac-P1-3CD have been evaluated by vaccinating macaque monkeys with VLP vaccine adjuvanted with alum. The monkeys responded positively and developed specific humoral and cellular immune responses to EVA71 VLP (Lin et al., 2012).

The low yield due to degradation and purity were the main issue that held up the expression of EVA71 VLPs in the Sf-9 using a baculovirus vector. The yield issue was addressed in two different studies. Chung et al., (2010) have proven that reduced expression of the 3CD to mitigate the competition with P1 expression have increased the yield of the EVA71 VLPs significantly. The reduced expression of the 3CD was achieved by constructing Bac-P1-C3CD under the CMV promoter and Bac-P1-I3CD under IE-1 promoters, and both are weaker promoters than p10 promoter. VLP characterisation has shown the enhancement of the extracellular EVA71 VLPs yield in Sf-9 cells. However, the yield was low in insect cells High Five™ (Hi-5) cells. The yield and the purity for industrial-scale production purposes were tackled by Zhao et al (2017) who have purified EVA71 VLPs using a novel multistep chromatography using specific columns: Capto Core 700, Capto Adhere resin, and Capto Butyl columns (GE Healthcare). This purification method has resulted in ~31.52% yield and >95% purity.

In another study aimed to generate EVA71 VLPs vaccines that exhibit cross-reactivity against the three sub-genotypes: (B3, B4, and C5), gene expression of baculovirus was enhanced by incorporating additional promoters in the form of open-reading frames described as transcription stimulators and known as AcMNPV (lef3, gp41, and chitinase), as well as cytomegalovirus immediately early (CMV-IE) (Kim et al., 2019). It was found that the Baculo-P1-3CD-gp41 produced a high yield in Hi-5 cells of approximately of 11.3 mg/L. This yield of VLPs was higher than that of Baculo-P1-3CD-lef3, and four times the yield obtained from Baculo-P1-3CD-CMV-IE. The potential of these VLPs as vaccines was proven by analysing the neutralizing antibody that was elicited in mice. As well the cross reactivity was proven among the four genotypes (Kim et al., 2019).

Yeast as an expression system was utilised to express the EVA71 VLPs. EVA71 VLPs were expressed in *Saccharomyces cerevisiae* using recombinant pYES2-P1 and pYES2-Trp- 3CD (Zhao et al., 2015). In the same study, the lethal EVA71 challenge test showed that VLPs generated in yeast can induce potent immune responses and VLP-immunized sera could protect neonate mice. The other yeast utilised to express EVA71 VLPs has been *Pichia pastoris* (Wang et al., 2013). This yeast has been utilised before in order to produce a subunit vaccine based on the expression of recombinant VP1 protein. This study demonstrated the vaccine potential of VP1 protein expressed in *Pichia pastoris.* The assessment of expressed recombinant VP1 was carried out in BALB/c mice. The anti-VP1 antibodies and neutralised EVA71 viruses. The antisera from VP1 vaccinated mice showed a prophylactic efficacy in neonatal mice.

To overcome the low levels of *S. cerevisiae* EVA71 VLPs, which was approximately 0.25 mg per liter yeast culture, Zhang et al., (2015) explored VLP expression in *P. pastoris*. The

recombinant expression of EVA71 in *P. pastoris* was carried out by co-expressing both vectors YE001 and YE003. The YE001 was engineered by the corporation of P1 polyprotein of the EVA71/G082 strain into pPink-HC (Invitrogen). Similarly, the YE002 was constructed by cloning the 3CD gene into pPink-HC to make plasmid YE002. The study demonstrated a high level of VLP recovery. The EVA71 VLP yield was high p to 4.9% TSP (or ∼150 mg VLP per liter yeast culture).

Regarding immunisation, studies have shown that these VLPs can elicit protective immunity. Yang et al., (2020) obtained a similar result of immunogenicity from the co-expression of the P1 gene and 3CD into *P. pastoris*. However, this study aimed to improve the yield of the VLPs, which resulted in 270 mg per litre yeast culture. The authors

attributed this improvement to some factors that could be related to the plasmid construction method where the AOXI promoter of 3C-pPICZαB was replaced by PEX8 promoter. Or it could be associated with the host strain (SMD1168H vs. PichiaPinkTM) or the fermentation condition.

A mammalian cells expression systems was also used to co-express EVA71 VLP vaccines. EVA71 VLPs using recombinant single Adenovirus vector known as Ad-5H that carried both P1 and 3CD in EK-293A cells (Tsou et al., 2015).

All the previous vaccines were monovalent and targeted EVA71 only. As HFMD can be caused by Coxsackievirus, e.g., CVA6, CVA10, and CVA16, the inactivated EVA71 vaccines failed to provide cross-protection against them. It was essential to develop a bivalent or multivalent HFMD vaccine to protect against two viruses or more. A bivalent chimeric vaccine was developed against EVA71 and CVA16 in *S. cerevisiae*. Passive immunisation with anti-ChiEV- A71 VLPs sera conferred full protection against lethal challenges (Zhao et al., 2015). Zhang et al., (2018) generated tetravalent VLPs vaccines that contain recombinant EVA71 VLPs, CVA6 VLPs, CVA10 VLPs, and CVA16 VLPs. Mice models were protected by antisera derived from immunisation with the tetravalent VLP vaccine, which suggests a promising candidate for vaccination.

## 1.4. Polio

Poliovirus is a serotype of the Enterovirus C species that belongs to the *Picornaviridae* and is considered one of the most famous viruses in this family as most of the modern virology studies were based on many studies that were conducted to understand it (Tuthill et al., 2006).

### 1.4.1. Molecular genetics of polio

Poliovirus is a single-strand RNA (+ssRNA) non-enveloped virus, a member of the genus Enterovirus that belongs to the *Picornaviridae* family. The polio genome consists of 7500 bases in length in a non-enveloped capsid comprising 60 copies; each copy is composed of viral structural proteins that are VP1, VP2, VP3 and VP4. Each structural proteins have an edge-shaped, eight-stranded β-sandwich core structure (Hogle, 2002). Within the 8-stranded β-fold of VP1 lies a pocket containing a sphingosine-like lipid (pocket factor) (Rossmann et al., 2002). The viral lifecycle of polio, including cell entry, genome replication and virus assembly or morphogenesis, is typical of *Picornaviridae*, and the general details are similar to the infectious cycle of EVA71 (as described in 2.3.5) (Figure 1.5) (reviewed in Jiang et al., 2014).

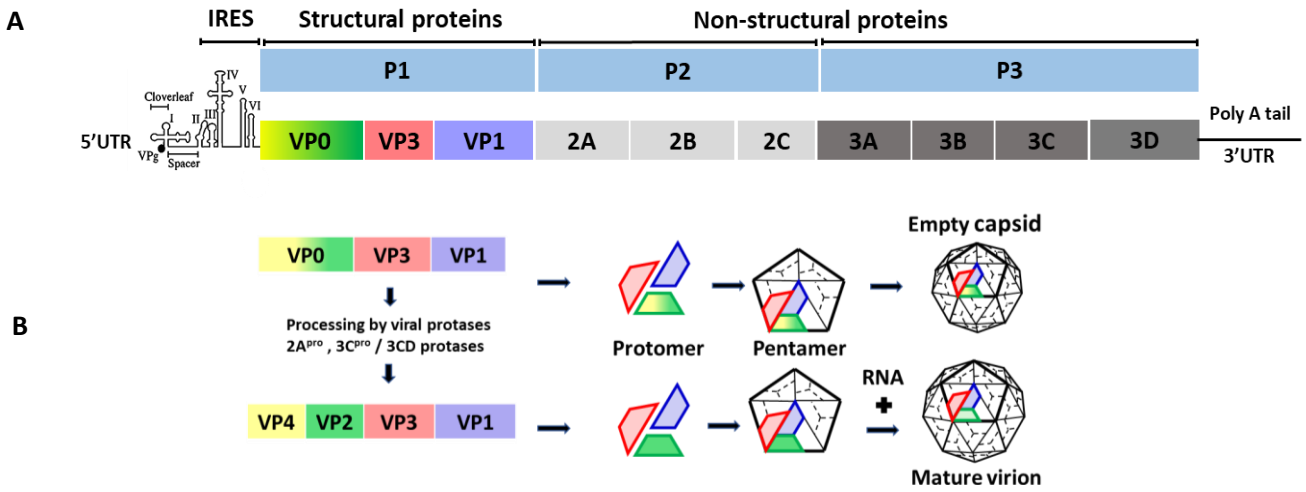


**Figure 1.5 Polio genome structure and morphogenesis:** (A) Like many other picornaviruses, poliovirus contains a single positive-strand RNA genome of approximately 7500 nucleotides. The viral RNA consists of an ORF flanked by two UTR, at the 5' and 3' end of the genome. at the 5' end is covalently linked to VPg, and the 3' end is connected to a poly(A) tail. The 5' UTR contains two elements essential for translation and replication: The internal ribosomal entry site (IRES) region which consist of five stem loop structures within the 5' UTR, and a cis-acting cloverleaf-like. (B) The ORF is translated into a single polyprotein comprising three proteins encoding regions P1 that encode the viral capsid proteins, and P2 and P3 encode proteins for proteolytic processing and replication. The P1 is cleaved by viral protease precursor 3CD into the capsid proteins VP0, VP1 and VP3. The viral RNA encapsidation to form the mature virion occur when VP0 cleaves into VP2 and VP4, whilst in naturally occurring ECs VP0 remains uncleaved. (Adapted from Adeyemi, 2017).

### 1.4.2. Polio pathogenesis

The natural host of poliovirus is humans, but also monkeys can be infected when the virus is inoculated directly into the central nervous system (CNS). Like other viruses, cell tissue tropism and host tropism for polio are influenced by the presence of cellular receptors that serve as the poliovirus receptor (PVR) and permits viral entry. The presence of these receptors can be natural or transgenic, as in the case of transgenic mice that carries the human polio receptor (hPVP/CD155) (reviewed in Nomoto 2007).

The virus is transmitted from person to person, and poliovirus is shed in the faeces; thus, the main route of spread is faecal-oral, although respiratory routes are possible. The virus enters the mouth and nose, multiplies in the pharynx and lower intestinal tract, and spreads through the blood and lymphatic systems (reviewed in Troy and Maldonado, 2012). Incubation is from 5 to 35 days, and virus shedding in faeces might be reduced within three weeks. However, in rare cases, the virus may present in the pharynx for 1-3 weeks and can be shed in stools for 4-8 weeks after infection, even in individuals with mild symptoms or asymptomatic. The usual incubation period of non-paralytic poliomyelitis is ranged between 3 to 6 days. Nevertheless, for the onset of paralysis in paralytic poliomyelitis, the incubation period is usually between 7 to 21 days (reviewed in Troy and Maldonado, 2012).

The virus spreads to gastrointestinal lymphatic tissues during intestinal replication and may enter the bloodstream. That would be followed by a minor viremia ensues, and the virus invades a number of sites, such as muscle, fat, liver, spleen, and bone marrow. The disease might be contained at this point, but further virus replication in these tissues will lead to significant viremia and the onset of clinical symptoms. During the viremic phase, the cell of the CNS is infected in 1% of cases. Like EVA71, polio cross to the CNS by crossing the Blood-Brain Barrier or retrograde axonal transport (Romero and Modlin, 2015).

### 1.4.3. Clinical manifestation

Polio infection can lead to subclinical infection, paralysis, and death. However, less than 1% of infected individuals suffer from paralytic poliomyelitis, 70% of polio-infected individuals are asymptomatic, and 25% have mild symptoms (CDC 2022). The mortality rate for acute paralytic polio ranges from 5–15%. Paralytic poliomyelitis could be spinal, bulbar and bulbospinal type according to the site of infected motor neurons. Meningitis is the first symptom of spinal poliomyelitis, followed by severe myalgia and sensory and motor symptoms such as hyperaesthesia and spasms (reviewed in Mehndiratta et al., 2014). Then weakness and paralysis occur within 1-2 days and are classified as asymmetrical and flaccid paralysis (AFP). The lower limbs are predominantly affected, although any combination of limbs may be paralysed. Bulbar poliomyelitis led to paralysis of the muscles innervated by the cranial nerves. This type of disease can result in dysphagia, nasal speech, pooling of secretions and dyspnoea. The progress of paralysis can occur within one week, and about 70% of the affected patients suffer from permanent weakness spasms (reviewed in Mehndiratta et al., 2014). Most reversible damage will disappear within 30 days, but some functions may return in nine months. However, recovered patients may suffer from post-polio syndrome, characterised by the onset of fatigue, muscle weakness and wasting (reviewed in Troy and Maldonado, 2012; Oluwasanmi et al., 2019).

### 1.4.4. Treatment and prevention

Supportive care is the main treatment, medication to relieve severe muscle spasms, intermittent catheterisation, and ventilators to support patients with respiratory compromise (reviewed in Troy and Maldonado, 2012). The vaccination is the only possible solution against poliomyelitis in the absence of effective treatment and the light of the

continued epidemics and futility of isolation and quarantine. Fortunately, vaccination has proved to be efficient at preventing poliomyelitis. Poliovirus has three individual and immunologically distinct strains (PV1, PV2, and PV2) (reviewed in Baicus 2012).

Currently, there are two polio vaccines: the inactivated poliomyelitis vaccine (IPV) and the attenuated oral poliomyelitis vaccine (OPV). The breakthrough in 1955, Jonas Salk developed the IPV, followed in 1960 by an OPV developed by Albert Sabin. Both were effective and helped to eradicate PV2 and PV3 Wild poliomyelitis globally, and PV3 was last detected in West Bihar, India, in 1999. The only wild-type circulated currently is PV1 in only two countries, Pakistan and Afghanistan, due to political instability and several other reasons (reviewed in Baicus 2012).

Several paralytic poliomyelitis cases of circulating vaccine-derived poliovirus (cVDPV) PV2 have been detected since 2000 (reviewed in Qiu 2017). In order to prevent paralytic polio caused by circulating vaccine-derived poliovirus type 2, the trivalent oral poliovirus vaccine (tOPV) will be replaced by the bivalent oral poliovirus vaccine (bOPV).

Several attempts were carried out to produce new polio vaccines to face the issue of attenuated vaccines. These attempts were either conducting attenuation by genetic engineering that is stable or may not revert to wild-type quickly (Yeh et al., 2020). The thermal selection was also applied to create stabilised VLPs vaccines against polio (Fox et al., 2017). Also, finding new strains that are slowly reverting to wild-type. Only these vaccines are currently on the list of emergencies of WHO, which is the nOPV (Martin et al., 2022).

## 1.5. Study rationale

In the era of polio post eradication, the EVA71 has the potential to cause massive outbreaks around the globe, especially in the absence of approved antiviral drugs. Vaccines have a significant role in controlling infectious diseases and substantially impact mitigating outbreaks and reducing the incidence, hospitalisations, and deaths. To obtain an effective vaccine, certain conditions must be considered, such as biosafety, stability, efficacy, and immunogenicity. Thus, a virus-free vaccine such as the VLP vaccine could be an ideal candidate.

## 1.6. Study objectives

The general objective of this project is to develop novel thermally stable EVA71 VLPs as novel vaccine candidates.

### 1.6.1. Selection and characterisation of thermal stable EVA71 mutants in mammalian cells.

- Molecular characterisation: identification of mutants within the viral genome; recapitulate and combine identified mutations in the infectious clone.
- Generation of EVA71 empty particles in mammalian cells using an infectious virus.
- Antigenic characterisation: assess the selected mutants' thermal stability and antigenic profile against the wild type using a panel of available antibodies (commercially and non) and antibodies generated by collaborators (Drs A Macadam and J. Martin, NIBSC).

### 1.6.2. Generation of EVA71 VLPs in yeast.

- Construction of a plasmid for yeast expression.
- Expression and purification of VLPs of wild type and mutants in yeast.
- Molecular and antigenic characterisation of yeast VLPs.
- Investigate whether the stabilised VLPs in the native antigenic conformation (NAg) has a superior immunogenicity over the expanded VLPs with the non-native antigenic conformation (HAg).
- Generate purified viral particles, empty capsids and VLPs (mutants and wild-type) for structural studies by cryo-EM and crystallography.

# Chapter 2

# Materials and methods

## 2.1. Techniques used for the generation of plasmids

### 2.1.1. Restriction digest of purified products for ligation

To prepare DNA plasmids and DNA insert for ligation, 5ug vector or purified PCR product (see section 2.2.5) were digested using 20 - 50 units of appropriate restriction enzymes (New England Biolabs (NEB)) in 2 µl of CutSmart Buffer (10X) (NEB) in a total reaction volume of 20 µl according to the manufacturer's protocol. Reactions were incubated at 37$^{o}$C for 2 hours. The 5' ends of the DNA plasmids were dephosphorylated by adding one unit of calf intestinal phosphatase (CIP)(NEB) to the vector digestion reaction. The reaction was re-incubated for 30 min at 37$^{o}$C. The CIP treated vector and the DNA insert were purified by gel electrophoresis (as described in section 2.1.7).

### 2.1.2. Ligation reaction

Ligation of purified vector and DNA inserts ligations were conducted according to the manufacturer instructions (NEB). Briefly, ligation mixture was prepared using 100ug of DNA at a 3:1 molar ratio of the insert to vector in a final volume of 20 µL. The reaction was incubated at room temperature for 30 min. Simultaneously, a vector without insert was treated with the same ligation reagents and included as a control. The ligation reactions were transformed into *E. coli* DH5α (see section 2.1.3).

### 2.1.3. *E. coli* DH5 α transformation

To transform a DNA plasmid, 1 - 10 ng of DNA plasmid or 10 µl of ligation mixture was added to 50 µl *E. coli* DH5α competent cells and incubated on ice for 30 min. Cells were heat-shocked at 42°C for 2 min and chilled immediately on ice for 2 min. Cells were recovered in 300 µl of Luria–Bertani (LB) broth (10 g/L tryptone, 5 g/L yeast extract, 10 g/L NaCl) for 1 hour at 37°C. The transformed cells were plated on an LB agar plate (10 g/L tryptone, 5 g/L yeast extract, 10 g/L NaCl, 15 g/L Agar) supplemented with 100 µg/ml ampicillin sodium salt and incubated for 16 - 18 hours at 37$^{o}$C.

### 2.1.4. Preparation of plasmid DNA

In order to expand plasmid DNA, a single colony of transformed *E. coli* DH5α cells containing the required plasmid was inoculated in 5 ml of LB broth containing 100 µg/ml ampicillin sodium salt. The colony was picked from a transformation LB agar plate or LB agar plate streaked from a glycerol stock, prepared by adding 750 µl of 80% glycerol added to 250 µl transformed *E. coli* DH5α cells. Cultures were incubated for 16 hours at 37$^{o}$C with agitation. Cells subsequently underwent miniprep (see section 2.1.5).

### 2.1.5. Miniprep

To isolate DNA plasmid from bacterial cells Miniprep was carried out according to the manufacturer instructions (Qiagen). Briefly, overnight bacterial cultures that were pelleted by centrifugation at 4,000 xg for 30 min. in a 1.5 ml microfuge tube cells were resuspended in 250 µl P1 buffer followed by the addition of 250 µl of P2 lysis buffer and were mixed thoroughly by inverting the tube 4 - 6 times to facilitate lysis. To neutralise the cell lysate, a

350 µl of N3 buffer was added to the tube and mixed by inverting the tube 4–6 times until a colourless precipitate formed. The tube was centrifuged at 16,000 rcf for 10 min at 4$^{o}$C. A 750 µl of the aqueous phase was transferred into the QIAprep spin column and centrifuged at 16,000 rcf for 1 min at 4$^{o}$C. The column was washed with 500 µl PB and centrifuged at 16,000 rcf for 1 min at 4$^{o}$C. That was followed by washing the column with 750 µl of PE buffer and centrifuged at 16,000 rcf for 1 min at 4$^{o}$C. Additional centrifugation at 16,000 rcf for 2 min at 4$^{o}$C was applied to fully dry the column. The spin-column was placed in a 1.5 ml collection tube. The plasmid was eluted by adding 60 µl of PCR grade water and leaving the tube to stand for 1 min then centrifuged at 16,000 rcf for 1 min at 4$^{o}$C. The concentration and purity of the plasmids were assessed NanoDrop (NanoDrop 1000 Thermo Scientific). DNA concentration was assessed using two absorbance ratios A260/A280 and purity by A260/A230. Accepted DNA absorbance ratios were ~1.8 and >2.0, respectively. Purified DNA plasmids were stored at -20°C until required.

### 2.1.6. Gel electrophoresis

To separate DNA fragments and estimate their size, DNA gel electrophoresis was used. To prepare the gel, 1% (w/v) agarose. Tris-borate-EDTA (TBE) buffer (90 mM Tris (pH 7.6), 90 mM boric acid, and 2 mM EDTA (Sigma-Aldrich) was prepared. The mixture was melted until all visible agarose crystals had dissolved. SYBR™ Safe (Invitrogen, Thermo Fisher) was added to this mixture at 1:100,000 and agarose was transferred into an assembled gel casting system. The agarose was left at room temperature until solidified. DNA samples were combined with an appropriate volume of 6x gel loading dye (NEB) before being added into a well. Samples were subjected to electrophoresis at 100 V for 45 - 60 min in 1 x TBE buffer until sufficient DNA separation was obtained. The appropriate size of DNA marker, either Quick-Load® Purple 1 kb DNA ladder (NEB) or Quick-Load® Purple 1 kb Plus DNA ladder (NEB), was loaded to estimate the size of the DNA bands produced. When an adequate separation of DNA ladder was obtained, the band of DNA fragments were visualised using blue light FastGene Blue LED Transilluminator, or long wave UV Transilluminator. The gel images were taking by Toshiba imaging system.

### 2.1.7. Gel extraction and purification of DNA

DNA products were extracted from agarose gels after separation using QIAEX II Gel Extraction Kit (Qiagen) according to the manufacturer's instructions. The band of interest was excised using a clean scalpel and was placed in a 1.5 ml microfuge tube. To dissolve the gel and release the DNA, 300–500 µl of buffer QX1 were added to the excised gel and incubated at 45$^{o}$C until the gel completely dissolved, 250 µl isopropanol was added to the melted gel and mixed by inverting the tube before samples were added to the column. 750 µl of the mixture

was transferred into QIAquick spin column and placed inside a 1.5 collection tube and centrifuged at 16,000 rcf for 30 - 60 sec at 4$^{o}$C. Columns were washed with 750 µl of PE buffer and centrifuged at 16,000 rcf for 30 - 60 sec at 4$^{o}$C. The column was dried by subsequent centrifugation for a further 1 min at 16,000 rcf at 4$^{o}$C. The extracted DNA fragment was eluted by adding 60 µl of PCR grade water and leaving the tube to stand for 1 min then centrifuged at 16,000 rcf for 1 min at 4$^{o}$C. The concentration and purity of the gel extracted DNA were determined by measuring nucleic acid concentration using DNA application in the NanoDrop (NanoDrop 1000 Thermo Scientific).

## 2.2. Molecular techniques

### 2.2.1. Primers

PCR sequencing primers (Table 2.1), and 3A primers (Table 2.2) were designed manually according to the sequence map of EVA71 pT7-HH-EVA71B2-IC mapped by SnapGene viewer available at: https://www.snapgene.com/snapgene-viewer/.

The length of the designed primers was between 18 - 40 bp, 40-60% GC content, and a melting temperature of about 72$^{o}$C. Primers were purchased from Integrated DNA Technologies (IDT). Upon arrival, oligonucleotides were resuspended in a DNase/RNase-Free Water to a 100 µM stock concentration. Further stock dilution into working concentrations required for PCR mix was carried out based upon the application requirements.

### 2.2.2. Designing primers for genome sequencing

In order to sequence the entire viral genome, a set of overlapping primers were designed based on the EVA71 B2 gene sequence EVA71 pT7-HH-EVA71B2-IC. The sequence was divided into regions that each consisted of 700 nucleotides. For each region a set of primers was designed and included a number of forward primers flanked by a forward primer at the 5' end and a reverse primer at the 3' end.

| Primer | Sequence |
|---|---|
| 41-51P1F | TTAAAACAGCCTGTGGGTTGCACC |
| #2 INT A 5' PIF | GATCAAGCATATCTGTTCCCCCGGAC |
| #3 INT B 5' P1 F | CTCACCATTGGAAACTCCACCATCACC |
| #4 INT C5' P1F | CCATGGCAATCAACAATGCTGGGC |
| #5 5' P1 R | GCCAGTATCCAGTCGATGACTGCT |
| #6 P2F | GCTATICAGGOGGATAGGGTG |
| #7 INT A P2 F | TGGGAAGACAGCTCTCGCGACCTA |
| #8 INT B P2 F | AAACACCGTATTGAACCTGTATGTCTCATCATCAGG |
| #9P2R | TIGGAATAGTGCTTCAATTGTGTTGCCAATAGC |
| #103' P3F | CTAGTGTGTGGGAAAGCTATCCAACTTAGAGAC |
| #11 INT A 3' P3 F | GCAAGCGAACAAGGCGAGATCCAA |
| #12 INT B 3' P3 F | GATGTGCTOGCTAGTTACCTTTTCT |
| #13 3° P3R | GCTATTCTGGTTATAACAAATTTACCCCCACCAGTCATT |
| 41-51P1F | TTAAAACAGCCTGTGGGTTGCACC |

**Table 2.1: EVA71 genome sequencing primers**

| Primer | Sequence |
|---|---|
| External primer FP | CCGCCCAGGGCTGTGACACAATTGC |
| External primer RP | CAGGCGCGCCTGGCTCTCCCTAGC |
| 3A F1 FP | CACCTCATTGGATCCGATGGAGCGGTT |
| 3A 3 UTR RP 2 | GCTATTCTGGTTATAACAAATTTACCCCCACCAGTCATTA |
| 3A F2 FP | AAGGGAGTTTCCTTCACATCTAAGTTT |
| 3A F3 FP | CTCACATTGGTGACACTAGATACTAAT |
| 3A F4 Fp | ATGACTTTTGGACATCTTTACGAGGTG |

**Table 2.2 PCR primers used to sequence P3 region encoding 3A**

### 2.2.3. Genome sequencing

Samples to be sent for Sanger sequencing were prepared by mixing 500 ng of plasmid DNA or 250 ng gel extracted PCR product with 25 pmol primer in a final volume of 10 µl. Samples were sent to Genewiz (Genomics from Azenta Life Sciences) for processing by sanger sequencing. The returned nucleotide sequence chromatograms were visualised and inspected using SnapGene viewer software (Interpreting Sequencing Chromatograms). Each generated nucleotide sequence was translated independently into a protein sequence using web-based Translate tool by ExPASY program available from Swiss Institute of Bioinformatics (SIB) at (https://web.expasy.org/translate/). The protein sequences were trimmed then combined to produce a complete and accurate sequence for the whole viral genome. To identify possible discrepancies or mutations the generated sequence was then aligned to the sequence of the wild-type by web-based Clustal Omega program available from the European Molecular Biological Laboratory, European Bioinformatics Institute (EMBL-EBI) available at (https://www.ebi.ac.uk/Tools/msa/ clustalo/). Alternatively, the sequence was aligned by using Pairwise Sequence Alignment, EMBOSS Stretcher from (EMBL-EB) (https://www.ebi.ac.uk/ Tools/psa/emboss_stretcher/)

### 2.2.4. Protein structure visualisation

To visualise the position of detected mutations in the viral capsid structure, the structure of wild-type sequence (3VBS) was retrieved from Protein Data Bank (PDB) at (https://www.rcsb.org/structure/3VBS), displayed in PyMOL (Schrödinger).

### 2.2.5. Next-generation sequencing

The genetic sequence of stabilised virus populations was determined by next-generation sequencing. RNA was extracted from virus samples and genomes were reverse transcribed, and then amplified cDNA was sequenced using a MiSeq flow cell (Illumina). Reads underwent quality trimming and assembly before mapping to parental reference sequences using Geneious R7 (Biomatters) software.

### 2.2.6. Sample preparation before sending for sequencing (end point PCR )

To amplify DNA segment from plasmid template, or cDNA from a RT-PCR reaction (see section 2.3.3), an endpoint PCR reaction was carried out using Phusion high-fidelity polymerase (NEB). The PCR reaction mixture was formed by combining 10 ng of DNA or cDNA as a reaction template, 1 µM of forward and reverse primers specific to the P1 region of EVA71, 10 µl of Phusion buffer (NEB), 200 µM of each dNTP (NEB) and PCR grade water to 50 µl. PCR cycling condition were illustrated in table 2.3.

| Step | Temperature (°C) | Duration | No. of cycles |
|---|---|---|---|
| Initial denaturation | 95°C | 2 min | x1 |
| Denaturation | 95°C | 15 sec | x35 |
| Annealing | 72°C | 15 sec | |
| Extension | 72°C | 1 min 30 sec/1 kb | |
| Final extension | 72°C | 5 min | x1 |
| Cooling | 4°C | ∞ | N/A |

**Table 2.3 PCR cycling conditions**

### 2.2.7. PCR products clean-up

To purify the PCR product, a QIAquick PCR Purification Kit was used according to the manufacturer's protocol (Qiagen). A 250 µl of PB buffer was added to PCR eproducts, and the mixture was added to the QIAquick spin column placed inside a 1.5 ml collection tube and centrifuged at 16,000 rcf for 30 - 60 sec 4$^{o}$C. This step was followed by adding a 750 µl of PE buffer and centrifuged at 16,000 rcf for 30 - 60 sec at 4$^{o}$C. The column was centrifuged further at 16,000 rcf for 1 min at 4$^{o}$C then placed in a fresh 1.5 ml collection tube. To elute the cleaned PCR products a 30 µl of PCR grade water was added, and the column was allowed to stand for 1 min before being centrifuged at 16,000 rcf for 1 min at 4$^{o}$C. DNA purity was assessed using gel with 3ul of sample to check that it is their band of 2.5 kb. Samples were stored at -20°C until required.

### 2.2.8. Overlap site direct mutagenesis (Overlap - SDM)

Site-directed mutagenesis (Overlap - SDM) (Figure 2.2) was employed to introduce thermal stability single mutation into the corresponding positions in structural P1 region in the pT7-HH-EVA71-B2 (Figure 2.1). This method was performed using the primers listed in table 2.6. The 3A A66T was introduce into the GFP replicon (Figure 2.1) using the same approach using primers in table 2.7. In order to generate a mutant DNA sequence, two PCR products were generated: the 5' prime end product (5' prime end product #1) and the 3' prime end product (3' prime end product #2) by PCR as described in Table 2.4. Both products were confirmed by 1% agarose gel, and were gel extracted and purified according to the gel extraction protocol (section 2.1.7).

To overlap the generated products: both 5’ prime end product #1 and 3’ prime end product #2 was mixed at a 1:1 molar ration with a final amount of 10 ng per reaction e.g., 7.2 ng of 5’ prime end product #1 was added to 2.8 ng of 3’ prime end product #2. The overlapping PCR was carried out through 10 cycles of PCR without external primers, allowing product 1 and 2 to prime each other as in table 2.5. Afterwards, the full length of the mutated DNA strand was amplified using two external primers through 25 PCR cycles. The PCR products were undergoing PCR cleanup, restriction digestion with suitable restriction enzymes e.g *BamHI* and *AatII* were used for the single point mutation SDM. Treated DNA was gel extracted before ligation into linearised pT7-HH-EVA71-B2 digested with *BamHI/AatII* and CIP treated (as described in 2.1.2). The ligated gene was transformed into competent *E. coli* DH5α cells (section 2.1.3).

| 5'prime end product # 1 | 3' prim end product #2 | The first round of overlap – SDM PCR thermal cycle |
|---|---|---|
| 1 µl (10 ng) of template infectious clone | 1 µl (10 ng) of template infectious clone | 95°C: 2 min |
| 1 µl External forward primer | 1 µl External reverse primer | 95°C: 15 sec. |
| 1 µl mutation reverse primer | 1 µl mutation forward primer | 72°C: 15 sec. } x 35 cycles |
| 1 dNTP | 1 dNTP | 72°C: 1.5 min |
| 10 µl of Phusion buffer | 10 µl of Phusion buffer | 72°C: 5 min. 1 min/1 kb |
| 0.5 µl Phusion enzyme | 0.5 µl Phusion enzyme | 4°C: Hold |
| 35.5 µl PCR grade water | 35.5 µl PCR grade water | Gel extraction |

**Table 2.4 The first round of overlap–SDM PCR thermal cycle (Generation of DNA products #1 and #2):** The Overlap–SDM PCR was initiated by generating two PCR products; the 5' prime end (product #1) and the 3' prime end (product #2).

| 5’prime product #1 and 3’ prim product #2 | The second round of PCR thermal cycle (overlap) |
|---|---|
| 10 ng in total mix the following:<br><br>7.2 ng of extracted 5’prime product #1<br><br>2.8 ng of extracted 5’prime<br><br>product #1<br><br>1 µl dNTP<br><br>10 µl of Phusion buffer<br><br>0.5 µl Phusion enzyme<br><br>35.5 µl PCR grade water | 95°C: 2 min<br><br>95°C: 15 sec<br><br>72°C: 15 sec } x 10 cycles<br><br>72°C: 2.5 min<br><br>72°C: 5 min<br><br>4°C: Hold |
| 5’prime product #1 and 3’ prim product #2 | The third round of PCR thermal cycle (amplified DNA fragment) |
| 5’ product #1+3’ product #2<br>+<br>1µl of flanking primers; forward and reverse primers | 95°C: 2 min<br><br>95°C: 15 sec<br><br>72°C: 15 sec } x25 cycles<br><br>72°C: 2.5 min<br><br>72°C: 5 min<br><br>4°C: Hold<br>⬇<br>Gel extraction |

**Table 2.5 The second and third rounds of overlap–SDM PCR thermal cycle: Synthesis of DNA insert by overlap–SDM PCR:** The second phase of the overlap - SDM by PCR was aimed to generate a DNA insert by overlapping the two previously produced PCR products: the 5’ prime end (product #1) and 3’ 5’ prime end (product #2). Both products were combined by applying two rounds of PCR cycles. The second-round aim to overlap the two PCR products through 10 cycles of PCR. The third round of PCR cycles was aimed to amplify the DNA insert by 25 cycles using the same protocol. Results of the PCR were confirmed by running 1 µl aliquots on 1% agarose gel.

A

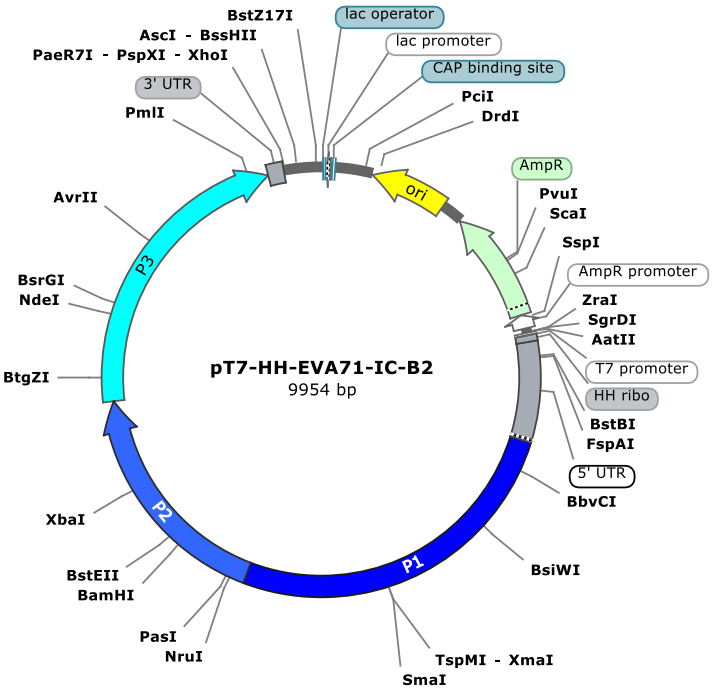


B

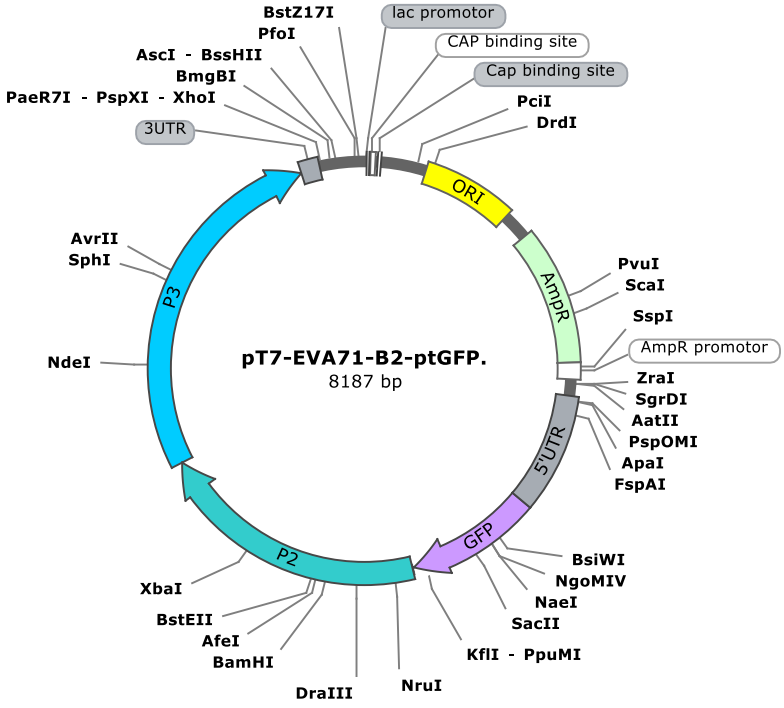


**Figure 2.1 (A) Infectious clone pT7-HH-EVA71-IC-B2 (B) Infectious clone pT7-EVA71-B2-ptGFP (replicon)**

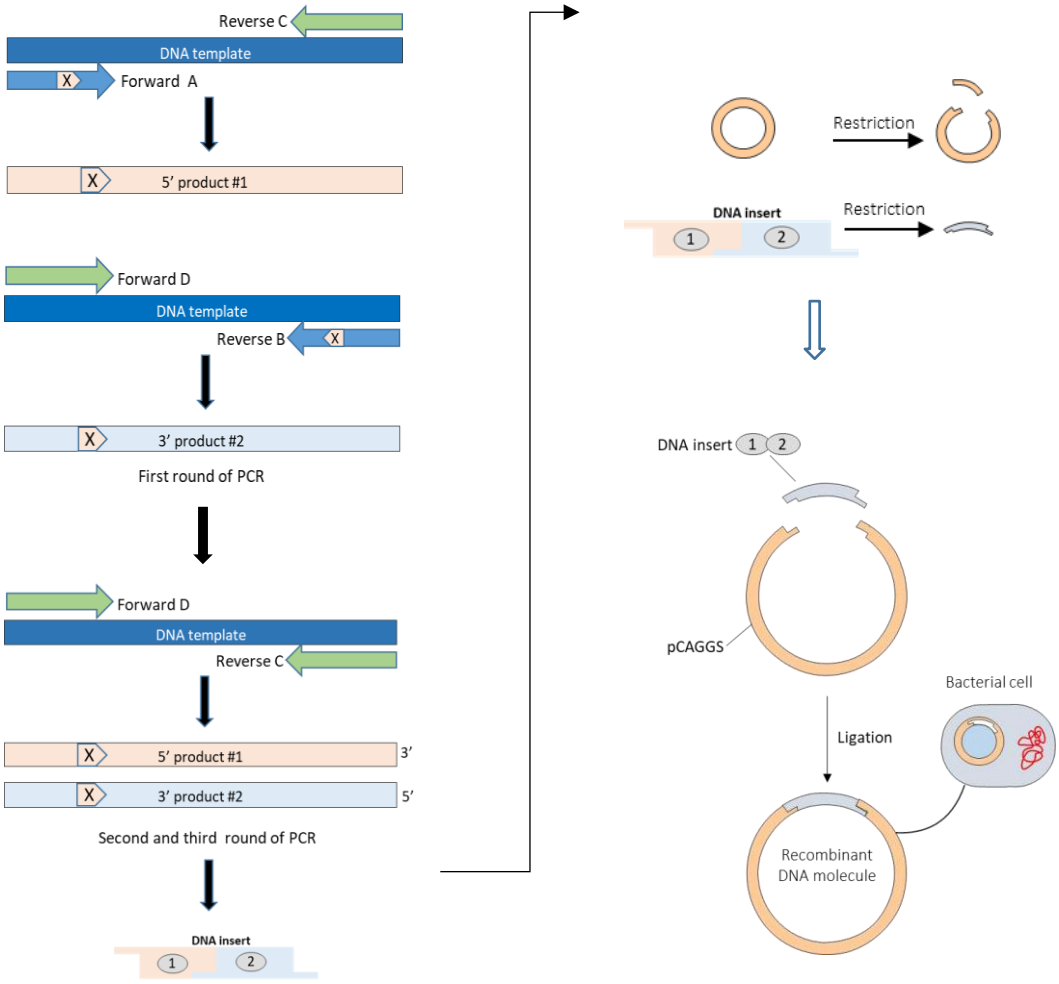


**Figure 2.2 Schematic diagram of SDM overlap PCR:** The SDM overlap PCR was performed in order to introduce single thermal resistance mutation into the corresponding positions of the pT7-HH-EVA71-IC-B2. Primers used in SDM were forward and reverse. Adapted by mutagenic primers (A & B) to introduce the required mutation in addition to two external primers for the targeted region (C & D). Overlap extension PCR was performed according to table 2.4 and table 2.5.

### 2.2.9. P1 single point mutation mutagenesis

The cloning of the single point mutation (Table 2.6) was carried out by SDM by PCR (see section 2.2.7). Generated DNA inserts were inserted into pT7-HH-EVA71-IC-B2 to obtain five independent pT7-HH-EVA71-B2 -P1. Each plasmid comprises a single point mutation was named according the mutation that it carries: (Y1116C), (K1162I), (V2085L), (13233M), and (P1246A).

| Mutation | Change | Sequence |
|---|---|---|
| NJK 0143 (EX) | | F=GTGOCACCTGACGTCGACGTAATACGACTCACTATAGGGCC |
| NJK 019 (EX) | | R= CTCAACCGCTCCATCGGATCCAATGAG |
| Y1116C | A-> G | F= ATAGACATAACTGGCTGCGCACAAATGCGCAGGAAA<br>R=GCGCATTTGTGCGCAGCCAGTTATGTCTATGTC |
| K11621 | A-> T | F=COCCTGGCGCTCCCATACCAGAATCCAGGGAATCA<br>R= COTGGATTOTGGTATGGGAGCGCCAGGGGGAAC |
| V2085L | G>C | F= GAAGTTCCCTGATCTATTGACAGAAACCGGAGTCT<br>R=GGTTTCTGTCAATAGATCAGGGAACTTCCAGT |
| 13233M | A>G | F=AAAGACACCAGTCACATGTTACAGACAGCCTCTATT<br>R=TGTCTGTAACATGTGACTGGTGTCTTTGCACA |

**Table 2.6 The PCR primers for SDM overlap PCR:** PCR primers that were designed to insert single mutation into wild-type infectious clone by SDM overlap by PCR.

### 2.2.10. 3A A66T mutagenesis

The cloning of the single point mutation A66T (GCT -> ACT) was carried out by Site Direct Mutagenesis overlap PCR (SDM- overlap PCR) (see section 2.2.7). Generated DNA inserts were inserted into pT7-HH-EVA71-B2-ptGFP with Green fluorescent protein (GFP) quantitative reporter of gene expression. The insertion was carried out with and without the 3D E250G mutation: E250 A66T and G250 A66T. The replication was carried out using primers in table 2.7.

| Primer | Sequence |
|---|---|
| 3A A -T 2 (GCT-ACA) FP | GCAATCCATCACGACTGTGGTGGC |
| 3AA-T 2 (AGC-TGC) RF | GCCACCACAGTCGTGATGGATTGC |
| 3A A66T 1 GCT- ACT FP | GCAATCCATCACTACTGTGGTGGCA |
| 3A A66T 1 (CGA-AGT) RF | GCCACCACAGTAGTGATGGATTGCAT |

**Table 2.7 The PCR primers for 3A:** These primers were designed to insert A66T mutation into pT7-HH-EVA71-B2-ptGFP.

### 2.2.11. Cloning mammalian VLP expression system pCAGGS-EVA71-B2-P1

To construct the mammalian cell VLP coexpression system pCAGGS-EVA71-B2-P1 and pCAGGS-EVA71-93-P1 (Figure 2.3), the P1 region of both the #9.1 and #9.3 from the infectious clone pT7-HH-EVA71-IC-B2 (Figure 2.1) that was constructed previously for both constructs, has been amplified, and the cleaned PCR products were digested with *XhoI* and *AgeI* along with the pCAGGS plasmid (as described in 2.1.1). The appropriate size digested products, where gel extract plasmids were digested with *RsrII* and *KpnI* to confirm cloning. The ligations (see section 2.1.2) were transformed in competent *E. coli* DH5 α cells in 1 ml of LB–Amp broth (see section 2.1.3). The mixture was kept on ice for one hour and was spread on LB–Amp plate and incubated overnight at 37$^{o}$C. The next day transformed plasmids were amplified by picking a colony from the LB–Amp plate and inoculated it in 10 ml LB–Amp broth with 10 µl ampicillin overnight in a shaking incubator at 37$^{o}$C and purified with the Qiagen Miniprep kit (as described in section 2.1.5).

The nucleotides sequences were confirmed by Sanger sequencing. Samples and sequencing primers mentioned in table 2.7 were sent for Sanger sequencing to Genewiz, UK following the company instructions (see section 2.2.2). The pCAGGS His-taq 3C was obtained from Dr Natlie Kingston, University of Leeds.

A

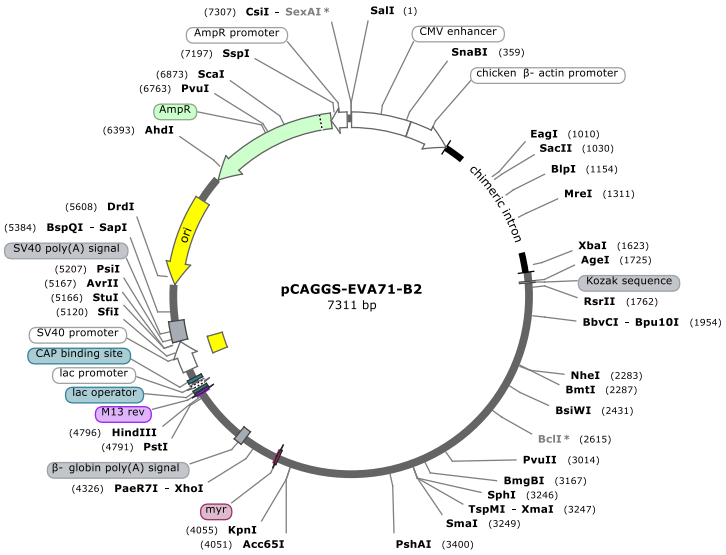


B

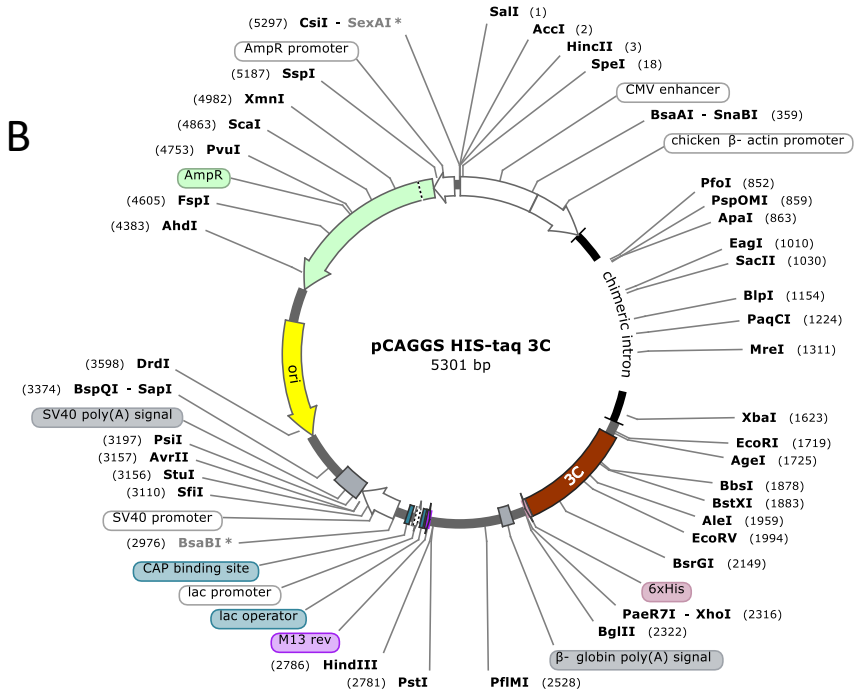


**Figure 2.3 The pCAGGS map of (A) pCAGGS-EVA71-B2-P1 (B) pCAGGS) HIS-taq 3C**

## 2.3. Techniques used for the generation of DNA from RNA

### 2.3.1. Isolation of Virus RNA

Viral RNA was extracted using TRIzol (Invitrogen). Cell membrane disruption and homogenisation were carried by adding TRIzol (1 mL per 10 $cm^2$) to adherent cells in the plate. Cells were lysed by repetitive pipetting up and down.

The cell lysate was incubated with TRIzol for 5 min at 25°C, 200 µl of chloroform was added to the mixture, and the tube was inverted repeatedly by hand for 15 seconds. After incubation at 25°C for 2–3 min the sample was centrifuged at 12,000 ×g for 15 minutes at 4°C. Around 400 µl of the colourless upper phase that contains the RNA was transferred to a fresh RNase free tube. An equal volume of 95-100% ethanol was added and mixed well before being processed through a directzol column (Zymoresearch) (see section 2.3.2).

### 2.3.2. RNA Clean & Concentrator

To purify and concentrate extracted viral RNA in the aqueous phase following TRIzol®/chloroform, a Direct-zol™ RNA Miniprep Plus TRIzol® In. RNA Out from (Zymoresearch) was used. Buffers were prepared as follows: PreWash was prepared by adding 10 ml or 40 ml ethanol (95-100%) to the 40 ml or 160 ml Directzol™ RNA PreWash concentrate. To prepare the Wash buffer, 48 ml 100% ethanol (52 ml 95% ethanol) was added to the 12 ml RNA Wash Buffer concentrate or 192 ml 100% ethanol (208 ml 95% ethanol) to the 48 ml RNA Wash Buffer concentrate. Lyophilised DNase I was reconstituted with DNase/RNase-Free Water, mixed by gentle inversion and stored frozen aliquots: add 275 µl DNase/RNase-Free Water #E1011-A (1500 U), or add 55 µl DNase/RNase-Free Water #E1009-A (250 U).

To purify the sample, an equal volume of the sample was added to an equal volume of ethanol (95-100%) e.g., 20 µl of sample in TRI reagent mixed with 20 µl of 95-100% ethanol. The mixture was transferred to the Zymo-Spin™ IIC Column and centrifuged at 16,000 xg for 30 sec. A 400µl of RNA Wash Buffer was added to the column and centrifuge at 16,000 xg for 30 sec.

The sample was treated with DNase by adding a mixture of DNase I and DNA Digestion Buffer (both reagents are part of the kit), to the column matrix and incubated at room temperature 25°C for 15 min. The mixture was prepared by adding 5 µl DNase I to 75 µl DNA Digestion Buffer, and the mixture was mixed by gentle inversion. The RNA sample was washed with 400 µl Direct-zol™ RNA PreWash5 and then centrifuged at 16,000 xg for 30 sec. Another wash was carried out by adding 700 µl Direct-zol™ RNA PreWash5, and the column was centrifuged at 16,000 xg for 1 min. The RNA was eluted in 1.5 ml RNase-free tube by adding 50 µl of DNase/RNase-Free Water and letting the tube stand for 1 min at room temperature before centrifuging at 16,000 xg for 1 min. The eluted RNA was either used immediately or stored at -80$^{o}$C.

### 2.3.3. Reverse transcription PCR (RT-PCR) of virus RNA into cDNA

To reverse transcription of extracted viral RNA into cDNA was carried out by PCR amplification of DNA and was performed using Transcriptor First Strand cDNA synthesis kit (Roche, Merck). Briefly, 1µg of total RNA was added to 1µl (2.5µM) of anchored-oligo$(dT)_{18}$ Primer 50 pmol/µl (vial 5). The total volume of the primer-template mix was adjusted to be 13µl with PCR grade water (vial 7 or 9), and the mixture was centrifuged briefly to collect the sample at the bottom of the tube. To denature secondary RNA structures, the PCR tube was heated for 10 min at 65°C in a block cycler and chilled on ice. Subsequently the following were added to the tube: 4µl of Transcriptor Reverse Transcriptase Reaction Buffer (5x conc) (vial 2), 0.5µl Protector RNaseInhibitor (40 U/µl) (vial 3), 2µl deoxynucleotide Mix, (10 mM each) and 0.5µl Transcriptor Reverse Transcriptase (20U/µl) (vial 1). The total volume was adjusted to 20µl, and the tube was incubated in PCR at 55 $^{o}$C for 60 min. The cDNA was used directly or stored at -20°C until required.

### 2.3.4. Generate EVA71 P1 PCR product

The P1 region of RNA genome sequence of either wild-type or mutant #9 was amplified from generated cDNA according to standard PCR method (as described in section 2.2.5) and conditions in table 2.3. The forward primer and a reverse primer were designed to match the sequences of either end of the region of interest. The primers were a 5' UTR upstream primer (5' - CTCAACCGCTCCATCGGATCCAATGAG - 3'), and a 3' UTR downstream primer (5' - GTGCCACCTGACGTCGACGTAATACGACTCACTATAGGGCC- 3').

### 2.3.5. Cloning P1 region into EVA71 wt infectious clone

In order to study the P1 region of #9, was introduce into pT7-HH-EVA71-IC-B2. The pT7-HH-EVA71-IC-B2 is an EVA71 reverse genetics system that was constructed by Dr Natalie Kingstone, University of Leeds. The construction was carried out by reverse transcribed cDNA (see section 2.3.3) from extracted viral RNA of genogroup B2 strain MS/7423/87 using specific primers, then the amplicon was introduced under a T7 promoter and downstream of hammerhead ribozyme (HH-Ribo).

The whole P1 region of mutant #9 comprising the thermal resistant mutants was extracted from PCR amplified cDNA by *BamHI* and *AatII.* Then, according to the protocol of SDM by overlap PCR (see section 2.2.7) and by using primers in table 2.6 extracted P1 region was ligated into the pT7-HH-EVA71-IC-B2 under a T7 promoter and downstream of HH-Ribo (Figure 2.1). The resulting plasmid pT7-HH-EVA71-IC-B2-P1-#9 was transformed incompetent *E. coli* DH5 α cells, amplified, and purified using miniprep kit (as described in 2.1.5). Successful cloning was confirmed by restriction enzyme digestion using *XhoI* and *AatII* (as described in 2.1.1). Samples

and sequencing primers mentioned in table 2.7 were sent for Sanger sequencing to Genewiz, UK following the company instructions (see section 2.2.2).

## 2.4. Technique used for T7 RNA transcription

### 2.4.1. Synthesis of RNA by *in vitro* transcription

#### 2.4.1.1. Preparation of plasmid DNA templates for in vitro transcription (Preamble to T7)

To prepare DNA plasmids for *in vitro* transcription, 5 µg of a full-length DNA construct containing T7 promotor was linearised with restriction digestion by the *XhoI* (NEB). The purity and concentration of linearised DNA was determined by NanoDrop and DNA agarose gel electrophoresis (see section 2.1.6).

To purify the linearised DNA constructs, an equal volume of the DNA sample and phenol/chloroform isoamyl solution were combined. The mixture was vortexed for 1 min and centrifuged for 10 min at 17,000 rcf max speed. The aqueous phase was extracted carefully and transferred to a 1.5 ml RNA tube. An equal volume of chloroform was added and vortexed for 1 min and centrifuged for 10 min at 17,000 rcf. The aqueous phase was carefully transferred into 1.5 ml RNA free tube. The purified DNA was precipitated by adding 1: 10 (v/v) 3M sodium acetate (pH 5.2) and a 2.5 x volume of 100% ethanol. The mixture was then incubated at -20oC for >30 minutes. The mixture was subsequently centrifuged for 30 min at 17,000 rcf to pellet the DNA. The supernatant was removed, and the precipitated DNA was washed 500ul of 70% ethanol and centrifuged for 30 min at 17,000 rcf. Following the centrifugation, the ethanol was removed, and the extracted DNA was then dried on a

heat block at 42°C and resuspend in 20 µl of DNase/RNase-Free Water. The purity andconcentration of linearised DNA was determined by nanodrop.

### 2.4.1.2. T7 RNA transcription

The T7 RNA transcription *in vitro* was carried out using the transcription kit T7 RiboMAX Express large-scale RNA production system from (Promega) according to manufacturer's instructions. Briefly, 10 µl RiboMAX Express T7 2X Buffer and 2 µl of the Enzyme Mix T7 Express was added to 1 µg of linearised and purified DNA template in a final volume of 20 µl. The reactions were mixed gently and incubated at 37°C for 1 hour and treated with 2 µl of RNAse free DNAse (Promega) for 15 min at 37°C to degrade DNA templates. Newly synthesised T7 RNA was purified and concentrated using the RNA Clean & Concentrator™-25 kit (Zymoresearch) (see section 2.3.2). Samples were quantified by Nanodrop and evaluated by RNA formaldehyde MOPS gel electrophoresis (see section 2.4.4) before being aliquoted and stored at -80

### 2.4.1.3. Purification of RNA transcripts

To purify and concentrate extracted T7RNA transcripts in the aqueous phase, an RNA Clean & Concentrator™-25 kit (Zymoresearch) was used. An equal amount of the sample was added to a mixture of DNA/RNA Binding Buffer and 95-100% ethanol that was prepared also by mixing equal amount of each. For example: 20µl of the sample was added to 20 µl of DNA/RNA Binding Buffer mixed with 20 µl of 100% ethanol. The mixture was transferred to the Zymo-Spin™ IICR Column and centrifuged at 16,000 rcf for 30 sec. A 400 µl of RNA Prep Buffer was added to the column and centrifuge at 16,000 x g for 30 sec. The RNA sample was washed by 700 µl of the DNA/RNA Wash Buffer and centrifuge at 16,000 rcf for 30 sec and

the flow-through was discarded. Another wash was carried out by adding 400 µl of the RNA Wash Buffer, and the column was centrifuged at 16,000 rcf for 2 min. The RNA was eluted in 1.5 ml RNase-free tube by adding a 20 µl of DNase/RNase-Free Water and let the tube stand for 1 min at room temperature before centrifuged at 16,000 rcf for 1 min. All the steps were carried out in room temperature 25$^{o}$C. The concentration of extracted RNA and purity were assessed using RNA application in the NanoDrop (NanoDrop 1000 Thermo Scientific). RNA purity was assessed using two absorbance ratios A260/A280 and A260/A230. Absorbance ratio of ~2.0 is generally accepted as "pure" for RNA. Samples were stored at -80$^{o}$C.

### 2.4.2. RNA Formaldehyde-MOPS gels

An RNA Formaldehyde-MOPS gel was run to determine the homogeneity of the T7-transcribed RNA. Gels were prepared by mixing 0.3 - 0.4 g of agarose (Fisher Bio Reagents) with 3.5 ml 10x MOPSbuffer (G-Biosciences) and 29.5 ml DEPC water (1:1000 dissolved diethylpyrocarbonate [C6H10O5] (DEPC) in water, and autoclaved) in a 50 ml tube. The mixture was dissolved in the microwave. Two ml formaldehyde (Sigma F8775-500ML) was added to the melted agarose gel before being transferred into a gel casting rig. To prepare RNA for electrophoresis, RiboRuler Low Range RNA ladder (Thermo Fisher) or 1 µg T7 RNA were combined at 1:1 ration with 2x RNA Gel Loading Dye (ThermoFisher) and heated for 85$^{o}$C for 10 min. Samples were loaded in the gel and separated at 60V for 1 hour in RNA-free running buffer prepared from 25 ml 10x MOPS and 225 ml DEPC water. A UV trans-illuminator box was used to examine the gel product details.

### 2.4.3. Infectious clone T7 RNA transfection

To transfect transcribed viral T7 RNA, a 6-well plate was seeded with L292 cells, at a density of 2 x $10^5$ cells/well in 2000 µl 10% GM (10% growth medium (DEME with 10% foetal bovine serum (FBS)) a day before transfection and were incubated at 37°C 5% $CO_2$ until 80-90%

confluence (approx. 16 - 18 hours later). Transfection master mix was prepared in a set of two separate 1.5 ml RNA free tubes and then mixed. Transfection was performed

by first diluting 2 µg of RNA in 100 µl of OptiMEM (Invitrogen). Simultaneously, 8 µl of lipofectin (Invitrogen) was diluted in 100 µl of OptiMEM. Both tubes were incubated for 15 min at room temperature before the contents of both tubes were combined and incubated at room temperature for 15-20 min. During the incubation of the transfection reactions, the cells were washed with 1 ml/well of sterile 1x PBS, before 2000 µl of OptiMEM was added to each well. The transfection mix was then added drop wise to each well. The cells were incubated 6 hours at 37°C in a humidified $CO_2$ incubator. The transfection medium in each well was replaced with 2000 µl of 10% GM. Cells were incubated at 37°C overnight. Cells were collected the next day after being examined under the microscope. The cell debris were pelleted at 16,000 xg for 5 min and analysed by SDS–PAGE and western blot using anti VP0/VP2 mAb 979 antibody (section 2.10.1 and 2.10.2). The infective titer of the rescued viruses was evaluated using plaque assay (section 2.8.2). The supernatants were stored at -80°C until required.

## 2.5. Cell culture methods

### 2.5.1. Cell lines

All cell lines in this project were mammalian cells from stocks maintained in the University of Leeds. HeLa Ohio cells are adherent cell originated from human epithelial cell carcinoma of the cervix (Henrietta Lacks) National Institute of Biological Standards and Control (NIBSC) UK. Vero cells are a primate cell line extracted from kidney epithelial cells of African green monkey from ATCC. Mouse L292 cells were obtained from mouse embryo fibroblast, Moloney Sarcoma Virus transformed murine fibroblasts from ATCC. All the cell lines have been used to grow EVA71 (reviewed in Kelly 2015; WHO 2022) and were recommended to use in researching and diagnose Enterovirus including EVA71 by WHO. Both Vero and RD cell express SCARB2 receptors, while the EVA71 receptors on HeLa cells have not been studied yet. The mouse cell is known to resist the other enteroviruses such as poliovirus as they do not bear the suitable receptors (reviewed in Kelly 2015; WHO 2022)

### 2.5.2. Recovery of -80$^{o}$C preserved cells

Cryovials containing preserved cells were retrieved from a -80$^{o}$C freezer and were thawed gradually in a biosafety cabinet at room temperature. Then, the content of the cryovials was transferred into 20% GM (20% growth medium (DEME with 20% fetal bovine serum (FBS) in a 1-T75 flask and incubated overnight at 37$^{o}$C in a 5% $CO_2$ humified incubator. The following day, the 20% GM was replaced with 10% GM in order to remove DMSO and re-incubated under the same conditions. Once an 80-90% monolayer had been observed, cells were sub- cultured into a T175 flask and 10% GM (see section 2.5.3).

### 2.5.3. Culturing and maintenance of cell line

#### 2.5.3.1. Maintenance of cell line

All cell lines were maintained in 10% GM prepared from a minimum essential media (DMEM) supplemented with 10% FBS (Thermo Fisher, Gibco) and 1% of penicillin/streptomycin (10,000 units/mL of penicillin and 10,000 µg/mL of streptomycin). (Thermo Fisher, Gibco) in T175 flasks (Corning). Cell passaging was performed every 2 - 3 days when cells reached 80 - 90% confluence. Old 10% GM was removed, and the cells were washed with 1 x PBS twice. Cells were incubated with pre-warmed trypsin at 37$^{o}$C to dissociate them from adherent surfaces. The split ratio was 1:20. Trypsinsed cells were resuspended in 10% GM to inactivate the trypsin, 90% of cells were discarded, and 20 ml of 10% GM was added. The T175 flask was then incubated at 37$^{o}$C with 5% $CO_2$ in a humidified incubator.

#### 2.5.3.2. Cell counting

Cells were counted under the microscope in two chambers of a haemocytometer after loading a 1:1 solution of diluted cell suspension with trypan blue. The following equation used to calculate the number of cells in each flask based on the mean cell count: Number of cells per square x dilution factor (DF) x $10^4$ (cells/ml).

#### 2.5.3.3. Cryopreservation of cell line

At 80-90% confluency, cell monolayers were trypsinised (as described as in section 2.5.3). Then, the contents were transferred into 50 ml falcon tube and centrifuged for 5 min at 500 rcf to pellet cells. The supernatant was removed, and the cell pellets were resuspended in cryopreserving mixture (10 % DMSO (Sigma) and 90% FCS). The cell mixture was then divided

into 1 ml aliquots containing $1x10^6$. Cells vials were stored at -80°C.

## 2.6. Virus methods

### 2.6.1. Parental virus

Here, one strain of EVA71 has been examined as proof of principle: EVA71 B2 (MS742387) kindly donated by SingVax (Singapore).

### 2.6.2. Virus stocks

To prepare a virus stock from the parental viruses, cells were seeded in a suitable number of T175 flasks with 10% GM 1-2 days prior to viral inoculation. When cells reached about 80% confluence, the media was removed, and the cell monolayer was washed with 1 x PBS. Cells were infected with viral supernatant obtained from a previously passaged virus and titrated by plaque assay was diluted with serum free DMEM at a defined multiplicity of infection (MOI) (0.1-1). Flasks were incubated at 37$^{o}$C in a 5% $CO_2$ humidified incubator for two to three days until a full clear cytopathic effect (CPE) was observed.

### 2.6.3. Virus harvesting from flasks (T175/T25)

In order to harvest propagated viruses, cells were collected once a full CPE was observed, usually within three days post-infection (dpi). The content of flasks was collected in 50 ml Falcon tubes and was frozen at -20$^{o}$C or -80$^{o}$C to enhance cell lysis. After two cycles of freeze-thaw, the harvested viral supernatant was clarified using centrifugation at 4000 xg at 4$^{o}$C for 30 min. The pellets were then discarded, and the supernatant was aliqouted in 1.5 ml screw-capped tubes and stored at -80$^{o}$C. The virus titer was assayed by plaque assay (section 2.8.2) before storage.

### 2.6.4. Virus harvesting from flasks (6-well plate/24-well plate)

In order to harvest propagated viruses, cells were collected according to a time interval (as described in 2.7.5), or once a full CPE was observed usually after overnight incubation. The content of wells was collected in 1.5 ml tubes. Cells were lysed with Laemmli buffer and proteins assayed by SDS-PAGE and western blot (as described in 2.10.1 and 2.10.2). infectious virus titer was assayed by plaque assay (see section 2.8.2).

### 2.6.5. One step growth curve

In order to study the virus kinetics, wild-type transcribed T7 RNA of EVA71 was transfected into L292 cells to ensure one cycle of infection. Transfection was performed as described in section (2.11.1). Samples were collected at 6, 8, 10, 12, 16, 20, 22, 24, and 36 hours post infection (hpi). Cells were lysed with Laemmli buffer and proteins assayed by SDS-PAGE and western blot (as described in 2.10.1 and 2.10.2). infectious virus titer was assayed by plaque assay (see section 2.8.2).

### 2.6.6. Virus expansion and purification

#### 2.6.6.1. Virus expansion

To expand virus 15 T175 flasks were seeded with HeLa cells as described previously (see section 2.5.3). Cells were infected with viral supernatant to at an MOI 0.1. Flasks were incubated at 37$^{o}$C in a 5% $CO_2$ humidified incubator until full CPE was observed. Infected cells were collected in 50 ml falcon tubes with 0.1% NP40 followed by one cycle of freeze and thaw. The virus solution was then centrifuged 4000 xg for 30 min to clarify the supernatant. The virus supernatant was supplemented with 1-2 mM MgCl, and with 12.5 units/ml of

benzonase nuclease ≥250 units/µL (Sigma-Aldrich). The mixture was incubated for around 2 hours at room temperature on mechanical rocker. To precipitate the viruses in every 30 ml of the supernatant mixture 20 ml of 20% PEG 8000 was added to obtain a final concentration of 8%, and the mixture was incubated overnight at 4$^{o}$C. The precipitate was pelleted using centrifugation at 4000 xg for 45 min. To every 15 ml of the initial supernatant, 5 ml PBS buffer was used to resuspend the viruses followed by centrifugation at 4000 xg for 30 min to remove the insoluble materials.

### 2.6.6.2. 30% Sucrose cushion pelleting

The resuspended virus particles were transferred to a SW32 Ti tube (Beckman Coulter), and pelleted through 5ml of a 30% sucrose cushion, which was pipetted underneath the viral supernatant. The SW32 Ti tubes were centrifuged at 150,000 rcf in a Beckman SW32 Ti rotor at 4$^{o}$C for 3.5 hours. Viral pellets were resuspended by adding 1ml of 1 x PBS with continuous gentle rocking at 4$^{o}$C overnight. Resuspended viruses were centrifuged at 10,000 xg for 10 min before carrying out sucrose gradient purification (see section 2.7.3).

### 2.6.6.3. 15 - 45% Sucrose gradient

The resuspended pellets were overlaid on the top of 15 - 45% discontinuous sucrose gradient in a SW41 Ti tube (Beckmen coulter) for final purification by ultracentrifuge at 50,000 rcf at 4$^{o}$C for 12 hours.

### 2.6.6.4. Manual fractionation

The gradient was fractionated by carefully by pipetting 1000 µl fractions from the top of the gradient. The protein content was analysed by assayed by SDS-PAGE and western blot (as described in 2.10.1 and 2.10.2). infectious virus titer was assayed by plaque assay (see section 2.8.2).

### 2.6.6.5. Concentration

To concentrate virus particles, fractions were pelted using SW55 Ti tube (Beckman Coulter) for final purification by ultracentrifuge at 300,000 rcf for 2 hours at 4$^{o}$C.

## 2.7. Determination of virus titer

### 2.7.1. EVA71 titer by 50% tissue culture infective dose $TCID_{50}$

To determine virus titer, a 96-well plate (Sigma Aldrich, Corning) was seeded with Vero cells at a seeding density of $1x10^4$ per ml to obtain $4x10^4$ cells at confluency. After overnight incubation at 37°C in 5% $CO_2$ humidified incubator, the 10% GM was replaced with serum free medium was added. Ten-fold serial dilutions of EVA71 were carried out. Dilutions (-2 to -8) were distributed on 96- well plate, so that each dilution was distributed on 10 wells, and each well was inoculated with 100 µl virus dilution. The last row was left uninfected as a control, and the plate was incubated at 37°C in 5% $CO_2$ humidified incubator. The reading CPE was obtained 5 dpi.

### 2.7.2. Plaque assay

To quantify virus by plaque assay 6-well plates (Sigma Aldrich, Corning) were seeded with HeLa cells at a density of $1 \times 10^6$ cells/well in 2.5 ml 10% GM to obtain 100% confluence monolayer after overnight incubation at 37°C in 5% $CO_2$ humidified incubator. The virus underwent 10-fold serial dilution in serum free medium (S/F). 1 ml of diluted virus was inoculated into the cells monolayer after removing the 10% GM and washing the cells by gentle pipetting using 1x PBS. The 6-well plates were incubated at 37°C for 1 hour with gentle manual rocking every 15 minutes to distribute the viral inoculum evenly across the cell monolayer. The inoculum was removed, and cells were overlaid with immobilizing medium 2 ml of 0.8% agarose. Initially, the 6% agarose overlay was prepared by adding 3 g.

of agarose (SeaPlaque GTG Agarose 25g (Lonza)) to 50 ml sterile 1xPBS. The mix was microwaved until completely dissolved. Directly after dissolving the agarose, 7 ml of it was mixed with 45 ml of 10% GM in a 50 ml Falcon tube and placed in 42℃ water-bath for 1 hour to equilibrate the temperature. Discard serial dilutions and overlay 2 ml immobilizing medium and was left to solidify inside a biosafety cabinet with the lid open, then the plate was incubated at 37°C in 5% $CO_2$ humidified incubator. Plaques and cells were fixed and stained with 2 ml of crystal violet/formaldehyde stain (0.5% crystal violet, 10% ethanol, 25% formaldehyde, and then add 100ml PCR grade water) 4 days post infection (dpi). After 1 hour at room temperature, the overlay was removed by washing with fresh water and the plates were air-dried. To determine the number of infectious viruses, the plaques were counted from the last well from which they can be counted. The number of infectious viruses was expressed as plaque formation unite (pfu) per millilitre (pfu/ml).

## 2.8. Methods of thermal stressing and characterisation

### 2.8.1. Thermal inactivation assay

To determine the inactivation temperature that was used to select the thermal resistance mutant, aliquots of EVA71 wt were thermally stressed in a Multi-Block PCR Thermal Cycler (ProFlex™ 3x32-well PCR System, Thermo Fisher Scientific) using a range of temperatures between 37 and 53°C for 30 min and cooled at 4°C. An aliquot was kept on ice 4°C as a non-thermally stressed control. The number of infectious viruses in thermally stressed aliquots were determined by plaque assay (see section 2.8.2) (Figure 2.4)

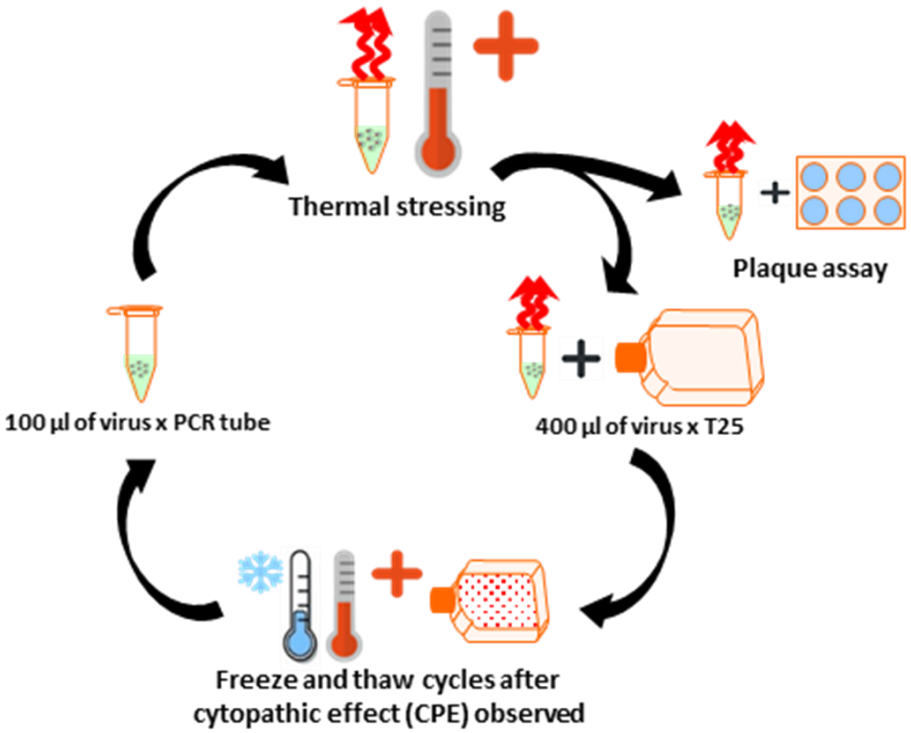


**Figure 2.4 Protocol for thermal stressing of EVA71:** This diagram shows the steps of a single EVA71 thermal stressing cycle. Aliquots of EVA71 were thermally stressed at 52.5°C and passaged into Vero cells x T25 flask until full CPE observed. Viral titer was measured after each thermal stressing cycle by plaque assay. Cycles of virus thermal stressing and passaging were repeated until the titer of thermally stressed virus yielded a similar titer as the not thermally stressed wt virus.

### 2.8.2. Thermal selection by $TCID_{50}$ assay

To carry out thermal selection using TCID50, virus samples were heated for 60 min at a range of temperatures (37$^{o}$C and 56.5$^{o}$C) using a thermocycler, (Master cycler nexus instrument, Eppendorf). One sample was chilled on ice at 4$^{o}$C as non–thermally stressed control and all conditions were cooled to 4°C within the thermal cycler. For each condition, the virus titer was determined using a $TCID_{50}$ assay (section 2.8.1).

### 2.8.3. Thermal selection by plaque assay

To carry out a cycle of thermal selection by plaque assay, 100 µl aliquots of wt virus was thermally stressed for 30 min using the inactivation temperatures 52.5°C in a Multi-Block PCR Thermal Cyclers (ProFlex™ 3 x 32-well PCR System, Thermo Fisher Scientific), The 4°C sample was left on ice as control, and all conditions were cooled to 4$^{o}$C within the thermal cycler. Two aliquots were obtained from each cycle, one aliquot was thermally stressed at 52.5$^{o}$C and directly assayed by plaque assay (see 2.8.2). The other aliquot was assayed also by plaque assay according to the plaque assay protocol prior to be being passaged in Vero cells seeded in T25 flasks with an MOI of 0.1 pfu/ml. The inoculated flask was incubated at 37$^{o}$C in 5% $CO_2$ humidified incubator. When a full CPE observed, the cells were subjected to one cycle of freeze and thaw to release the virus from cellular material and centrifuged for 5 min at 4000 rcf to pellet the cells. The thermal selection was carried out until the titer of thermally stressed viruses was approximately equal to the titer of the wt controls that were passaged serially without heating in parallel with each thermal cycle.

### 2.8.4. Genetic stability assessment of thermal resistant mutants

To determine the genetic stability of viruses in the absence of thermal pressures resistant mutants were passaged five times in the absence of thermal selection pressure and titers determined by plaque assay.

Subsequently, the thermal resistance profile of viruses was determined by incubating $1x10^6$ pfu of wt or mutant virus at thermally 37°C-57°C for 30 minutes. The heat- treated samples were titrated by plaque assays to assess infectivity. The viral genome was extracted according to the RNA extraction protocol (see section 2.3.1). The cDNA was generated from extracted RNA and sent for sequencing (see section 2.2.2).

## 2.9. Characterisation of viral proteins

### 2.9.1. 12% SDS-polyacrylamide gel electrophoresis

To analyse the structural proteins of virus particles or virus like particles (VLPs), samples were first diluted with Laemmli buffer at a ratio of 1:1, denatured at 95$^{o}$C for 10 minutes and pelleted for 5 minutes at 4$^{o}$C. Samples were loaded alongside a PageRuler™ Prestained Protein Ladder, 10 to 180 kDa (Thermo Fisher Scientific) were loaded on 12% SDS-PAGE (5 ml Tris 0.5M-pH 8.8, 6.6 ml water, 8 ml 30% Acrylamide-Bis 37.5:1, 200 µl 10% SDS, 200 µl 10% AP, and 15 µl TEMED) with 5% stacking gel (1.3 ml Tris 1.5M-pH 6.8, 5.5 ml water, 1.3 ml 30% Acrylamide-Bis 37.5:1, 50 µl 10% SDS, 80 µl 10% AP, and 10 µl TEMED). Samples were separated at 200 V constant for 1 hour.

### 2.9.2. Western blot

To transfer the proteins from 12% SDS - PAGE onto PVDF membrane, a semi-dry transferring unit was used. The 12% SDS - PAGE gel was placed on the top of methanol-activated transfer membrane, and both were sandwiched between four filter papers soaked with transfer buffer saline with Tween 20 (TBST). The 100 mL of 1x TBST was prepared from 10X TBS stock solution and 1 mL Tween 20 detergent to 900 mL of water. The 1 L of TBS 10x stock solution was prepared as follows: dissolve 190 Mm glycine, 25 mM Tris base 20% methanol, and add SDS with final concentration of .01% in 1.8 L water then adjust the pH to 7.6 and final volume to 1 L. The assembly was placed in a transferring instrument (Trans-Blot® Turbo™ Transfer System), and the electrophoretic transfer was carried out at 25 V for 30 min. The membrane was blocked using 5% milk in 1x TBST for 1 hour at room temperature before overnight incubation

in primary antibody at 4°C. The membrane was washed three times with 1x TBST buffer, followed by incubating the membrane with anti VP0/VP2 mAb 979, at room temperature for 1 hour with agitation, to detect EVA71 structural proteins. In addition to an α anti-tubulin (alpha- tubulin N-acetyltransferase (MyBioSource)) was used as a loading control. After the 1 hour incubation, the membrane was washed three times with 1xTBST buffer, followed by adding anti-mouse HRP (Sigma Aldrich) diluted at 1:10000 10% milk buffer/1x TBST at room temperature for 1 hour with agitation. Membranes were washed further 3 times in 1 x TBST and incubated with Promega ECL Western Blotting Substrate, which is an enhanced luminol-based chemiluminescent substrate reagent (Promega), for 1 minute before exposure to X-ray film in dark room. The exposure time was gradual starting from 30 sec up to 1 minute.

### 2.9.3. Sandwich ELISA

Sandwich ELISA was employed in order to assess the antigenicity and thermal stability of virus particles or VLPs. High-binding 96-well EIA/RIA (Sigma Aldrich) plates were incubated overnight at 4° C with polyclonal rabbit EVA71 Abs as capture antibody that were resuspended in at 1 : 2000 in filtered carbonate coating buffer pH 7.4 Plates were blocked by wash/block buffer made with 1x PBS with 2% skim milk powder and 0.01% Tween) and incubated at room temperature for 30 min to 1 hour. Buffer was removed and 50 µl of each sample was added to wells, plates were then incubated for 1-2 hours at 37$^{o}$C. Plates were washed three times before the addition of 50 µl of primary antibody (mAb 979) diluted at 1:1 000 in 10% milk buffer in 1x TBST buffer and incubated for 1 hour at 37$^{o}$C. Plates were washed three times before the addition of the secondary antibody (Sigma Aldrich). The anti-mouse HRP was used at 1: 2000 in 10% milk buffer in 1x TBST, and plates were incubated for 1 hour at 37°C. After washing the plates five times, 100 µl of OPD substrate solution (Sigma-fast) was added to each well and plates were incubated in the dark at room temperature for 30 min. This reaction was stopped by the addition of 50 µl 3M hydrochloric acid and plates were read in an ELISA plate reader measuring absorbance at 492 nm. The optical density (OD) for the duplicate standards and samples was calculated and the background (filtered carbonate coating buffer) absorbance readings was subtracted from the mean. Standard curves were plotted in Excel (Micrisoft Office) and used to determine the VLPs concentrations of the samples.

## 2.10. Mammalian VLP production

### 2.10.1. DNA transfection

To carry out DNA transfection, a ratio of 1: 1 of both mammalian VLPs co-expression plasmids: pCAGGS-EVA71–B2–P1 (P1) and pCAGGS His-tag 3C (3C) (Figure), were combined and with a 6µl Poly (ethylenimine) (PEI) (prepared in house by Dr Natalie Kingston). Empty pCAGGS plasmid (pCAGGS) and 3C plasmid were used as controls. The pCAGGS plasmid is useful for efficient gene expression in various mammalian cells using under the control of the AG promoter and the human CMV-IE enhancer in various mammalian cells. The AG promoter sequence consists of the chicken β-actin promoter linked to a rabbit β-globin fragment (Alexopoulou, Couchman and Whiteford, 2008). The transfection master mix was transfected into HeLa cells seeded in a 6-well plate to obtain $1x10^6$ cells per well after overnight incubation. The cell lysate and supernatant were harvested sequentially after 48 hours in 1.5 ml protein low binding tubes and pelleted by centrifugation at 16,000 rcf for 10 min. NP40 lysis buffer (30 ml of 5 M NaCl, 100 ml of 10% NP-40, 50 ml of 1 M Tris, pH 8.0) was added to pelleted cells to free the VLPs. 12% SDS-PAGE and western blot analyses (as described in 2.10.1 and 2.10.2), using anti-VP2/VP0 mAb979 antibody as primary antibody. Anti α Tubulin antibody was also used to indicate loading of an equal amount of the protein into the gel.

### 2.10.2. Optimisation of 3C/P1 ratio in HeLa cells

An optimal ratio of 3C to P1 was determined by testing various concentrations of the 3C using a fixed concentration of wild-type P1 plasmid (1µg P1 DNA/ml culture). The optimisation was carried out in a 12-well plate seeded with HeLa Ohio cells at 70% confluence. As each well should contain 2µg of DNA in total, the plasmids concentrations were adjusted by alternating the quantity of the added pCAGGS to the 3C while the P1 quantity was stabilised to be 1000 ng/µl (see table 2.8). The concentration of pCAGGS was added as follows: 900ng/µl, 700 ng/µl, 500 ng/µl, and 1000 ng/µl. The 3C concentrations were added as follows: 100 ng/µl, 300 ng/µl, 500 ng/µl, and 1000 ng/µl. A total of four controls were used: mock, pCAGGS, 3C, and P1. The cells lysate was collected after 72 hours in 1.5 ml protein low binding tubes. All collected cells were processes and examined (as described in sections 2.7.4).

| 3C concentration ng/µl | Empty pCAGGS concentration ng/µl | wt concentration ng/µl |
|---|---|---|
| 100 | 900 | 1000 |
| 300 | 700 | 1000 |
| 500 | 500 | 1000 |
| 1000 | …….. | 1000 |

**Table 2.8 3C concentration optimisation in HeLa Ohio:** The optimisation was carried out in HeLa Ohio cells using different concentrations of 3C, pCAGGS vector, and wt. Samples were collected at 72 hours. The experiments were characterised by western blot using mAbs 979. (n=4).

### 2.10.3. Optimisation of co-expression VLPs harvesting time

To optimise the harvesting time of the co-expression of VLPs, the DNA transfection protocol was followed. The cell lysate and supernatant were harvested sequentially after 24, 48, and 72 hours in 1.5 ml protein low binding tubes. Processing and examining were carried out as described in sections (2.11.1, 2.10.1, and 2.10.2).

### 2.10.4. Large scale co-expression EVA71 recombinant VLPs in mammalian cells

To produce recombinant VLPs in a large scale, 8-T175 flasks were seeded with HeLa cells for RC93 and wild-type. Cells at 70% confluence were cotransfected at a 1:1 ratio of the P1 and 3C plasmids. After 48 hours the cells were harvested according to a, optimised purification protocol previously optimised by Dr Natalie Kingston, University of Leeds). Briefly, HeLa cells were pelleted by centrifugation for 30 min at 4000 xg at 4$^{o}$C. VLPs were released from pelleted cells by NP40 lysis buffer, and 820 ml of water. Store at 4°C. Lysates were clarified by centrifugation at 4000 rcf for 30 minutes before particles were pelleted by ultracentrifugation through a 30% (w/v) sucrose cushion at 150,000 rcf for 3.5 hours at 4$^{o}$C. Pellets were resuspended in 1x PBS then loaded on a sucrose gradient 15 - 30% (w/v) and were ultracentrifuged at 50,000 xg for 12 hours at 4$^{o}$C. Purified fractions were collected from the top to the bottom (as previously described, section 2.7.3). The collected fractions were analysed for protein expression by 12% SDS-PAGE and Western blot using anti VP0/VP2 mAb 979 antibody (as described in sections 2.10.1, and 2.10.2). Fractions were also tested with sandwich ELISA using A9 and CT11F9 (see section 2.10.3).

### 2.10.5. Antigenicity and thermal stability

To estimate the thermal stability and proportion of native and expanded of the mammalian VLPs, sandwich ELISA assay was performed using anti-VP0/VP2 mAb979 (as described in section 2.10.3). Briefly, nine aliquots from the peak fraction were incubated at 30, 35, 40, 45, 50, 55, 60 & 65 °C for 10 min and then chilled on ice. ELISA assay was then carried out according to the protocol**.**

### 2.10.6. Yeast VLP expression

#### 2.10.6.1. Yeast VLP large scale expression

Pichia-pink cells were transformed with DNA sequences for wt or mutant EVA71 P1 (Figure2.5 ) and PV 3CD under the inducible AOX promoter (The vector and cells were prepared by Dr Natalie Kingston, University of Leeds). The pPINK-HC vector is a high-copy number vector (Thermofisher). It is built around the *ADE2* gene to complement the *ade2* deletion in the *Pichia pastoris* and use the methanol-induced AOX1 promoter to express targeted protein. The plasmid has encoded for Ampicillin (bla) resistance gene for selection in *E. coli*, and CYC1 transcription terminator for expression in yeast.

To express EVA71 VLPs in *Pichia pastoris* 10 ml cultures for 2 days, 200 ml of a sterile filtered Yeast Extract–Peptone–Dextrose media (YPD) (Bacto Peptone 20 g, yeast extract dissolved in 950 ml water), supplemented with 100ug/ml of ampicillin and 50ug/ml of Kanamycin was placed in 2-liter baffled flask. For every 100 ml of YPD culture, 1-5 ml of starter culture was added and incubated at 28°C with 250 rpm shaking for 48 hours. The following day, the yeast cells were pelleted at 1500 rpm for 10 min, and the YPD media was discarded.

Pelleted yeast cells were resuspended in a 200 ml of a sterile filtered YPM media supplemented with 100ug /ml of ampicillin and 50ug/ml of kanamycin, and the flask was incubated at 28°C shaking at 250 rpm for 24 hours. The culture was supplemented with methanol at a final concentration of 1%. The flask was kept at 28°C with 250 rpm shaken for 24 hours. The yeast culture was collected after 48 hours of methanol induction, the cells were pelleted at 1500 rcf for 30 minutes, and the supernatant was discarded. The pelleted cells were resuspended in a breaking buffer consisting of 50 mM sodium phosphate, 1 mM EDTA, and 5% Glycerol at pH 7.4. Yeast cells were stored at -20$^{o}$C and a sample was kept for SDS-PAGE and Western blot analysis (as described in 2.10.1 and 2.10.2)

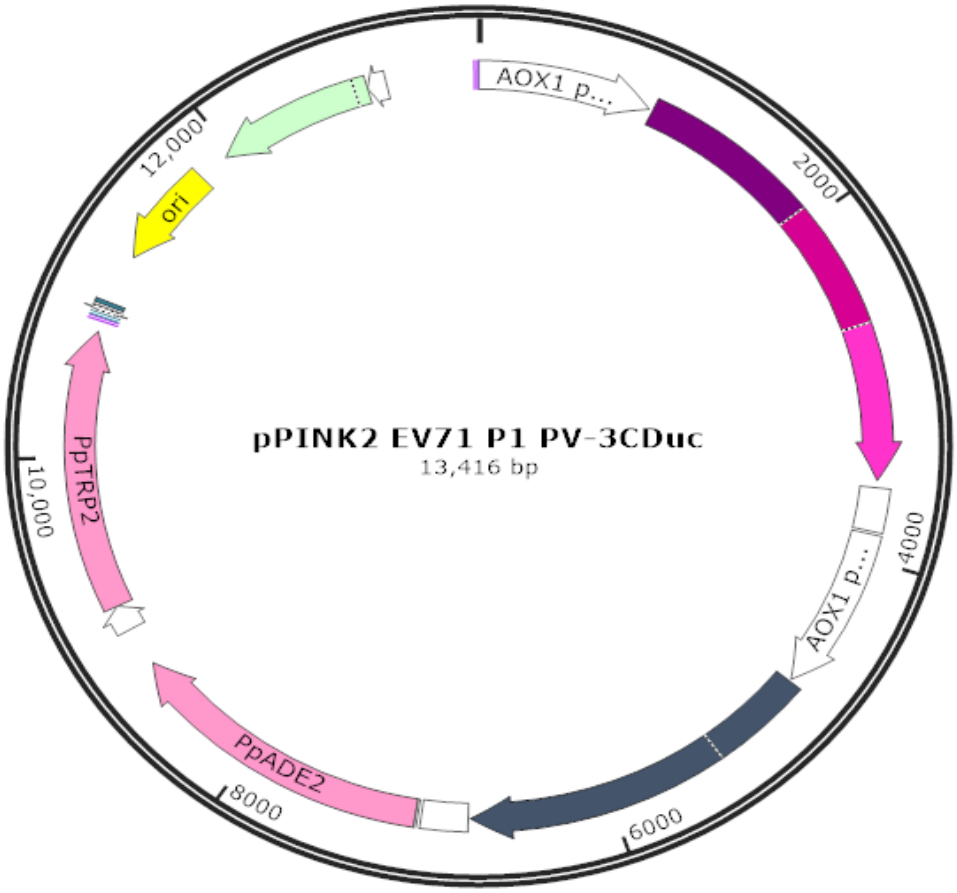


**Figure 2.5 The *Pichia Pastori* vector pPINK EVA71 P1 PV – 3CDuc**

### 2.10.7. Purification of yeast VLPs

For yeast VLP purification, the harvested yeast suspension stored at -20°C earlier was supplemented with Triton-X100 solution to a final concentration of 0.1% and the tube was incubated on a rocker for 30 min. Yeast were resuspended in Breaking buffer (see section 2.12.1). Cells were disrupted at 40 Knots Per Square Inch (kpsi) with cooling (Models CF1 and CF2 High pressure cell disruption - research to production from Constant Systems Ltd) The flow through mode can take a minimum of 60 ml of suspension with a maximum of 200 ml whilst cooling the sample. Samples were harvested and the insoluble materials were pelleted at 4000 xg for 30 minutes at 4°C. A second clarifying spin was carried out to remove the remaining insoluble material at 10,000 xg for 30 minutes at 4°C. To break down the cellular DNA 25 U/10 ml of benzonase and 1-2 mM of $MgCl_2$ was added to the yeast supernatant and incubated on a shaker at room temperature for 2 hours. Samples were incubated overnight in 8% (w/v) a PEG 8000 at 4°C overnight. The precipitated proteins were centrifuged at 4000 rcf for 30 minutes at 4°C. After removing the supernatant, pellets were resuspended in 30 ml 1x PBS per 200 ml culture. The mixture was centrifuged at 4000 rcf for 30 minutes at 4°C to remove insoluble materials. Another clarifying step was carried out to remove any insoluble material by centrifugation at 10,000 rcf for 30 minutes at 4°C. The supernatant was pelleted using 30% sucrose cushion and ultracentrifuged in a SW32 Ti bucket at 151,000 xg for 3.5 hours at 4°C (as previously described in section 2.7.2). Pellets were resuspended in buffer consisting of 1 ml of 1x PBS + 1% NP-40 + 0.5% sodium deoxycholate and incubated at 4°C overnight. Pellets were pipetted briefly to break up the pellet and release VLPs effectively.

A 15-45% sucrose gradient was carried out as previously described. The resuspended pellet was centrifuged for 10 minutes at 10,000 xg at 4$^{o}$C to remove insoluble materials. The supernatant was overlaid on the top of the gradient in the SW32 Ti tube. The gradient was balanced and ultracentrifuged using the SW32 Ti rotor at 151,000 xg for 3 hours at 4$^{o}$C. Fractions of 1 ml each were collected from top to bottom using a 1000 µl pipette and placed in a 1.5 ml low binding protein tube. Samples were assessed by 12% SDS-PAGE and western blot (see section 2.10.1 and 2.10.2), ELISA (see section 2.10.3), and plaque assay (see section 2.8.2).

### 2.10.8. Characterisation of replicon replication

#### 2.10.8.1. GFP replicon T7 RNA transfection

The reporter gene GFP measures the level of viral replication in cells by measuring the level of GFP fluorescence as a result of the gene expression. It can be inserted into either a full-length virus or into a replicon into a subgenomic replicon (Ge et al., 2007, Hertzig et al., 2004). To transfect transcribed viral T7 RNA of GFP replicon (Figure 2.6) to cell, a 24-well plate was seeded with HeLa cells at a density of 1 x $10^5$ cells/well 16 - 24 hours before transfection and were 80 - 90% confluence at the time of transfection. Complete DMEM (cDMEM) was prepared in advance by mixing phenol red free DMEM with 10% FBS and Glutamax. The transfection master mix was prepared in a 1.5 ml RNA free tube by adding 2 µg of RNA in 50 µl of OptiMEM (Invitrogen) (1 µg: in 25 µl /well). As well, a 3 µl of Lipofectamine 2000 reagent (Thermo Fisher Scientific) was added to 50 µl of OptiMEM per well. Tube was vortexed and centrifuge briefly and incubated for 10 min at room temperature. Afterward, 50 µl of the reagent mix was added to each RNA tube to create 100 µl and mixed by pipetting and incubated at room temperature for 15 - 20 min.

While the transfection reactions were incubated, the media were removed from the cells and the cells were washed with 500 µl of cDMEM. Then 500 µl of cDMEM was added to each well and returned to the incubator. A50 µl volume of transfection mix was added drop wise to each well after incubation of the RNA transfection reactions completed. The cells were incubated for 18-24 hours at 37$^{o}$C in a Incucyte incubator.

### 2.10.8.2. IncuCyte analysis of replication

The replication of 3A GFP replicon and live-cell imaging were analysed with IncuCyte Dual Colour Zoom FLR (Essen Bioscience) housed within a 37$^{o}$C humidifying $CO_2$ incubator. After transfection of replicon-transcribed RNA, cells were placed in the IncuCyte and cells were monitored hourly for 24 hours. The images of each well were taken, and the number of GFP expressing cells were counted as green GFP object and the measurements analysed by using the integrated algorithm within the IncuCyte Zoom.

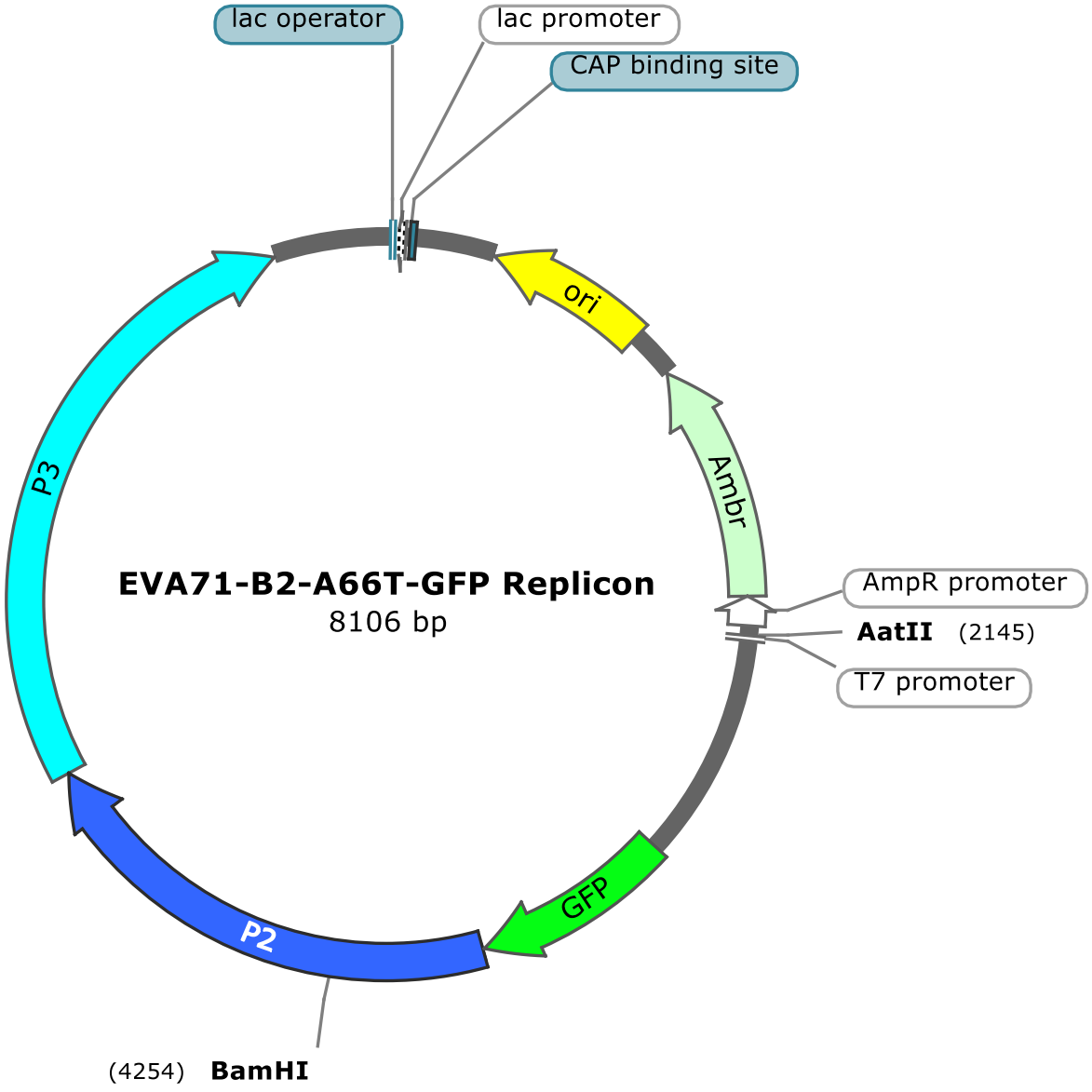


**Figure 2.6 The vector map of EVA71-B2-A66T-GFP replicon**

# Chapter 3

## Results

### Stabilising EVA71 empty capsid structure by thermal stressing

## 3.1. Introduction

Three EVA71 inactivated vaccines have been recently marketed but only for the Chinese market (reviewed in Li et al., 2021). Production of these vaccines requires the propagation of a huge amount of virus, which poses a risk of live virus escape into the vaccine formulation or into the environment. VLP vaccines mimicking naturally occurring empty capsids (ECs) and can serve as an effective and safer alternative if they possess epitopes with the same conformation as infectious virions (Nooraei et al., 2021). However, this type of recombinant vaccine faces a significant challenge as naturally occurring picornaviral EC have been documented to be less stable than viral particles and are likely to undergo conformational changes (Adeyemi et al., 2016; Fox et al., 2017). Therefore, improving EC stability to display epitopes appropriately in the native form may be important to produce an effective EVA71 VLP vaccine.

Most of the EC stability data have been informed by intensive research undertaken on polio virus (PV) (reviewed in Mehndiratta et al., 2014). The PV virion has an organised internal network comprised of N terminus extensions of VP1, VP2, and VP3 together with VP4 decorating the inner surface of the capsid, that contributes considerably to stabilising it. The lack of such structure may affect the stability of generated VLPs (Basavappa et al., 1998). In contrast, the internal network is disordered including the entire N-terminal extension of VP1 and parts of N-terminal extension of VP0. This disorder may distort the interaction between different EVA71 pentamers or protomers, which may provide a possible explanation of ECs liability and readiness for expansion (Basavappa et al., 1998).

Similar to polio, EVA71 particles have both antigenic forms, NAg and HAg. From structural data on purified samples of EVA71, ECs appear noticeably expanded and the hydrophobic pockets within the capsid are collapsed (Wang et al., 2012). EVA71 ECs are unstable and readily convert from a state with NAg form to HAg state with altered antigenic properties resembling those of 135S intermediate or the virion capsid after receptor bindings (Liu et al., 2011; Wang et al., 2012; Cifuente et al., 2013).

RNA viruses have error-prone replication due to the lack of proofreading of the virus- encoded RNA polymerase (Domingo et al., 1996). Rapid evolution (resulting from their high mutation rates and short replication times), allow RNA viruses to escape the immune system, become resistant to antiviral drugs, gain virulence, and rapidly adapt to a new environment (Domingo et al., 1996). The replication of RNA viruses, including enteroviruses such as PV and EVA71, generates heterogeneous but genetically related spectra of mutants as a diverse cloud of virus sequences defined as a quasispecies (Domingo et al., 2012). The frequency of variants in a quasispecies is impacted by genetic variation, competition, natural selection, and random drift. Variants arise continually and change in relative frequency, but they co-operate functionally and collectively to give the virus population its unique phenotype (Domingo et al., 2012). Continuous rounds of replication and high mutation rate will expand the sequence space of the quasispecies away from the dominant master sequence by generating a diverse range of genotypes (Domingo et al., 1996). The framework of quasispecies is determined by environment and selective pressure. In a specific environment, natural selection optimises

fitness by selecting beneficial mutations and trimming existing genetic variation. However, not all generated mutations are beneficial but, mostly, they can be deleterious or neutral, which means the population can become extinct as a result (Martínez et al., 2012). The effective strategy to compensate that effect and adapt rapidly to a changeable environment is by the generation of a large population size.

The vast genetic diversity of the RNA quasispecies allow these to adapt rapidly to changes in the environment (Martínez et al., 2012). Some of these mutants within a quasispecies will have different properties including increased resistance to certain conditions due to a single or a number of mutations in the virus genome. These features may confer the ability to escape from the immune system, adapt to different cell types, or resist high temperatures and pH (Domingo et al., 2012; Domingo and Perales, 2019). These variants might be generated previously under certain selective pressures but remain as minority within quasispecies until exposed again to the same selection. The enormous adaptive capacity of RNA viruses has been exploited in many direct evolution experiments. As these experiments relied on natural selection, virus populations were subjected to certain conditions such pH or thermal stress to select a desired phenotype or modify existing one (Martínez et al., 2012). Thermal adaptation is vital for viruses in natural selection and evolution; therefore, temperature can be utilised as a stressor in the experimental evolution and thermal adaptation of viruses (Chen and Shakhnovich, 2010). Several studies have shown that picornaviruses have adapted to elevated environmental temperatures, and acquired superior thermal fitness comparing to the viruses at 37°C.

For PV, the native or NAg form of particles is considered suitable for use as a vaccine as it can induce a long-lasting protective immune response, unlike the expanded or HAg form that does not. The potency or immunogenicity of the vaccine is determined by NAg content, and a high antigen content vaccine should contain mainly NAg form. Selecting stable mutants, either by increasing pH or through thermal stressing, was applied for some picornaviruses to stabilise or maintain NAg conformation of ECs, which in turn was used to inform the generation of VLPs that are able to elicit a potent immune response. Recent studies have demonstrated the possibility of stabilising the NAg form of VLPs (Adeyemi et al., 2017, Fox et al., 2017).

The consequence of these antigenic forms on vaccine efficacy and long-term immune response is still unknown for EVA71. In order to understand their role, we aim in this chapter to stabilise the NAg form of ECs by first employing molecular evolution of EVA71 to select a virus population with enhanced thermally resistance. An established protocol with PV was used as a starting point (Adeyemi et al., 2017). The results could inform the generation of a stabilised EVA71 VLP vaccine candidate.

EVA71 mutants with increased thermal resistance can be selected from the quasispecies by employing cycles of thermal selection and passaging surviving viruses. The thermal stressing temperature or selection temperature is set at the highest temperature at which almost all the virus is inactivated. For PV 51$^{o}$C, with 53$^{o}$C, and 57$^{o}$C were employed in successive rounds of selection (Adeyemi et al., 2017). Here, the first step was to identify the temperature for thermal selection for a thermal resistance virus population selection from quasispecies that will inform the generation of stabilised VLP. After selection the structural region of the genome incorporating the thermal resistance mutations, either individually or in

combination, can be expressed along with the viral protease 3CD in a heterologous expression system (Yee and Poh., 2015). These systems could be yeast e.g., *Pichia pastoris* (Zhang et al., 2015), mammalian cells (Tsou et al., 2015) for example HEK-293A cells or Hela Ohio cells, or *Spodoptera frugiperda* (Sf-9) insect cells (Hu et al., 2003; Chung et al., 2006).

Several different EVA71 strains are known to cause hand, foot, and mouth disease (HFMD). Here, one strain of EVA71 has been used as proof of principle: EVA71 B2 (MS/7423/87) kindly donated by SingVac (Singapore).

## 3.2. The assessment of EVA71 thermal stressing by $TCID_{50}$ assay

As described above, generating EVA71 ECs with native conformation will inform the generation of stabilised EVA71 VLPs with native conformation that could be used as a VLP vaccine candidate. The stabilisation was carried out by selecting thermally resistant virus population using repeated cycles of thermal inactivation and passaging of surviving virus. This was preceded by identifying the temperature at which ≈ 99.9% of infectious titer were lost as an initial step (Figure 3.1).

In this context, this experiment was undertaken in order to determine the ideal temperature of thermal selection to be used to select a mutant with increased thermal stability. Consequently, we first sought primarily to thermally stress samples of EVA71 wild- type using a range of temperatures (37-53.5$^{o}$C) for 30 min and cooled immediately at 4$^{o}$C. A sample was kept on ice (4$^{o}$C) as a non-thermally stressed control.

EVA71 quantification and initial thermal stressing experiments were undertaken by the cytopathic effect (CPE) microtitration assay, expressed as 50% tissue culture infective dose per milliliter ($TCID_{50}$/ml). This endpoint dilution assay was used to identify the thermal selection temperature at which ≈ 99.99% of EVA71 virus population was inactivated. The results of EVA71 titer were presented as a logarithmic plot of virus titer against the increasing temperatures (see method section 2.8.1).

Initial viral titer was around 1.31 x $10^{8}$ $\log_{10}$ $TCID_{50}$ per ml. Then viral titer started to decrease down to 7.9.6 x $10^{4}$ $\log_{10}$ $TCID_{50}$ per mL between 40.6$^{o}$C and 45.5$^{o}$C until a full inactivation of the virus occurred between 52$^{o}$C and 53$^{o}$C (Figure 3.1). However, the data also showed that there was a small but unexplained increase in the virus titer at 37$^{o}$C.

In our hands, it was technically challenging to obtain convincing replicated data by $TCID_{50}$ assay (data not shown). Another method for titrating virus is the plaque assay. One advantage of plaque assays over $TCID_{50}$ is that both plaque phenotypes as well as an absolute titer can be obtained from a single assay. Thus, investigating a plaque assay as an alternative to $TCID_{50}$ may allow more information about potential phenotypes to be obtained. Hence, this method was replaced by plaque assay to assess EVA71 titer for the remainder of this project.

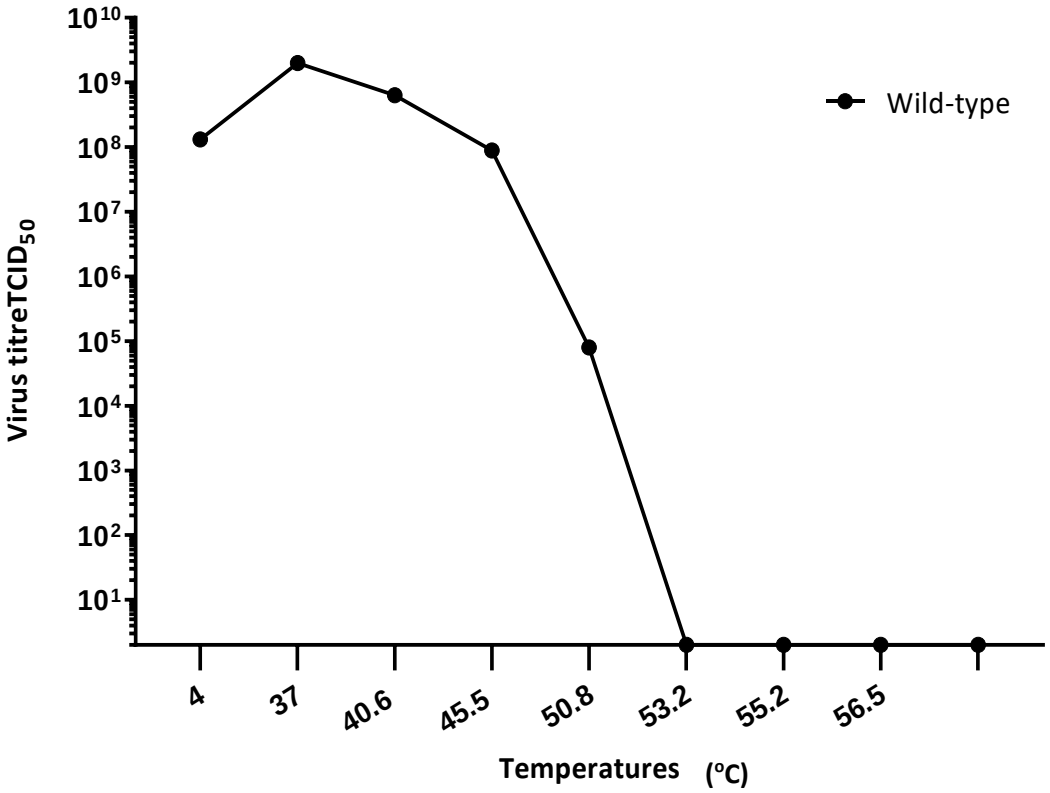


**Figure 3.1 Thermal selection of EVA71 by $TCID_{50}$:** The EVA71 samples were thermally stressed for 30 min at a range of temperatures between (37°C and 56°C), then cooled immediately at 4°C. A non – thermally stressed control at 4°C was included. $TCID_{50}$ assay was performed in Vero cells to measure the virus titer. Samples of virus were tenfold serially diluted ($10^{-1}$ – $10^{-8}$) and inoculated in 96 well plates with cell density of 2.5 x $10^4$ cell / well and at ~90% confluence. The results were presented by a logarithmic plot of virus titer against the increasing temperatures. This experiment is one experiment that was carried out one time (n=1).

## 3.3. Plaque assay optimisation for EVA71

Plaque assay is one of most used method to quantify samples of infectious viruses of unknown concentration that has been serially diluted. The virus titer is determined by counting plaques that are “dead zones” formed in a monolayer of cells by individual infectious virions. Plaques can also be used to isolate infectious viruses.

Obtaining a consistent virus titer by plaque assay depends upon several parameters such as cell line, the virus inoculum, cell culture practices, incubation time, and/or the final concentration of the agarose overlay (Shurtleff et al., 2012). Assay validation and parameter optimisation must be undertaken prior to the application of a plaque assay in any new viral research (Shurtleff et al., 2012). In this project, some of the parameters of a previous plaque assay protocol (provided by Dr Elisabetta Groppelli, University of Leeds), were optimised to accurately measure the EVA71 titer. According to Shurtleff et al (2012), one of these parameters is a permissive cell line that can produce a confluent and intact monolayer for an effective viral plaque formation. For the EVA71 plaque assay, Vero cells and HeLa Ohio cells were evaluated. Both cell lines are permissive for EVA71, based on the previous experience of other laboratories to measure the titer of both EVA71 and PV by plaque assay (e.g., Baer and Kehn-hall, 2014; Kelly., 2015; Adeyemi et al., 2017). EVA71 was able to produce plaques in both cell lines. However, HeLa appeared to be easier to manipulate as it produces a confluent monolayer that remained intact during all the stages of the plaque assay. EVA71 plaques in HeLa cells were clear, small, most of them were with a defined circular border though some were not.

The second modified parameter was the continuous rocking of the inoculated 6-well plate for 1 hour to spread the virus inoculum across the cell monolayer. This rocking was previously performed mechanically but it disturbed the cell monolayer, thus was replaced with a gentle manual rocking every 15 min for 1 hour.

The final parameter was the volume of the overlay media (5% GM + 0.6% agarose gel), was reduced from 3 ml to 2 ml. The volume adjustment allowed the overlay to gel faster while being sufficiently solid to restrict viral spread, preventing cellular infection, and for effective plaque formation (Figure 3.2).

The EVA71 plaques were small and visible three days-post infection (dpi). The cells and plaques were fixed and stained 4 dpi to enhance plaque visualisation.

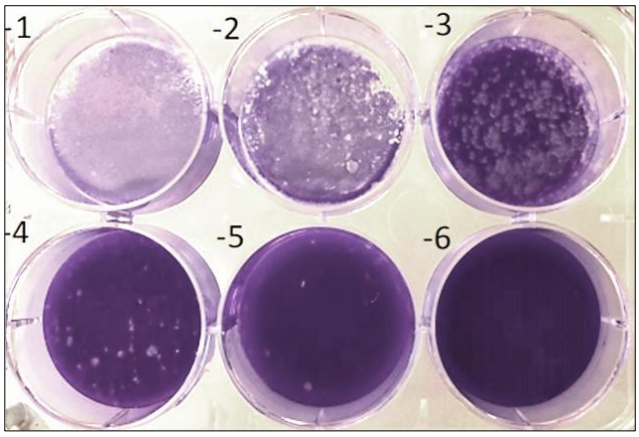


**Figure 3.2 Optimisation of EVA71 plaque assay:**
HeLa cells were plated with cell density between 8 x $10^5$ – 1 x $10^6$ cell/ml in 2.5 - 3 ml of 5% GM in 6 well plates a day prior to the assay. Virus samples that were tenfold serially diluted ($10^{-1}$ - $10^{-6}$) in serum free DMEM, were inoculated into ~90% confluent monolayer the day after plating. After 60 min of virus adsorption, 2 ml of overlay media (5% GM + 0.6% agarose) was added. At 4 dpi, the cellular monolayer and plaques were fixed and stained with crystal violet/formaldehyde for 1 hr at room temperature. The overlay was removed, and the plaques were counted.

## 3.4. The assessment of EVA71 thermal stressing by plaque assay

A subsequent thermal inactivation curve was established using the plaque method in order to determine the selection temperature at which most of EVA71 virus population is inactivated and would be used to stress the EVA71 virus population (Figure 3.3) (method section 2.9.1 and (method section 2.8.2). Thermal characterisation of EVA71 wt was performed by incubating aliquots of EVA71 at a range of temperatures between (37$^{o}$C and 53.5$^{o}$C) for 30 min. A separate aliquot was kept on ice (4$^{o}$C) as a non-thermally stressed control. The initial titer for EVA71 at 4$^{o}$C was 4.8 x $10^5$ pfu/ml. The results of EVA71 titer were presented as a logarithmic plot of virus titer against the increasing temperatures between 37$^{o}$C and 56.5$^{o}$C, and 4$^{o}$C as control (Figure 3.3).

Aliquots of the surviving pool of viruses were assayed for infectivity by plaque assay. The thermally stressed viruses showed a reduction in titer with the increase in temperature until a complete inactivation of EVA71 occurred at 53$^{o}$C. The infectivity of EVA71 was reduced from 100% (4.8 x $10^5$ pfu/ml) at 4$^{o}$C (non-thermally stressed control) to 0.06% (2.8 x $10^2$ pfu/ml) at 52.5$^{o}$C. This result suggested that a selection temperature between 52.5$^{o}$C and 53$^{o}$C could be employed as this is where ≈99.99% of viruses are inactivated (Figure 3.3). The thermal characterisation was conducted only once, however, the data broadly agree with those reported by $TCID_{50}$ assay in section where complete inactivation of the virus occurred at 52.5$^{o}$C (Figure 3.1).

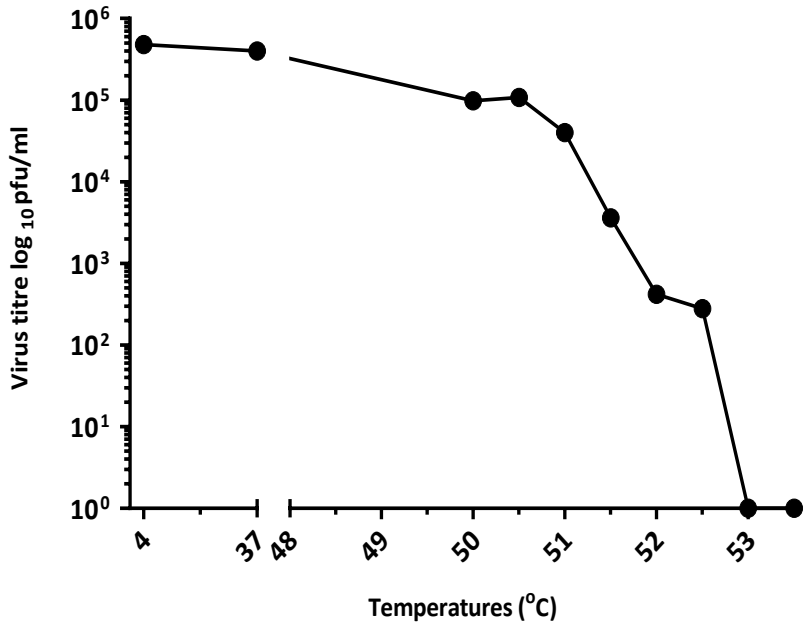


**Figure 3.3 Thermal inactivation of EVA71 by plaque assay:** The EVA71 samples were thermally stressed for 30 min at a range of temperatures (37°C – 53°C), then cooled immediately at 4°C. A non-thermally stressed control at 4oC was included. The plaque assay was performed in HeLa cells. Samples of virus were tenfold serially diluted ($10^{-1}$ – $10^{-8}$) and inoculated in 6 well plates, plated with cell density of 8 x $10^5$– 1 x $10^6$ cell/ well and at ~90% confluence. The results were presented by a logarithmic plot of virus titer against the increasing temperatures and the number of plaques was represented using plaque forming units (pfu) per millilitre. This experiment is one experiment that was carried out one time (n=1).

## 3.5. Thermal stressing of EVA71

In order to select thermally stable mutants from the EVA71 quasispecies, thermal stressing assays were employed using the thermal selection temperature (52.5$^{o}$C). Aliquots of EVA71 B2 were subjected to successive cycles of thermal selection at 52.5$^{o}$C for 30 min and surviving viruses were passaged in Vero cells at 37°C until full CPE observed. The cycles were initiated by heating an aliquot ~ $1x10^6$–$2x10^6$ pfu / ml of wt virus passaged in Vero cells. At the end of each cycle, two aliquots were obtained; one aliquot was further heated and passaged, while the other was assayed by plaque assay to determine the titer of surviving viruses (Figure 3.4). The cycles were then repeated eight times until the heated virus titer was approximately equal to the titer of unheated controls.

To assess the thermal stability of thermally selected populations, the titer of heated viruses was compared to titer of non-heated wt control. The results have shown that there was an initial significant fitness cost of 4-$\log_{10}$ reduction in infectious titer after selection for one cycle. That was followed by observing 2 $\log_{10}$ increase in titer at cycle two, and the increase was continued until cycle four followed by slight reduction in titer at cycle five for unknown reason. This increase in virus titer or infectivity could be an indication of possible selection of thermally stable mutants that adapted to heating at 52.5$^{o}$C. Selection was continued for another four rounds. From cycle six onward, the virus titers were increased slightly over this time until the heated virus titer was approximately equal to the unheated wt control virus (Figure 3.5). The pool of viruses that was isolated from the ninth thermal cycle was termed #9.

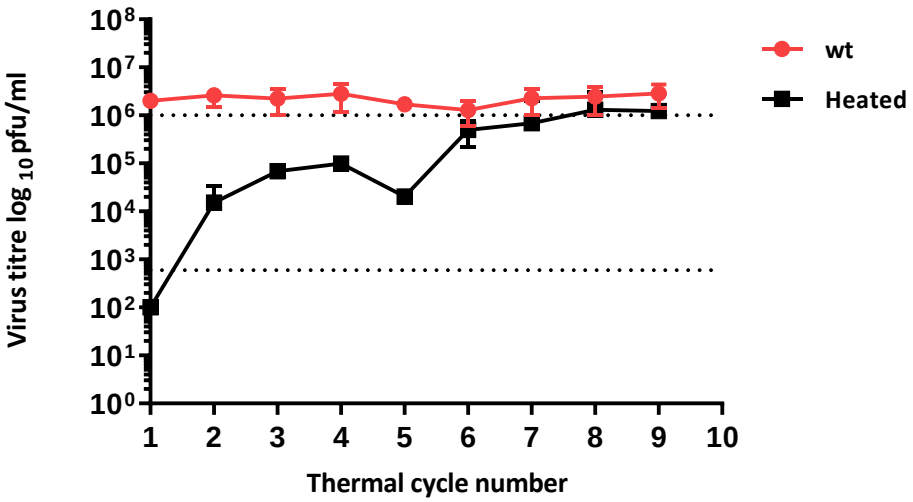


**Figure 3.4 Thermal selection:** Thermal selection was carried out at the selection temperature of 52.5°C. Successive thermal cycles were undertaken by incubating virus aliquots at 52.5°C for 30 min, cooling at 4°C, and passaging the surviving viruses at 37°C without thermal selection. As control, non-thermally stressed wild-type aliquot was passaged serially without heating. The heated virus titer and control titer was evaluated by plaque assay after each cycle. The thermal selection cycles were repeated until titer of thermally stressed virus and the wild-type were similar. The resulting virus was designated as #9. The results were presented by a logarithmic plot of virus titer against the number of thermal stressing cycles. This experiment is one experiment that was carried out in triplicate (n=3). Error bars often represent one standard deviation.

## 3.6. Thermal characterisation of selected viruses

Prior to proceeding with thermal characterisation of #9, it was essential to assess any possible reversion to wild-type genotype. This genetic stability was examined by serially passaging aliquots of #9 virions population in Vero cells seeded in a T75 flask (seeded with Vero cells) at 37$^{o}$C five times using a high multiplicity of infection (MOI) of 0.1 (MOI= virus particles (pfu)/ number of cells). After the final passage, the recovered virus pool, termed #9x5, was subjected to Sanger sequencing.

To characterise the thermal resistance of both #9 and #9x5, samples from both virus pools were thermally stressed using range of temperatures (37-57$^{o}$C) (Figure 3.6). Samples of wt were characterised using the same range of temperatures. Similar to the thermal selection experiment (in section 3.1.4), the virus infectivity of each virus pool was examined by plaque assay after each thermal characterisation cycle and presented as a logarithmic plot of virus titer against the number of thermal stressing cycles (Figure 3.6). The results indicated that the infectivity of EVA71 wild-type was reduced from 2 x $10^6$ pfu/ml at 37$^{o}$C to

1.3x $10^2$ pfu/ml at 52$^{o}$C. This corresponds to a reduction of >99.99%. The infectivity of #9 was reduced from 2.5x $10^6$ at 37$^{o}$C to 1.88 x $10^3$ at 57$^{o}$C. The infectivity of #9x5 was reduced from 1 x $10^6$ at 37$^{o}$C to 1.66 x $10^3$ at 57$^{o}$C. These results indicate that the #9 and #9x5 virus pools have an enhanced stability at higher temperatures in comparison to the wild-type. Interestingly, #9x5 appears to have slightly higher stability than wild type for unknown reasons.

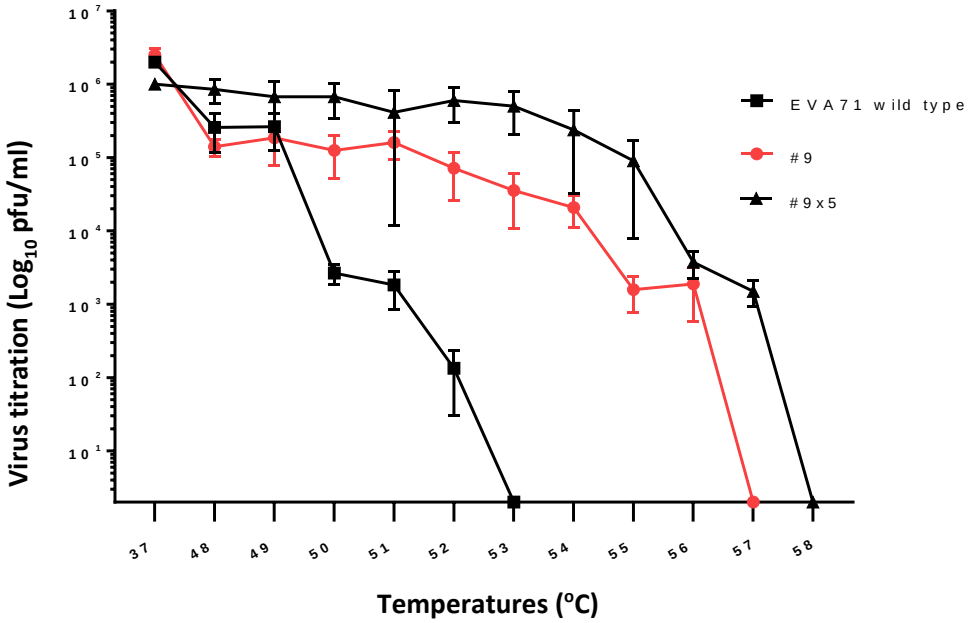


**Figure 3.5 Thermal characterisation of heat-selected viruses:** Thermal resistance profile of #9 and #9x5 virus pools were assessed alongside a wild-type control. Each virus pool was incubated at a range of temperatures (between 37°C and 57°C) for 30 min and cooled to 4°C. The virus titers were determined by plaque assays. The data represent titers of each virus pool at each temperature. This experiment is one experiment that was carried out in triplicate (n=3). Error bars often represent one standard deviation.

## 3.7. The identification of capsid thermal resistance mutations

Sanger sequencing was used to identify the capsid mutations in the P1 capsid-encoding region of #9 potentially contributing to the observed thermal resistance of #9. cDNA of extracted viral RNA of #9 was amplified and sent for Sanger sequencing (see method section 2.2.3). The nucleotide sequence was translated using the ExPASY tool and was aligned by ClustalW with the sequence of EVA71 B2 wt that was obtained earlier (Figure 3.6).

The sequence analysis revealed that #9 acquired five non-synonymous substitutions within the structural region. Three of them were located in the VP1 protein; Y1116C, K1162I, and P1246A, though P1246A appears to be a tissue culture adaptation mutation as it has been found in a previous wild-type passage virus in our lab (Table 1.3). The V2085L in VP2, while I3235M was found in VP3 (Table 1.3). Importantly, #9 appears to be genetically stable as no reversion to wt was detected in the #9x5 virus population (Appendix 2).

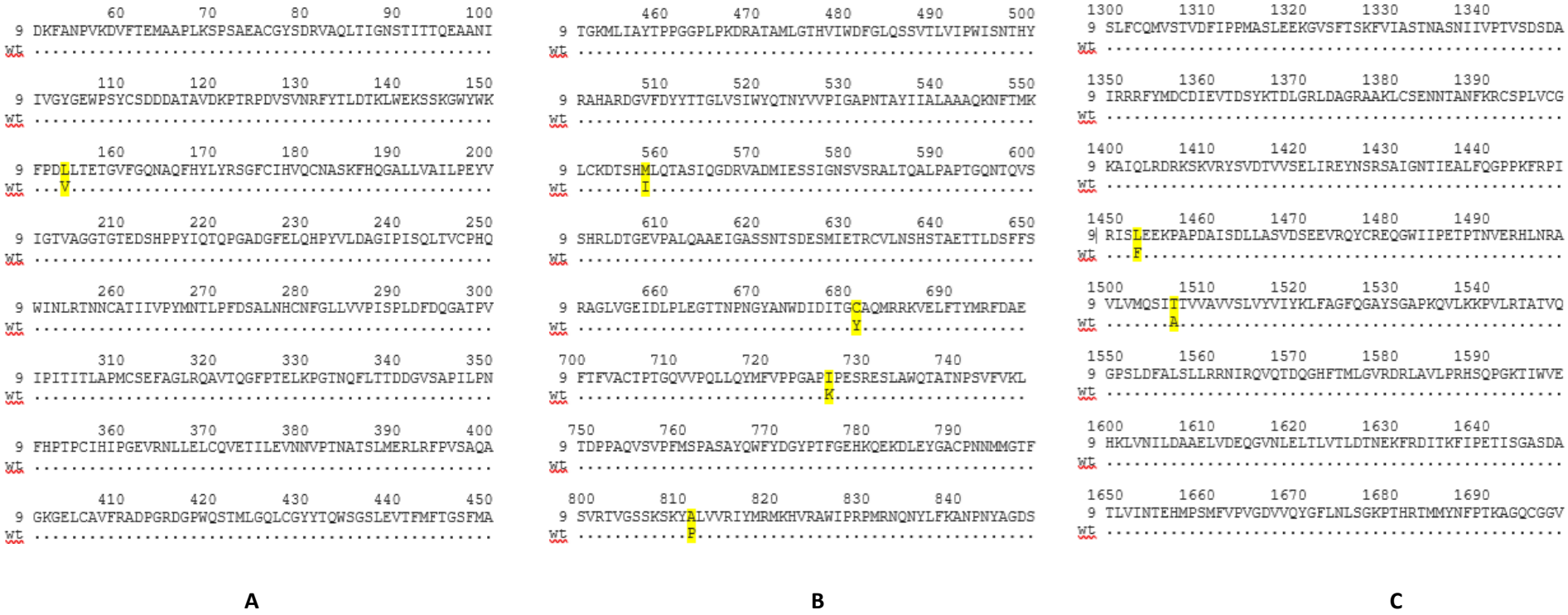


**A** **B** **C**

**Figure 3.6 Sanger sequencing results:** Alignment of the #9 with wt sequence using Pairwise Sequence Alignment, EMBOSS Needle from EMBL-EBI. (A) & (B) Show the thermal resistance mutations that were found in structural region of the genome: V2085L, I3235M, Y1116C, K1162I, and P1246A (C) F5101 and A66T in the non-structural region 3A.

| Mutation | Structural protein | Location on protomer |
|---|---|---|
| P1246A | VP1 | Within the VP1 HI-loop atop the five-fold mesa |
| I3235M | VP3 | Near the flexible C-terminal end of VP3 above VP1 |
| K1162I | VP1 | Outer canyon region and within the quasi 3-fold region between VP1 and VP3 |
| V2085L | VP2 | In Helix of the VP2 on the external surface of the capsid near the two-fold symmetry axis |
| Y1116C | VP1 | Whitin a helical above the canyon and near to the pocket |

**Table 3.1: Capsid mutations of #9:** Thermal resistance mutated residues and their location in the capsid

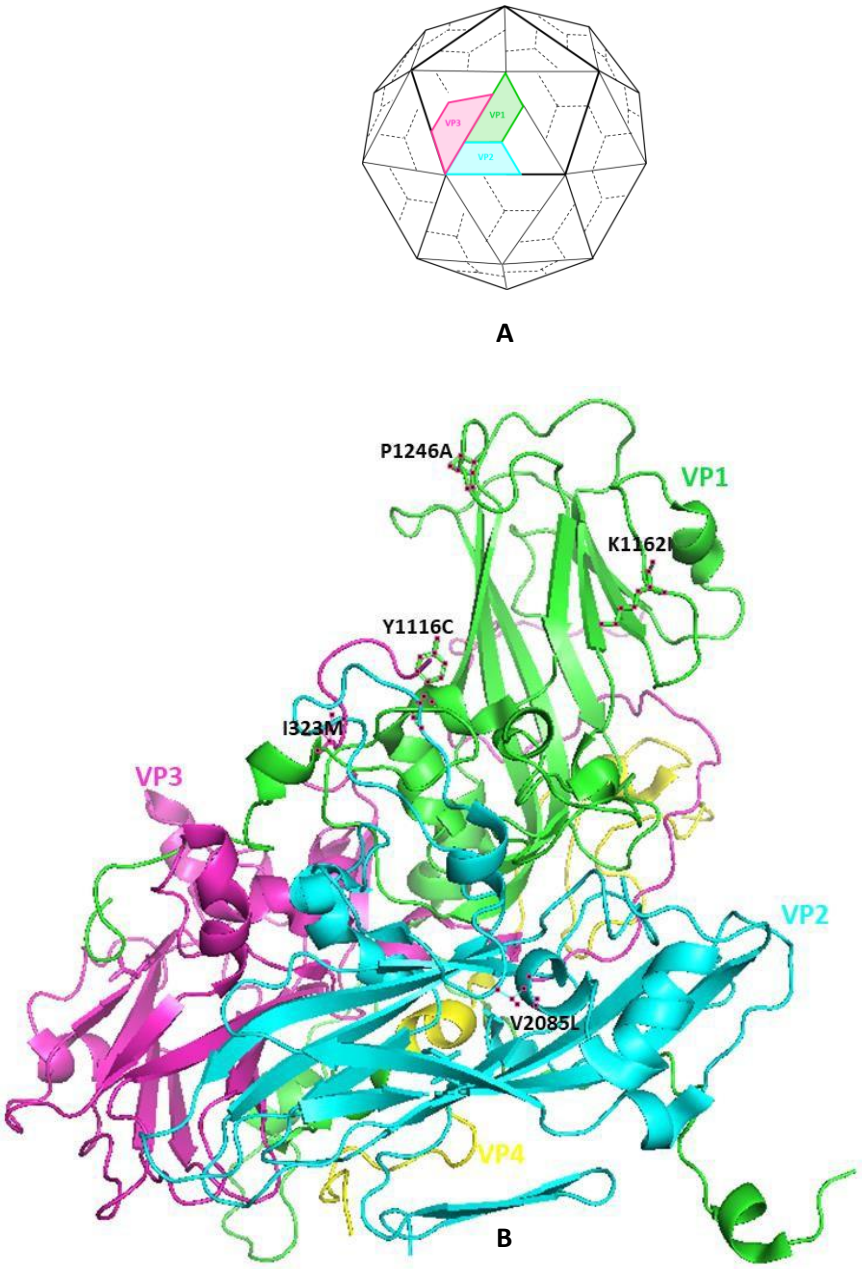


**Figure 3.7 Mutations within P1 capsid-encoding region of #9 mapped on 3BVS:** Mutations within P1 capsid-encoding region of #9 were mapped on 3BVS by PyMOL. (A) The viral capsid with the location of each protomer illustrated by colour VP1 (green), VP3 (purple), VP2 (blue), and VP0 (yellow (B) The capsid structural proteins are represented by ribbon models of an EVA71 protomer. The positions of #9 mutations are highlighted in yellow spheres and indicated on the cartoon modelling of EVA71 viral capsid. All the mutations occurred on external surface residues of the capsid.

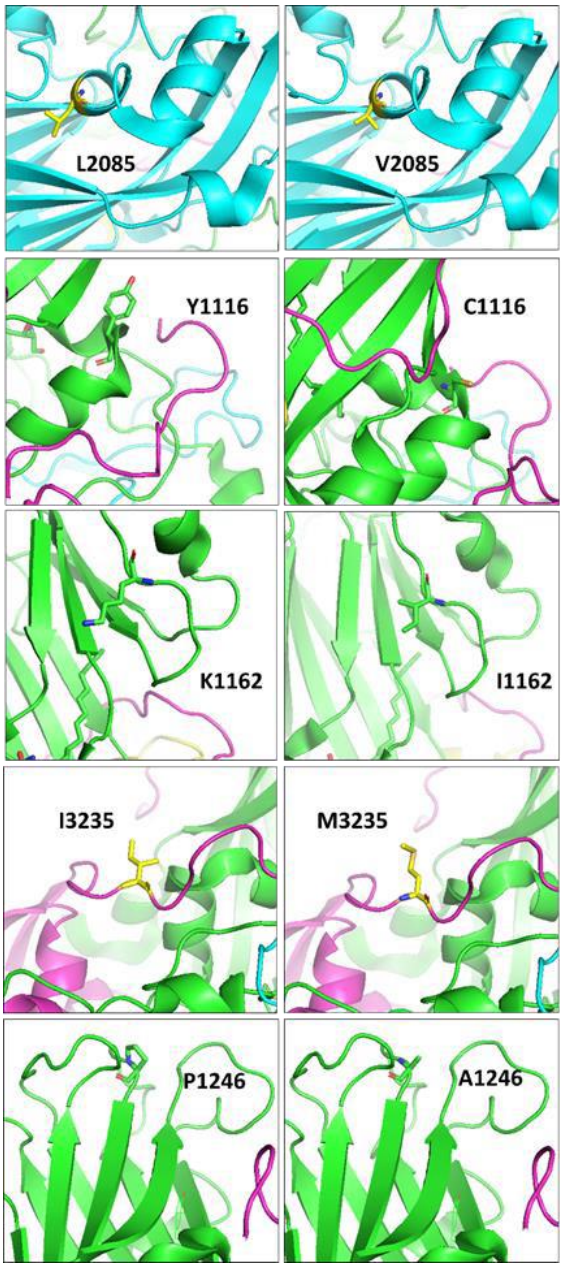


**Figure 3.8 Thermal resistance mutated residues within P1 capsid-encoding region of #9 mapped on 3BVS:** Mutations within P1 capsid-encoding region of #9 were mapped on 3BVS by PyMOL. The images at the right are showing the original protein secondary structure before genetic changes. While the images at the left are showing the thermal resistance mutated residues.

## 3.8. Identification of stabilising mutations through NGS sequencing

Next generation sequencing (NGS) offers a robust analysis and quantification tool that provides an in-depth insight into the evolution of highly diverse RNA viral quasispecies (Lu et al., 2020). This method was employed in this project to determine genetic variation that might correlate to the increased thermal stability of #9.

To identify mutations that may confer the capsid thermal stability, aliquots were obtained from five thermal cycles: #4, #5, #7, #8, and #9 and sequenced by NGS (carried out by Helen Fox, NIBSC) (Figure 3.10). The NGS confirmed the presence of the five non- synonymous substitutions within the structural region that were identified by Sanger sequencing (Figure 3.7) (Table 3.1). A non-structural mutation, 3A F12L was suggested to a tissue culture adaptation as this mutation was detected within the wt population before stressing and the mutant #9.3 (Table 3.1). Other non-synonymous substitutions, including N3225D, I1052I, and Q1145L, were found in cycle #4 and #5, but were extinct after (Figure 3.9). Synonymous substitutions were also detected, but as these have not altered the amino acid sequence, they were excluded from further investigation. Genetic changes were also detected within the 5' UTR and 3' UTR In the non-structural region two mutations were found: the 3A A66T and the 3C I157V. The 3A A66T was further investigated as it was found to be associated with the transmembrane domain. The frequency of 3C I157V was low, and it was excluded from further investigation.

## 3.9. Frequency of non-synonymous mutations within the structural protein-encoding region

The analysis of the frequency of the non-synonymous mutations has shown that all of them were detected during earlier cycles of thermal stressing but with different frequencies. Some increased in abundance by repeated cycles of thermal stressing but some remained less frequent even after being stressed repeatedly. Both I3235M and P1246A (tissue culture adaptation mutation) were fixed at early cycles and have the highest frequency as they are presented in >95% of sequences of cycle #4 and the frequency increased through the cycles until it became 99.7% at cycle #9. K1162I was less frequent at cycle #4 but then the frequency of this mutation had increased and presented in 99.9% of #9 sequence. The least frequent mutations were Y1116C and V2085L. V2085L presented in 24.3% of the sequence of cycle 4, and the frequency remained fluctuating through the cycles until it reached 43.1% at cycle 9. Y1116C had the lowest frequency in the sequences of earlier cycles: 2.3% in 4 and 5, but the sequence frequency increased to present in 69.5% of sequence of cycle 9. (Figure 3.10).

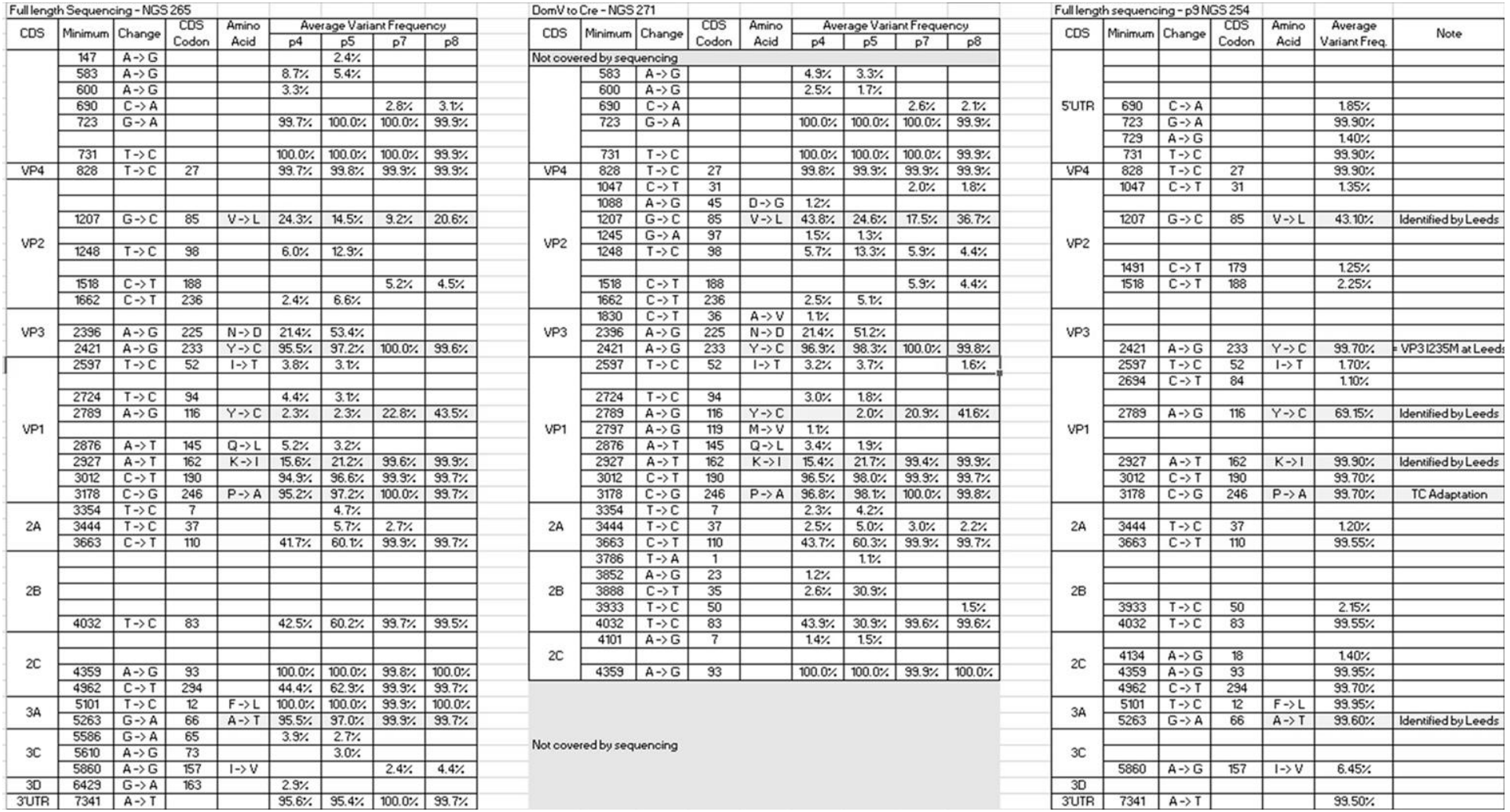

Full length Sequencing - NGS 265

| CDS | Minimum | Change | CDS Codon | Amino Acid | Average Variant Frequency p4 | p5 | p7 | p8 |
|---|---|---|---|---|---|---|---|---|
| | 147 | A -> G | | | | 2.4% | | |
| | 583 | A -> G | | | 8.7% | 5.4% | | |
| | 600 | A -> G | | | 3.3% | | | |
| | 690 | C -> A | | | | | 2.8% | 3.1% |
| | 723 | G -> A | | | 99.7% | 100.0% | 100.0% | 99.9% |
| | | | | | | | | |
| | 731 | T -> C | | | 100.0% | 100.0% | 100.0% | 99.9% |
| VP4 | 828 | T -> C | 27 | | 99.7% | 99.8% | 99.9% | 99.9% |
| | | | | | | | | |
| | | | | | | | | |
| | 1207 | G -> C | 85 | V -> L | 24.3% | 14.5% | 9.2% | 20.6% |
| VP2 | | | | | | | | |
| | 1248 | T -> C | 98 | | 6.0% | 12.9% | | |
| | | | | | | | | |
| | 1518 | C -> T | 188 | | | | 5.2% | 4.5% |
| | 1662 | C -> T | 236 | | 2.4% | 6.6% | | |
| | | | | | | | | |
| VP3 | 2396 | A -> G | 225 | N -> D | 21.4% | 53.4% | | |
| | 2421 | A -> G | 233 | Y -> C | 95.5% | 97.2% | 100.0% | 99.6% |
| | 2597 | T -> C | 52 | I -> T | 3.8% | 3.1% | | |
| | | | | | | | | |
| | 2724 | T -> C | 94 | | 4.4% | 3.1% | | |
| | 2789 | A -> G | 116 | Y -> C | 2.3% | 2.3% | 22.8% | 43.5% |
| VP1 | | | | | | | | |
| | 2876 | A -> T | 145 | Q -> L | 5.2% | 3.2% | | |
| | 2927 | A -> T | 162 | K -> I | 15.6% | 21.2% | 99.6% | 99.9% |
| | 3012 | C -> T | 190 | | 94.9% | 96.6% | 99.9% | 99.7% |
| | 3178 | C -> G | 246 | P -> A | 95.2% | 97.2% | 100.0% | 99.7% |
| | 3354 | T -> C | 7 | | | 4.7% | | |
| 2A | 3444 | T -> C | 37 | | | 5.7% | 2.7% | |
| | 3663 | C -> T | 110 | | 41.7% | 60.1% | 99.9% | 99.7% |
| | | | | | | | | |
| | | | | | | | | |
| 2B | | | | | | | | |
| | | | | | | | | |
| | 4032 | T -> C | 83 | | 42.5% | 60.2% | 99.7% | 99.5% |
| | | | | | | | | |
| 2C | | | | | | | | |
| | 4359 | A -> G | 93 | | 100.0% | 100.0% | 99.8% | 100.0% |
| | 4962 | C -> T | 294 | | 44.4% | 62.9% | 99.9% | 99.7% |
| 3A | 5101 | T -> C | 12 | F -> L | 100.0% | 100.0% | 99.9% | 100.0% |
| | 5263 | G -> A | 66 | A -> T | 95.5% | 97.0% | 99.9% | 99.7% |
| | 5586 | G -> A | 65 | | 3.9% | 2.7% | | |
| 3C | 5610 | A -> G | 73 | | | 3.0% | | |
| | 5860 | A -> G | 157 | I -> V | | | 2.4% | 4.4% |
| 3D | 6429 | G -> A | 163 | | 2.9% | | | |
| 3'UTR | 7341 | A -> T | | | 95.6% | 95.4% | 100.0% | 99.7% |

DomV to Cre - NGS 271

| CDS | Minimum | Change | CDS Codon | Amino Acid | Average Variant Frequency p4 | p5 | p7 | p8 |
|---|---|---|---|---|---|---|---|---|
| Not covered by sequencing | | | | | | | | |
| | 583 | A -> G | | | 4.9% | 3.3% | | |
| | 600 | A -> G | | | 2.5% | 1.7% | | |
| | 690 | C -> A | | | | | 2.6% | 2.1% |
| | 723 | G -> A | | | 100.0% | 100.0% | 100.0% | 99.9% |
| | | | | | | | | |
| | 731 | T -> C | | | 100.0% | 100.0% | 100.0% | 99.9% |
| VP4 | 828 | T -> C | 27 | | 99.8% | 99.9% | 99.9% | 99.9% |
| | 1047 | C -> T | 31 | | | | 2.0% | 1.8% |
| | 1088 | A -> G | 45 | D -> G | 1.2% | | | |
| | 1207 | G -> C | 85 | V -> L | 43.8% | 24.6% | 17.5% | 36.7% |
| VP2 | 1245 | G -> A | 97 | | 1.5% | 1.3% | | |
| | 1248 | T -> C | 98 | | 5.7% | 13.3% | 5.9% | 4.4% |
| | | | | | | | | |
| | 1518 | C -> T | 188 | | | | 5.9% | 4.4% |
| | 1662 | C -> T | 236 | | 2.5% | 5.1% | | |
| | 1830 | C -> T | 36 | A -> V | 1.1% | | | |
| VP3 | 2396 | A -> G | 225 | N -> D | 21.4% | 51.2% | | |
| | 2421 | A -> G | 233 | Y -> C | 96.9% | 98.3% | 100.0% | 99.8% |
| | 2597 | T -> C | 52 | I -> T | 3.2% | 3.7% | | 1.6% |
| | | | | | | | | |
| | 2724 | T -> C | 94 | | 3.0% | 1.8% | | |
| | 2789 | A -> G | 116 | Y -> C | | 2.0% | 20.9% | 41.6% |
| VP1 | 2797 | A -> G | 119 | M -> V | 1.1% | | | |
| | 2876 | A -> T | 145 | Q -> L | 3.4% | 1.9% | | |
| | 2927 | A -> T | 162 | K -> I | 15.4% | 21.7% | 99.4% | 99.9% |
| | 3012 | C -> T | 190 | | 96.5% | 98.0% | 99.9% | 99.7% |
| | 3178 | C -> G | 246 | P -> A | 96.8% | 98.1% | 100.0% | 99.8% |
| | 3354 | T -> C | 7 | | 2.3% | 4.2% | | |
| 2A | 3444 | T -> C | 37 | | 2.5% | 5.0% | 3.0% | 2.2% |
| | 3663 | C -> T | 110 | | 43.7% | 60.3% | 99.9% | 99.7% |
| | 3786 | T -> A | 1 | | | 1.1% | | |
| | 3852 | A -> G | 23 | | 1.2% | | | |
| 2B | 3888 | C -> T | 35 | | 2.6% | 30.9% | | |
| | 3933 | T -> C | 50 | | | | | 1.5% |
| | 4032 | T -> C | 83 | | 43.9% | 30.9% | 99.6% | 99.6% |
| | 4101 | A -> G | 7 | | 1.4% | 1.5% | | |
| 2C | | | | | | | | |
| | 4359 | A -> G | 93 | | 100.0% | 100.0% | 99.9% | 100.0% |

Not covered by sequencing

Full length sequencing - p9 NGS 254

| CDS | Minimum | Change | CDS Codon | Amino Acid | Average Variant Freq. | Note |
|---|---|---|---|---|---|---|
| | | | | | | |
| | | | | | | |
| | | | | | | |
| 5'UTR | 690 | C -> A | | | 1.85% | |
| | 723 | G -> A | | | 99.90% | |
| | 729 | A -> G | | | 1.40% | |
| | 731 | T -> C | | | 99.90% | |
| VP4 | 828 | T -> C | 27 | | 99.90% | |
| | 1047 | C -> T | 31 | | 1.35% | |
| | | | | | | |
| | 1207 | G -> C | 85 | V -> L | 43.10% | Identified by Leeds |
| VP2 | | | | | | |
| | | | | | | |
| | 1491 | C -> T | 179 | | 1.25% | |
| | 1518 | C -> T | 188 | | 2.25% | |
| | | | | | | |
| | | | | | | |
| VP3 | | | | | | |
| | 2421 | A -> G | 233 | Y -> C | 99.70% | = VP3 I235M at Leeds |
| | 2597 | T -> C | 52 | I -> T | 1.70% | |
| | 2694 | C -> T | 84 | | 1.10% | |
| | | | | | | |
| | 2789 | A -> G | 116 | Y -> C | 69.15% | Identified by Leeds |
| VP1 | | | | | | |
| | | | | | | |
| | 2927 | A -> T | 162 | K -> I | 99.90% | Identified by Leeds |
| | 3012 | C -> T | 190 | | 99.70% | |
| | 3178 | C -> G | 246 | P -> A | 99.70% | TC Adaptation |
| | | | | | | |
| 2A | 3444 | T -> C | 37 | | 1.20% | |
| | 3663 | C -> T | 110 | | 99.55% | |
| | | | | | | |
| | | | | | | |
| 2B | | | | | | |
| | 3933 | T -> C | 50 | | 2.15% | |
| | 4032 | T -> C | 83 | | 99.55% | |
| | | | | | | |
| 2C | 4134 | A -> G | 18 | | 1.40% | |
| | 4359 | A -> G | 93 | | 99.95% | |
| | 4962 | C -> T | 294 | | 99.70% | |
| 3A | 5101 | T -> C | 12 | F -> L | 99.95% | |
| | 5263 | G -> A | 66 | A -> T | 99.60% | Identified by Leeds |
| | | | | | | |
| 3C | | | | | | |
| | 5860 | A -> G | 157 | I -> V | 6.45% | |
| 3D | | | | | | |
| 3'UTR | 7341 | A -> T | | | 99.50% | |

**Figure 3.9 NGS results analysis:** Summary spreadsheet showing the mutations that were present in the duplicate PCRs, above 1% for both NGS runs. The second run confirmed the results from the first, but also identified mutations at lower frequency.

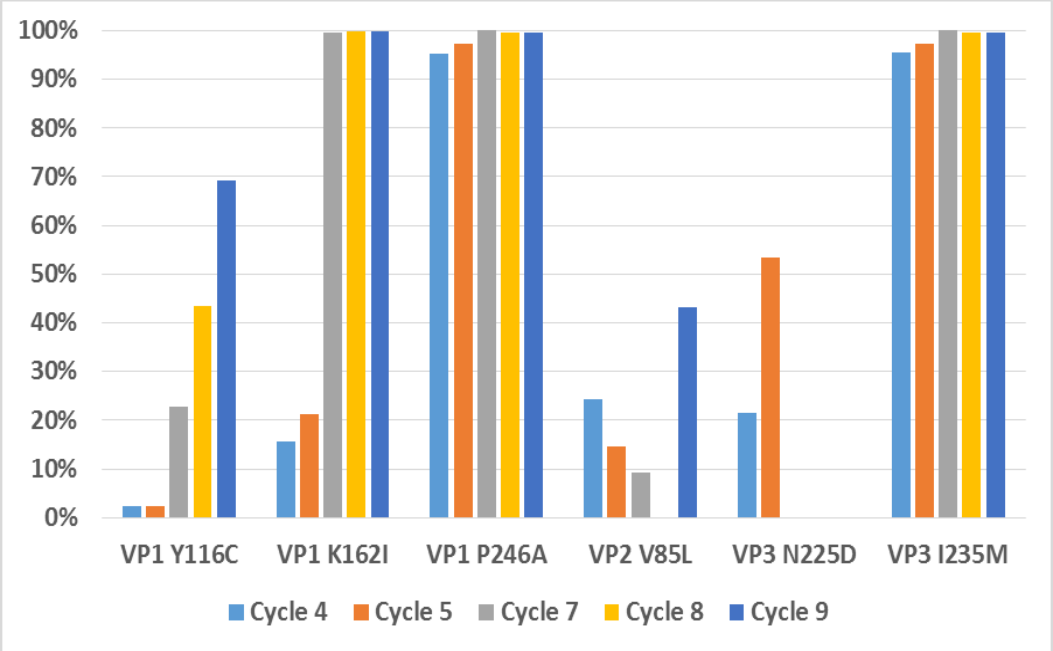


**Figure 3.10 Next generation sequencing results: analysis of five thermal cycles:** The mutation frequency analysis was carried out by NGS over five different thermal cycles #4, #6, #7, #8, and #9. Each cycle is represented by a different coloured bar and shown as percentage. Cycle #4 was represented by light blue, cycle #5 by orange, cycle #7 by grey, cycle #8 by yellow and cycle #9 by dark blue.

## 3.10. Cloning of the nonsynonymous mutations of #9 into EVA71 wild-type infectious clone

To study the role of the five non-synonymous identified mutations found in the structural encoding region P1 in enhancing the thermal stability of #9 capsid, these mutations were incorporated into an EVA71 reverse genetics system with T7 promoter. This wt infectious clone that named pT7-HH-EVA71-IC-B2 was constructed by Dr Natalie Kingston, University of Leeds (see section 2.3.5). Two strategies of cloning were followed in order to insert these mutations. First, each mutated residue was inserted individually into WT-IC by overlap site direct mutagenesis (overlap-SDM). This cloning procedure yielded five recombinant clones each carrying one mutation and, they were named according to the inserted mutation, e.g., V2085L.

The second strategy was aimed to insert all the five identified mutations into wild-type infectious clone. Here, the #9 RNA was isolated, and reverse transcribed into cDNA. The P1 encoding region was amplified by PCR, and then inserted into wt infectious clone by overlap-SDM. This cloning strategy had resulted in two independent clones designated as #9.1 and #9.3. Sequencing showed that both clones comprised three mutations that are: I3235M, K1162I, and P1246A (Figure 3.12) (see method 2.16.3). Interestingly, #9.1 also included the = V2085L mutation that was found in #9 in addition to a novel K2069R mutation. The K2069R has not been detected previously by either sequencing approach, which may indicate that it could have emerged during the cloning process. On the other hand, #9.3 consisted of four mutations: K1162I, P1246A, I3235M, and Y1116C but not V2085L (Figure 3.11). It is important to note that the cloned viruses will be referred to through this study as #9.1 and #9.3, while the VLPs will be termed as #9.1 and #9.3.

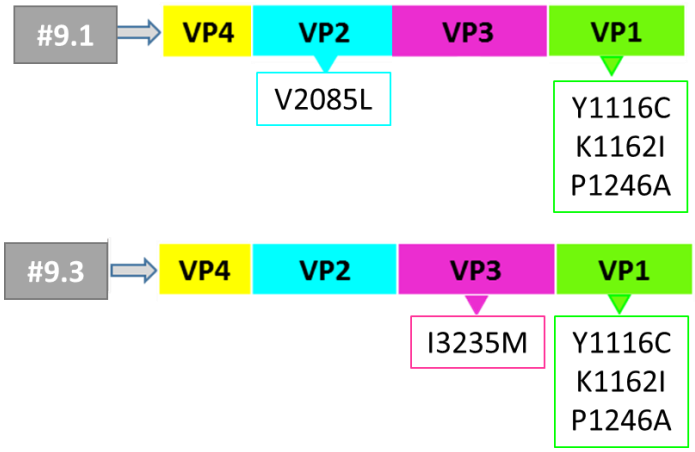


**Figure 3.11 Combined mutations set of #9.1 and #9.3:** Schematic diagram shows the P1 capsid-encoding region of #9.1 and #9.3. The P1 region was extracted from a transcribed cDNA of viral genomic RNA of an infectious virus passaged in Vero cells and inserted into wt infectious clone. The positions of all the identified mutations were indicated on the model of structural proteins. K1162I and P1246A were located in VP1, I3235M in VP3 were common between both mutants. V2085L was in VP2 of #9.1, and Y1116C was in VP1 of #9.3.

## 3.11. Characterisation and assessing the infectivity of #9 mutations.

To characterise #9 stabilising mutations and assessing their infectivity and antigenicity, viruses carrying individual mutation or combined mutations were rescued from constructed reverse genetics systems. The rescue was undertaken by transfecting L929 cells with the *in vitro* transcribed T7 RNA of sequences encoding the capsid stabilised mutants. The transfection was performed in L929 cells as they lack EVA71 receptors to ensure single cycle of infection and minimise the possibility of generating new mutations (Fox et al., 2017).

L929 cell were transfected with *in vitro* transcribed RNA from: wt, #9.1, #9.3, I3235M, K1162I, Y1116C, and V2085L. P1246A was not included as it occurs as a cell culture adaptation mutation and was therefore not investigated further. Cells were collected after full CPE (after 24 hours post transfection (hpt)) to be examined by western blot and plaque assay.

Pelleted cells were lysed with Laemmli buffer to release the intracellular virus, and the viral proteins were examined by western blot. In parallel, another set of rescued viruses in L929 cells was prepared and subjected to a single freeze, thaw cycle. The supernatant was used to measure the virus titer by plaque assay.

Despite a clear CPE bring observed in transfected L929 cells at 24 hpt, no viral protein bands were detected by western blot (figure not included). In order to investigate whether the virus rescue from transcribed T7 RNA was successful, the L929 cell lysate of each mutant was passaged into Vero cells. Clear CPE was observed for each mutant within 3 dpi except #9.1, which was also inconsistence with western blot results (Figure 3.12 A and B).

Further characterisation was carried out by assessing the infectivity of the mutants by plaque assay. All mutants were infectious except #9.1, and they showed no obvious changes in the phenotype as all mutants produced similar plaques in terms of size and shape (no figure included).

| Clone | +CPE |
|---|---|
| Mock | No CPE |
| wt | Day 1 |
| #9.1 | No CPE |
| #9.3 | Day 1 |
| I3235 | Day 1 |
| K1162 | Day 4 |
| V2085 | Day 1 |
| Y1116 | No CPE |

A

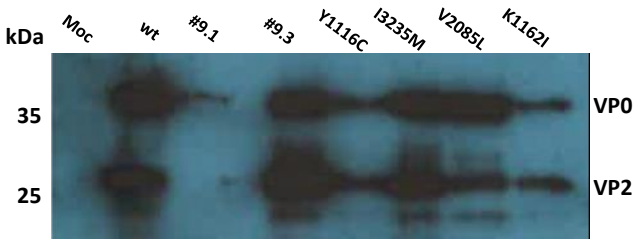


B

**Figure 3.12: The infectivity assessment of rescued viruses of recombinant clones and wild-type infectious clone:** Aliquots of rescued viruses of recombinant clones and wt infectious clone in L929 cell were passaged into Vero cells and incubated for 10 days at 37°C. (A) This table shows CPE development through the incubation period (B) Western blot analysis of viral proteins of passaged rescued viruses detected by mAb 979.

## 3.12. Optimising L929 cells transfection protocol

Failure to detect the viral proteins of the rescued viruses from L929 cells by western blot indicated the need to revise the transfection protocol. One of the possible reasons for inefficient transfection could be related to cell harvesting time. Accordingly, it was important to establish and perform time course and replication kinetics assay to determine the optimum time of cell harvesting. The other reason might be related to the density of cells. Regarding the previous transfection protocol, cells were trypsinised, cleaned and mixed with transfection mixture and plated. The transfection method in general leads to some degree of cell death. Thus, it was necessary to exclude the effect of transfection manipulation on the cell quality and density by simply plating the appropriate number of cells overnight prior to transfection.

## 3.13. Replication kinetics of transfected RNA of EVA71 wild-type and time course of structural viral protein expression in L929 cells (kinetics of RNA transfection)

EVA71 viral replication kinetics and time courses of viral protein expression aims to understand virus pathogenesis and host-pathogen interaction (Lu et al., 2011; Lui et al.,2013). These experiments were performed using different *in vitro* models (e.g., Vero cells), on either virus-infected cells or cells transfected with RNA transcripts. Assessing viral infectivity can be carried out by qRT-PCR to measure levels of intracellular viral RNA (Lu et al., 2011). Plaque assay can also be applied to determine the viral titer (Chang et al., 2019). Here plaque assay was employed as it was used throughout this study.

The aim of performing the EVA71 wild-type viral replication kinetics and time courses of viral protein expression was to determine the optimum time point to harvest EVA71 transfected

cells. A one-step growth curve was established by transfecting L929 cells with wild-type RNA generated by *in vitro* transcription (Figure 3.14 A). The virus titer was measured by plaque assay (Figure 3.14 B).

Samples were collected at: 6, 8, 12, 16, 20, 24, and 36 hpt. The viral titer was measured by plaque assay and expression of viral proteins VP0/VP2 was determined by western blot using mAb 979.

The results of the protein expression (Figure 3.13) have shown that the viral protein VP0 was detected as early as 6 hpt before VP2, which may indicate that the precursor accumulating formed at the early stage of the virus life cycle before the generation of nascent genome required for virion assembly and generation of infectious virions. The synthesis of particles was evidenced by the detection of VP2 that started after 8 hpt in addition to VP0. The protein expression started to increase until it reaches the peak between 16 hpt and 22 hpt and then declined slightly. That would be explained by cell lysis and the release of newly generated virions.

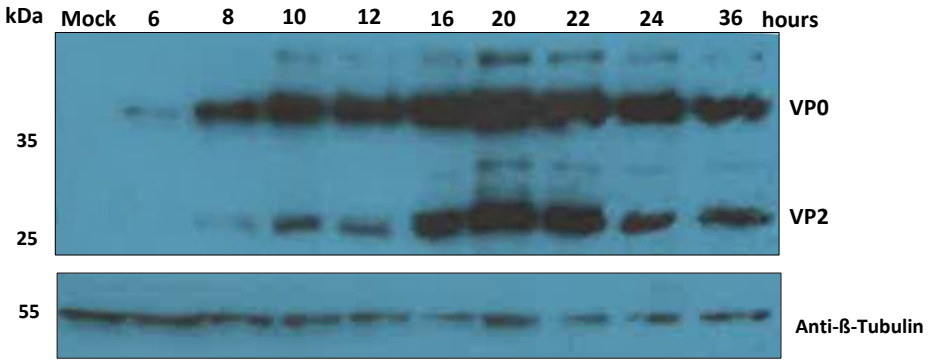


**Figure 3.13 Time course of wild-type EVA71 structural viral protein expression in L292 cells**: 24 well plates were plated with 2 x $10^5$ cells per well and incubated at 37°C overnight. Each well was transfected with 2 µg of RNA of wt EVA71 Samples were collected at 6, 8, 10, 12, 16, 20, 22, 24, and 36 hpt. Cells were lysed with Laemmli buffer and proteins assayed by western blot. Viral proteins were detected with mAb 979. Anti-ß-Tubulin was used as a control for protein loading.

Studying virus infectivity by plaque assay at each time-point has revealed that the generation of infectious virions started 6 hpt (Figure 3.14 A & B). These results indicate the differences in sensitivity of the assays, where mAb 979 appears unable to detect the presence of low-level VP2, while infectious titers as low as 10 pfu/ml were detectable, thus the presence of VP2 can be inferred.

**A**

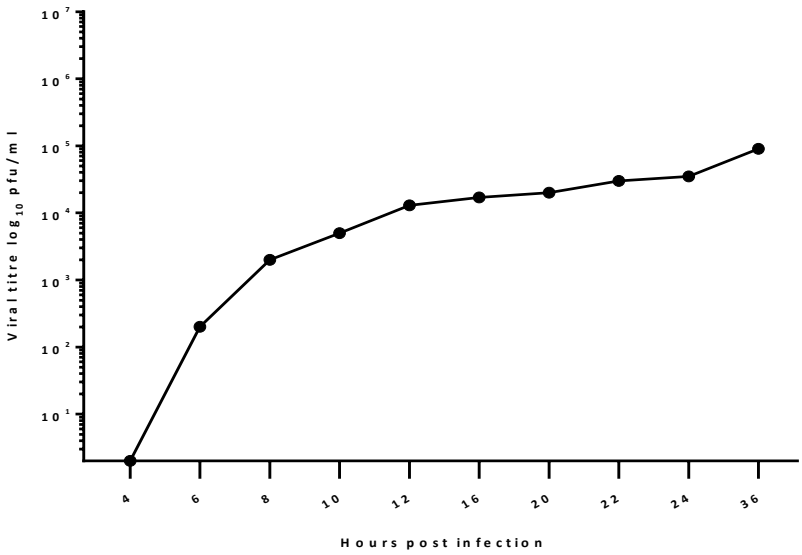


**B**

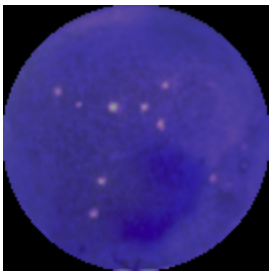

**Figure 3.14 Replication kinetics of wild-type EVA71 in L929cells:** (A) 24-well plates were plated with 2 x $10^5$ cells per well and incubated at 37$^o$C overnight. Each well was transfected with 2 µg of RNA of wt EVA71. First time-point sample was collected 6 hpt. The next samples were collected as follows (8, 10, 12, 16, 20, 22, 24, and 36 hpt). The cells of each time point were subjected to one cycle of freeze and thaw and the infectious virus titer was determined by plaque assay. (B) Plaque morphology of wild-type EVA71 from 36 hpt sample. This experiment is one experiment that was carried out one time (n=1).

## 3.14. Assessing the infectivity of cloned mutants using optimised L292 cell protocol

Another round of T7RNA transfection into L929 cells was undertaken to assess the infectivity of all available cloned mutants after optimising the L929 cell transfection protocol. The transfection was carried out using the same amount of *in vitro* transcribed T7RNA of K1162I, I3235M, Y1116C, V2085L, P1246A, #9.1 and #9.3, and wt.

All the mutants induced CPE in transfected L929 cells at 24 hpt. Transfected cells were harvested, pelleted, and lysed to release viral proteins that was analysed by western blot and SDS-PAGE using mAb979. The virus titer of supernatants was assessed by plaque assay.

As is evident from the results shown in (Figure 3.15 A), all the samples produced bands corresponding to the expected size of capsid proteins VP0 ≈35 kDa and VP2 25 kDa. However, the variation in the intensity of these bands suggested that the mutations, either single mutations or combined mutations exert a different effect on the cleavage and assembly of capsid proteins.

The infectivity of each recovered virus population was assessed by plaque assay (Figure 3.15 B). The data showed that the titer of the viruses rescued in L929 cells were low as mostly none of the rescued viruses titer exceeded a $1 \times 10^4$ pfu/ml. The other observation was that the variants with single point mutations were less infective compared to the wt. The exception was the tissue culture adaptation mutation P1246A, which generated almost a similar quantity of viruses as wt. The mutant #9.1 was infectious but the least infectious with only few colonies $9 \times 10^2$ pfu/ml. In contrast, #9.3 was infectious, but the virus titer

around 5 x $10^4$ pfu/ml was less than the wild-type and P1246A. Plaque morphology of all mutants were like the wt  only the plaque assay of wild-type, #9.1 and #9.3 (Figure 3.15 C)

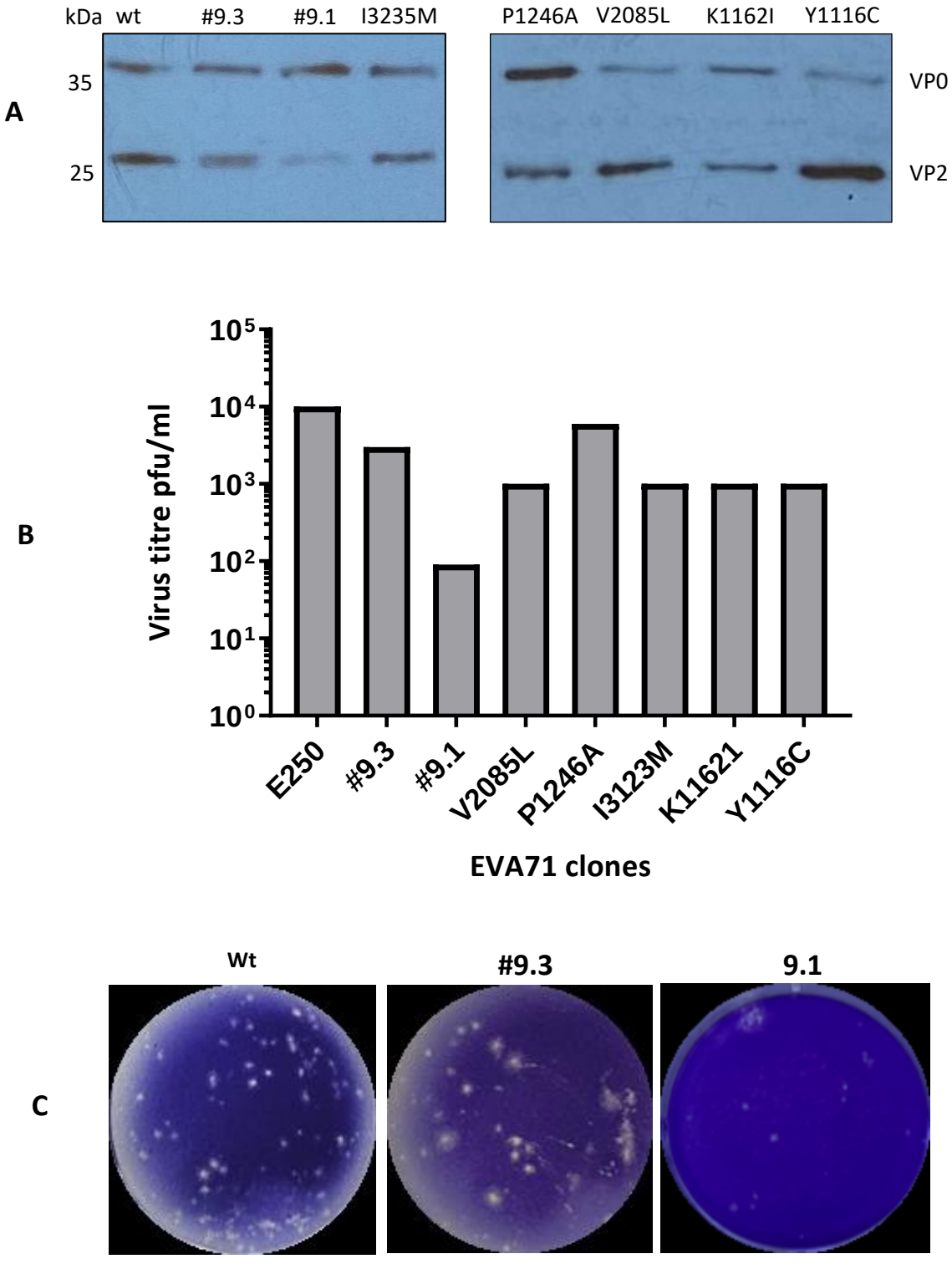


**Figure 3.15 Rescuing cloned and wild-type viruses in L292 cells: (**A) 24 well plates were plated with 2 x $10^5$ cells per well and incubated at 37°C overnight. For each mutants, L292 cells were transfected with *in vitro* transcribed 2 µg of T7RNA. Cells were collected 20 hpt, lysed with Laemmli buffer and examined by Western blot for viral proteins using mAb 979. Anti-ß-Tubulin was used as a control for protein loading. (B) & (C) The plaque assay of EVA71 mutants and wild-type was performed in HeLa cells according to optimised protocol.

## 3.15. Thermal characterisation of selected viruses

To examine the thermal stability of #9.3 against both the #9 and wild-type, aliquots from L929 cell virus pools were thermally stressed for 30 min using the following temperatures (37$^{o}$C, 53$^{o}$C, 55$^{o}$C, and 57$^{o}$C) (Figure 3.16). Samples of wild-type viruses were used as a control. Similar to the thermal characterisation experiment that was carried out earlier to examine the stability of the #9 and #9x5 (in section 3.1.4), the virus infectivity was assessed by plaque assay. The titer of the virus suspension was adjusted to 1 x $10^6$ pfu/ ml. #9.1 was excluded from the experiment as it was impossible to obtain enough titer to carry out this experiment.

The results (Figure 3.16) showed #9.3 was as stable as #9 as it was not inactivated until 56$^{o}$C. In contrast, the titer of EVA71 wild-type was reduced from 1 x $10^6$ pfu/ml at 37$^{o}$C to 1x $10^2$ pfu/ml at 52$^{o}$C. This corresponds to a reduction of ~ 99.99%. The infectivity of #9 was reduced from 1x $10^6$ at 37$^{o}$C to 1 x $10^3$ at 57$^{o}$C. The infectivity of #9x5 was reduced from 1 x $10^6$ at 37$^{o}$C to 1 x $10^3$ at 57$^{o}$C. These results show that both the #9.3 and #9 virus pools have an enhanced stability at higher temperatures in comparison to the wild-type.

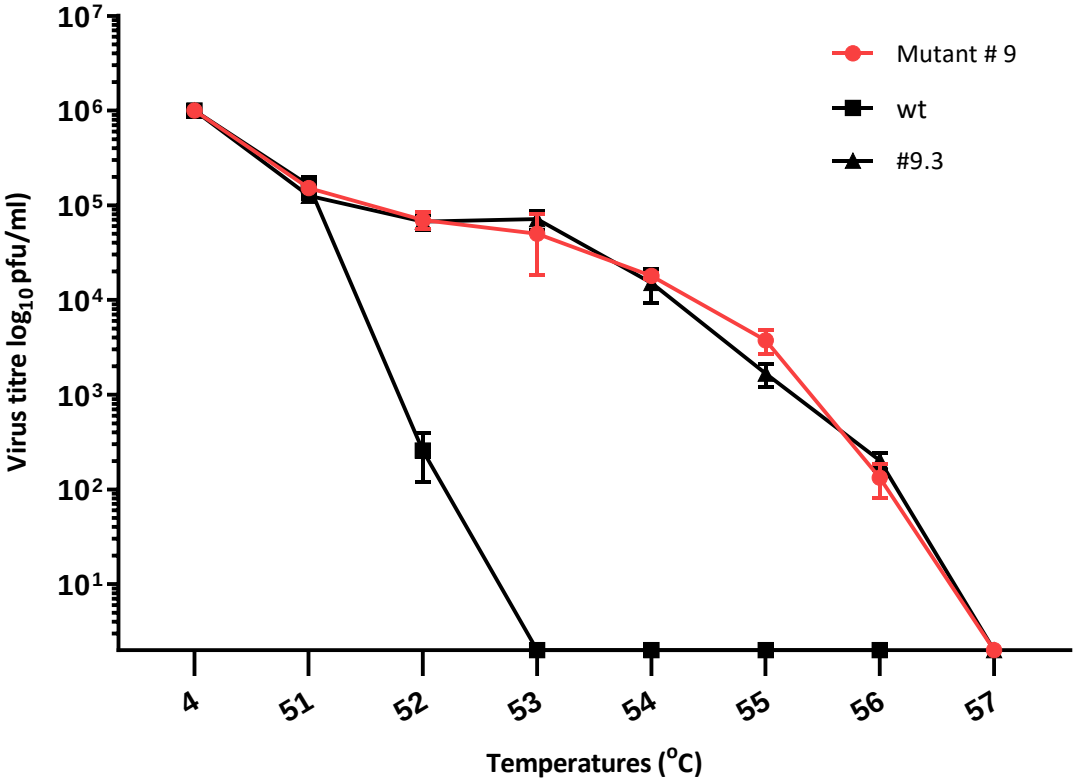


**Figure 3.16 Thermal characterisation of w, #9, and #93*:*** Thermal resistance profile of #9 and #93 virus pools were assessed alongside a wt control. Each virus pool was incubated at a range of temperatures (between 3C and 57°C) for 30 min and cooled to 4°C. The virus titers were determined by plaque assays. The data represent titers of each virus pool at each temperature. This experiment is one experiment that was carried out in triplicate (n=3). Error bars often represent one standard deviation.

## 3.16. Purification of EVA71 viruses #9, #9.3, and wild-type

To scale up production of EVA71 #9, #9.3 and the wild-type were inoculated into 8x T175 with 80-90% cell confluency, HeLa cells was infected with 0.1 MOI of L292 cell rescued viruses. Using an optimised protein purification protocol (provided by Dr Kingston, University of Leeds), harvested viruses were purified in 15-45% (w/v) sucrose gradients by ultracentrifugation at 18,000 xg for 12 hours at 4$^{o}$C. Fractions were collected from the top to the bottom. Each fraction was analysed for by Western blot using anti-VP2/VP0 mAb979 antibody. Bands corresponding to VP0 were distributed across the gradient between fraction 9 and fraction 18. Fractions corresponding to ECs peaked between fraction 11 and 12, while the peak of virus particles was detected lower in the gradient, at fractions 17 and 18 (Figure 3.17). The top fractions contain mostly VP0 with molecular weight ≈ 35 kDa, which indicate a EC. While bottom fractions contained VP2 with molecular weight ≈ 25 kDa, which correspond viral particles. Traces of uncleaved VP0 also appeared in these fractions.

The antigenicity of the fractions was examined by sandwich ELISA using the detection antibodies A9 and CT11F9. Both A9 and CT11F9 have the ability to detect both native and expanded forms of the EVA71 virus particles. However, both preferentially bind to the expanded conformation and neither of them can efficiently detect exclusively native form. Each fraction was evaluated individually, and the reaction to antibodies was consistent with western blot. Here, the antigenicity characterisation has showed that the empty capsid reacted in the wild-type better with A9 (Figure 3.17). However, the virions were not well detected. On the other hand, both virus particles in #9 and #9.3 (Figure 3.18) & (Figure 3.19) have shown a reactivity with CT11F9 in fractions corresponding to both EC and virion, though

A9 appeared to detect ECs almost exclusively. Importantly, both 9# and 9.3# particles reacted similarly to both antibodies.

A

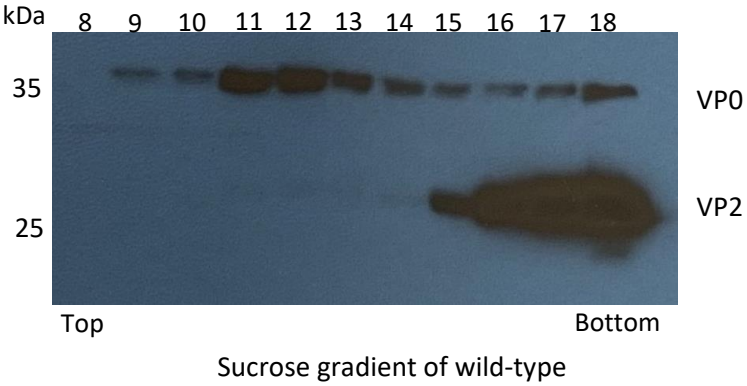


Sucrose gradient of wild-type

B

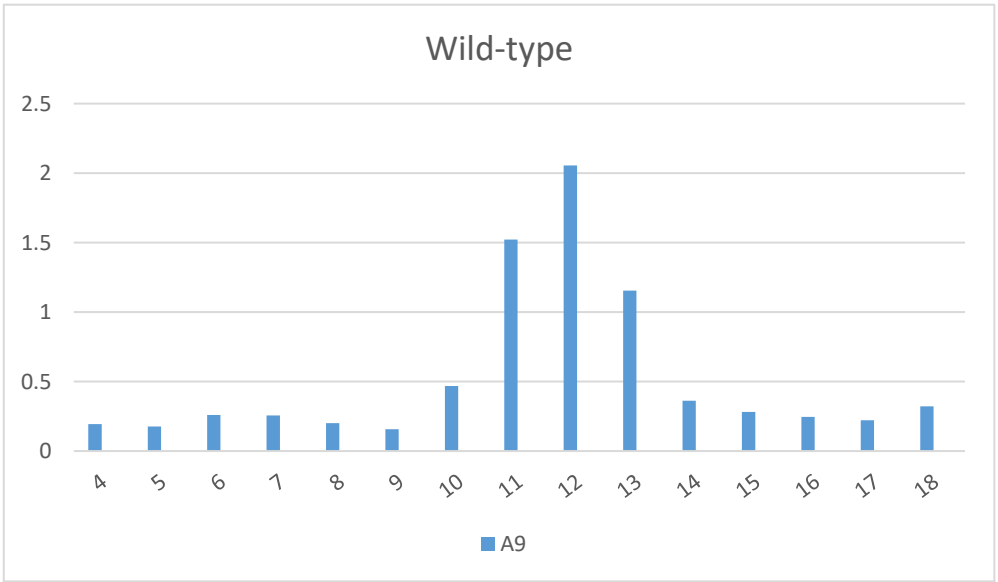


C

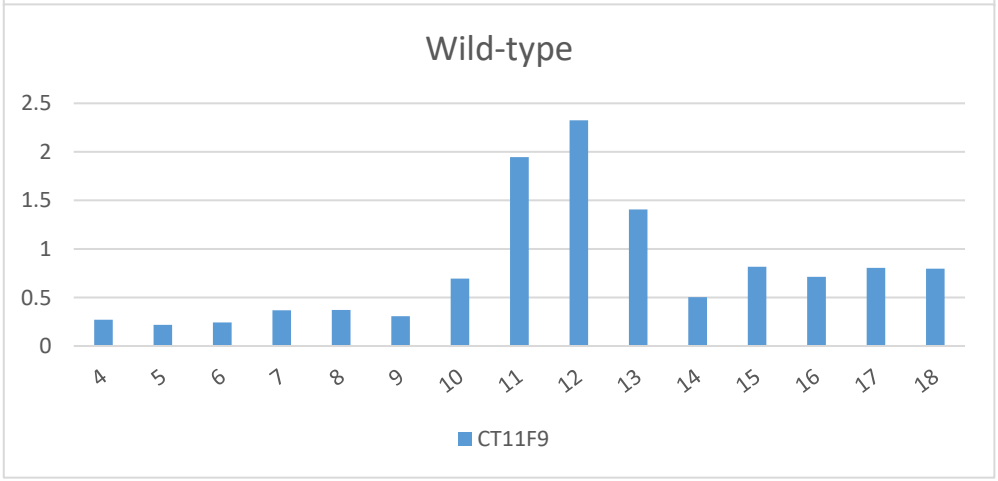


**Figure 3.17 EVA71 wt sucrose gradient (15-30%):** Sucrose gradient analysis of empty capsid and mature virions from EVA71 wild-type. HeLa cells were infected with MOI of 0.1 that equal to $1x10^6$ pfu/ml of L 292 cells rescued viruses. Cells were lysed and viral particles were purified after 72 hours. On 15-30% sucrose gradients. Fractions were collected from the top to the bottom. (A) The proteins were analysed by SDS-PAGE and western blot using VP0/VP2 monoclonal antibody mAb 979. (B & C) ELISA using two monoclonal antibodies A9 and CT11F9 assayed viral particles for antigenicity.

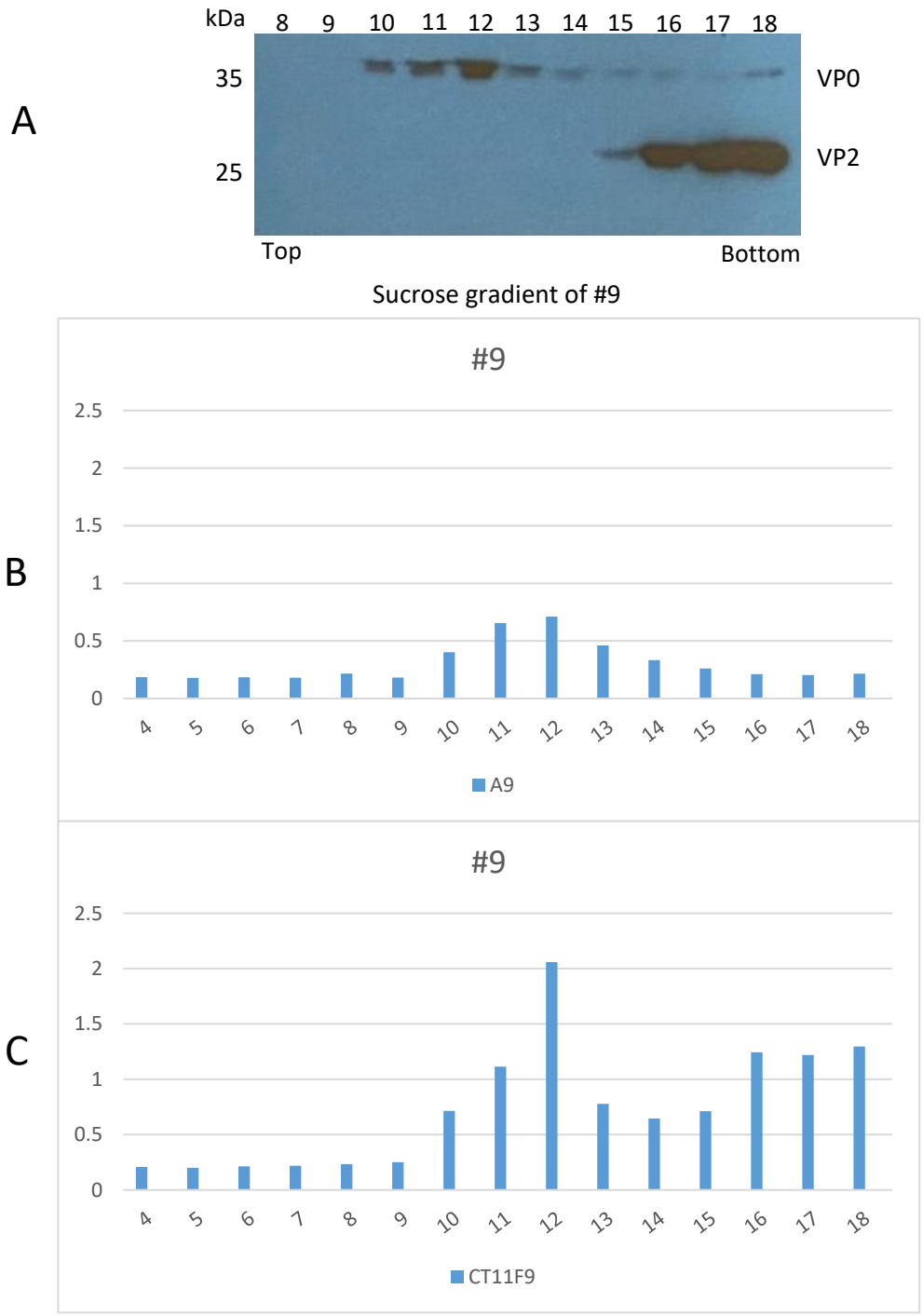


**Figure 3.18 EVA71 #9 sucrose gradient (15-30%):** Sucrose gradient analysis of empty capsid and mature virions from EVA71 #9. HeLa cells were infected with MOI of 0.1 of a $1x10^6$ pfu/ml from L 292 cells rescued viruses. Cells were lysed and viral particles were purified after 72 hours. On 15-30% sucrose gradients. Fractions were collected from the top to the bottom. (A) The proteins were analysed by SDS-PAGE and western blot using against VP0/VP2 monoclonal antibody mAb 979. (B & C) ELISA using two monoclonal antibodies A9 and CT11F9 assayed viral particles for antigenicity.

A

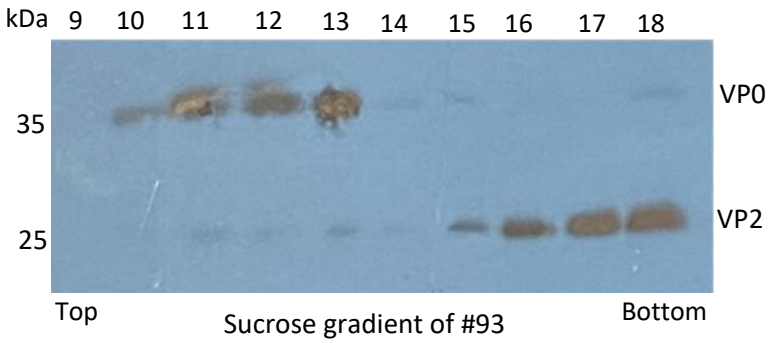


B

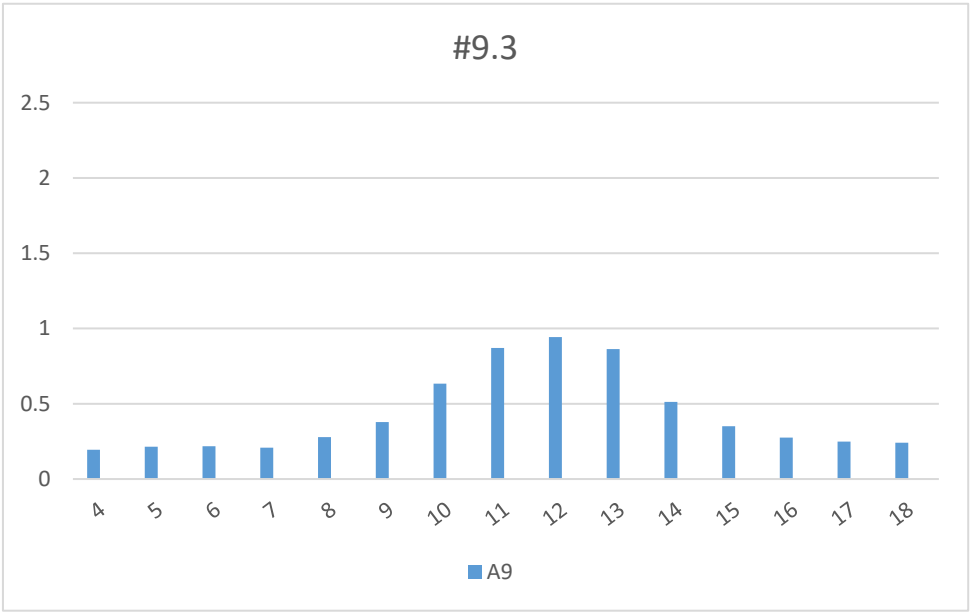


C

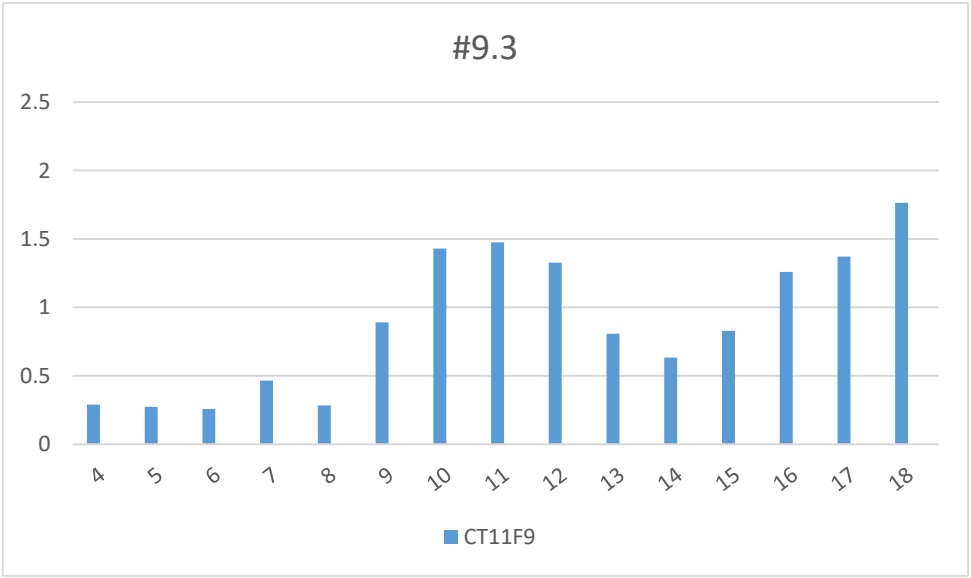


**Figure 3.19 EVA71 #9.3 sucrose gradient (15-30%):** Sucrose gradient analysis of empty capsid and mature virions from EVA71 #9.3. HeLa cells were infected with MOI of 0.1 of a $1x10^6$ pfu/ml from L292 cell rescued viruses. Cells were lysed and viral particles were purified after 72 hours. On 15-30% sucrose gradients. Fractions were collected from the top to the bottom. (A) The proteins were analysed by SDS-PAGE and western blot using against VP0/VP2 monoclonal antibody mAb 979. (B & C) ELISA using two monoclonal antibodies A9 and CT11F9 assayed viral particles for antigenicity.

## 3.17. 3A A66T GFP replicon assay

A66T mutation was detected by NGS sequencing of #9 within the non-structural coding sequence for the 3A. It was detected at early cycles and was maintained throughout the selection process. To study the possible replication effect of this mutation, four GFP replicons were constructed by site-directed mutagenesis by Dr Kingston. They include wild- type polymerase variants G250 (G) and E250 (E), each in the presence of the 3A mutant G A66T (GA) and mutant E A66T (EA). A polymerase knockout (GNN) replicon was also included to assess background fluorescence generated from the translation of input RNA. The clones were handed to Dr Dobson to carry out RNA synthesis and replicon assay. An equal size RNA was synthesised for each replicon (Figure 3.20A) and the transfections were performed in duplicate using lipofectamine 2000 and imaged using the Incucyte S3 every 30 mins (Figure 3.20B). All the replicons showed about

>100,000-fold increase in the number of fluorescent cells per well compared to the GNN. Both mutants replicated at the same level of wt with small variations in replication observed. GA showed a slightly higher replication rate compared to the G, while the EA to have a lower replication rate compared to the E. The experiment was halted at this point and was not repeated.

A

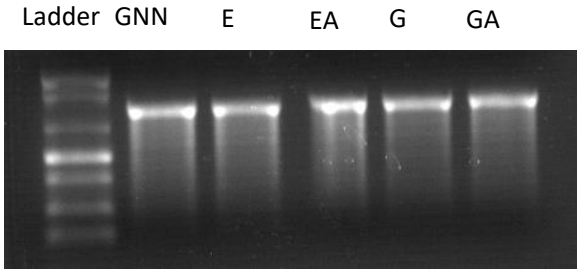


B

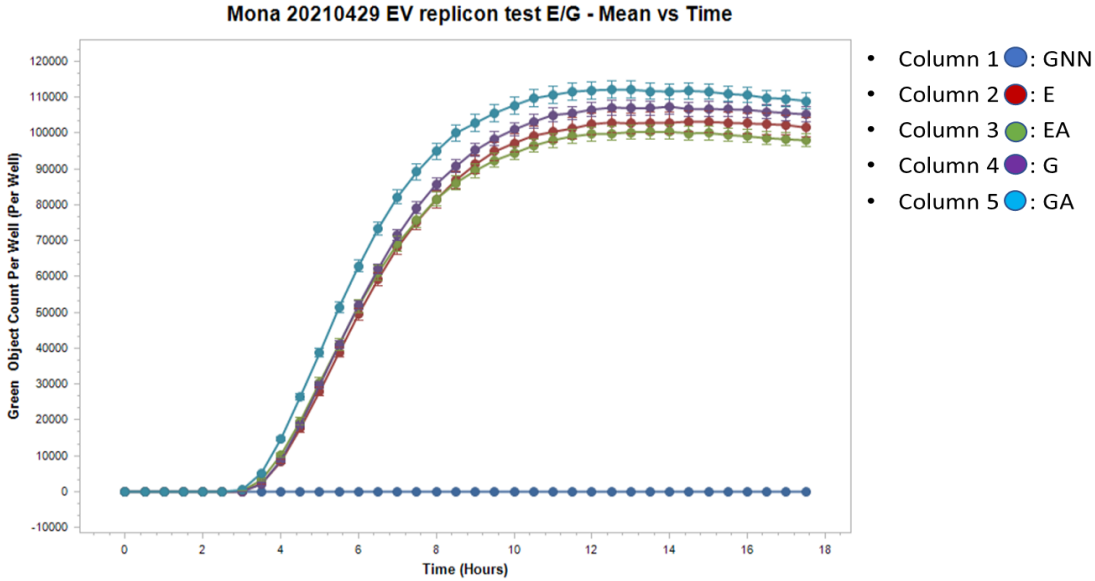


**Figure 3.20 3A A66T GFP replicon assay:** To study the possible replication effect of this mutation, four GFP constructs: wild-type G250 (G), wild-type E250 (E), mutant G A66T (GA) and mutant E A66T (EA). (A) An equal size RNA was synthesised for each replicon. (B) The transfections were performed in duplicate using lipofectamine 2000 and imaged using the Incucyte S3 every 30 mins. This experiment was one experiment that was carried out in duplicate (n=2).

## 3.18. Discussion

The experiments described above aimed, through employing thermal selection, to obtain structurally stable and immunogenic EVA71 ECs that can elicit a potent immune response similar to a native virus. Selection was based upon the ability of EVA71 as RNA viruses to readily adapt to a stressful environment probably by selecting from mutations existing within the viral quasispecies. This strategy allows RNA viruses to resist an antiviral drug, escape the immune system, or persist infection (Domingo et al., 2012; Domingo and Perales, 2018).

After employing successive cycles of heating and passage by using a selection temperature of 52.5$^{o}$C, a thermally stable population of EVA71 virus (termed #9) was generated. The efficacy of the thermal stressing on stabilising the EVA71 capsid was evaluated by allowing #9 to replicate in the absence of thermal selection pressure. The sequencing data showed that #9 exhibited genetic stability as no reversion to the wt phenotype was detected, and there was no evidence of developing new mutations even after being passaged five times at physiological temperatures.

The sequence of stabilised #9 was determined by first Sanger sequencing and then the results confirmed by NGS. The NGS helped to obtain high resolution and detect low abundant variants in the virus population. Several synonymous and non-synonymous mutations were detected in the #9 genome. However, only five of the non-synonymous capsid mutations, which were detected in the structural protein encoding region P1, were incorporated into the recombinant stabilised viruses to be expressed. On the other hand, none of the mutations that were found in 5' UTR and 3' UTR or in the non-structural protein encoding region P3 were selected for further investigation.

The selected mutations were found to be efficient to enhance the thermal stability of the generated viruses, which is a clear indication that the other mutations were not critical for gaining a thermally resistance profile. This observation is contradicting another observation that were made in poliovirus, where non-structural mutations within 2A were required for a thermal-resistance phenotype (Adeyemi et al., 2019). In their study, Adeyemi et al (2019) showed that the selected mutation was complementing the role of the structural mutations in stabilising the PV capsid (Adeyemi et al., 2019).

The five non-synonymous capsid mutations that were identified in the structural protein P1 showed that each mutant consisted of a distinctive set of combined mutations. Interestingly, it was found that #9.1 carries K2069 residue, which is a new mutation that was not detected previously, possibly arisen due to cloning error, which is not uncommon when using a non-proof-reading polymerase, such as reverse transcriptase. Both mutants included K1162I and P1246A (TC adaptation mutation) and I3235M. Mapping the non-synonymous mutations onto capsid structure facilitated a better understanding of their impact on the viral capsid stability. It has been suggested for PV that thermal stability mutations increase the stability of the internal network of the ECs by increasing the internal interactions within the protomers (Adeyemi et al., 2016). However, this seems unlikely be the case here as the mutations detected mostly localise to the external capsid surface.

Previous vaccine research and diagnostic studies have focused on EVA71 VP1, as it is known to be a highly conserved protein that consists of many immunologically relevant epitopes (Zhang et al., 2017). Positively charged residues in VP1 appear to play a significant role in the stability of the virus, or with the interaction with a host cell. Tan et al (2017) demonstrated that positively charged lysine residues K1162, K1242 and K1244 (the latter two

located at the fivefold axis) were essential for heparan sulphate (HS) binding, and they found that the attachment depends on a cluster of such charged residues.

a similar study, and in order to understand the role of VP1, Yuan et al (2016) also performed a charge-to-alanine scanning on all lysine positively charged residues in VP1. They found that some of the positively charged amino acids residues were essential for infectious particle production. However, the change of lysine to alanine in residue 162 in VP1 had not affected the generation of infectious virus particles, and the mutant was replication competent, consistent with results here. They also found that when the lysine in K1215 in the VP1 GH-loop mutated into alanine, a substantial increase in thermal stability occurred, suggesting the possibility of generating a thermostable mutant by altering the charge characteristics of VP1.

The K1162 is located outside the canyon region at the q-3-fold axis; in our study, positively charged lysine at position K1162 was replaced with a non-polar, uncharged, hydrophobic isoleucine (I). The nature of the substituted amino acid may have contributed to the conformational change and might have helped in enhancing the thermal stability of #9. These assumptions could be confirmed by solving the structure of #9.

P1246 is also found in VP1 and is located in the HI-loop around the fivefold axis. The HI-loop in VP1 was found to be essential for PSGL-1 receptor viral interaction, according to Nishimura et al (2013). They showed that mutation in K1242 and K1244 on this loop has led to significant attenuation in PSGL- 1 viral interaction. However, P1246A appears to be a TC adaptation mutation and exhibited no deleterious effect on viral replication or infectivity. Remarkably, in their attempt to study the host-virus interaction, Qing et al (2014) demonstrated that the host

factor cyclophilin A (CypA) regulates viral uncoating through interacting with the conformation of HI-loop of VP1. They suggested that the proline residue located in the HI-loop is essential in the interaction between CypA and EVA71 leading to correct conformation of viral capsid and further virus uncoating. They found that the P1246A was incapable of binding CypA. Proline at this position is conserved$_{130}$ among most of the EVA71 sequences. We suggest that this mutation is tolerated in tissue culture but may not be tolerated *in vivo*. The detection of P1246A mutation in EVA71 drug-resistant strains might be another evidence on the essential role of this mutation in enhancing the virus adaptability. When paired with S1184T mutation, it confers high resistance to MADAL385, which is a novel class of tryptophan dendrimers (Sun et al., 2019). This drug can prevent binding to PSGL-1 and heparan sulphate receptor and block the virus attachment to the cell.

The Y1116 residue is located in VP1 at the external surface of the capsid at the helix. For the Y1116C mutation, tyrosine was replaced with cysteine. This mutation was studied by Brandt and Kolb (2003) during their research with the Herpes simplex virus type 1 (HSV-1). They found that multiple genes are involved in ocular virulence. One of these is the US1 gene that encodes the host range, is an ocular virulence determinant in a strain OD4, and is required for peripheral virulence (keratitis). The US1 encodes the immediate early α22 (IEα22) protein that performs several functions, such as regulating the expression of a subset of HSV-1 genes and regulating the phosphorylation state and localisation of RNA polymerase II. The defective α22 has related to the infectious capacity reduction of the mutant viruses and the latency phenotype alteration of the mutant viruses. They found that the tyrosine at position 116 in the α22 gene is required for ocular virulence of OD4, demonstrating that both

S34A and Y1116C mutations can act independently and affect ocular virulence in strain OD4. The I3235M was one of the mutations found in #9. The I3235 residue is located close to the C- terminus loop of VP3 that is exposed on the virion surface. Loops exposed on the surface are some of the most variable regions of picornavirus virions and form neutralising immunogenic sites (Plevka et al., 2012). The replacement of isoleucine with methionine may enhance the stability of the loop since it can create a Met-aromatic motif and can stabilise protein-protein binding interactions (Valley et al., 2012; Aledo, 2019).

Methionine can also form hydrogen bonds similar to cysteine due to the sulphur (Mundlapati et al., 2015). The possible stability created by methionine may affect the interaction of the loop with other loops and hence leading to stability enhancement by unknown mechanisms. The V2085 residue in the α-helix within VP2 is exposed on the surface and known as a poor helix forming residue (Gregoret and Sauer, 1998). The positioning of valine at this location could suggest possible localised flexibility that is required by the virus to allow expansion at the 2-fold axis required for genome release. This flexibility might be transformed into rigidity by replacing the valine with leucine that can generate strong bonds (Moitra et al., 1997).

The K2069 residue was found in the β-sheet of VP2 and was replaced by arginine in #9.1, though this mutation was never detected in the #9 virus population. Both the lysine and arginine are positively charged residues usually found at protein surfaces and have an essential role in protein stability (Sokalingam et al., 2012). However, as arginine residue may improve the stability of the protein structure by forming electrostatic interactions such as creating salt bridges. This mutation was only detected after cloning the recombinant #9.1 that was not included in further investigation as it showed extremely low infectivity.

More investigation could be undertaken in the future to understand the reasons behind that defect. In the view of mapping the location of each non-synonymous mutation, it could be concluded that identified mutations were located in positions that are critical to the virus capsid expansion and antigenic stability. According to Kingston et al (2022), the presence of V2085L mutation residues in proximity to the helices at the 2-fold axis, and Y1116C and I3235M atop the canyon, in addition to presence of K1162I at the q3-fold axis, may play an essential role in the antigenic shift from a native to expanded state. This hypothesis is emphasised by acknowledging that the capsid expansion requires the expansion at the 2-fold axis to externalise the VP4 and the genome, and the expansion at the q3-fold axis to externalise the VP1 N-terminal region. The expansion also requires the expulsion of stabilising lipid with the pocket factor located in VP1.

The NGS analysis of different viral populations obtained from different thermal cycles has elucidated the dynamics of molecular evolution of EVA71 over the cycles of thermal stressing. By this approach, emergence and accumulation, or disappearance of mutations, were tracked effectively over the course of the thermal stressing experiment. The data analysis showed that all non-synonymous mutations have emerged during the initial thermal cycles. But some of them were fixed directly, while others accumulated gradually. The early fixed mutations were found to dominate the final virus population #9. These mutations were P1246A in VP1 and I3235M in VP3. Both were emerged and fixed at early thermal stressing cycles and dominated the final cycle #9. Another mutation was K1162I in VP1, which also emerged early but was fixed later. Interestingly, these three beneficial mutations were found in both #9.1 and #9.3, which agrees with the mutation frequency analysis. Their role requires

further investigation, but it can be suggested that they might functions co-operatively as with compensatory mutations. It also could be concluded that the viral population of #9 was not diverse since the same nonsynonymous mutations were detected by Sanger sequencing and NGS.

The viral evolution pattern that was observed here was previously described by Morley and Turner (2017). They found that when a virus population experiences a sudden change in their environment, beneficial mutations tend to be more readily fixed early in contrast to the less beneficial mutations. They said that the clustered mutations were more readily fixed than a single mutation. In general, this pattern changes if the environmental changes occurred gradually.

The impact of each mutation on infectivity tested. All virus clones harbouring single mutation were infectious, but the virus titer was varied among them. The #9.3 was infectious but the #9.1 was either not infectious or the titer was extremely low. That could be related to one of the mutations, or the combined mutations, has conferring a high stability on the capsid that might affect the uncoating of the virus. The affected infectivity of #9.1 mutant might be an indication of an extremely stable capsid.

Compared with the same study on PV, the selection was carried out through one set of successive thermal stressing cycles that resulted in a significant viral adaptation. That may indicate a rapid and profound adaptation behaviour exhibited by EVA71, which could be applied to other enteroviruses to select thermally stable strains.

The finding of this study was different from previously obtained results by Kelly (2015). Kelly's

research and the current project have used the same strain to carry out the thermal stressing experiments. The mutations detected by Kelly (2015) were V1179A and viL1183V in the pocket of VP1. None these mutations were found in the current project despite applying a similar method of thermal stressing, which might indicate the vast virus population of EVA71 quasispecies, and multiple possible mechanisms for inducing thermal resistance. Hypothetically, these observations may help to understand some characteristics of the thermal response of EVA71 that may lead to predictable thermal resistance dynamics. Thus, shedding light on the mechanism of how the virus evades the host immune system and be able to establish persistent infection.

Primarily, the effect of stabilising mutations on the antigenicity of wt, #9, and #9.3 was investigated by assessing the antigenicity of their purified ECs and virions using sandwich ELISAs with A9 and CT11F9. These monoclonal antibodies were able to detect both antigenic forms: the NAg and HAg. However, the variation in reactivity to these antibodies between the viruses and the ECs may provide some hints on the antigenic content of the fractions. All the viruses showed a better reactivity to the CT11F9 comparing to A9. Moreover, ECs were more reactive to both antibodies than the virions in all viruses. Given the relative abundance of VP0/VP2 detected by western blot, this suggests both antibodies have a binding-preference for the HAg state. As was expected both #9 and recombinant virus #9.3 show a similar antigenicity indicating similar conformation. Though the uncertainty of these results emphasised the need to develop an antibody able to detect the NAg.

Sequencing the non-structural coding region of #9 showed the occurrence of a mutation (A66T) in the 3A encoding region. The A66T mutation arose at early cycles of thermal stressing

and was maintained throughout selection cycles. It seems that there is no significant effect of this mutation on replication despite the small variations that were observed, which may occur due to a variation in the experiment itself. This result, in addition to the fact that this mutation or other non-structural mutations was not included in #9.3 clone, it could be concluded that it has no contribution to #9 thermal resistance (Kingston et al., 2022). The contribution of mutation beyond the capsid region to stability of the capsid was studied by Adeyemi et al (2018). They showed that a mutation that was arose in 2A protease slowed the kinetics of viral polyprotein processing, which may improve the correct folding of the mutant capsid precursor protein to permit virion assembly.

The thermal characterisation and antigenic characterisation have suggested that the #9.3 is the ideal candidate for VLP generation. #9.3 will be synthesised using recombinant techniques to express the P1 structural protein precursor and a protease. There are many expression systems that could be used (e.g., insect cells, *Pichia pastoris*, or mammalian cells) (Wang et al., 2016; Zhang, C. et al., 2015), as described in the next chapter.

# Chapter 4

# Results

## EVA71 VLP expression and characterisation

## **4.1.** Introduction

In the previous chapter, a thermally stabilised mutant virus termed #9.3 was obtained through a series of thermal stressing experiments. The capsid mutations present in this mutant were used to inform the synthesis of possible stable VLPs by extracting the P1 region of the mutated virus and cloning the sequence into a suitable vector for co-expression with the viral protease. The antigenicity of generated VLPs was assessed, while the immunogenicity testing is not part of this project (Figure 4.1).

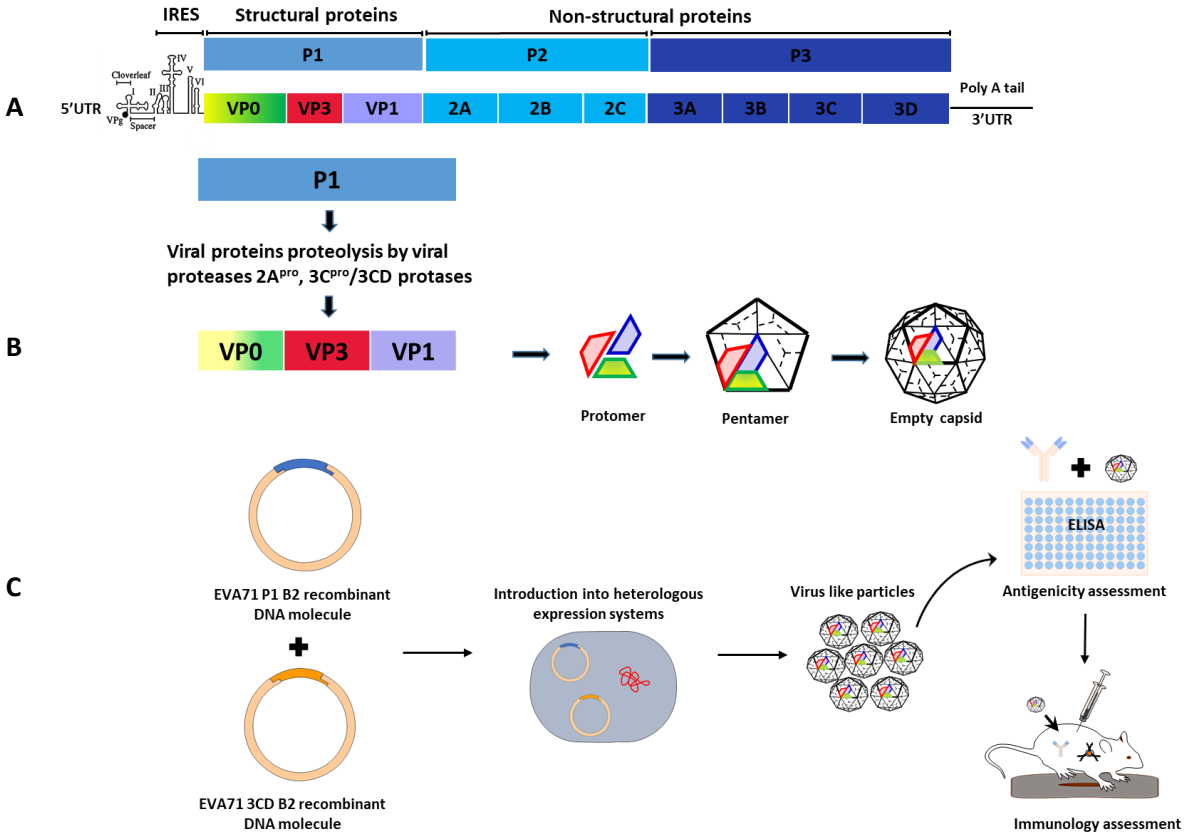


**Figure 4.1 EVA71 VLPs genome and co-expression system:** (A) Schematic representation of EVA71 empty capsid genome that comprises structural P1 region that consist of VP1, VP3, and non-cleaved VP0. It also shows the two non - structural regions: the P2 region and the P3 region, that includes the 3C protease that is needed for P1 processing. (B) Schematic diagram shows the P1 region proteolysis with 3C and the assembly of capsid protein subunit. (C) Schematic of co-expression flow of VLPs in mammalian cells, which achieved by the co-expression of two independent vectors cloned with P1 and 3C protease.

## 4.2. Virus-like particles (VLPs) and VLP vaccines

VLPs can self-assemble from virus capsid proteins but are unable to replicate and are non-infectious as they are devoid of genetic material (reviewed in Vicente et al., 2011). These particles can present a highly structured construct with a high antigenic and structural resemblance to the native virus (Dong et al., 2014). Mimicking the native structure and displaying repetitive high-density surface epitopes allows the VLPs to elicit a potent immune response (Nooraei et al., 2021).

VLP vaccines possess a high safety profile, are highly stable and highly immunogenic. Also, they can be manufactured on a large-scale at an affordable cost (reviewed in Vicente et al., 2011). Consequently, they can be optimal vaccine vehicles that can overcome the limitations of attenuated or inactivated vaccines while being equally efficient.

VLP can be produced in different expression systems such as bacteria, insect cells, plant cells, yeast, mammalian cells, and cell-free expression systems (reviewed in Tariq 2022). Multiple factors determine the selection of an appropriate expression system, as each system has advantages and disadvantages that must be considered (reviewed in Vicente et al., 2011). VLP expression systems may differ in their ability to express VLPs, for instance mammalian cells are preferred to express proteins from enveloped viruses over yeast. They also differ in their ability to perform protein folding and post-translational modification, e.g., glycosylation, phosphorylation, or disulphide bond formation, these properties may ultimately affect the immunogenicity of VLP vaccines. Simple non-enveloped VLPs can be expressed in both eukaryotic and prokaryotic systems, e.g., human papillomavirus (HPV) VLPs formed from a single capsid protein. However, the generation of complex VLPs with multi- capsid components are more challenging and usually expressed in eukaryotic expression systems

such as yeast or insect cells. Another consideration is the ability to produce contamination-free products during the large-scale purification. The contaminants are usually cell debris, DNA, lipid and proteins derived from host cells. In some cases, further treatment might be required, which might affect the antigenic structure of the VLPs themselves. Other factors also should be considered, such as cost, yield and ease of system manipulation. Another critical factor is contamination with biologically compatible zoonotic viruses.

## 4.3. VLP vaccine expression platforms

### 4.3.1. Bacteria

The bacterial cell has been the most widely used system to produce recombinant proteins and many non-enveloped VLPs. However, it is not preferred to produce enveloped VLPs (eVLPs) as this system cannot perform post-translational modification such as glycosylation. The non-enveloped VLPs expressed in such a system are simple structures with one or two proteins. In developing countries where the cost of developing vaccines is a burden, bacteria are seen as a safe and cost-effective expression systems. They can be cultivated without expensive media and production can be scaled up easily. However, bacteria such as *E.coli* have some drawbacks, such as endotoxin contamination and it can be challenging to express large protein (reviewed in Nooraei et al., 2021; Tariq et al., 2022).

### 4.3.2. Baculovirus/insect cells (B/IC)

The B/IC system is a eukaryotic system used extensively to express enveloped and non-enveloped VLPs. The baculovirus-insect cell line has several advantages, production of high cell density cultures and high yields of expressed proteins. Also, the most critical factor is their ability to perform post-translational modification and attain protein folding. The most well used insect cell line is the *Trichoplusia ni* High Five™ (Hi5) cells. *Spodoptera frugiperda* (Sf9)

are also used as they are easy to manipulate and can achieve high density VLPs (reviewed in Nooraei et al., 2021; Tariq et al., 2022).

EVA71 VLPs have been produced in insect cells. EVA71 recombinant baculoviruses (Bac-P1 and Bac-3CD) were constructed and proteins were coexpressed in Sf9 cells resulted in successful self-assembly and expression of EVA71 VLPs. However, the yield was low but was improved in further studies (Hu et al., 2003; Lin et al., 2015).

There are drawbacks of using this expression system: first, the co-produced enveloped baculovirus particles complicate the purification process. Their removal can necessitate complex procedures to provide high-grade VLP preparations.

### 4.3.3. Plant cells

Plant cells have demonstrated a great potential for recombinant protein expression and the expression of both enveloped and non-enveloped VLPs. Plant cells have many advantages over other expression systems (reviewed in Tariq et al., 2022). They have a high expression level, high performance, are cost-effective, free from mammalian pathogens, and have low contamination risk. However, the essential features are that their eukaryotic processing machinery can perform post-translational modification similar to those in mammalian cells. Unlike mammalian cells, plants have a simple N-glycan processing pathway and no O-glycosylation. However, mammalian cells require significant genome engineering to produce more uniformed glycans. In contrast, genome editing is required to achieve that in the plant. The introduction of the novel N-glycan and O-glycan *Nicotiana benthamiana* was tolerated quite well. Polio VLPs have been produced successfully in plant cells. Although this technique is cheap, none of the expressed VLPs have reached the commercialized standard yet (Schoberer and Strasser, 2018).

### 4.3.4. Mammalian cells

Mammalian expression systems remain the most favorable choice to produce multiple structural proteins of both non-enveloped and enveloped VLPs (Bahar et al., 2021). Animal cell expression platforms can efficiently perform post-translational modifications essential for protein folding and glycosylation. Also, the expressed proteins in mammalian cells have structural similarities and biochemical properties to parental or native proteins derived from mammalian pathogens. This system can grow to a very high cell density and scale-up. Vero cell lines have been used to synthesize EVA71 VLPs (Liu et al., 2011). However, the mammalian system has many disadvantages such as low protein yield, high production cost, the media is expensive, long-expression time, cells can be difficult to transfect. They are susceptible to contamination with clinically relevant pathogens, and the purification is complicated (reviewed in Nooraei et al., 2021; Tariq et al., 2022).

### 4.3.5. Yeast

Yeast is a recombinant protein expression system frequently used for VLP generation. This system can be used to produce enveloped and non-enveloped VLPs. They are relatively easy to cultivate and manipulate (Kim et al., 2017). They also can grow rapidly, have a high yield, cost-effective production, and have a low level of contamination; thus, their purification process is more straightforward. Furthermore, yeast cells can perform complex post-translational modification including glycosylation. Moreover, the high fermentation abilities of yeast allow the large-scale expression of VLPs. One of the limitations of this system is that the yeast post-translational modification of proteins is different from mammalian cells, in particular glycosylation, in which high density mannose is favoured over the addition of more complex, branched glycans.

## 4.4. Cell-free protein synthesis (CFPS) system

The cell-free protein synthesis (CFPS) system or cell-free gene expression (CFE) is an *in vitro* protein expression system that emerged as an alternative approach to *in vivo* or cellular expression systems (reviewed in Gregorio et al., 2019; Garenne et al., 2021). This approach is a simple, rapid, effective expression tool consisting of essential cellular machineries and substrates that are required for generating required proteins. In the absence of the actual cell, the chances of contamination with biological materials are less, and the generated proteins are free from toxic protein or unnatural amino acids, making CFPS a powerful tool in biological research.

The CEPS was employed to produce different proteins, virus assembly, metabolic engineering, therapeutics, antibodies, and VLPs production. By applying CEPS technology, the environment where desired VLPs are produced is better controlled, thus offering the production of VLPs free from host-derived contamination that may result in unpredictable immune responses. The CFPS system is a single tube experiment based on exploiting the components from crude cellular lysates of *E. coli,* rabbit reticulocytes, or insect cells (reviewed in Khambhati et al., 2019). To prepare the crude cell lysate, cells overnight grown are harvested after reaching a specific optical density and then sonicated to disrupt the cell membrane to release the cells contents. The lysate is further buffered to adjust the pH and mixed with essential growth material such as amino acids, nucleotides, substrates, cofactors, energy sources and DNA (linear or plasmid). Combining *in vitro* VLP assembly with CFPS offers excellent potential for a safe, efficient technology for vector VLP vaccines. However, the process of in vitro VLP generation may vary between different viral capsids, and the production conditions need to be optimised for each VLP candidate to increase the yields and improve VLP assembly.

However, the potential of *in vitro* VLPs needed more research. The disadvantages of this system are high cost and limited scalability. The high price of CFPS systems can be reduced by regenerating energy and cofactors (Woodyer et al., 2006).

## 4.5. Production of recombinant EVA71 VLPs

The EVA71 genome encodes the structural P1 region, which is proteolytically processed into VP1, VP3, and VP0 that can self-assemble into empty capsids (Yuan et al., 2018a). The EVA71 genome also encodes non-structural encoding regions P2 and P3. To overcome the small size of their genome, RNA viruses such as PV and EVA71 encode precursor polyproteins within these regions. These proteins are multifunctional as they can shut down host cell functions to favour of viral replication, and they are also participating in virus multiplication. Moreover, the processing of these proteins will result in subset of proteins that exhibit a different activity from the precursor. Both $3C^{pro}$ and its precursor 3CD play important roles in processing of the EVA71 structural polyprotein into mature products during viral morphogenesis. In addition, $3C^{pro}$ can shutdown host-protein synthesis, and is known to be cytotoxic to cells, this is particularly apparent when carrying out recombinant protein expression. The 3CD precursor retains P1-specific proteolytic activity but is less toxic to cells.

In this study, mammalian and yeast expression of VLPs was carried out by the co-transfection of two independent vectors; one carries the P1 structural polyprotein precursor and the other provides the 3C protease (or its precursor 3CD) necessary for P1 processing. During the co-expression the precursor EVA71 structural polyprotein P1 is cleaved by 3C/3CD to form structural capsid proteins VP1, VP3, and VP0 (Figure 1B).

## 4.6. Expression of EVA71 VLP in mammalian cells

EVA71 VLPs have been expressed in different platforms such as yeast cells (Li et al., 2013), insect cells (Chung et al., 2006), and mammalian cells (Tsou et al., 2015). It is essential to optimise several variables of the process to ensure efficient production in terms of the yield and purity of the desired proteins. The parameters include expression vector design, cell expression type, and 3CD levels to balance processing and toxicity. Variable also include the cultivation time, temperature, growth medium and purification method (Jeong and Seong, 2017). For the work described here, HeLa cells were selected to express recombinant EVA71 VLPs. This cell line has been used as an effective viral host in many virological experiments and structural studies (Khan, 2013), as was used to cultivate EVA71 viruses through this project. Producing proteins in mammalian cell lines offers a native-like transcription and translation environment similar to where the native virus is originally processed. Such an environment should allow efficient protein folding and particle assembly to resemble the native structure more closely (Almo and Love, 2014; Khan, 2013).

Similar to PV, EVA71 produces two different types of particles with distinct antigenic structures (Le Bouvier, 1959; Marsian et al., 2017 ; Bahar et al., 2021). The virus particles exist in N-Antigen (NAg) native conformation or H-Antigen (HAg), which is the expanded non-native conformation. Both EVA71 particles with NAg form and HAg form can induce neutralising antibodies, unlike PV where the HAg form particles are unable to induce neutralising antibodies. Overall, this study aims develop VLPs that have enhanced native antigenicity. This hypothesis was first examined by estimating the proportions of NAg and HAg particles in the mammalian expressed EVA71 VLP preparations.

## 4.7. Mammalian cell expression and purification of EVA71 VLPs

To express recombinant EVA71 VLPs in HeLa cells, the P1 regions of the #9.3 and wild-type or the 3C region were introduced into the pCAGGS vector. Prior to large-scale co-expression, optimisation of parameters that influence the expression in mammalian cells was undertaken. These parameters include the co-transfection ratio of 3C and P1 and the VLP harvesting time.

## 4.8. Optimisation of P1-3C co-transfection ratios

Previous studies have reported the expression of EVA71 VLPs and other enterovirus VLPs by co-expression of the viral capsid precursor P1 and the viral protease 3C. However, 3C can trigger cell apoptosis and can be toxic to the cells. The toxicity of the 3C can be attenuated by manipulating the relative expression efficiency of 3C protease. Here, the attenuated toxic activity of 3C was approached by balancing the 3C to the P1 plasmid ratio during plasmid co-transfection.

An initial small-scale experiment was conducted to optimise the ratio of 3C to P1 for co-transfection for later large-scale production. The experiment was performed in a six-well plate seeded with $1x10^6$ cells/well HeLa cells. The co-transfection was carried out by changing the added 3C plasmid ratio while maintaining the level of P1 plasmid constant. Cells were collected after 72 hours.

The optimum 3C to P1 ratio was determined by the examination of the VP0 band intensity on western blot film (Figure 4.2) using the anti-VP0-VP2 mAb 979 antibody. It was found that an equal amount of both plasmids (1:1) is the optimal co-transfection ratio. This ratio was used for optimisation of harvesting time and later for large scale production.

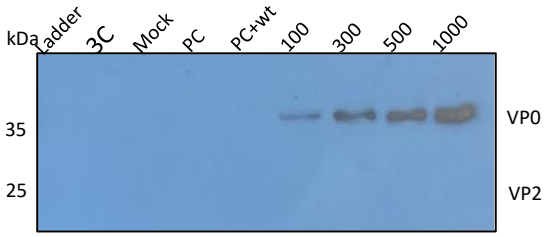


**Figure 4.2 Optimisation of 3C/P1 ratio in HeLa cells:** The optimisation was carried in six-well plate seeded with HeLa Ohio cells and incubated overnight. Each well was transfected with certain concentrations of 3C: 100 ng/µl, 300 ng/µl, 500 ng/µl, 1000 ng/µl. The concentration of each 3C inoculum was corrected to equal 1000 ng by adding relevant amount of pCAGGS concentration, which were respectively 900 ng/µl, 700 ng/µl, 500 ng/µl, and 1000 ng/µl. The wild-type concentration was (1000 ng/µl). Four controls were included: 3C control, Mock, pCAGGS vector, pCAGGS vector + wt. Cell lysate of each ratio was collected at 72 hours and analysed by SDS-Page and western blot using primary anti-VP0-VP2 MBA979 and HRP anti-mouse secondary antibody. A representative image shown. This experiment is one experiment that was carried out in triplicate (n=3).

## 4.9. Optimisation of VLP harvesting time

A time-course assay was performed to define the optimum time-point to harvest the highest yield of expressed VLPs through studying the kinetics of protein expression. HeLa cells were transfected at a 1:1 ratio of 3C and P1 expressing plasmids. Cell lysates and supernatants were harvested after 24, 48 and 72 hours and analysed via western blot with anti-VP2/VP0 mAb 979. Anti-α-tubulin antibody was used as a loading control. VP0, was detected at 24 hours post-transfection and protein signal reached the maximum at 48 hours without further increase at 72 hours, suggesting 48 hours is a suitable timepoint to harvest mammalian-expressed samples (Figure 4.3).

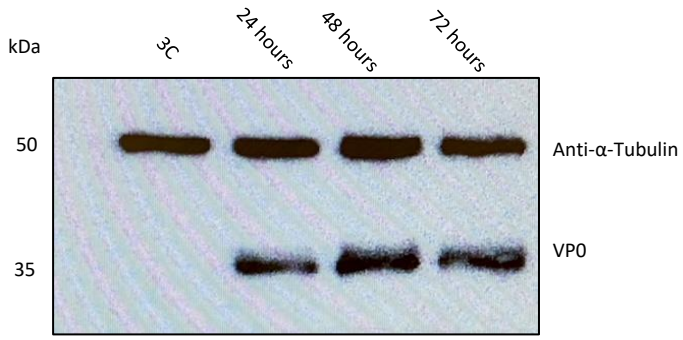


**Figure 4.3 Optimisation of co-expression VLPs harvesting time:** HeLa cells seeded in six-well plate were transfected with equal ratio of 3C/P1 vectors. Cell lysate and supernatant were harvested sequentially after 24, 48, and 72 hours and analysed via SDS-PAGE and western blot with anti-VP2/VP0 mAb979 antibody. The film was probed also by anti α tubulin antibody to indicate loading of equal amounts of the material. A representative blot is shown is one the result one experiment that was carried out in triplicate (n=3).

## 4.10. Large scale co-expression EVA71 recombinant VLPs

Larger scale EVA71 mammalian VLPs were produced by the co-transfection of the HeLa cells with a 1:1 ratio of the P1/3C constructs in 10 x T175 flasks. VLPs were harvested and purified using protocol previously optimised by Dr Natalie Kingston (University of Leeds). VLPs were separated along a 15-30% (w/v) sucrose gradient at 50,000 xg for 12 hours at 4$^{o}$C. Fractions were collected from the top to the bottom of the tube.

Fractions were analysed by SDS-PAGE and western blot using antiVP0/VP2 mAb979 and indicated the presence of a band consistent with the predicted molecular weight of VP0 ~35 kDa. This was located within the gradient, which indicates the successful P1/3C expression and resultant VLP assembly. Smaller protein bands were detected to a lesser extent, likely minor degradation products.

The VP0 band was distributed across the gradient between 9 and 14. The peak of the wild-type was detected in fraction 12, while the peak of #9.3 was detected in fraction 13. These data indicates that the VLPs showed a similar sedimentation rate to the ECs produced from wild-type and 9.3 infectious virus of mammalian cells (Figure 4.4) (See chapter 3).

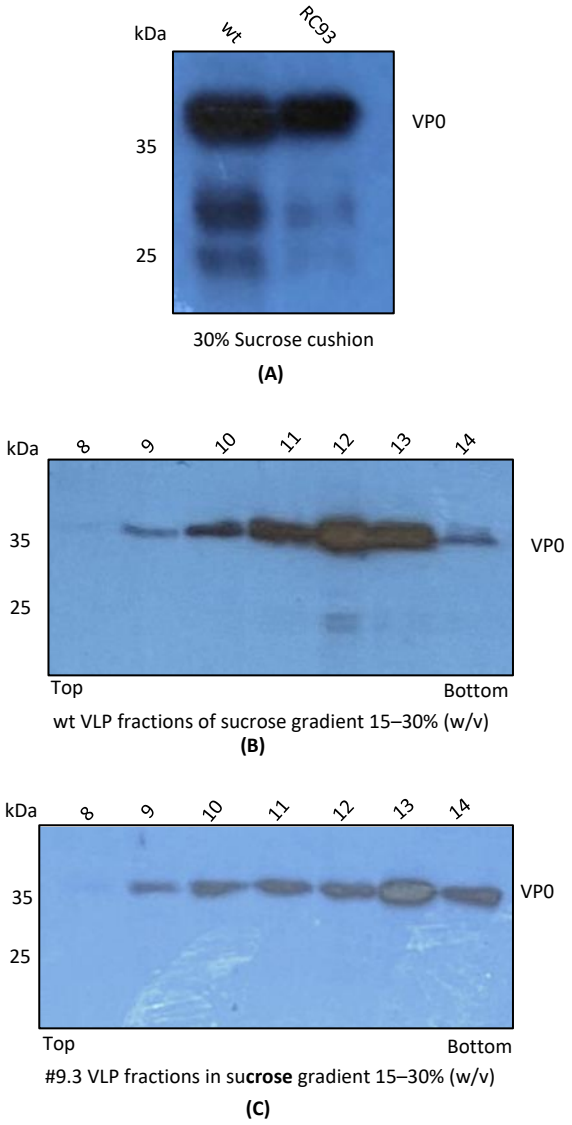


**Figure 4.4 Sucrose gradient of mammalian VLPs:** The mammalian VLPs of both wild-type and #9.3 were expressed by co-transfecting a ratio of 1:1 3C/P1 in 70% confluent of HeLa cells seeded in eight T175 flasks. (A) Cell lysate was sucrose cushioned. (A) and (B) Purified fractions were collected from the top to the bottom. The collected fractions were analysed for protein expression by 12% SDS-PAGE and western blot with anti-VP0/VP2 mAb979.

## 4.11. Characterisation of mammalian expressed VLPs

The antigenicity of wild-type and #9.3 VLPs which were expressed in HeLa cells were evaluated using mAb 979, A9 and CT11F9. Both the A9 and CT11F9 have the ability to detect both NAg and HAg forms of EVA71. On the other hand, mAb 979 recognises an epitope that corresponded to residues 136–150 of VP2 (Liu et al., 2011). mAb 979 exclusively detects the HAg conformation which may be either naturally occurring or induced through heating particles. However, there is currently no antibody that can exclusively detect the NAg conformation in ELISA.

Analysing the antigenicity of wt (Figure 4.5) and #9.3 (Figure 4.6) VLPs was determined. Antigenically, the VLPs were detected between fraction 9 and 14 the gradient with the peak fraction of wt located at fractions 12, while #9.3 peak was at peak 13. These data are consistent with the location of particles within the gradient, determined by western blot (Fig 4.4). The assessment of NAg and HAg reactivity by ELISA indicate that VLPs of both wt (Figure 4.5) and #9.3 (Figure 4.6) were more reactive with A9 and CT11F9 compared to mAb979. Moreover, both VLPs were slightly more reactive with CT11F9 comparing to A9. On the other hand, the VLPs of wt were more reactive to mAb979 comparing to #9.3.

A

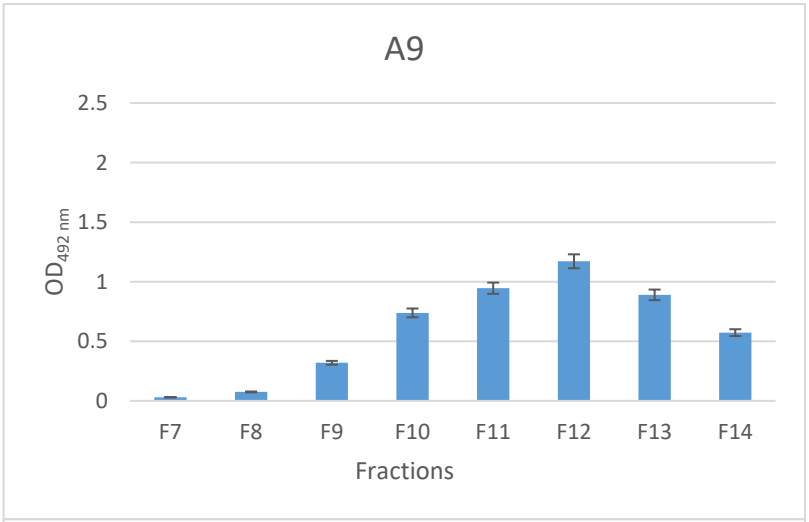


B

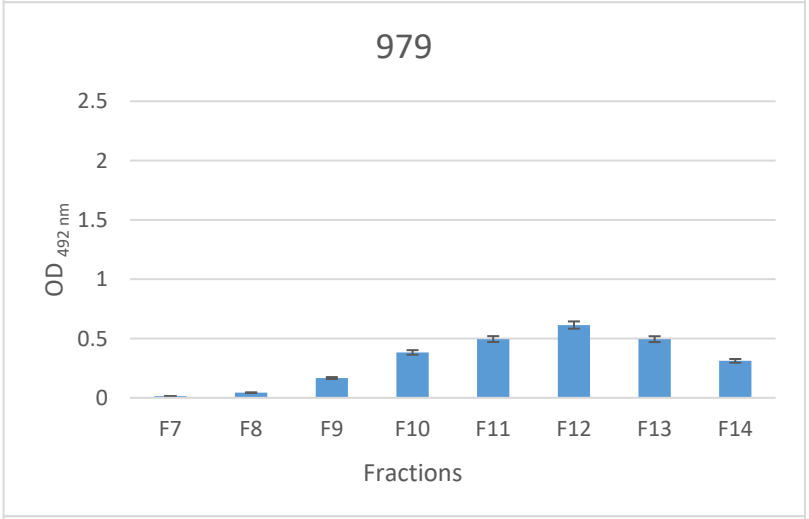


C

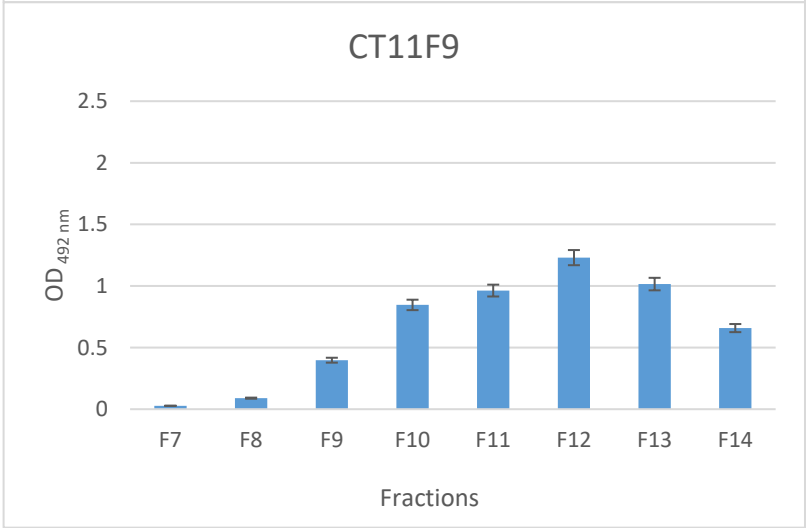


**Figure 4.5 Mammalian wild-type VLP antigenicity evaluation by sandwich ELISA:** Mammalian VLPs wt fractions of 15-30% (w/v) sucrose gradient was collected from top to bottom. ELISA was performed to analyse the VLPs antigenicity using a panel of antibodies anti VP0/VP2 (A) A9 (B) mAb979, and (C) CT11F9 This experiment is one experiment that was carried out in triplicate (n=3). Error bars often represent one standard deviation.

A

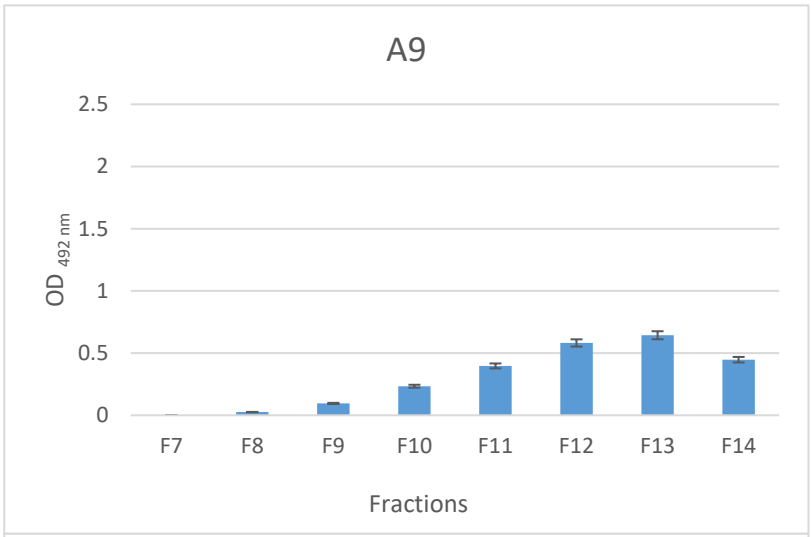


B

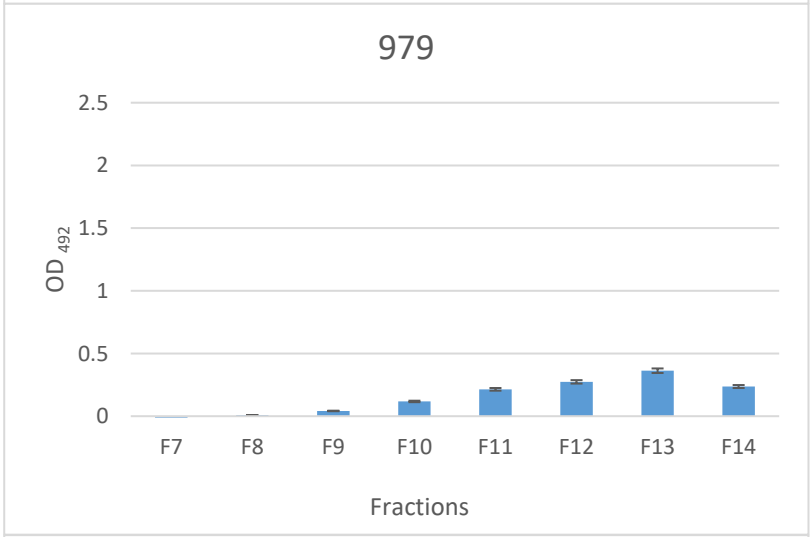


C

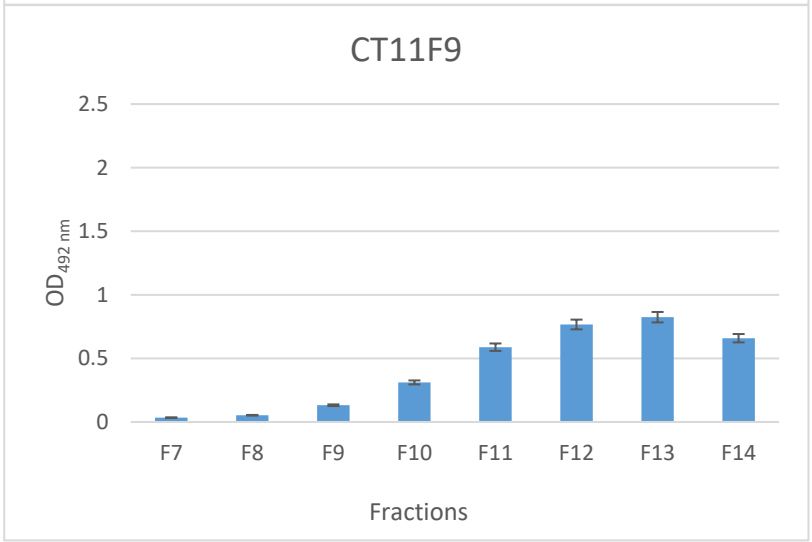


**Figure 4.6 Mammalian #9.3 VLPs antigenicity evaluation by sandwich ELISA:** Mammalian VLPs #9.3 fractions of 15-30% (w/v) sucrose gradient was collected from top to bottom. ELISA was performed to analyse the VLPs antigenicity using a panel of antibodies anti VP0/VP2 (A) A9 (B) mAb979, and (C) CT11F9. This experiment is one experiment that was carried out in triplicate (n=3). Error bars often represent one standard deviation.

## 4.12. Evaluating the heat inactivation of mammalian wild-type and # 9.3 VLPs by Sandwich ELISA

Sandwich ELISA and anti VP0/VP2 mAb979, which is able to detect the HAg, was performed to evaluate the effect of heat inactivation on the mammalian VLPs. This assay aimed to give an estimate of the effect of heat inactivation on gaining antigenicity of the non-native HAg form and relies on the specificity of VP0/VP2 mAb979 for detecting the expanded form of EVA71. 100 µl of the nine aliquots from the peak fraction were thermally stressed at a range of temperatures between 30$^{o}$C and 65$^{o}$C for 10 min and then chilled on ice. The OD of each sample was read at 492 nm (n=2). A slight decrease in reactivity of wild-type VLPs was observed from at 52$^{o}$C which then continued until 60$^{o}$C. In contrast, although #9.3 VLPs were less reactive than the wild-type VLPs, most importantly there was a slight increase at 56$^{o}$C.

A

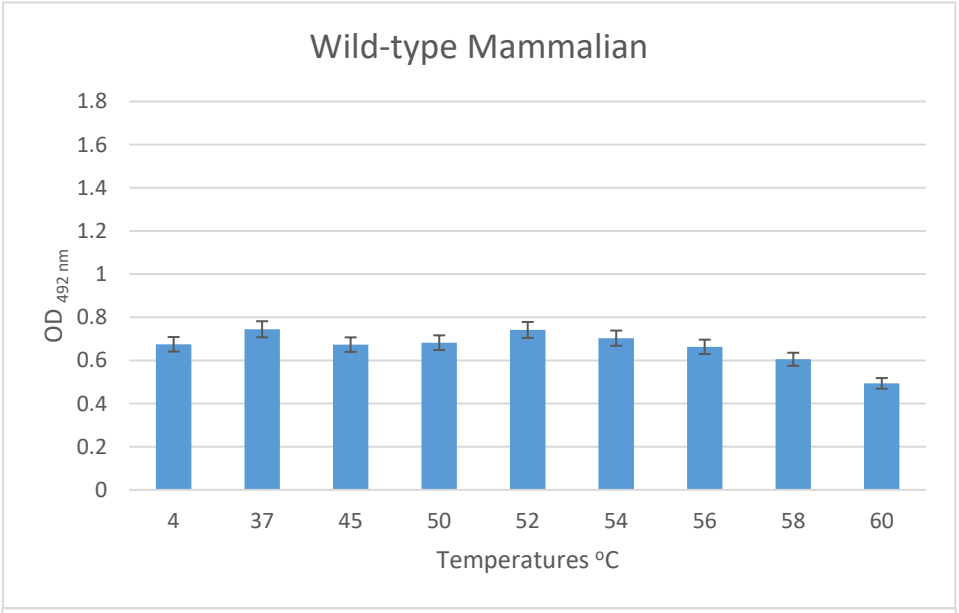


B

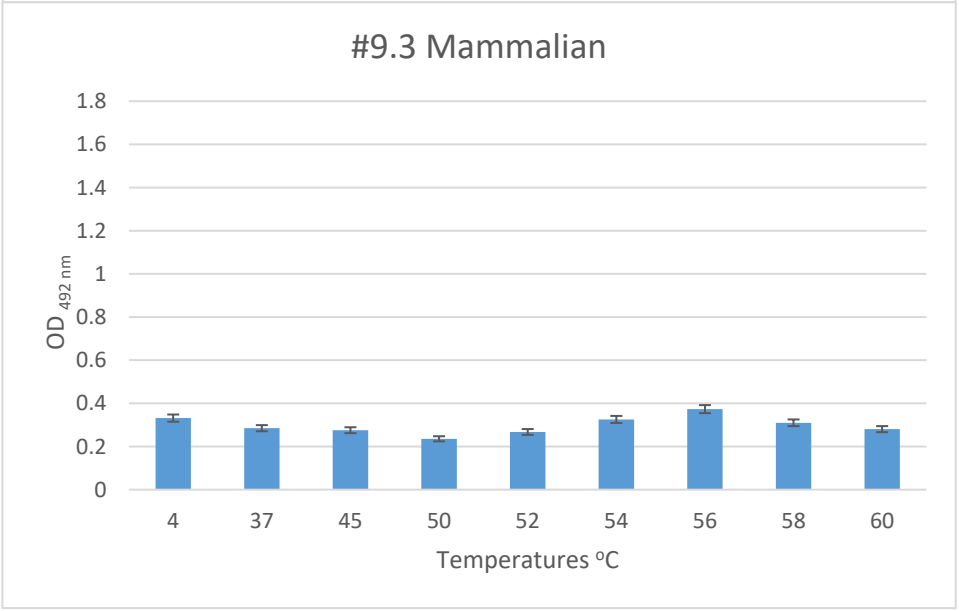


**Figure 4.7 Heat conversion of mammalian VLPs by sandwich ELISA:** ELISA was performed with anti-VP0/VP2 mAb979 to estimate the thermo-stability of the mammalian (A) Wild-type and (B) #9.3 VLPs. For thermostability assays, 100 µl nine aliquots from the peak fraction were thermally stressed at a range of temperatures between 30°C and 65°C for 10 min and then chilled on ice. The OD of each sample was read at 492nm. This experiment is one experiment that was carried out in triplicate (n=3). Error bars often represent one standard deviation.

## 4.13. Evaluating the antigenic conversion of mammalian wild-type and #9.3 VLPs by sandwich ELISA

Sandwich ELISA using anti-VP0/VP2 mAb979, which detects the HAg, was performed to evaluate the effect of heating on the mammalian VLPs and antigenic conversion. This assay aimed to understand the effect of heat on gaining HAg reactivity and relies on the specificity of VP0/VP2 mAb979 for detecting the expanded form of EVA71. Nine 100 µl aliquots from the peak fraction were heated using temperatures between 30°C and 65°C for 10 min and then chilled on ice before assessment in a mAb979-specific ELISA. The OD of each sample was read at 492 nm (n=2). A slight decrease in reactivity of wild-type VLPs was observed from 52°C which then continued until 60°C. In contrast, although #9.3 VLPs were less reactive than the wild-type VLPs, most importantly there was a slight increase at 56°C.

ELISA readings are dose-dependent but can vary between assays. Thus, the relationship between changing OD and HAg concentration must be internally defined for each assay. A reference standard curve was generated to determine the relationship between loss of OD (incline) and 50% reduction in antigen. The reference standard curve was generated by including a series of 4 two-fold dilution references in duplicate. The mean of each reference was plotted against a $\log_2$ dilution to generate the reference standard curve.

To estimate the thermal stability and proportion of NAg/HAg content of VLPs, 100 µl aliquots of VLP were heated using a range of temperatures between 30°C and 65°C. The mean of each duplicate was calculated and normalised to the mean of the negative control (no VLP wells). For each temperature the proportion of HAg (pHn) in sample n as follows: Proportion HAg = $1/ (2 ((OD^{heated} – OD^{unheated})/incline))$.

The proportion of NAg (pNn) in sample n defined as the inverse of the HAg proportion. These calculations indicate that the mammalian #9.3 VLPs lost detectable of the NAg content by 40°C, whereas the wild-type VLPs converted to HAg conformation at temperatures above 35°C. It also showed that more than >90% of unheated wild-type VLPs were already in the HAg form, and only 30% of #9.3 VLPs were in the native NAg form (Figure 4.8).

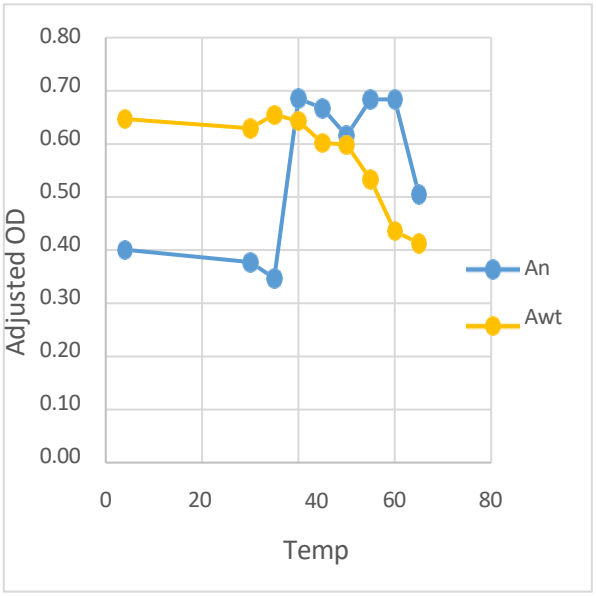


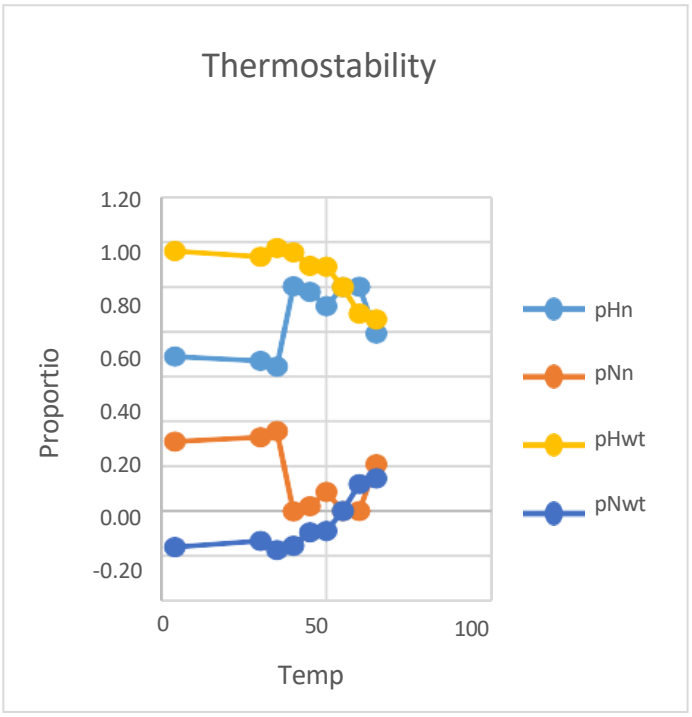


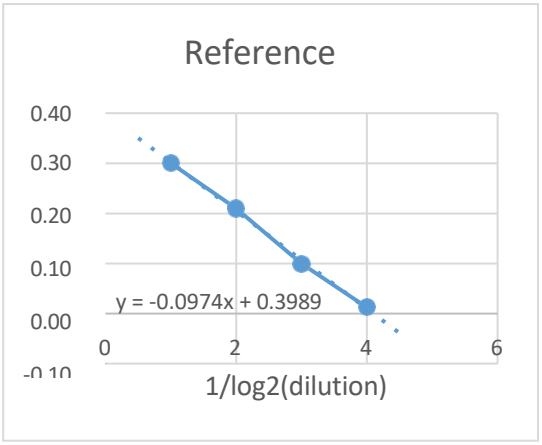


**Figure 4.8 Antigenic conversion of mammalian VLPs:** Sandwich ELISA was performed to estimate the thermo stability proportion of the NAg/HAg content of thermally stressed yeast VLPs of wild-type and #9.3. 100 µl aliquots from the peak fraction were thermally stressed at this range of temperatures: 30oC and 65oC for 10 min and then chilled on ice. NAg/ HAg contents were referred to as: pNwt = NAg wt, pHwt = HAg wt, pNn = NAg #9.3, pHn = HAg #9.3, Awt = wt and An = #9.3. The OD of each sample was read at 492nm This experiment is one experiment that was carried out twice (n=2). Error bars often represent one standard deviation.

## 4.14. Expression of VLPs in *Pichia pastoris*

Yeast is an attractive platform that has been used for generating recombinant proteins and was utilised to express EVA71 VLPs. These particles were expressed firstly in *Saccharomyces cerevisiae* and later in *Pichia pastoris*. The yeast generated VLPs were able to induce robust immune response in murine models of EVA71 in neonatal mice (Li et al., 2013).

As mentioned previously*, P. pastoris* has been used successfully to generate EVA71 VLPs through the co-expression of the structural protein precursor P1 and the viral 3CD protease pastoris (Zhang et al., 2015).

*P. pastoris* was employed here as an alternative host system for the expression of EVA71 VLPs. To express EVA71 VLPs, a *P. pastoris* protocol that was optimised by Dr Lee Sherry (University of Leeds) for production of PV VLPs was used.

## 4.15. Large-Scale Pichia pink expression and purification of EVA71 VLPs

The large-scale production of EVA71 VLPs in *P. pastoris* was carried out using the pPINK-HC expression vector encoding wt or #9.3 EVA71 P1 and PV 3CD under the inducible AOX promoter in a dual promoter system. Vectors were generated and transformed into Pichia pink strain 1 by Dr Natalie Kingston, University of Leeds (see section 2.11.4). Transformed Pichia pink cells were used to generate a starter culture. Cultures were scaled up and expression was induced with methanol as described in section (2.11.4). Cells were lysed and VLPs were purified by sucrose cushion and through 15-45% (w/v) sucrose gradients as in the section (2.7.2). Fractions of 1ml were collected from the top to the bottom and protein content of the fractions was analysed for VP0 by SDS-PAGE and western blot using the anti-VP2/VP0 mAb 979 antibody (Figure 4.9).

Western blot indicates the presence of a major protein band with molecular weight corresponding to VP0 ~35kDa. The presence of this within the gradient suggests the successful expression of P1/3C and indicates VLPs assembly. Wt protein signals were detected from fraction 8 onward, while #9.3 signals were detected from fraction 8 onward and the peak of #9.3 was detected at fraction 10.

.

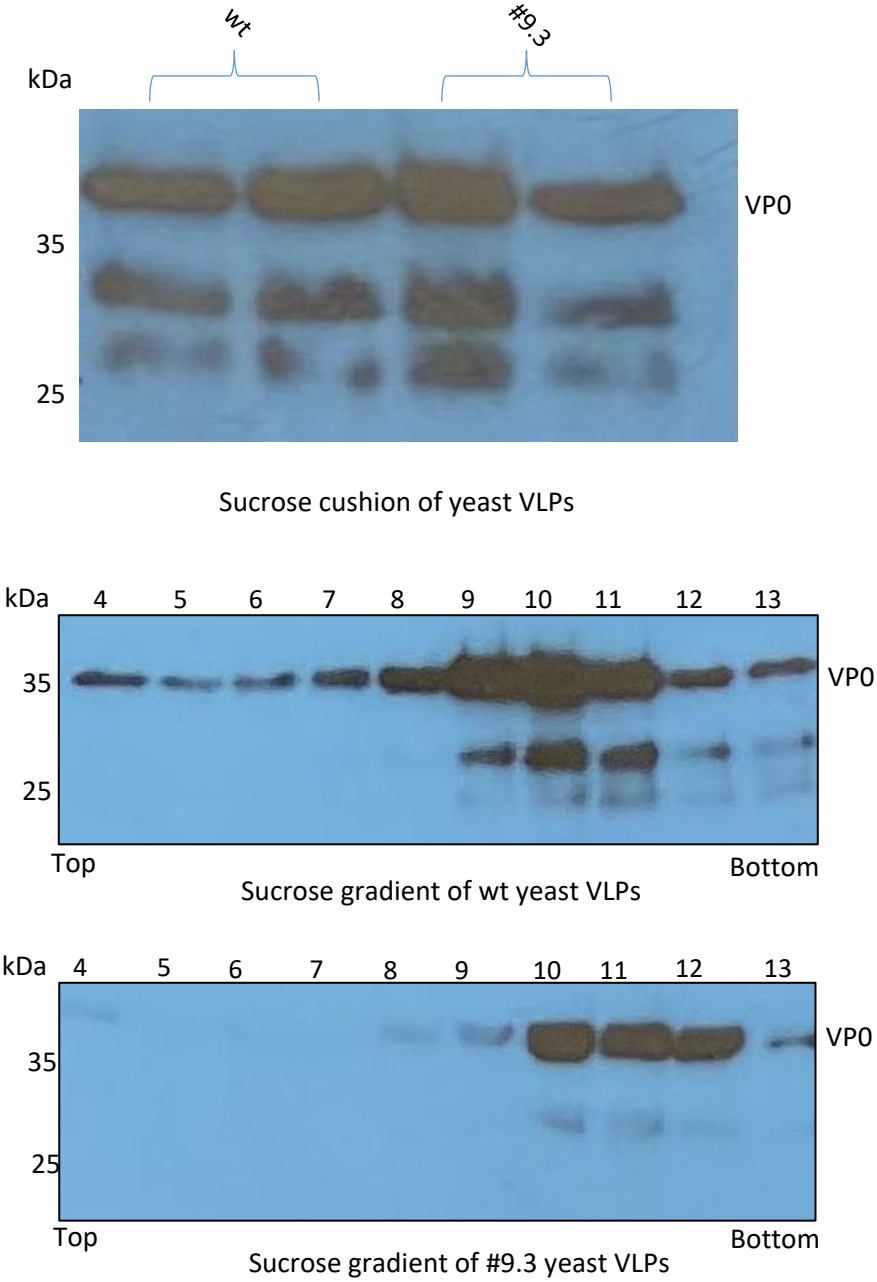


**Figure 4.9 The large-scale co-expression of EVA71 VLPs in *Pichia pastoris*:** Yeast VLPs wild-type or #9.3 were expressed using EVA71 P1 and PV 3CD vectors with the inducible AOX promoter (both were prepared and transformed by Dr Natalie Kingston, University of Leeds). The yeast culture was collected and purified according to standard protocol. The proteins were analysed by SDS-PAGE and western blot analysis using mAb979.

## 4.16. Characterisation of yeast co-expressed VLPs by TEM

Samples of #9.3 VLPs produced in *P. pastoris* were visualised by negative stain transmission electron microscopy (TEM). Samples of #9.3 ECs were included as a control. The two samples appearing similar in terms of size and gross morphology. (The material for #9.3 VLP (Pichia) was giving by Dr Natalie Kingston, University of Leeds) (All TEM images were provided by Joe Snowden, University of Leeds) (Figure 4.10).

(A) #9.3 EC

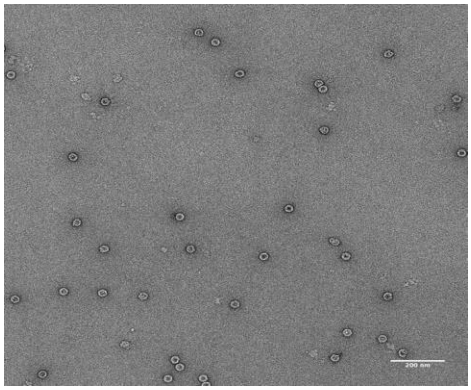

(B) #9.3 yeast VLPs (*Pichia*)

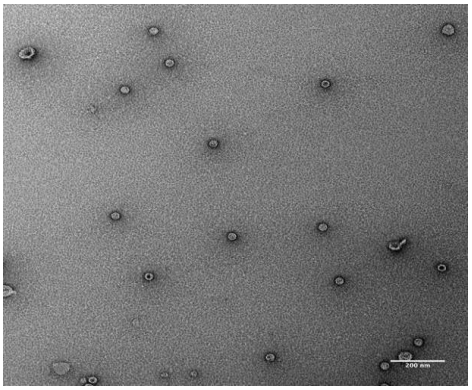

**Figure 4.10 Photographs of EVA71 particles as analysed by Transmission Electron Microscopy (TEM):** (A) #9.3 EC (B) #9.3 VLPs (*Pichia)*. Both the ECs and yeast VLPs can be estimated to be approximately 30–32 nm in diameter.

## 4.17. Antigenicity characterisation of yeast co-expressed VLPs

Similar to mammalian-produced VLPs, the antigenicity of yeast-expressed VLPs were assessed by ELISA using mAb979, A9 and CT11F9. The signal was detected in ELISA between fraction 7 and 14 the gradient with a peak around fraction 9. The results of the wild-type were corresponded to the results of the SDS-PAGE and western blot analysis (Figure 4.9). However, regarding #9.3 the result was slightly different, as the peak in western blot seems to in consistence with the ELISA results. ELISA indicates that VLP-containing fractions of both wild-type (Figure 4.11) and #9.3 (Figure 4.12) were more reactive with A9 and CT11F9 compared to mAb979. Moreover, both VLP types were slightly more reactive with CT11F9 compared to A9. Despite both particle types having similar reactivity with A9 and CT11F9, the wild-type samples were more than twice as reactive with mAb979 compared to #9.3.

A

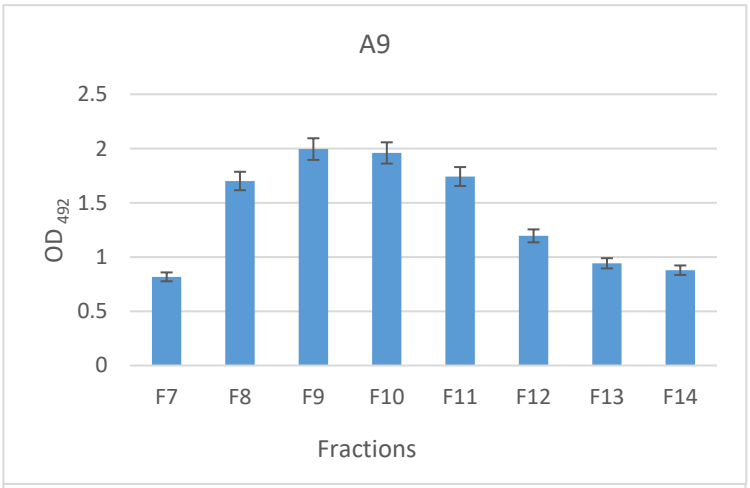


B

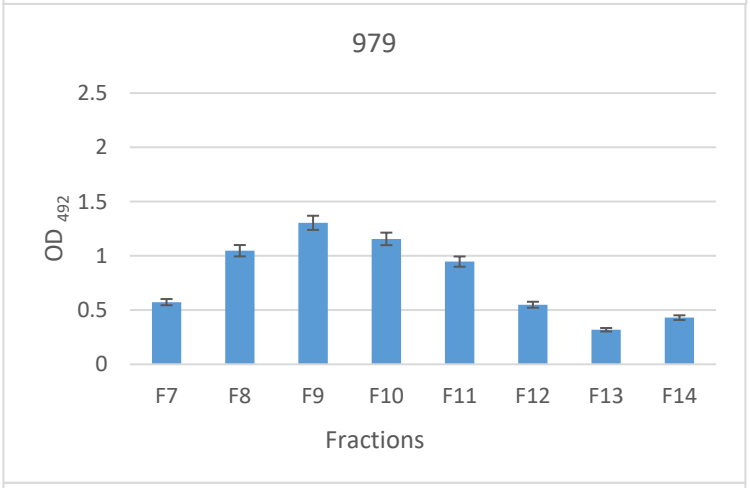


C

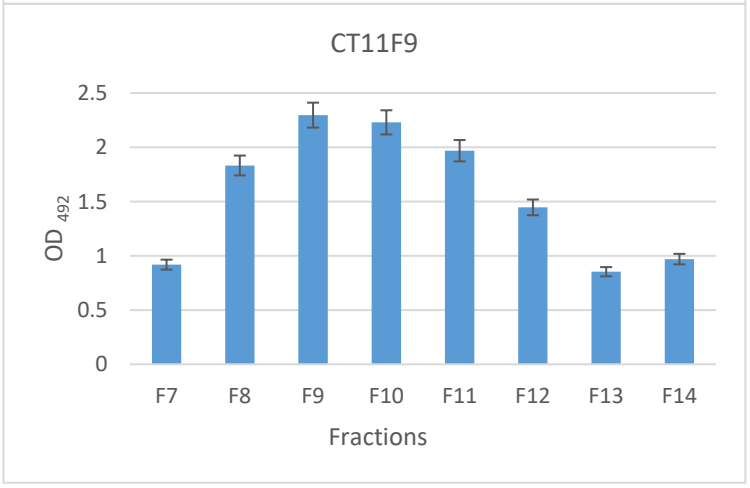


**Figure 4.11 Antigenicity assessment of wild-type yeast VLPs by sandwich ELISA:** Wild-type yeast-expressed VLPs fractions of 15-30% (w/v) sucrose gradient was collected from bottom to top and assessed by sandwich ELISA using the monoclonal antibodies (A) A9 (B) mAb979, and (C) CT11F9 in the detection phase. The results were read using 492 nm. This experiment is one experiment that was carried out in triplicate (n=3). Error bars often represent one standard deviation.

A

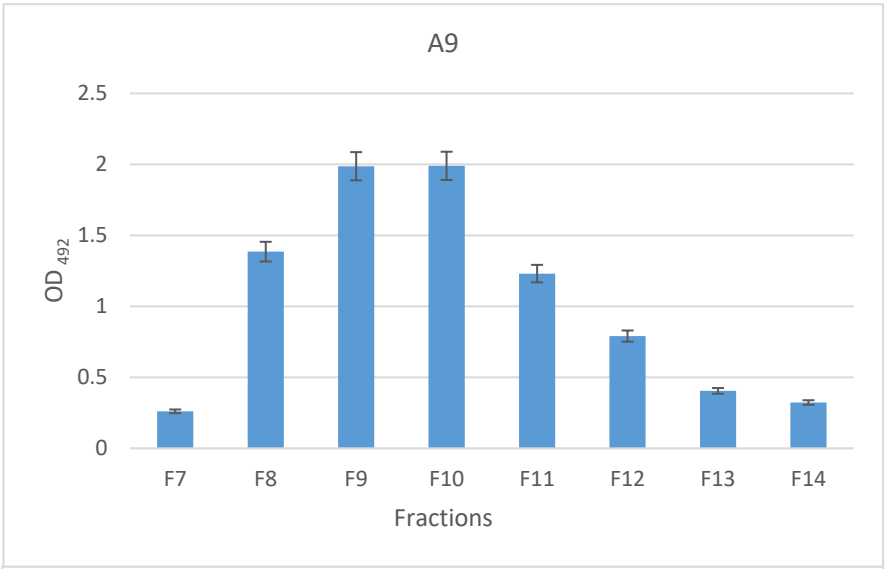


B

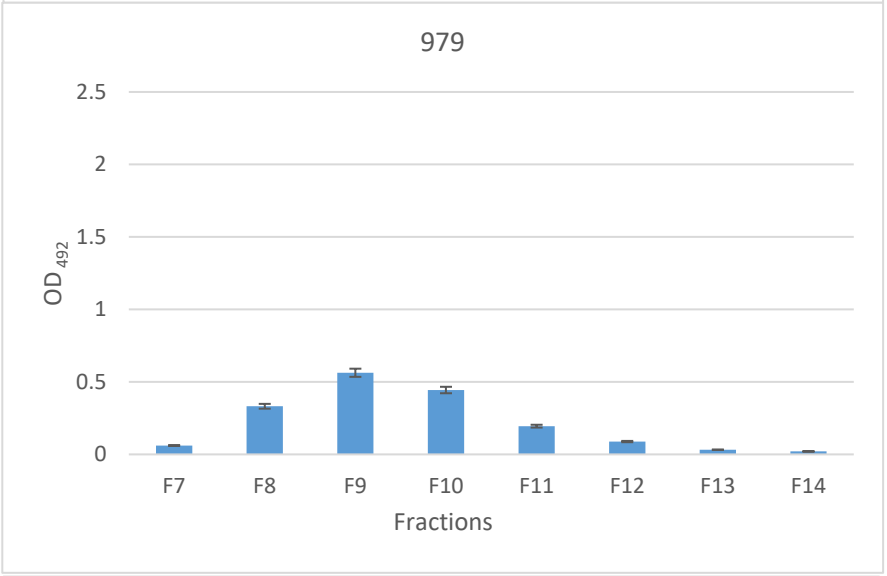


C

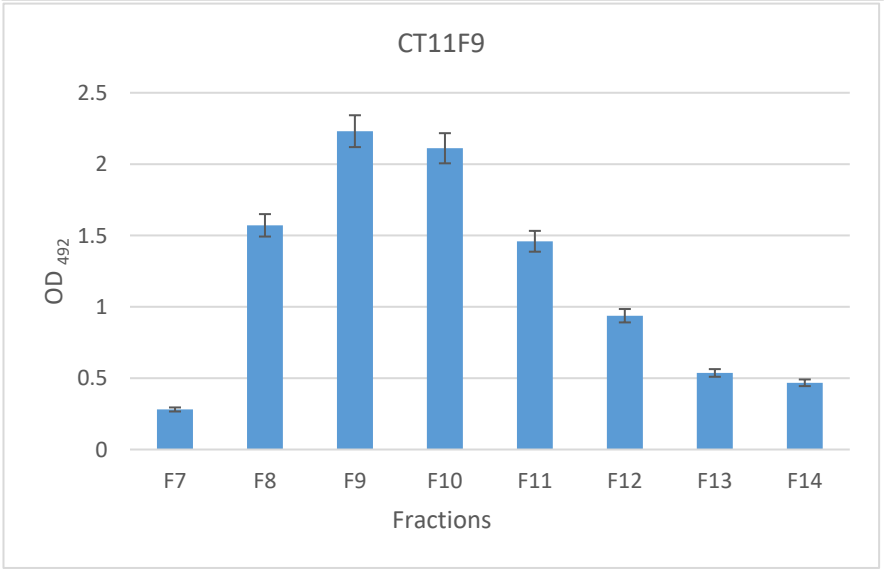


**Figure 4.12 Antigenicity assessment of #93 yeast VLPs by Sandwich ELISA:** The antigenicity of purified #9.3 yeast VLPs fractions were examined using a number of primary antibodies: anti VP0/VP2 (A) mAb 979, (B) A9, and (C) CT11F9. The polyclonal rabbit EVA71 Abs diluted at 1: 2000 was used as capture antibody. The secondary antibody was anti mouse HRP Abs. The results were read using 492 nm. This experiment is one experiment that was carried out in triplicate (n=3). Error bars often represent one standard deviation.

## 4.18. Antigenicity and stability analysis of VLPs with monoclonal antibody 979

To determine the antigenicity of the yeast-expressed VLPs, 100 µl aliquots from the peak fraction were incubated at a range of temperatures between (37$^{o}$C and 60$^{o}$C). Sandwich ELISA was performed using anti-VP0/VP2 mAb979 antibody to monitor any increase of the HAg form. Estimating the conversion of NAg form to the HAg form indicates that the wild-type VLPs were stable across different temperatures. However, the reactivity of the #9.3 VLPs to VP0/VP2 mAb979, increased at 45$^{o}$C (Figure 4.13).

To determine the antigenic stability of yeast expressed VLPs, 100 µl aliquots from the peak fraction were incubated at a range of temperatures between 37$^{o}$C and 60$^{o}$C. Sandwich ELISA was performed using anti-VP0/VP2 mAb979 to monitor any change in HAg reactivity. The OD did not appear to change substantially after wt particles were incubated at each temperature indicating that the wild-type VLPs were likely already predominantly in the HAg conformation, thus did not gain mAb979 reactivity with heating. Conversely, the reactivity of the #9.3 VLPs to VP0/VP2 mAb979 increased at 45$^{o}$C suggesting that particles were converting from the non-reactive NAg conformation to the reactive HAg conformation (Figure 4.13). Sandwich ELISA was performed with anti-VP0/VP2 mAb979 to estimate the converted NAg to HAg of wild-type and #9.3 VLPs after heating at 55$^{o}$C (Figure 4.14). The results of heating the #9.3 VLPs have shown that there was an increasing in reactivity by increase heating, which was not observed with the wild-type. It seems that the wild-type VLP consist mainly of HAg as before and after the heating there was no evidence of shifting between native VLPs or HAg form, while the #9.3 reactivity changed substantially after heating, which may indicate that most of the particles are in NAg form before heating.

The proportion of the NAg/HAg contents of the yeast VLPs and their thermostability were estimated following the same procedure described in section (4.4.6). In this assay, the data indicated that the yeast-expressed #9.3 VLPs contained approximately 60% NAg which was stable until approximately 40°C. Whereas the wild-type EVA71 VLPs appeared to contain approximately 24% and was stable until approximately 37°C. (Figure 4.15).

A

B

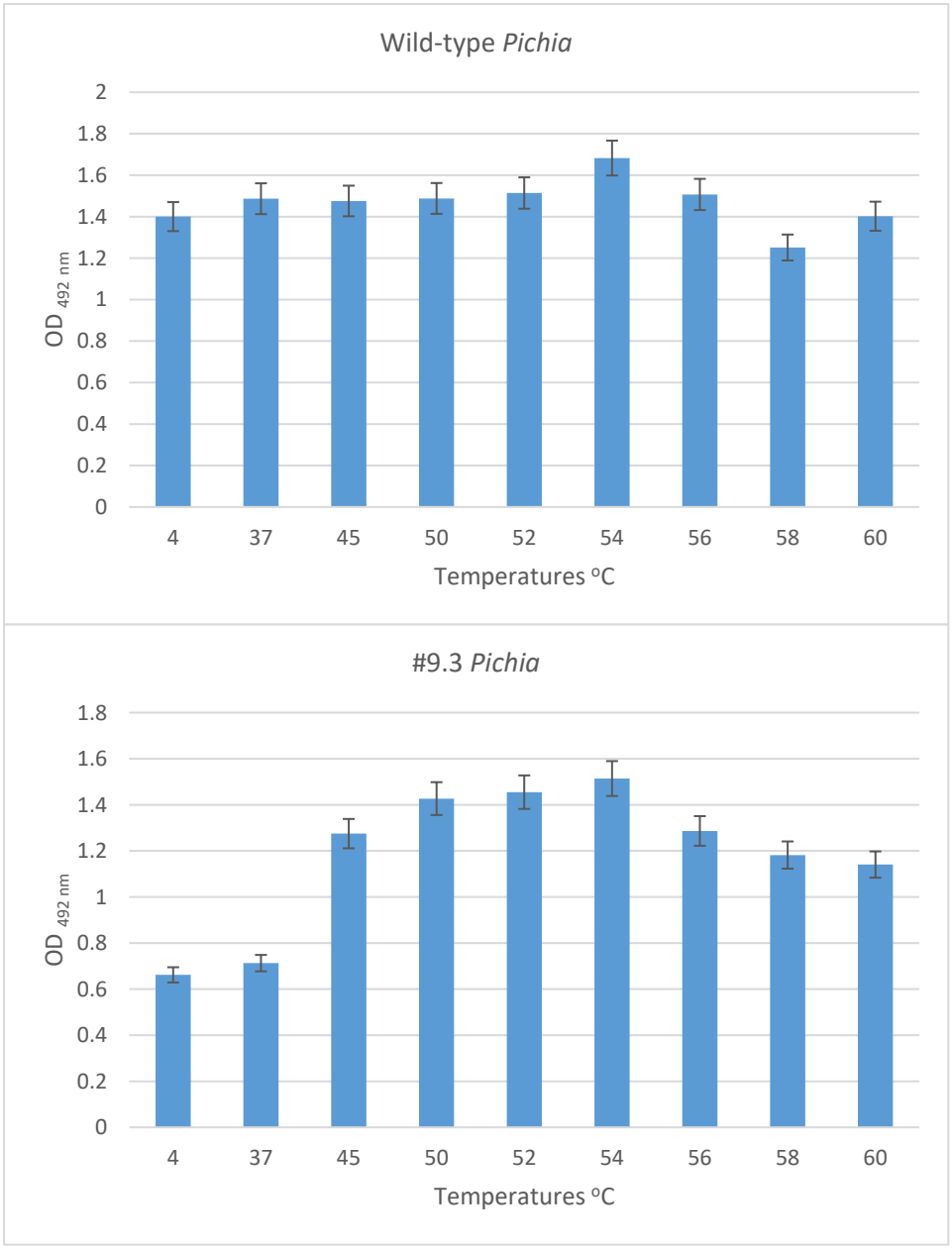


**Figure 4.13 Heat conversion of yeast VLPs by sandwich ELISA assay:** ELISA was performed with anti-VP0/VP2 mAb979 to estimate the thermo-stability of the yeast VLPs of (B) wild-type and (A) #9.3. For thermostability assays, 100 µl nine aliquots from the peak fraction were thermally stressed at this range of temperatures: 30°C and 65°C for 10 min and then chilled on ice. The OD of each sample was read at 492nm This experiment is one experiment that was carried out twice (n=2). Error bars often represent one standard deviation.

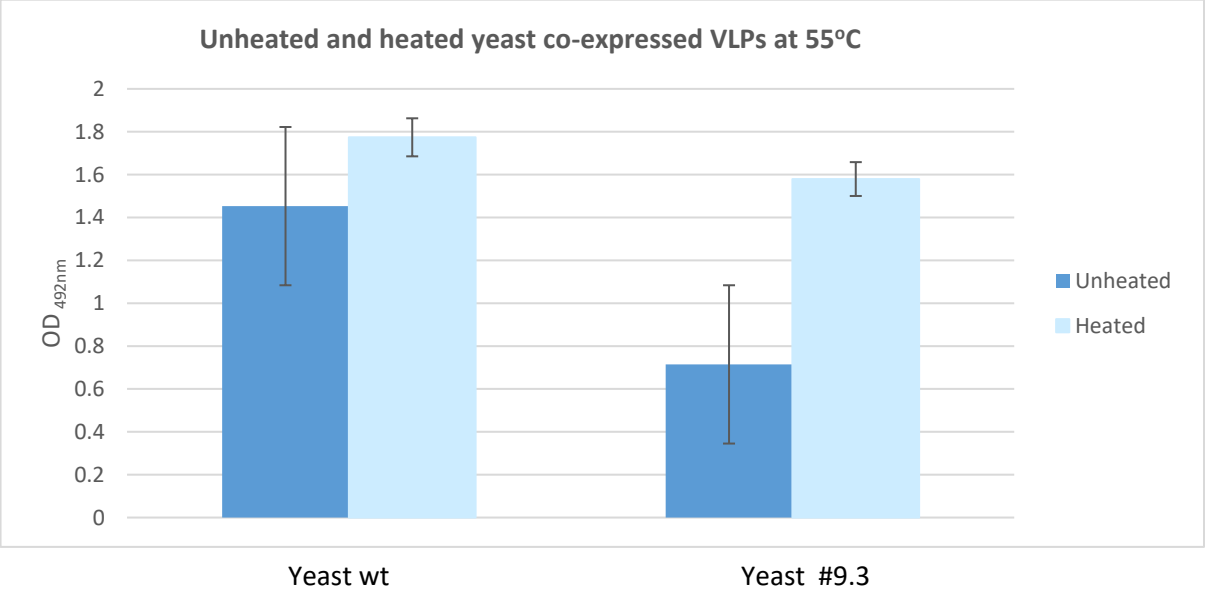


**Figure 4.14 Antigenicity conversion**: Testing the proportion of the NAg/HAg content of wild-type and #9.3 VLPs by sandwich ELISA after heating at 55°C: ELISA was performed with to estimate the thermo-stability of yeast VLPs. Aliquots of the peak fraction were heated at 55°C for 10 min and then chilled on ice. ELISA was carried out using anti-VP0/VP2 mAb979. The OD of each sample was read at 492nm. This experiment is one experiment that was carried out twice (n=2). Error bars often represent one standard deviation.

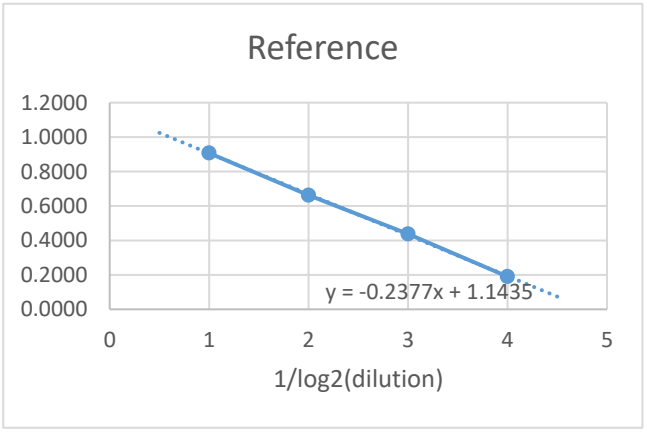


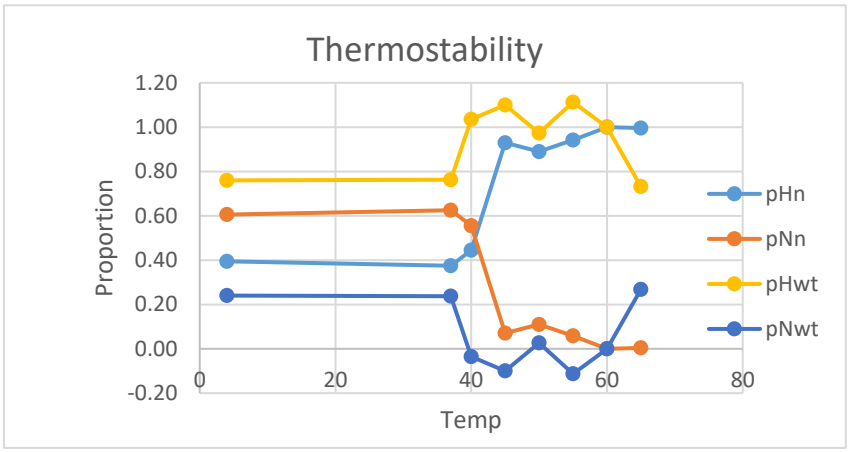


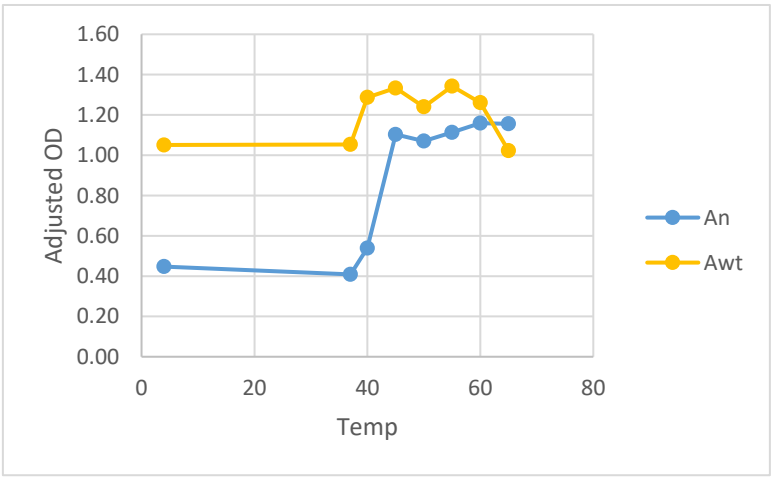


**Figure 4.15 Antigenic conversion of yeast VLPs:** Sandwich ELISA was performed to estimate the thermo stability proportion of the NAg/HAg content of thermally stressed yeast VLPs of wt and #9.3. 100 µl aliquots from the peak fraction were thermally stressed at this range of temperatures: 30°C and 65°C for 10 min and then chilled on ice. NAg/ HAg contents were referred to as: pNwt = NAg wt, pHwt = HAg wt, pNn = NAg #9.3, pHn = HAg #9.3, Awt = wt and An = #9.3. The OD of each sample was read at 492nm This experiment is one experiment that was carried out twice (n=2). Error bars often represent one standard deviation.

## 4.19. Discussion

As previously mentioned in the introduction, many EVA71 VLP candidates have been developed in different platforms, such as baculovirus and insect expression system, S. cerevisiae, *and P. pastoris* by the co-expression of the structural polyprotein P1, and the viral protease 3C or its precursor 3CD. The potential of these VLP vaccine candidates was evaluated and found to elicit a long-lasting humoral immune response and high IgG titer. They were found to protect against lethal viral challenges in murine models. By comparing the VLP immunisation with the heat inactivated EVA71 virus, it was found that VLPs to were superior or comparable to the latter in terms of inducing an immune response (Yang et al., 2020).

The successful strategy behind generating EVA71 VLPs is based on generating particles that mimic the EC structure that lacks the genetic material while maintaining intact conformational epitopes. When initially produced, EVA71 ECs are structurally and antigenically indistinguishable from infectious viruses, they are unstable, and their antigenic conformation can convert easily from NAg to HAg. This expansion includes conformational changes that closely resemble the changes of EVA71 uncoating intermediates due to cellular receptor attachment or the conformation changes induced by environmental stress, such as decreasing pH or heating. Chyi-Liu et al (2011) carried out formalin inactivation of viral particles and ECs to confirm the differences in their physical structures for vaccine production. These particles were examined by a virus neutralisation assay, which showed that the neutralising antibodies induced by the formalin-inactivated ECs were less potent than the formalin-inactivated full virus. However, antibodies generated from both particles recognised the same linear neutralisation epitope of VP1 reported previously (residues 211–225).

The two antigenic forms have been studied extensively for PV for vaccine production purposes to determine the reliability of vaccine potency. However, previous studies have not evaluated the antigenic reactivity of EVA71 VLPs, presumably due to a lack of suitable tools. Therefore, measuring, quantification, or estimating the NAg and HAg content of EVA71 VLPs may provide an indication of its potency.

This chapter demonstrates the successful expression and assembly of EVA71 VLPs of the wild-type and the thermally stabilised #9.3 in HeLa cells and yeast. Mammalian expression conditions were optimised to ensure an efficient expression of recombinant VLPs. Before initialising the large-scale production of VLPs, the 3C:P1 ratio was assessed to minimise the 3C apoptosis-inducing effect on cells, and we found that an equal level of 3C and P1 was ideal to obtain the highest VLP yield. It was also found that the optimal harvesting time should be 48 hours as the VLP yield reached its maximum and then plateaued at 72 hours.

Sandwich ELISA with the available antibodies was an essential tool to help the stability of the generated VLPs. The antibodies A9 and CT11F9, and mAb979 were exploited to assess and characterise the VLPs in terms of yield and antigenicity. The results of mammalian #9.3 VLPs suggested being less reactive compared to all of these antibodies than wild-type. However, there was an obvious low yield of mammalian VLPs, which was expected as this is one of the disadvantages of this expression system. Despite this successful expression of VLPs in HeLa cells, the amount of generated VLPs was low and has affected proceeding with other essential characterisation experiments such as cryo-EM.

In comparison, the yeast system produced substantially more VLPs and highlighted one of the critical advantages of the yeast expression system. Yeast is known for producing a large amount of proteins, especially *P. pastoris*. Despite several successful attempts to express EVA71 VLPs in either the baculovirus and insect expression system, or *S. cerevisiae*, the low yield of both systems remains an issue. To overcome that, *P. pastoris* was used to express EVA71 VLPs to increase the yield, which was successful. While the yield of *S. cerevisiae* was about 0.25 mg/L, *P. pastoris* produced about 150 mg/L, which is also higher than the VLP expression level in insect cells that reached 64.3 mg/L. The low yield is one of the drawbacks of mammalian cells besides being an expensive system. Some studies suggested a possible optimisation step that could be considered to increase the VLPs yield in mammalian cells by combining P1 and 3C in a single vector to perform a single co-transfection (Porta et al., 2013; Bahar et al., 2021; Sherry et al, 2020). However, it was not considered here due to the time limitation, but it could be tested in the future.

The native conformation of EVA71 VLPs, produced in mammalian and yeast cells, was examined by ELISA using mAb979 due to the absence of an antibody that can exclusively detect the NAg form. The presence of the NAg form was implied from the increase in the reactivity of the VLPs to a HAg antigen that mAb979 still recognised upon heating the particles. This approach allowed the thermal stability of the VLPs to be assessed and the proportion of NAg/HAg determined.

The amount of HAg reactive wild-type VLPs from both expression systems remained relatively constant over temperatures, which suggested that most VLPs were already in the HAg form. In contrast, the yeast #9.3 VLPs exhibited an enhanced signal corresponding with increased

temperatures, likely due to the increase of HAg in the #9.3 VLP samples included more native particles than wild-type samples. These correspond with the results obtained by Marsian et al

(2017) In their study on plant-expressed polio VLPs, stabilised VLPs had enhanced thermal stability compared to the wild-type, and their antigenic reactivity increased with temperature as an indication of NAg conversion to the HAg. However, here NAg- specific antibodies were used. The high NAg content of #9.3 suggests that they could be superior to wild-type VLPs in inducing neutralising antibodies, thus, inducing better protective immune responses.

The thermal stability of #9.3 VLPs might be driven by the change of a conserved positively charged lysine residue in the VP1 loop to hydrophobic uncharged isoleucine in K1162C. The lysine residue was found to interact with a negatively charged aspartate presented on an adjacent VP3 loop when it is extended outwards in the fully expanded conformation of wild-type. Thus, the change in charge means that the interaction with the aspartate cannot occur CryoEM reconstructions of EVA71 #9.3 has provided evidence about the conformation of these VLPs (VLP particles generated by Dr Natlie Kingston, University of Leeds) (EM data provided by Joseph Snowden, University of Leeds) (the data showed here have not been published until this thesis submission).

The NAg #9.3 VLPs structure was determined to be 2.4 Å (Figure 4.16). The 3D classification sorted particles into two groups according to their structural similarities (Figure 4.17). Group 1 has displayed characteristics of a canonically NAg particle, while group 2 appears to have a region of poor resolution and partially expanded. The classifications indicated that approximately ~90% of particles were in the native conformation (24,000 particles) and approximately 10% (2,700 particles).

The density map indicated additional density for a sphingosine-like pocket factor present in the pocket of NAg particles, a narrow opening at the 2-fold symmetry axis, for some of the VP1 N-terminal region (Figure 4.18). That could be due to the presence of a VP3 GH-loop that is

extended outwards in expanded particles toward the 2-fold axis at the quasi-3-fold. However, this loop is folded back in native particles but extended, which might result from the K1162I mutation. This assumption is based on investigating the published confirmation of expanded EVA71(PDB: 3VBU). In this model the VP3 GH-loop appears to extend away from the capsid surface, and the K1162 within the EF-loop of an adjacent VP1 protomer appears to form a salt bridge with the side chain of VP3-D183. This salt bridge might lock the GH-loop in the extended HAg conformation, but this salt bridge might not be formed due to the presence of the K1162I mutation. Consequently, the extended VP3 GH-loop confirmation may not occur, thus reducing the possibility of transition from NAg to HAg (Figure 4.19).

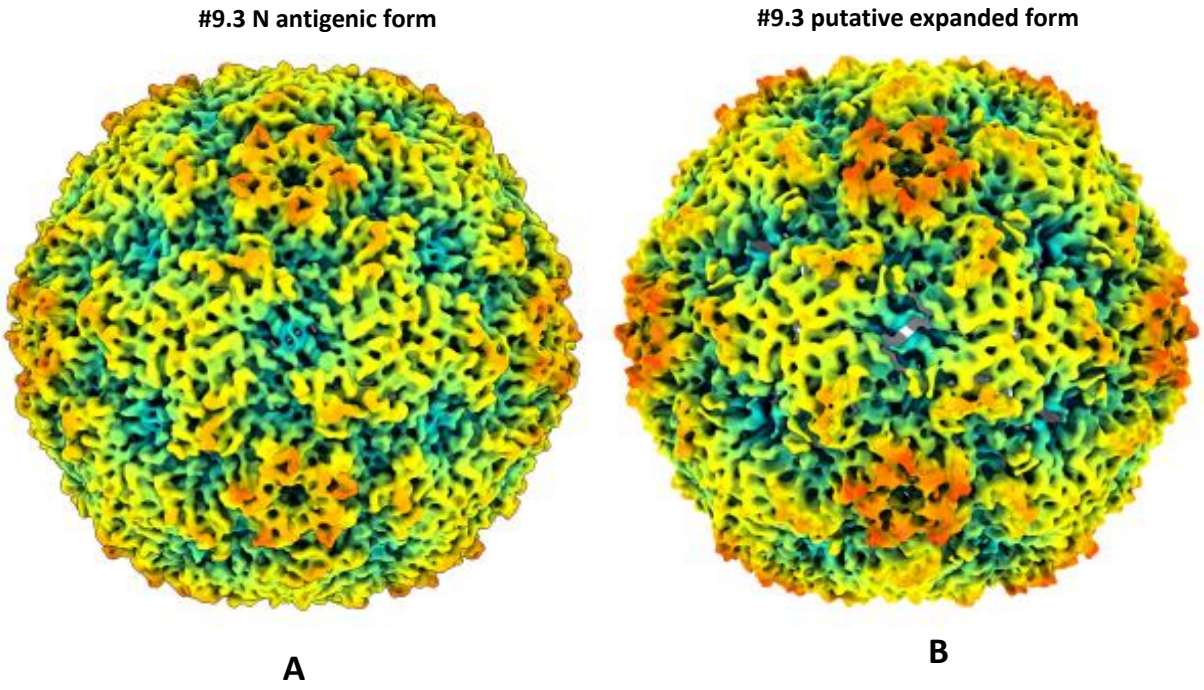


**Figure 4.16 Crystal structure of #9.3 VLPs:** Both density maps were 5 Å low-pass filtered (A) N antigenic #9.3 VLPs (B) Putative expanded #9.3 VLPs.

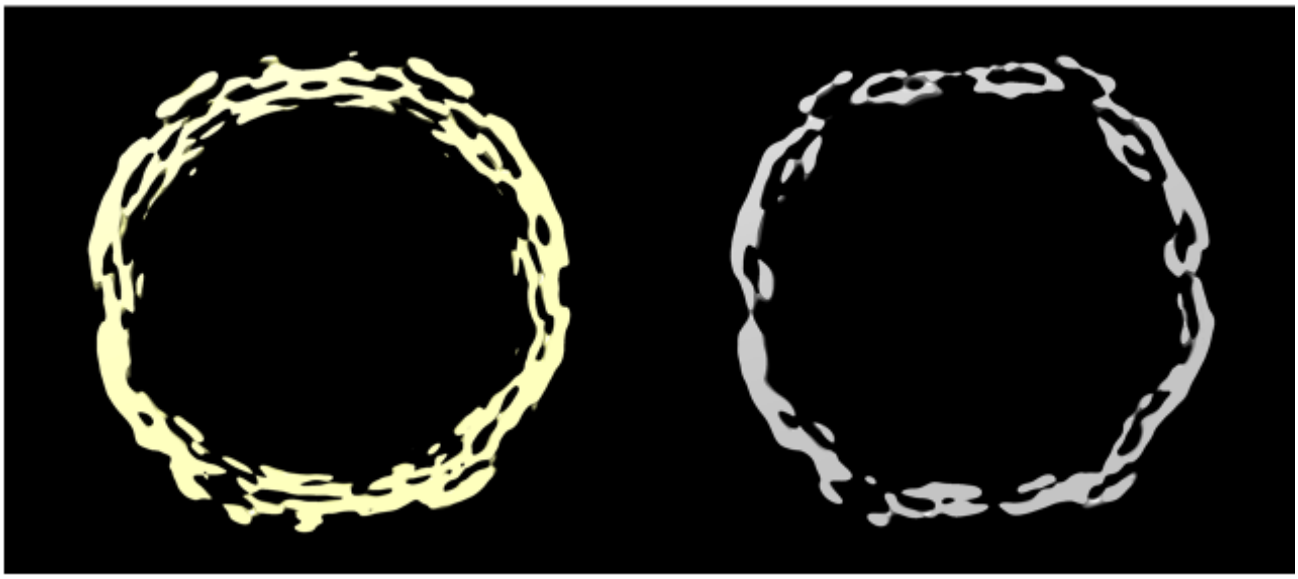

**Figure 4.17 3D classification of the #9.3 VLPs particles:** (A) Native #9.3 VLPs (24,000 particles) (B) expanded #9.3 VLPs (2,7000 particles).

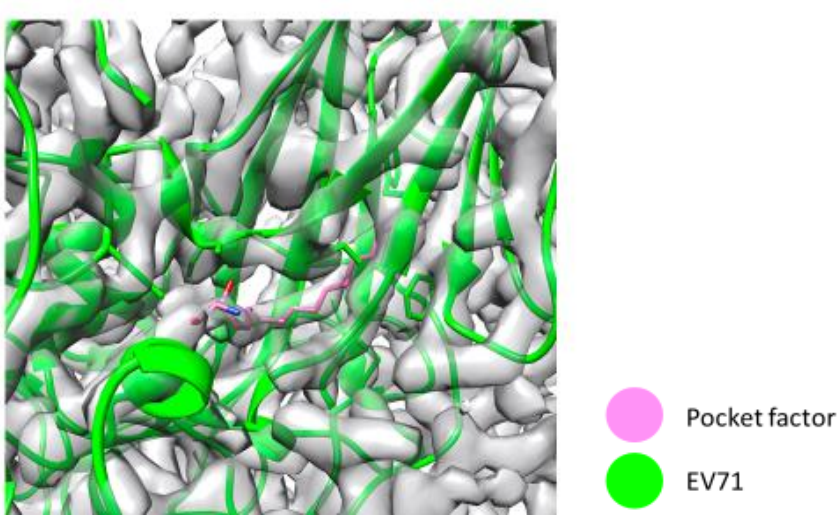


**Figure 4.18 Pocket factor in #9.3 VLPs:** The pocket factor was modelled on density map of expanded crystal structure of wild-type EVA71 (PDB: 3VBU).

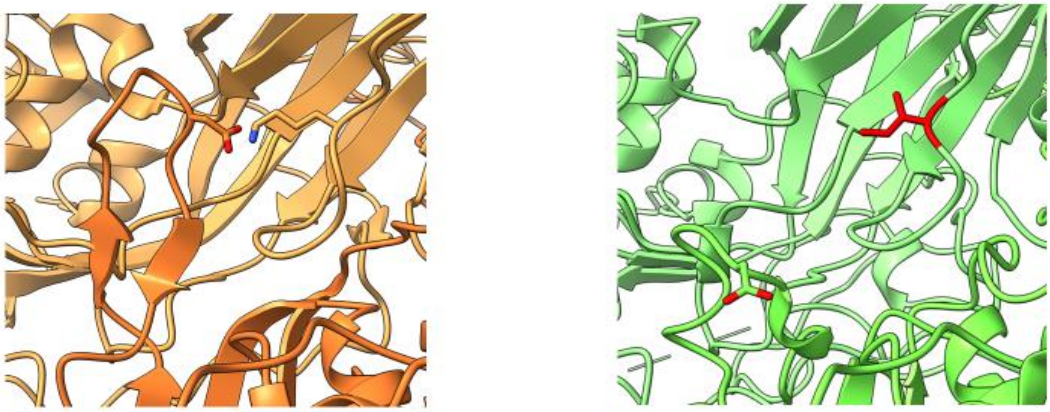


**Figure 4.19 Mechanism of stabilisation of #9.3 VLP:** (A) Expanded crystal structure of wild-type EVA71(PDB: 3VBU).

It seems that this is a key interaction of VLP expansion. Losing this in #9.3 VLPs might play an important role in the subsequent thermal stability of the VLP structure by making the expanded state less energetically favourable. Interestingly, that most of the particles are in the native conformation which comes in agreement with previous antigenic studies that were carried out by Dr Kingston who provide the cyro-EM data. She found that #9.3 yeast VLPs consist of 90% Nag form. The cryo EM also showed that the #9.3 VLPs possess a pocket factor, which helps in stabilising the assembly of the VLPs similar to many other picornaviruses. A further study could be undertaken to study the effect of acidic pH in expulsion of this factor after receptor recognition destabilises the #9.3 VLPs.

On the other hand, animal testing of the VLPs as possible vaccine is ongoing work during the writing of this thesis. It aims to compare the immunological responses of BALB/c mice to NAg or HAg conformations of EVA71 particles, or PBS in the presence or absence of Alhydrogel.

# Chapter 5

## General discussion, limitations, and future work

## 5.1. Discussion

The EVA71 ECs possess a structure with conformation antigenicity identical to the NAg confirmation of infectious virus, but they are unstable and can convert readily into HAg form, especially if exposed to high temperatures or high pH. Both confirmational forms of EVA71 can induce similar immune responses, although whether the NAg has superior immunogenicity over the HAg is still unknown. This study aimed to investigate this hypothesis by designing a stable and immunogenic EVA71 VLP that mimics the native virus conformation, to be used as a possible effective VLPs vaccine candidate. In order to achieve this, we applied a protocol used previously to stabilise PV VLPs by applying thermal selection. This is in contrast to the approach used by Fox et al (2021) where stabilised PV capsids were generated by starting with thermostable viruses.

### 5.1.1. Thermal selection of antigenically stable EVA71

Initially, an inactivation curve was generated to establish a selection temperature at which most of the virus was inactivated. This showed that at 52.5$^{o}$C, most of the virus population was non-infectious.

Thermal stressing using the identified selection temperature was the bottleneck event that acted upon the EVA71 quasispecies, resulting in a virus population with enhanced thermal stability. Using the thermal selection temperature of 52.5$^{o}$C, nine repeated cycles of thermal stressing and passage yielded #9. This population was characterised by improved thermal stability and significant sequence deviation from the initial wild-type consensus sequence.

Allowing #9 to replicate five times without thermal selection pressure demonstrated genetic stability, as no reversion to the wild-type phenotype was observed.

### 5.1.2. Mutations and the EVA71 capsid stability

Five non-synonymous mutations were identified in the P1 capsid-encoding region of the genome. Consequently, both VP1 P246A and 3A F12L are present in unheated, #9 and all infectious clone recovered viruses. This mutation with I3235M had a high frequency at cycle 4, (95.5%), which increased to 99.7% at passage 9. Additional mutations appeared at early cycles but with a lower frequency. K1162I started to increase at cycle 7 until it reached 99.9% at cycle 9. The frequency of Y1116C and V2058L was low compared to other non-synonymous mutations, with a frequency of 43.1% and 69.5%, respectively. These data suggested that I3235M may have offered some thermal resistance to the capsid and that resistance was enhanced by K1162I, and possibly also Y1116C and V2085L.

To investigate the role of these non-synonymous mutations in thermal stability, they were incorporated into a wild-type infectious clone, which resulted in two mutants, termed #9.3 and #9.1 (Figure 3.11). Both shared P1246A, I3235M, and K1162I, with the presence of Y1116C in #9.3 and V2058L in #9.1. As a result of low infectivity, #9.1, was excluded from further study.

Mapping the mutations onto the structure of EVA71 has shown that P1246A lies at the five-fold axis, I3235M is located at the C-terminus of VP3 atop the canyon. Y1116C was within VP1/VP1 interface, in proximity to helices atop the canyon. The K1162I was located at the three-fold axis. In contrast, V2085L lies at the two-fold axis of VP2 in proximity to loops. All the mutations were located at the external surface of the capsid. It seems more probable that the conformational changes which would lead to expansion of wt particles are not favoured in the presence of the stabilising mutations.

Characterising the infectivity of #9.3 comparing to wild-type and #9 have showed that #9.3 is stable similar to the #9. These results were consistent with the results of antigenicity profile assessment of both mutant along with wild-type. The reactivity of both mutants were similar, which was another indication that the #9.3 as stable as #9. Accordingly, the genome sequence of #9.3 has informed the expression of VLP.

### 5.1.3. Expression of wild-type and #9.3 VLPs

Successful expression of wild-type and #9.3 VLPs was achieved in the mammalian system and in *P. pastoris*, using constructs expressing the PI region and a protease. However, the yield from the mammalian system was low, which hindered further VLP characterisation. In contrast, the yield from yeast was sufficient to proceed with characterisation of both antigenicity and structure. The antigenic stability of VLPs and the ratio of NAg form to the HAg form were investigated using ELISA and by applying thermal stressing using a range of temperatures. mAb979 was used, due to the lack of an antibody capable of exclusively detecting the NAg form. Therefore, the ELISA was designed to investigate increases in signal with temperature. This could therefore only correspond to an increase in Hag. The #9.3 VLPs were found to be less reactive to mAb979 than wild-type. Reactivity was increased after heating as a possible indication of capsid expansion, however, this was much more evident for wild-type than the #9.3 VLPs (Kingston et al., 2022).

From the cryo-EM analysis of #9.3 VLPs, the K1162I mutation was found to be very interesting. The positively charged lysine residue in the VP1 loop would interact with a negatively charged aspartate presented on the adjacent VP3 loop when extended outwards in the fully expanded

(NAg) conformation of wild-type. However, change to a hydrophobic isoleucine would prevent that interaction, hence destabilizing the expanded (HAg) conformation.

Therefore, the phenotype of #9.3 VLPs appears to be as a result of destabilising the expanded HAg conformation, rather than stabilisation of NAg.

## 5.2. Study limitation and future work

Overall, this thesis provides several important pieces of information: stabilisation of the capsid of EVA71 through thermal selection and successful incorporation and expression of the selected mutation into VLPs. It also provided information on the stability of the expressed VLPs via ELISA, suggesting that #9.3 VLPs predominantly possess a NAg conformation and wild-type VLPs possess HAg conformation. In addition, it provides some insight into how EVA71 evolves and adapts to high temperatures.

During this study, some challenges were encountered. One of these challenges was the low yield of the mammalian cell expression system, which is one of the platform's known drawbacks. The yield might be enhanced by using a variety of expression cassettes with different or doubled promotors or using a single vector that carries both the P1 and 3CD or the 3C.

It should be noted that none of the stabilising mutations present in #9.3 are in proximity of the 2-fold axis, where mAb 979 reacts (VP2 residues 136-150). The lack of proximity therefore suggests that the mutations in #9.3 are unlikely to directly influence antibody binding (Kingston et al., 2022). Use of available antibodies were able to analyse and characterise the antigenic properties and structural features on the VLPs surface to a certain extent, however, it remains challenging to differentiate between the NAg and HAg forms of VLPs. Thus, it is essential to develop antibodies that can be used to effectively distinguish between the two antigenic conformational forms of EVA71 VLPs for future vaccine development.

Quantification of VLPs using well-established virus quantification techniques such as plaque assay or $TCID_{50}$ is not possible as they are not infectious. Generally, VLPs lack genomic materials, it is therefore not feasible to quantify using PCR. Usually, transmission electron microscopy (TEM) can provide visual evidence of the size, concentration, and purity of the VLPs, though it cannot provide the exact amount of VLPs present in the sample. To overcome this issue, it is possible to use visualization method that allow to visualise the VLPs in suspension, e.g., by measuring the UV absorption spectrum. The findings of this current study have given rise to more questions. Adeyemi et al (2017) used a total of three selections (at increasing temperatures) to generate stable capsids. It is possible that additional rounds of selection might be useful for EVA71. It is also possible that some of the mutations generated are de-stabilising as there still needs to be a balance between stabilising and destabilising mutations to allow virus infectivity. However, perhaps the most critical question is there a difference between the NAg and HAg conformation in terms of eliciting a potent immune response. This question will be answered through undertaking potency assays and challenge studies in animals immunised by NAg confirmation.

Potency can be defined as biological response, which can be quantified, elicited by drug substance or antigen formulated as the vaccine product (reviewed in Moreira et al., 2022; Sanyal 2022). Potency testing ensures that the consistently manufactured vaccines are safe, pure, potent, and effective according to the standard determined in the original study. Every manufacturer should monitor the quality of manufactured products and demonstrate the consistency between different vaccine lots using reference vaccines that were initially proven effective in a host animal (reviewed in Moreira et al., 2022; Sanyal 2022).

The potency test is mainly carried out by vaccinating laboratory animals and challenging them with the live pathogenic agent. However, *in vitro* testing or serological assays can be an alternative to animal testing due to many issues regarding cost, safety, and animal welfare. However, to consider the serology testing effective, the antibody response to the targeted vaccine antigen needed to be a primary protective response in the vaccinated host (reviewed in Moreira et al., 2022; Sanyal 2022).

Many *in vitro* assays, such as hemagglutination SDS-PAGE and ELISA, were developed to measure vaccine antigens. However, one concern in developing serological assays is finding appropriate target antigens for the assay. The ideal assays could use either monoclonal antibody to the passive protective protein from a challenged animal, neutralising antibodies *in vitro*, or purified protein that could elicit protection in a vaccinated animal (reviewed in Moreira et al., 2022; Sanyal 2022).

The potency of inactivated poliovirus vaccines (IPV) is based on the content of the DAg form of poliovirus. Immunisation with a vaccine mainly consisting of DAg will induce protective immunity in the vaccinated host with protective immunity. In contrast, the CAg does not induce protective immunity. The DAg can be easily converted into CAg with heating at 56°C or higher and become ineffective in inducing protective immunity. Consequently, the content of native DAg is the biomarker of IPV potency and is commonly determined by a DAg ELISA (Le Bouvoir 1955; Mayer et al., 1957).

In the unpublished data of evaluating the potency of #9.3 yeast VLP, the potency test of yeast VLPs was carried out on 10 groups of 8 female BALB/c mice by immunizing them intraperitoneally with 100 AgU EVA71 antigen or PBS in the presence or absence of

Alhydrogel. The immunization was carried out twice with 3 weeks apart. Serum samples was taken 14 days after the final vaccine dose was administered. The serological tests have included neutralisation assay and measuring the total reactive antibody content of serum

The work presented in this thesis provides evidence for the successful application of thermal stressing to stabilise EVA71 mutants. However, more work is needed in order to generate more mAbs antibodies that can provide a precise antigenicity mapping of the EVA71. Dissecting the capsid antigenicity may led to a better understanding of the mechanism of particle stabilization, and whether there is a difference between NAg and HAg in term of antigenicity. These mAbs will also be helpful as unlimited reagents for future sensitive diagnostic antigens in ELISA assays. Likewise, they could be precise tool for evaluating vaccine potency.

Investing towards expressing the stabilised VLPs in other platforms, is another prospective goal in the future. Although the *Pichia pastori* is a robust heterologous protein expression system, a plant expression system might provide a cheaper platform to generate EVA71 VLP vaccines. Moreover, as future goal, it could be essential to move this project towards the application of identified mutations into other viruses either the other genotypes of the EVA71 or other viruses such as CAV16, which is a major causative agent of this HFMD as EVA71.

## *References*

Adeyemi, O. O., Sherry, L., Ward, J. C., Pierce, D. M., Herod, M. R., Rowlands, D. J., & Stonehouse, N. J. (2019). Involvement of a Nonstructural Protein in Poliovirus Capsid Assembly. *Journal of Virology*, *93*(5).

Aledo, J. C. (2019). Methionine in proteins: The Cinderella of the proteinogenic amino acids. *Protein Science*, *28*(10), 1785–1796.

Arthur Huang, K.-Y., Chen, M.-F., Huang, Y.-C., Shih, S.-R., Chiu, C.-H., Lin, J.-J., Wang, J.-R., Tsao, K.-C., & Lin, T.-Y. (2017). Epitope-associated and specificity-focused features of EV71-neutralizing antibody repertoires from plasmablasts of infected children. *Nature Communications*, *8*(1), 762.

Anasir, M., & Poh, C. (2019). Advances in Antigenic Peptide-Based Vaccine and Neutralizing Antibodies against Viruses Causing Hand, Foot, and Mouth Disease. *International Journal of Molecular Sciences*, *20*(6), 1256.

Ansardi, D. C., Morrow, C. D., Ansardi, C., Porter, D. C., Morrow, C. D., & Virol, J. (1993). Poliovirus capsid proteins derived from P1 precursors with glutamine-valine cleavage sites have defects in assembly and RNA encapsidation. *Journal of Virology*, *67*(12), 7284.

Arnon, R., & Ben-Yedidia, T. (2003). Old and new vaccine approaches. *International Immunopharmacology*, *3*(8), 1195–1204.

Alexopoulou, A. N., Couchman, J. R., & Whiteford, J. R. (2008). The CMV early enhancer/chicken β actin (CAG) promoter can be used to drive transgene expression during the differentiation of murine embryonic stem cells into vascular progenitors. *BMC Cell Biology*, *9*(1), 2.

Brandenburg, B., Lee, L. Y., Lakadamyali, M., Rust, M. J., Zhuang, X., & Hogle, J. M. (2007). Imaging poliovirus entry in live cells. *PLoS Biology*, *5*(7), 1543–1555.

Bible, J. M., Iturriza-Gomara, M., Megson, B., Brown, D., Pantelidis, P., Earl, P., Bendig, J., & Tong, C. Y. W. (2008). Molecular epidemiology of human enterovirus 71 in the United Kingdom from 1998 to 2006. *Journal of Clinical Microbiology*, *46*(10), 3192–3200.

Bodian, D. (1955). Emerging concept of poliomyelitis infection. *Science*, *122*(3159), 105–108.

Brandt, C. R., & Kolb, A. W. (2003). Tyrosine 116 of the herpes simplex virus type 1 IEalpha22 protein is an ocular virulence determinant and potential phosphorylation site. *Investigative Ophthalmology & Visual Science*, *44*(11), 4601–4607

Bahar, M. W., Porta, C., Fox, H., Macadam, A. J., Fry, E. E., & Stuart, D. I. (2021). Mammalian expression of virus-like particles as a proof of principle for next generation polio vaccines. *Npj Vaccines 2021 6:1*, *6*(1), 1–11.

Budowsky, E. I., Bresler, S. E., Friedman, E. A., & Zheleznova, N. v. (1981). Principles of selective inactivation of viral genome. *Archives of Virology*, *68*(3–4), 239–247.

Brisse, M., Vrba, S. M., Kirk, N., Liang, Y., & Ly, H. (2020). Emerging Concepts and Technologies in Vaccine Development. *Frontiers in Immunology*, *11*.

Bouvier, G. L. L. (1955). The modification of poliovirus antigens by heat and ultraviolet light. *The Lancet*, *266*(6898), 1013–1016.

Basavappa, R., Gómez-Yafal, A., & Hogle, J. M. (1998). The Poliovirus Empty Capsid Specifically Recognizes the Poliovirus Receptor and Undergoes Some, but Not All, of the Transitions Associated with Cell Entry. *Journal of Virology*, *72*(9), 7551–7556.

Bessaud, M., Razafindratsimandresy, R., Nougairède, A., Joffret, M. L., Deshpande, J. M., Dubot-Pérès, A., Héraud, J. M., de Lamballerie, X., Delpeyroux, F., & Bailly, J. L. (2014). Molecular Comparison and Evolutionary Analyses of VP1 Nucleotide Sequences of New African Human Enterovirus 71 Isolates Reveal a Wide Genetic Diversity. *PLOS ONE*, *9*(3), e90624.

Baicus A. (2012). History of polio vaccination. *World journal of virology*, *1*(4), 108–114.

Chang, Y.-K., Chen, K.-H., & Chen, K.-T. (2018). Hand, foot and mouth disease and herpangina caused by enterovirus A71 infections: a review of enterovirus A71 molecular epidemiology,

pathogenesis, and current vaccine development. *Revista Do Instituto de Medicina Tropical de São Paulo*, *60*(0).

Chang, C. K., Wu, S. R., Chen, Y. C., Lee, K. J., Chung, N. H., Lu, Y. J., Yu, S. L., Liu, C. C., & Chow, Y. H. (2018). Mutations in VP1 and 5'-UTR affect enterovirus 71 virulence. *Scientific Reports 2018 8:1*, *8*(1), 1–11.

Carter, J. R., Nawtaisong, P., Balaraman, V., & Fraser, M. J. (2014). Design and Analysis of Hammerhead Ribozyme Activity Against an Artificial Gene Target. *Methods in Molecular Biology (Clifton, N.J.)*, *1103*, 57.

Chang, P. C., Chen, S. C., & Chen, K. T. (2016). The Current Status of the Disease Caused by Enterovirus 71 Infections: Epidemiology, Pathogenesis, Molecular Epidemiology, and Vaccine Development. *International Journal of Environmental Research and Public Health*, *13*(9).

Carrat, F., & Flahault, A. (2007). Influenza vaccine: The challenge of antigenic drift. *Vaccine*, *25*(39–40), 6852–6862.

Choi, J. Y., Park, J. H., Jo, C., Kim, K. C., & Koh, Y. H. (2022). SARS-CoV-2 spike S1 subunit protein-mediated increase of beta-secretase 1 (BACE1) impairs human brain vessel cells. *Biochemical and Biophysical Research Communications*, *626*, 66–71.

Chia, M. Y., Chiang, P. S., Chung, W. Y., Luo, S. T., & Lee, M. S. (2014). Epidemiology of enterovirus 71 infections in Taiwan. *Pediatrics and Neonatology*, *55*(4), 243–249.

Chen, C.-S., Yao, Y.-C., Lin, S.-C., Lee, Y.-P., Wang, Y.-F., Wang, J.-R., Liu, C.-C., Lei, H.-Y., & Yu, C.-K. (2007). Retrograde Axonal Transport: a Major Transmission Route of Enterovirus 71 in Mice. *Journal of Virology*, *81*(17), 8996–9003.

Chong, P., Hsieh, S.-Y., Liu, C.-C., Chou, A.-H., Chang, J.-Y., Wu, S.-C., Liu, S.-J., Chow, Y.-H., Su, I.-J., & Klein, M. (2012). Production of EV71 vaccine candidates. *Human Vaccines & Immunotherapeutics*, *8*(12), 1775–1783

Chong, P., Liu, C. C., Chow, Y. H., Chou, A. H., & Klein, M. (2015). Review of Enterovirus 71 Vaccines. *Clinical Infectious Diseases*, *60*(5), 797–803.

Chea, S., Cheng, Y. B., Chokephaibulkit, K., Chotpitayasunondh, T., Rogier van Doorn, H., Hafy, Z., Kawichai, S., Liu, C. C., Nam, N. T. ran, Ooi, M. H. ow, Wolbers, M., & Zeng, M. (2015). Workshop on Use of Intravenous Immunoglobulin in Hand, Foot and Mouth Disease in Southeast Asia. *Emerging Infectious Diseases*, *21*(1).

Chen, P., & Shakhnovich, E. I. (2010). Thermal Adaptation of Viruses and Bacteria. *Biophysical Journal*, *98*(7), 1109–1118.

Chung, C.-Y., Chen, C.-Y., Lin, S.-Y., Chung, Y.-C., Chiu, H.-Y., Chi, W.-K., Lin, Y.-L., Chiang, B.-L., Chen, W.-J., & Hu, Y.-C. (2010). Enterovirus 71 virus-like particle vaccine: Improved production conditions for enhanced yield. *Vaccine*, *28*(43), 6951–6957.

Chia, M.-Y., Chung, W.-Y., Chiang, P.-S., Chien, Y.-S., Ho, M.-S., & Lee, M.-S. (2014). Monitoring Antigenic Variations of Enterovirus 71: Implications for Virus Surveillance and Vaccine Development. *PLoS Neglected Tropical Diseases*, *8*(7), e3044.

Corsino, C. B., Ali, R., & Linklater, D. R. (2022). Herpangina. Pediatric Clinical Advisor, 267–267. (Corsino, Ali and Linklater, 2022).

Cheng, H. Y., Huang, Y. C., Yen, T. Y., Hsia, S. H., Hsieh, Y. C., Li, C. C., Chang, L. Y., & Huang, L. M. (2014). The correlation between the presence of viremia and clinical severity in patients with enterovirus 71 infection: a multi-center cohort study. BMC Infectious Diseases, 14(1).

Crawt, L., Atkinson, E., Tedcastle, A., Pegg, E., Dobly, A., Wei, C., Lei, S., Ling, P., Li, C., Zheng, J., Wang, Y., Liqun, H., Jorajuria, S., Cozic, G., Ugiyadi, D., Kurniati, N., Ochiai, S., Miyazawa, M., Someya, Y., … Martin, J. (2019). Differences in Antigenic Structure of Inactivated Polio Vaccines Made From Sabin Live-Attenuated and Wild-Type Poliovirus Strains: Impact on Vaccine Potency Assays. *The Journal of Infectious Diseases*.

Chung, Y.-C., Ho, M.-S., Wu, J.-C., Chen, W.-J., Huang, J.-H., Chou, S.-T., & Hu, Y.-C. (2008). Immunization with virus-like particles of enterovirus 71 elicits potent immune responses and protects mice against lethal challenge. *Vaccine*, *26*(15), 1855–1862.

Chung, Y.-C. (2006). Expression, purification and characterization of enterovirus-71 virus-like particles. *World Journal of Gastroenterology*, *12*(6), 921.

Cifuente, J. O., & Moratorio, G. (2019). Evolutionary and Structural Overview of Human Picornavirus Capsid Antibody Evasion. In *Frontiers in Cellular and Infection Microbiology* (Vol. 9).

Chow, M., Newman, J. F. E., Filman, D., Hogle, J. M., Rowlands, D. J., & Brown, F. (1987). Myristylation of picornavirus capsid protein VP4 and its structural significance. *Nature*, *327*(6122), 482–486.

Chang, Y.-K., Chen, K.-H., & Chen, K.-T. (2018). Hand, foot and mouth disease and herpangina caused by enterovirus A71 infections: a review of enterovirus A71 molecular epidemiology, pathogenesis, and current vaccine development. *Revista Do Instituto de Medicina Tropical de São Paulo*, *60*(0).

Centers for Disease Control and Prevention (CDC). (2022). Polio Disease and Poliovirus *CDC*. [Accessed 25 October 2022]. Available from: https://www.cdc.gov/cpr/polioviruscontainment/diseaseandvirus.htm.

de La Peña, M., García-Robles, I., & Cervera, A. (2017). The Hammerhead Ribozyme: A Long History for a Short RNA. *Molecules 2017, Vol. 22, Page 78*, *22*(1), 78.

Debaisieux, S., Encheva, V., Chakravarty, P., Snijders, A. P., & Schiavo, G. (2016). Analysis of signaling endosome composition and dynamics using silac in embryonic stem cell-derived neurons. *Molecular and Cellular Proteomics*, *15*(2), 542–557.

David, G., Reboutier, D., Deschamps, S., Méreau, A., Taylor, W., Padilla-Parra, S., Tramier, M., Audic, Y., & Paillard, L. (2022). The RNA-binding proteins CELF1 and ELAVL1 cooperatively control the alternative splicing of CD44. *Biochemical and Biophysical Research Communications*, *626*, 79–84.

Domingo, E., Sheldon, J., & Perales, C. (2012). Viral Quasispecies Evolution. *Microbiology and Molecular Biology Reviews*, *76*(2), 159–216.

Domingo, E., Escarmís, C., Sevilla, N., Moya, A., Elena, S. F., Quer, J., Novella, I. S., & Holland, J. J. (1996). Basic concepts in RNA virus evolution. *The FASEB Journal*, *10*(8), 859–864.

Domingo, E., & Perales, C. (2019). Viral quasispecies. *PLOS Genetics*, *15*(10), e1008271.

Excler, J.-L., Saville, M., Berkley, S., & Kim, J. H. (2021). Vaccine development for emerging infectious diseases. *Nature Medicine*, *27*(4), 591–600.

Esposito, S., & Principi, N. (2022). Hand, foot and mouth disease: current knowledge on clinical manifestations, epidemiology, aetiology and prevention. *Morbidity and Mortality Weekly Report (MMWR)* 17;71(24):786-790

Centers for Disease Control and Prevention (CDC). (2021). Hand, Foot, and Mouth Disease (HFMD) [Online]. [Accessed 17 Nov 2021]. Available from: http://www.hawking.org.uk/https://www.cdc.gov/hand-foot-mouth/index.html

Fujii, K., Nagata, N., Sato, Y., Ong, K. C., Wong, K. T., Yamayoshi, S., Shimanuki, M., Shitara, H., Taya, C., & Koike, S. (2013). Transgenic mouse model for the study of enterovirus 71 neuropathogenesis. *Proceedings of the National Academy of Sciences of the United States of America*, *110*(36), 14753–14758.

Foo, D. G. W., Alonso, S., Phoon, M. C., Ramachandran, N. P., Chow, V. T. K., & Poh, C. L. (2007). Identification of neutralizing linear epitopes from the VP1 capsid protein of Enterovirus 71 using synthetic peptides. *Virus Research*, *125*(1), 61–68.

Fox, H., Knowlson, S., Minor, P. D., & Macadam, A. J. (2017). Genetically Thermo-Stabilised, Immunogenic Poliovirus Empty Capsids; a Strategy for Non-replicating Vaccines. *PLOS Pathogens*, *13*(1), e1006117.

Fujii, K., Sudaka, Y., Takashino, A., Kobayashi, K., Kataoka, C., Suzuki, T., Iwata-Yoshikawa, N., Kotani, O., Ami, Y., Shimizu, H., Nagata, N., Mizuta, K., Matsuzaki, Y., & Koike, S. (2018). VP1 Amino Acid Residue 145 of Enterovirus 71 Is a Key Residue for Its Receptor Attachment and Resistance to Neutralizing Antibody during Cynomolgus Monkey Infection. *Journal of Virology*, *92*(15).

Galiza, E., & Heath, P. (2017). Immunization. *Medicine (United Kingdom)*, *49*(10), 618–623.

Guttman, N., & Baltimore, D. (1977). Morphogenesis of poliovirus. IV. existence of particles sedimenting at 150S and having the properties of provirion. *Journal of Virology*, *23*(2), 363.

Guerra, A. M., Orille, E., & Waseem, M. (2022). Hand Foot And Mouth Disease. *StatPearls*.

Greenbaum, B. D., & Ghedin, E. (2015). Viral evolution: beyond drift and shift. *Current Opinion in Microbiology*, *26*, 109–115.

Gregorio, N. E., Levine, M. Z., & Oza, J. P. (2019). A User's Guide to Cell-Free Protein Synthesis. *Methods and Protocols*, *2*(1), 24. .

Garenne, D., Haines, M. C., Romantseva, E. F., Freemont, P., Strychalski, E. A., & Noireaux, V. (2021). Cell-free gene expression. *Nature Reviews Methods Primers*, *1*(1), 49.

Groppelli, E., Levy, H. C., Sun, E., Strauss, M., Nicol, C., Gold, S., Zhuang, X., Tuthill, T. J., Hogle, J. M., & Rowlands, D. J. (2017). Picornavirus RNA is protected from cleavage by ribonuclease during virion uncoating and transfer across cellular and model membranes. *PLOS Pathogens*, *13*(2), e1006197.

Gregoret, L. M., & Sauer, R. T. (1998). Tolerance of a protein helix to multiple alanine and valine substitutions. *Folding and Design*, *3*(2), 119–126.

Huang, Y. feng, Li, Y., Chen, J. ying, Lin, J. hui, Liu, L., Ye, J. zhou, & Su, Y. bin. (2022). Promoting effect of Fe3+ on gentamicin resistance in *Escherichia coli*. *Biochemical and Biophysical Research Communications*, *625*, 134–139.

Gao, F., Wang, Y. P., Mao, Q. Y., Yao, X., Liu, S., Li, F. X., Zhu, F. C., Yang, J. Y., Liang, Z. L., Lu, F. M., & Wang, J. Z. (2012). Enterovirus 71 viral capsid protein linear epitopes: Identification and characterization. *Virology Journal*, *9*(1), 1–7.

Garon, J., Seib, K., Orenstein, W. A., Gonzalez, A. R., Blanc, D. C., Zaffran, M. & Patel, M. (2016). Polio endgame: the global switch from tOPV to bOPV. *Expert Review of Vaccines* 15, 693-708.

Hagiwara, A., Tagaya, I., & Yoneyama, T. (1978). Epidemic of hand, foot and mouth disease associated with enterovirus 71 infection. *Intervirology*, *9*(1), 60–63.

Hu, Y. C., Hsu, J. T. A., Huang, J. H., Ho, M. S., & Ho, Y. C. (2003). Formation of enterovirus-like particle aggregates by recombinant baculoviruses co-expressing P1 and 3CD in insect cells. *Biotechnology Letters*, *25*(12), 919–925.

Hogle, J. M. (2002). Poliovirus cell entry: common structural themes in viral cell entry pathways. *Annu Rev Microbiol* 56, 677-702.

Hagiwara, A., Tagaya, I., & Yoneyama, T. (1978). Epidemic of hand, foot and mouth disease associated with enterovirus 71 infection. *Intervirology*, *9*(1), 60–63.

Han, X., Ying, X. L., Zhou, S. L., Han, T., Huang, H., Jin, Q., Yang, F., Sun, Q. Y., & Sun, X. X. (2014). Characterization of the enterovirus 71 P1 polyprotein expressed in Pichia pastor as a candidate vaccine. *Human Vaccines & Immunotherapeutics*, *10*(8), 2220.

He, Y., Ong, K. C., Gao, Z., Zhao, X., Anderson, V. M., McNutt, M. A., Wong, K. T., & Lu, M. (2014). Tonsillar crypt epithelium is an important extra-central nervous system site for viral replication in EV71 encephalomyelitis. The American Journal of Pathology, 184(3), 714–720.

Jiang, P., Liu, Y., Ma, H.-C., Paul, A. v., & Wimmer, E. (2014). Picornavirus Morphogenesis. *Microbiology and Molecular Biology Reviews*, *78*(3), 418–437.

Jin, Y., Sun, T., Zhou, G., Li, D., Chen, S., Zhang, W., Li, X., Zhang, R., Yang, H., & Duan, G. (2021). Pathogenesis Study of Enterovirus 71 Using a Novel Human SCARB2 Knock-In Mouse Model. *MSphere*, *6*(2).

Jia, Q., Ng, Q., Chin, W., Meng, T., Chow, V. T. K., Wang, C. I., Kwang, J., & He, F. (2017). Effective in vivo therapeutic IgG antibody against VP3 of enterovirus 71 with receptor-competing activity. *Scientific Reports 2017 7:1*, *7*(1), 1–14.

Jiang, Y., Yu, K., Zhang, H., Zhang, P., Li, C., Tian, G., Li, Y., Wang, X., Ge, J., Bu, Z., & Chen, H. (2007). Enhanced protective efficacy of H5 subtype avian influenza DNA vaccine with codon optimized HA gene in a pCAGGS plasmid vector. *Antiviral Research*, *75*(3), 234–241.

Jiao, W., Tan, S. R., Huang, Y. F., Mu, L. H., Yang, Y., Wang, Y., & Wu, X. E. (2019). The Effectiveness of Different Doses of Intravenous Immunoglobulin on Severe Hand, Foot and Mouth Disease: A Meta-Analysis. *Medical Principles and Practice*, *28*(3), 256–263.

Jin, Y., Li, D., Sun, T., Du, Y., Gao, Y., Ding, R., Ji, W., Zhang, W., Yang, H., Chen, S., & Duan, G. (2021). Pathological Features of Enterovirus 71-Associated Brain and Lung Damage in Mice Based on Quantitative Proteomic Analysis. *Frontiers in microbiology*, *12*, 663019.

Koh, W. M., Bogich, T., Siegel, K., Jin, J., Chong, E. Y., Tan, C. Y., Chen, M. I. C., Horby, P., & Cook, A. R. (2016). The Epidemiology of Hand, Foot and Mouth Disease in Asia: A Systematic Review and Analysis. *The Pediatric Infectious Disease Journal*, *35*(10), e285.

Koike, S., Taya, C., Aoki, J., Matsuda, Y., Ise, I., Takeda, H., Matsuzaki, T., Amanuma, H., Yonekawa, H., & Nomoto, A. (1994). Characterization of three different transgenic mouse lines that carry human poliovirus receptor gene-influence of the transgene expression on pathogenesis. *Archives of Virology*, *139*(3–4), 351–363

Kouiavskaia, D., Puligedda, R. D., Dessain, S. K., & Chumakov, K. (2020). Universal ELISA for quantification of D-antigen in inactivated poliovirus vaccines. *Journal of Virological Methods*, *276*, 113785.

Khambhati, K., Bhattacharjee, G., Gohil, N., Braddick, D., Kulkarni, V., & Singh, V. (2019). Exploring the Potential of Cell-Free Protein Synthesis for Extending the Abilities of Biological Systems. *Frontiers in Bioengineering and Biotechnology*, *7*.

Kuo, R. L., & Shih, S. R. (2013). Strategies to develop antivirals against enterovirus 71. *Virology Journal*, *10*(1), 1–8.

Kingston, N. J., Shegdar, M., Snowden, J. S., Fox, H., Groppelli, E., Macadam, A., Rowlands, D. J., & Stonehouse, N. J. (2022). Thermal stabilization of enterovirus A 71 and production of antigenically stabilized empty capsids. Journal of General Virology, 103(8), 001771.

Kim, H., Webster, R. G., & Webby, R. J. (2018). Influenza Virus: Dealing with a Drifting and Shifting Pathogen. *Viral Immunology*, *31*(2), 174–183.

Kelly, James Thomas (2015) *The enterovirus 71 particle: An evolutionary approach to investigate structure and function with implications for drug and vaccine development.* PhD thesis, University of Leeds.

Kim, H.-J., Son, H. S., Lee, S. W., Yoon, Y., Hyeon, J.-Y., Chung, G. T., Lee, J.-W., & Yoo, J. S. (2019). Efficient expression of enterovirus 71 based on virus-like particles vaccine. *PLOS ONE*, *14*(3), e0210477

Ke, X., Zhang, Y., Liu, Y., Miao, Y., Zheng, C., Luo, D., Sun, J., Hu, Q., Xu, Y., Wang, H., & Zheng, Z. (2020). A Single Mutation in the VP1 Gene of Enterovirus 71 Enhances Viral Binding to Heparan Sulfate and Impairs Viral Pathogenicity in Mice. *Viruses*, *12*(8), 883.

Kiener, T. K., Jia, Q., Lim, X. F., He, F., Meng, T., Kwong Chow, V. T., & Kwang, J. (2012). Characterization and specificity of the linear epitope of the enterovirus 71 VP2 protein. *Virology Journal*, *9*(1), 55.

Kamau, E., Nguyen, D., Celma, C., Blomqvist, S., Horby, P., Simmonds, P., & Harvala, H. (2021). Seroprevalence and Virologic Surveillance of Enterovirus 71 and Coxsackievirus A6, United Kingdom, 2006–2017. *Emerging Infectious Diseases*, *27*(9), 2261.

Karlsson Hedestam, G. B., Fouchier, R. A. M., Phogat, S., Burton, D. R., Sodroski, J., & Wyatt, R. T. (2008). The challenges of eliciting neutralizing antibodies to HIV-1 and to influenza virus. *Nature Reviews Microbiology*, *6*(2), 143–155.

Li, H.-Y., Han, J.-F., Qin, C.-F., & Chen, R. (2013). Virus-like particles for enterovirus 71 produced from *Saccharomyces cerevisiae* potently elicits protective immune responses in mice. *Vaccine*, *31*(32), 3281–3287.

Lin, Y.-L., Yu, C.-I., Hu, Y.-C., Tsai, T.-J., Kuo, Y.-C., Chi, W.-K., Lin, A.-N., & Chiang, B.-L. (2012). Enterovirus type 71 neutralizing antibodies in the serum of macaque monkeys immunized with EV71 virus-like particles. *Vaccine*, *30*(7), 1305–1312.

Li, M.-L., Shih, S.-R., Tolbert, B. S., & Brewer, G. (2021). Enterovirus A71 Vaccines. *Vaccines*, *9*(3), 199.

Luo, S. T., Chiang, P. S., Chao, A. S., Liou, G. Y., Lin, R., Lin, T. Y., & Lee, M. S. (2009). Enterovirus 71 maternal antibodies in infants, Taiwan. Emerging infectious diseases, 15(4), 581–584.

Le Bouvier, G. L. (1959). Poliovirus D and C antigens: their differentiation and measurement by precipitation in agar. *British Journal of Experimental Pathology*, *40*.

Liu, B., Luo, L., Yan, S., Wen, T., Bai, W., Li, H., Zhang, G., Lu, X., Liu, Y., & He, L. (2015). Clinical Features for Mild Hand, Foot and Mouth Disease in China. *PLOS ONE*, *10*(8), e0135503.

Liu, C.-C., Guo, M.-S., Lin, F. H.-Y., Hsiao, K.-N., Chang, K. H.-W., Chou, A.-H., Wang, Y.-C., Chen, Y.-C., Yang, C.-S., & Chong, P. C.-S. (2011). Purification and Characterization of Enterovirus 71 Viral Particles Produced from Vero Cells Grown in a Serum-Free Microcarrier Bioreactor System. *PLoS ONE*, *6*(5), e20005.

Li, M. L., Shih, S. R., Tolbert, B. S., & Brewer, G. (2021). Enterovirus A71 Vaccines. *Vaccines*, *9*(3), 1–10.

Lei, X., Cui, S., Zhao, Z., & Wang, J. (2015). Etiology, pathogenesis, antivirals and vaccines of hand, foot, and mouth disease. *National Science Review*, *2*(3), 268–284.

Lalani, S., Gew, L. T., & Poh, C. L. (2021). Antiviral peptides against Enterovirus A71 causing hand, foot and mouth disease. *Peptides*, *136*, 170443.

Lucas, M., Karrer, U., Lucas, A., & Klenerman, P. (2001). Viral escape mechanisms – escapology taught by viruses. *International Journal of Experimental Pathology*, *82*(5), 269.

Lin, J. Y., Kung, Y. A., & Shih, S. R. (2019). Antivirals and vaccines for Enterovirus A71. *Journal of Biomedical Science 2019 26:1*, *26*(1), 1–10.

Lai, R. H., Chow, Y. H., Chung, N. H., Chen, T. C., Shie, F. S., & Juang, J. L. (2022). Neurotropic EV71 causes encephalitis by engaging intracellular TLR9 to elicit neurotoxic IL12-p40-iNOS signaling. *Cell Death & Disease 2022 13:4*, *13*(4), 1–9.

Lee, K. Y. (2016). Enterovirus 71 infection and neurological complications. *Korean Journal of Pediatrics*, *59*(10), 395.

Lin, C., Yang, H., Zhao, W., & Wang, W. (2022). CTSB+ macrophage repress memory immune hub in the liver metastasis site of colorectal cancer patient revealed by multi-omics analysis. *Biochemical and Biophysical Research Communications*, *626*, 8–14.

Lai, M. C., Chen, H. H., Xu, P., & Wang, R. Y. L. (2020). Translation control of Enterovirus A71 gene expression. *Journal of Biomedical Science*, *27*(1), 1–9.

Lee, M. S., & Chang, L. Y. (2014). Development of enterovirus 71 vaccines. *Expert Rev. Vaccines 9*(2), 149–156.

Mayer et al. (1957). The Purification of Poliomyelitis Virus as Studied by Complement Fixation. *Journal of Immunology*, *78*(6), 435–455.

Mehndiratta, M. M., Mehndiratta, P., & Pande, R. (2014). Poliomyelitis: historical facts, epidemiology, and current challenges in eradication. *The Neurohospitalist*, *4*(4)

Morag Ferguson, D. J. W. and P. D. M. (1993). Antigenic structure of poliovirus in inactivated vaccines. *Journal of General Virology*, *74*, 685–690.

Martín, J., Samoilovich, E., Dunn, G., Lackenby, A., Feldman, E., Heath, A., Svirchevskaya, E., Cooper, G., Yermalovich, M., & Minor, P. D. (2002). Isolation of an Intertypic Poliovirus Capsid Recombinant from a Child with Vaccine-Associated Paralytic Poliomyelitis. *Journal of Virology*, *76*(21), 10921–10928.

Ma, S.-H., Liu, J.-S., Wang, J.-J., Shi, H.-J., Yang, H.-J., Chen, J.-Y., Liu, L.-D., & Li, Q.-H. (2009). Genetic Analysis of the VP1 Region of Human Enterovirus 71 Strains Isolated in Fuyang, China, During 2008 *. *VIROLOGICA SINICA*, *24*(3), 162–170.

Martínez, M. A., Martrus, G., Capel, E., Parera, M., Franco, S., & Nevot, M. (2012). Quasispecies Dynamics of RNA Viruses. In *Viruses: Essential Agents of Life* (pp. 21–42). Springer Netherlands.

Mao, Q., Wang, Y., Bian, L., Xu, M., & Liang, Z. (2016). EV71 vaccine, a new tool to control outbreaks of hand, foot and mouth disease (HFMD). *Expert Review of Vaccines*, *15*(5), 599–606.

Morley, V. J., & Turner, P. E. (2017). Dynamics of molecular evolution in RNA virus populations depend on sudden versus gradual environmental change. *Evolution*, *71*(4), 872–883.

Mundlapati, V. R., Ghosh, S., Bhattacherjee, A., Tiwari, P., & Biswal, H. S. (2015). Critical Assessment of the Strength of Hydrogen Bonds between the Sulfur Atom of Methionine/Cysteine and Backbone Amides in Proteins. *The Journal of Physical Chemistry Letters*, *6*(8), 1385–1389.

Marsian, J., Fox, H., Bahar, M. W., Kotecha, A., Fry, E. E., Stuart, D. I., Macadam, A. J., Rowlands, D. J., & Lomonossoff, G. P. (2017). Plant-made polio type 3 stabilized VLPs-A candidate synthetic polio vaccine. *Nature Communications*, *8*(1).

McMinn, P. C. (2002). An overview of the evolution of enterovirus 71 and its clinical and public health significance. *FEMS Microbiology Reviews*, *26*(1), 91–107.

Maday, S., Twelvetrees, A. E., Moughamian, A. J., & Holzbaur, E. L. F. (2014). Axonal Transport: Cargo-Specific Mechanisms of Motility and Regulation. *Neuron*, *84*(2), 292–309.

Melnick, J. L. (1993). The Discovery of the Enteroviruses and the Classification of Poliovirus Among Them. *Biologicals*, *21*(4), 305–309.

Maciej Serda, Becker, F. G., Cleary, M., Team, R. M., Holtermann, H., The, D., Agenda, N., Science, P., Sk, S. K., Hinnebusch, R., Hinnebusch A, R., Rabinovich, I., Olmert, Y., Uld, D. Q. G.

L. Q., Ri, W. K. H. U., Lq, V., Frxqwu, W. K. H., Zklfk, E., Edvhg, L. v, … ح ,فاطمی. (2013). Synteza i aktywność biologiczna nowych analogów tiosemikarbazonowych chelatorów żelaza. *Uniwersytet Śląski*, *7*(1), 343–354.

Minor, P. D. (2016). An introduction to poliovirus: Pathogenesis, vaccination, and the endgame for global eradication. *Methods in Molecular Biology*, *1387*, 1–10.

McMinn, P. C. (2002). An overview of the evolution of enterovirus 71 and its clinical and public health significance. *FEMS Microbiology Reviews*, *26*(1), 91–107.

Mong, H. O., Solomon, T., Podin, Y., Mohan, A., Akin, W., Yusuf, M. A., del Sel, S., Kontol, K. M., Boon, F. L., Clear, D., Chae, H. C., Blake, E., Perera, D., See, C. W., & Cardosa, J. (2007). Evaluation of Different Clinical Sample Types in Diagnosis of Human Enterovirus 71-Associated Hand-Foot-and-Mouth Disease. *Journal of Clinical Microbiology*, *45*(6), 1858.

Man-Li, T., Szyporta, M., Fang, L. X., & Kwang, J. (2012). Identification and characterization of a monoclonal antibody recognizing the linear epitope RVADVI on VP1 protein of enterovirus 71. *Journal of Medical Virology*, *84*(10), 1620–1627.

Min Feng, Q. L. (2014). EV71, A Virus with Complicated Pathogenesis in the CNS. *Journal of Infectious Diseases and Therapy*, *02*(05).

Mao, Q. Y., Wang, Y., Bian, L., Xu, M., & Liang, Z. (2016). EV71 vaccine, a new tool to control outbreaks of hand, foot and mouth disease (HFMD).

Morrison, P. (2016). Viral Vaccines: Fighting Viruses with Vaccines. *Viral Pathogenesis: From Basics to Systems Biology: Third Edition*, 253–269.

Marcotte, L. L., Wass, A. B., Gohara, D. W., Pathak, H. B., Arnold, J. J., Filman, D. J., Cameron, C. E., & Hogle, J. M. (2007). Crystal Structure of Poliovirus 3CD Protein: Virally Encoded Protease and Precursor to the RNA-Dependent RNA Polymerase. *Journal of Virology*, *81*(7), 3583–3596.

Nooraei, S., Bahrulolum, H., Hoseini, Z. S., Katalani, C., Hajizade, A., Easton, A. J., & Ahmadian, G. (2021). Virus-like particles: preparation, immunogenicity and their roles as nanovaccines and drug nanocarriers. *Journal of Nanobiotechnology*, *19*(1), 59.

Nims, R. W., & Plavsic, M. (2013). Polyomavirus inactivation – A review. *Biologicals*, *41*(2), 63–70.

Nomoto A. (2007). Molecular aspects of poliovirus pathogenesis. *Proceedings of the Japan Academy. Series B, Physical and biological sciences*, *83*(8), 266–275.

Nayak, G., Bhuyan, S. K., Bhuyan, R., Sahu, A., Kar, D., & Kuanar, A. (2022). Global emergence of Enterovirus 71: a systematic review. Beni-Suef University Journal of Basic and Applied Sciences, 11(1), 78.

Nakatsukasa, K., Fujisawa, M., Yang, X., Kawarasaki, T., Okumura, F., & Kamura, T. (2022). Triacylglycerol lipase Tgl4 is a stable protein and its dephosphorylation is regulated in a cell cycle-dependent manner in *Saccharomyces cerevisiae*. Biochemical and Biophysical Research Communications, 626, 85–91.

Nagata, N., Shimizu, H., Ami, Y., Tano, Y., Harashima, A., Suzaki, Y., Sato, Y., Miyamura, T., Sata, T., & Iwasaki, T. (2002). Pyramidal and extrapyramidal involvement in experimental infection of cynomolgus monkeys with enterovirus 71. Journal of Medical Virology, 67(2), 207–216.

Ohka, S., Sakai, M., Bohnert, S., Igarashi, H., Deinhardt, K., Schiavo, G., & Nomoto, A. (2009). Receptor-Dependent and -Independent Axonal Retrograde Transport of Poliovirus in Motor Neurons. Journal of Virology, 83(10), 4995–5004.

Offit, P. A. (2017). *The Cutter Incident*. Yale University Press.

Ohka, S., Matsuda, N., Tohyama, K., Oda, T., Morikawa, M., Kuge, S., & Nomoto, A. (2004). Receptor (CD155)-Dependent Endocytosis of Poliovirus and Retrograde Axonal Transport of the Endosome. Journal of Virology, 78(13), 7186–7198.

Ohka, S., Yang, W. X., Terada, E., Iwasaki, K., & Nomoto, A. (1998). Retrograde transport of intact poliovirus through the axon via the fast transport system. Virology, 250(1), 67–75.

Ohka, S., Hao Tan, S., Kaneda, S., Fujii, T., & Schiavo, G. (2022). Retrograde axonal transport of poliovirus and EV71 in motor neurons. Biochemical and Biophysical Research Communications, 626, 72–78.

Ong, K. C., & Wong, K. T. (2015). Understanding Enterovirus 71 Neuropathogenesis and Its Impact on Other Neurotropic Enteroviruses. Brain Pathology, 25(5), 614-624

Oluwasanmi, O. J., Mckenzie, D. A., Adewole, I. O., Aluka, C. O., Iyasse, J., Olunu, E., & Fakoya, A. O. (2019). Postpolio Syndrome: A Review of Lived Experiences of Patients. *International journal of applied & basic medical research*, *9*(3), 129–134.

Onvimala, N., Kosoltanapiwat, N., Pumirat, P., Vanaporn, M., Nimmanitya, S., Tacharoenmuang, R., Guntapong, R., & Leaungwutiwong, P. (2021). Genotyping of non-polio enteroviruses associated with acute flaccid paralysis in Thailand in 2013 and 2014. Virology Journal, 18(1), 1–8.

Ooi, M. H., Wong, S. C., Lewthwaite, P., Cardosa, M. J., & Solomon, T. (2010). Clinical features, diagnosis, and management of enterovirus 71. The Lancet Neurology, 9(11), 1097–1105.

Plevka, P., Perera, R., Cardosa, J., Kuhn, R. J., & Rossmann, M. G. (2012). Crystal structure of human enterovirus 71. *Science* (New York, N.Y.), 336(6086), 1274.

Plevka, P., Perera, R., Yap, M. L., Cardosa, J., Kuhn, R. J., & Rossmann, M. G. (2013). Structure of human enterovirus 71 in complex with capsid-binding inhibitor. *Proceedings of the National Academy of Sciences of the United States of America*, 110(14), 5463–5467.

Plevka, P., Perera, R. & Rossmann, M.G., 2012. Structure determination of enterovirus 71 research papers. *Biological Crystallography*, 68, pp.1217–1222.

Paul, A. v., & Wimmer, E. (2015). Initiation of protein-primed picornavirus RNA synthesis. *Virus Research*, *206*, 12–26.

Pathak, H. B., Arnold, J. J., Wiegand, P. N., Hargittai, M. R. S., & Cameron, C. E. (2007). Picornavirus Genome Replication. *Journal of Biological Chemistry*, *282*(22), 16202–16213.

Paton, D. J., di Nardo, A., Knowles, N. J., Wadsworth, J., Pituco, E. M., Cosivi, O., Rivera, A. M., Kassimi, L. B., Brocchi, E., de Clercq, K., Carrillo, C., Maree, F. F., Singh, R. K., Vosloo, W., Park, M.-K., Sumption, K. J., Ludi, A. B., & King, D. P. (2021). The history of foot-and-mouth disease virus serotype C: the first known extinct serotype? *Virus Evolution*, *7*(1).

Porta, C. et al., 2013. Rational Engineering of Recombinant Picornavirus Capsids to Produce Safe, Protective Vaccine Antigen. *PLoS Pathogens*, 9(3), p.e1003255.

Puenpa, J., Wanlapakorn, N., Vongpunsawad, S., & Poovorawan, Y. (2019). The History of Enterovirus A71 Outbreaks and Molecular Epidemiology in the Asia-Pacific Region. *Journal of Biomedical Science*, *26*(1), 75.

Phanthong, S., Densumite, J., Seesuay, W., Thanongsaksrikul, J., Teimoori, S., Sookrung, N., Poovorawan, Y., Onvimala, N., Guntapong, R., Pattanapanyasat, K., & Chaicumpa, W. (2020). Human Antibodies to VP4 Inhibit Replication of Enteroviruses Across Subgenotypes and Serotypes, and Enhance Host Innate Immunity. *Frontiers in Microbiology*, *11*, 2253.

Qing, J., Wang, Y., Sun, Y., Huang, J., Yan, W., Wang, J., Su, D., Ni, C., Li, J., Rao, Z., Liu, L., & Lou, Z. (2014). Cyclophilin A Associates with Enterovirus-71 Virus Capsid and Plays an Essential Role in Viral Infection as an Uncoating Regulator. *PLoS Pathogens*, *10*(10), e1004422.

Qiu, J., Yang, Y., Huang, L., Wang, L., Jiang, Z., Gong, J., Wang, W., Wang, H., Guo, S., Li, C., Wei, S., Mo, Z., & Xia, J. (2017). Immunogenicity and safety evaluation of bivalent types 1 and 3 oral poliovirus vaccine by comparing different poliomyelitis vaccination schedules in China: A randomized controlled non-inferiority clinical trial. *Human vaccines & immunotherapeutics*, *13*(6), 1–10.

Ren, R., & Racaniello, V. R. (1992). Poliovirus Spreads from Muscle to the Central Nervous System by Neural Pathways. *Journal of Infectious Diseases*, *166*(4), 747–752.

Rossmann, M. G., He, Y. & Kuhn, R. J. (2002). Picornavirus-receptor interactions. *Trends in microbiology* 10, 324-331.

Romero, J. R., & Modlin, J. F. (2015). Poliovirus. *Mandell, Douglas, and Bennett's Principles and Practice of Infectious Diseases*, *2*, 2073-2079.e2.

Rowlands, D. J. (2015). Picornaviruses. In eLS (pp. 1–12). Wiley.

Rozovics, J. M., Virgen-Slane, R., & Semler, B. L. (2011). Engineered Picornavirus VPg-RNA Substrates: Analysis of a Tyrosyl-RNA Phosphodiesterase Activity. *PLoS ONE*, *6*(3), e16559.

Riedel, S. (2005). Edward Jenner and the History of Smallpox and Vaccination. *Baylor University Medical Center Proceedings*, *18*(1), 21–25.

Racaniello, V. R. (2013). Picornaviridae: The viruses and their replication. In *Fields Virology: Sixth Edition* (Vol. 1).

Rattanapisit, K., Chao, Z., Siriwattananon, K., Huang, Z., & Phoolcharoen, W. (2019). Plant-Produced Anti-Enterovirus 71 (EV71) Monoclonal Antibody Efficiently Protects Mice Against EV71 Infection. *Plants*, *8*(12).

Sinclair, C., Gaunt, E., Simmonds, P., Broomfield, D., Nwafor, N., Wellington, L., Templeton, K., Willocks, L., Schofield, O., & Harvala, H. (2014). Atypical hand, foot, and mouth disease associated with coxsackievirus A6 infection, Edinburgh, United Kingdom, January To February 2014. *Eurosurveillance*, *19*(12), 20745.

Shabram, P., & Aguilar-Cordova, E. (2000). Multiplicity of infection/multiplicity of confusion. *Molecular Therapy*, *2*(5), 420–421.

Shingler, K. L., Yoder, J. L., Carnegie, M. S., Ashley, R. E., Makhov, A. M., Conway, J. F., & Hafenstein, S. (2013). The Enterovirus 71 A-particle Forms a Gateway to Allow Genome

Sherry, L., Grehan, K., Snowden, J. S., Knight, M. L., Adeyemi, O. O., Rowlands, D. J., & Stonehouse, N. J. (2020). Comparative Molecular Biology Approaches for the Production of Poliovirus Virus-Like Particles Using *Pichia pastoris*. *MSphere*, *5*(2).

Shimizu, H., Utama, A., Yoshii, K., Yoshida, H., Yoneyama, T., Sinniah, M., bin Yusof, M. A., Okuno, Y., Okabe, N., Shih, S. R., Chen, H. Y., Wang, G. R., Kao, C. L., Chang, K. S. S., Miyamura, T., & Hagiwara, A. (1999). Enterovirus 71 from fatal and nonfatal cases of hand, foot and mouth disease epidemics in Malaysia, Japan and Taiwan in 1997-1998. *Japanese Journal of Infectious Diseases*, *52*(1), 12–15.

Song, C., Li, Y., Zhou, Y., Liang, L., Turtle, L., Wang, F., Wu, P., Qiu, Q., Yang, J., Wang, K., Cui, P., Cheng, Y., Zhang, T., Guo, C., Zeng, M., Long, L., Peiris, M., Zhou, C., Cowling, B. J., & Yu, H. (2020). Enterovirus genomic load and disease severity among children hospitalised with hand, foot and mouth disease. EBioMedicine, 62, 103078.

Schindelin, J., Arganda-Carreras, I., Frise, E., Kaynig, V., Longair, M., Pietzsch, T., Preibisch, S., Rueden, C., Saalfeld, S., Schmid, B., Tinevez, J. Y., White, D. J., Hartenstein, V., Eliceiri, K., Tomancak, P., & Cardona, A. (2012). Fiji: An open-source platform for biological-image analysis. *Nature Methods*, *9*(7), 676–682.

Shiroki, K., Ishii, T., Aoki, T., Kobashi, M., Ohka, S., & Nomoto, A. (1995). A new cis-acting element for RNA replication within the 5' noncoding region of poliovirus type 1 RNA. *Journal of Virology*, *69*(11), 6825–6832.

Simmonds, P., & Welch, J. (2006). Frequency and Dynamics of Recombination within Different Species of Human Enteroviruses. *Journal of Virology*, *80*(1), 483–493.

Solomon, T., Lewthwaite, P., Perera, D., Cardosa, M. J., McMinn, P., & Ooi, M. H. (2010). Virology, epidemiology, pathogenesis, and control of enterovirus 71. *The Lancet Infectious Diseases*, *10*(11), 778–790.

Sabanathan, S., Tan, l., Thwaites, L., Wills, B., Qui, P. T., & Rogier van Doorn, H. (2014). Enterovirus 71 related severe hand, foot and mouth disease outbreaks in South-East Asia: current situation and ongoing challenges. *Journal of epidemiology and community health*, 68(6), 500–502.

Swain, S. K., Gadnayak, A., Mohanty, J. N., Sarangi, R., & Das, J. (2022). Does enterovirus 71 urge for effective vaccine control strategies? Challenges and current opinion. *Reviews in Medical Virology*, *32*(4), e2322.

Soboleski, M. R., Oaks, J., & Halford, W. P. (2005). Green fluorescent protein is a quantitative reporter of gene expression in individual eukaryotic cells. *The FASEB Journal : Official Publication of the Federation of American Societies for Experimental Biology*, *19*(3), 440.

*Safe and Objective Assay of Enterovirus 71 Neutralizing Antibodies via Pseudovirus*. (n.d.). Retrieved October 7, 2022

Schoberer, J., & Strasser, R. (2018). Plant glyco-biotechnology. *Seminars in Cell & Developmental Biology*, *80*, 133–141.

Schneider, C. A., Rasband, W. S., & Eliceiri, K. W. (2012). NIH Image to ImageJ: 25 years of image analysis. *Nature Methods*, *9*(7), 671–675.

Sabin, A. B. (1956). Pathogenesis of poliomyelitis. *Science*, *123*(3209), 1151–1157.

Sokalingam, S., Raghunathan, G., Soundrarajan, N., & Lee, S.-G. (2012). A Study on the Effect of Surface Lysine to Arginine Mutagenesis on Protein Stability and Structure Using Green Fluorescent Protein. *PLoS ONE*, *7*(7), e40410.

Sun, Y., Wang, Y., Shan, C., Chen, C., Xu, P., Song, M., Zhou, H., Yang, C., Xu, W., Shi, P.-Y., Zhang, B., & Lou, Z. (2012). Enterovirus 71 VPg Uridylation Uses a Two-Molecular Mechanism of 3D Polymerase. *Journal of Virology*, *86*(24), 13662–13671.

Sabin, A. B., & Boulger, L. R. (1973). History of Sabin attenuated poliovirus oral live vaccine strains. *Journal of Biological Standardization*, *1*(2), 115–118.

Sanjuán, R., & Domingo-Calap, P. (2016). Mechanisms of viral mutation. *Cellular and Molecular Life Sciences*, *73*(23), 4433–4448.

Strauss, M., Filman, D. J., Belnap, D. M., Cheng, N., Noel, R. T., & Hogle, J. M. (2015). Nectin-Like Interactions between Poliovirus and Its Receptor Trigger Conformational Changes Associated with Cell Entry. *Journal of Virology*, *89*(8), 4143–4157.

Tan, C. W., Sam, I.-C., Lee, V. S., Wong, H. V., & Chan, Y. F. (2017). VP1 residues around the five-fold axis of enterovirus A71 mediate heparan sulfate interaction. *Virology*, *501*, 79–87.

Tan, S., & Ponstein, N. (2019). Jonas Salk (1914–1995): A vaccine against polio. *Singapore Medical Journal*, *60*(1), 9–10.

Tee, K. K., Lam, T. T.-Y., Chan, Y. F., Bible, J. M., Kamarulzaman, A., Tong, C. Y. W., Takebe, Y., & Pybus, O. G. (2010). Evolutionary Genetics of Human Enterovirus 71: Origin, Population Dynamics, Natural Selection, and Seasonal Periodicity of the VP1 Gene. *Journal of Virology*, *84*(7), 3339–3350.

Tsou, Y.-L., Lin, Y.-W., Shao, H.-Y., Yu, S.-L., Wu, S.-R., Lin, H.-Y., Liu, C.-C., Huang, C., Chong, P., & Chow, Y.-H. (2015). Recombinant Adeno-Vaccine Expressing Enterovirus 71-Like Particles against Hand, Foot, and Mouth Disease. *PLOS Neglected Tropical Diseases*, *9*(4), e0003692.

Teo, K. W., Lai, F. Y., Bandi, S., Allen, D. J., & Tang, J. W. (2019). Emergence of Coxsackie A6 hand-foot-and-mouth disease and comparative severity of Coxsackie B vs. echovirus infections, 2014–2016, UK. *Journal of Infection*, *78*(1), 75–86.

Troy, S. B., & Maldonado, Y. A. (2012). Polioviruses. *Principles and Practice of Pediatric Infectious Diseases: Fourth Edition*, 1168-1172.e1.

Tenforde, M. W., Kondor, R. J. G., Chung, J. R., Zimmerman, R. K., Nowalk, M. P., Jackson, M. L., Jackson, L. A., Monto, A. S., Martin, E. T., Belongia, E. A., McLean, H. Q., Gaglani, M., Rao, A., Kim, S. S., Stark, T. J., Barnes, J. R., Wentworth, D. E., Patel, M. M., & Flannery, B. (2021). Effect of Antigenic Drift on Influenza Vaccine Effectiveness in the United States—2019–2020. *Clinical Infectious Diseases*, *73*(11), e4244–e4250.

Tuthill, T. J., Bubeck, D., Rowlands, D. J., & Hogle, J. M. (2006). Characterization of Early Steps in the Poliovirus Infection Process: Receptor-Decorated Liposomes Induce Conversion of the Virus to Membrane-Anchored Entry-Intermediate Particles. *Journal of Virology*, *80*(1), 172–180.

Tong, W. bin, Wu, X. Q., He, M., Yang, F. J., Jiang, Y., Zhang, G., & Zeng, P. bin. (2021). Epidemiological and etiological characteristics of hand, foot, and mouth disease before and after introducing enterovirus 71 vaccines in Sichuan, China: a 6-year retrospective study. *Chinese Medical Journal*, *134*(24), 3017.

Tong, W. bin, Wu, X. Q., He, M., Yang, F. J., Jiang, Y., Zhang, G., & Zeng, P. bin. (2021). Epidemiological and etiological characteristics of hand, foot, and mouth disease before and after introducing enterovirus 71 vaccines in Sichuan, China: a 6-year retrospective study. *Chinese Medical Journal*, *134*(24), 3017.

Techasaensiri, C., Wongsa, A., Puthanakit, T., Chokephaibulkit, K., Chotpitayasunondh, T., Charoonruangrit, U., Sombatnimitsakul, S., Puthavathana, P., Lerdsamran, H., Auewarakul, P., & Tassaneetrithep, B. (2021). Response of severe ev71-infected patients to hyperimmune plasma treatment: A pilot study. *Pathogens*, *10*(5).

Tariq, H., Batool, S., Asif, S., Ali, M., & Abbasi, B. H. (2022). Virus-Like Particles: Revolutionary Platforms for Developing Vaccines Against Emerging Infectious Diseases. *Frontiers in microbiology*, *12*, 790121.

Vogt, D. A., & Andino, R. (2010). An RNA Element at the 5'-End of the Poliovirus Genome Functions as a General Promoter for RNA Synthesis. PLOS Pathogens, 6(6), e1000936.

Várnai, A., Tang, C., Bengtsson, O., Atterton, A., Mathiesen, G., & Eijsink, V. G. H. (2014). Expression of endoglucanases in Pichia pastoris under control of the GAP promoter. Microbial Cell Factories, 13(1), 57.

Valley, C. C., Cembran, A., Perlmutter, J. D., Lewis, A. K., Labello, N. P., Gao, J., & Sachs, J. N. (2012). The Methionine-aromatic Motif Plays a Unique Role in Stabilizing Protein Structure. *Journal of Biological Chemistry*, *287*(42), 34979–34991.

World Health Organization (WHO). Regional Office for the Western Pacific (2011). *A guide to clinical management and public health response for hand, foot and mouth disease (HFMD)* [Online]. WHO Regional Office for the Western Pacific. [Accessed 25 October 2022]. Available from: https://apps.who.int/iris/handle/10665/207490.

World Health Organization (WHO). (2021). *Recommendations to assure the quality, safety and efficacy of enterovirus 71 vaccines (inactivated*) Annex 3, TRS No 1030. Geneva, Switzerland: WHO Press [Online]. [Accessed 25 August 2021]. Available from: https://www.who.int/publications/m/item/ev71-recommendations

World Health Organization (WHO). (2022). *Recommended composition of influenza virus vaccines for use in the 2022-2023 northern hemisphere influenza season*. Geneva, Switzerland: WHO Press [Online]. [Accessed 25 Nov 2021]. Available from :https://www.who.int/publications/m/item/recommended-composition-of-influenza-virus-vaccines-for-use-in-the-2022-2023-northern-hemisphere-influenza-season

Wang, M., Jiang, S., & Wang, Y. (2013). Recombinant VP1 protein expressed in Pichia pastoris induces protective immune responses against EV71 in mice. *Biochemical and Biophysical Research Communications*, *430*(1), 387–393.

Wang, J., Hu, Y., & Zheng, M. (2022). Enterovirus A71 antivirals: Past, present, and future. *Acta Pharmaceutica Sinica B*, *12*(4), 1542–1566.

Wang, B., Li, J., Wang, Y., Du, N., Sun, L., Xiao, H., Zhao, Y., Bao, W., & Zhang, W. (2019). Understanding the epidemiological characteristics of EV71 and CVA16 infection to aid the diagnosis and treatment of hand, foot, and mouth disease. *Journal of Medical Virology*, *91*(2), 201–207.

Wang, S. M., & Liu, C. C. (2014). Enterovirus 71: epidemiology, pathogenesis and management. *Http://Dx.Doi.Org/10.1586/Eri.09.45*, *7*(6), 735–742.

Woodman, A., Lee, K.-M., Janissen, R., Gong, Y.-N., Dekker, N. H., Shih, S.-R., & Cameron, C. E. (2019). Predicting Intraserotypic Recombination in Enterovirus 71. *Journal of Virology*, *93*(4).

WONG, S. S. Y., YIP, C. C. Y., LAU, S. K. P., & YUEN, K. Y. (2010). Human enterovirus 71 and hand, foot and mouth disease. *Epidemiology and Infection*, *138*(8), 1071–1089.

Wang, W., Sun, J., Wang, N., Sun, Z., Ma, Q., Li, J., Zhang, M., & Xu, J. (2020). Enterovirus A71 capsid protein VP1 increases blood–brain barrier permeability and virus receptor vimentin on the brain endothelial cells. *Journal of Neurovirology*, *26*(1), 84.

Woodyer, R. D., Johannes, T. W., & Zhao, H. (2006). Regeneration of Cofactors for Enzyme Biocatalysis. *Enzyme Technology*, 85–103.

Xu, L., He, D., Li, Z., Zheng, J., Yang, L., Yu, M., Yu, H., Chen, Y., Que, Y., Shih, J. W. K., Liu, G., Zhang, J., Zhao, Q., Cheng, T., & Xia, N. (2014). Protection against Lethal Enterovirus 71 Challenge in Mice by a Recombinant Vaccine Candidate Containing a Broadly Cross-Neutralizing Epitope within the VP2 EF Loop. *Theranostics*, *4*(5), 498–513.

Yuan, J., Shen, L., Wu, J., Zou, X., Gu, J., Chen, J., & Mao, L. (2018). Enterovirus A71 proteins: Structure and function. *Frontiers in Microbiology*, *9*(FEB), 286.

Yeh, M. te, Wang, S. W., Yu, C. K., Lin, K. H., Lei, H. Y., Su, I. J., & Wang, J. R. (2011). A Single Nucleotide in Stem Loop II of 5'-Untranslated Region Contributes to Virulence of Enterovirus 71 in Mice. *PLoS ONE*, *6*(11).

Yuan, S., Li, G., Wang, Y., Gao, Q., Wang, Y., Cui, R., Altmeyer, R., & Zou, G. (2016). Identification of Positively Charged Residues in Enterovirus 71 Capsid Protein VP1 Essential for Production of Infectious Particles. *Journal of Virology*, *90*(2), 741–752.

Yamaoka, S., Ito, N., Ohka, S., Kaneda, S., Nakamura, H., Agari, T., Masatani, T., Nakagawa, K., Okada, K., Okadera, K., Mitake, H., Fujii, T., & Sugiyama, M. (2013). Involvement of the Rabies Virus Phosphoprotein Gene in Neuroinvasiveness. *Journal of Virology*, *87*(22), 12327–12338.

Yamayoshi, S., Yamashita, Y., Li, J., Hanagata, N., Minowa, T., Takemura, T., & Koike, S. (2009). Scavenger receptor B2 is a cellular receptor for enterovirus 71. *Nature Medicine*, *15*(7), 798–801.

Yip, C. C. Y., Lau, S. K. P., Woo, P. C. Y., & Yuen, K. Y. (2013). Human enterovirus 71 epidemics: what's next? *Emerging Health Threats Journal*, *6*, 19780.

Yi, L., Lu, J., Kung, H. F., & He, M. L. (2011). The virology and developments toward control of human enterovirus 71. *Critical Reviews in Microbiology*, *37*(4), 313–327.

Yadav, D. K., Yadav, N., & Khurana, S. M. P. (2013). Vaccines: Present Status and Applications. *Animal Biotechnology: Models in Discovery and Translation*, 491–508.

Yeh, M. te, Bujaki, E., Dolan, P. T., Smith, M., Wahid, R., Konz, J., Weiner, A. J., Bandyopadhyay, A. S., van Damme, P., de Coster, I., Revets, H., Macadam, A., & Andino, R. (2020). Engineering the Live-Attenuated Polio Vaccine to Prevent Reversion to Virulence. *Cell Host & Microbe*, *27*(5), 736-751.e8.

Yajima, T., & Knowlton, K. U. (2009). Viral Myocarditis. *Circulation*, *119*(19), 2615–2624.

Yin, X. guang, Yi, H. xing, Shu, J., Wang, X. ju, Wu, X. jun, & Yu, L. hua. (2014). Clinical and epidemiological characteristics of adult hand, foot, and mouth disease in northern Zhejiang, China, May 2008 - November 2013. BMC Infectious Diseases, 14(1), 1–8.

Yang, F., Zhang, N., Chen, Y., Yin, J., Xu, M., Cheng, X., Ma, R., Meng, J., & Du, Y. (2022). Role of Non-Coding RNA in Neurological Complications Associated With Enterovirus 71. *Frontiers in cellular and infection microbiology*, *12*, 873304.

Yang, Z., Gao, F., Wang, X., Shi, L., Zhou, Z., Jiang, Y., Ma, X., Zhang, C., Zhou, C., Zeng, X., Liu, G., Fan, J., Mao, Q., & Shi, L. (2020). Development and characterization of an enterovirus 71 (EV71) virus-like particles (VLPs) vaccine produced in *Pichia pastoris*. *Human Vaccines & Immunotherapeutics*, *16*(7), 1602–1610.

Zhang, J., & Tao, A. (2015). *Antigenicity, Immunogenicity, Allergenicity* (pp. 175–186).

Zhang, W., Huang, Z., Huang, M., & Zeng, J. (2020). Predicting Severe Enterovirus 71-Infected Hand, Foot, and Mouth Disease: Cytokines and Chemokines. *Mediators of Inflammation*, *2020*, 1–11.

Zhao, R., Pevear, D. C., Kremer, M. J., Giranda, V. L., Kofron, J. A., Kuhn, R. J., & Rossmann, M. G. (1996). Human rhinovirus 3 at 3.0 å resolution. *Structure*, *4*(10), 1205–1220.

Zhao, M., Bai, Y., Liu, W., Xiao, X., Huang, Y., Cen, S., Chan, P. K., Sun, X., Sheng, W., & Zeng, Y. (2013). *Immunization of N terminus of enterovirus 71 VP4 elicits cross-protective antibody responses*.

Zhang, Y.-X., Huang, Y.-M., Li, Q.-J., Li, X.-Y., Zhou, Y.-D., Guo, F., Zhou, J.-M., & Cen, S. (2017). A highly conserved amino acid in VP1 regulates maturation of enterovirus 71. *PLOS Pathogens*, *13*(9), e1006625.

Zoll, J., Heus, H. A., van Kuppeveld, F. J. M., & Melchers, W. J. G. (2009). The structure-function relationship of the enterovirus 3'-UTR. *Virus Research*, *139*(2).

Zhang, W., Dai, W., Zhang, C., Zhou, Y., Xiong, P., Wang, S., Ye, X., Liu, Q., Zhou, D., & Huang, Z. (2018). A virus-like particle-based tetravalent vaccine for hand, foot, and mouth disease elicits broad and balanced protective immunity. *Emerging Microbes & Infections*, *7*(1), 1–12.

Zhang, C., Ku, Z., Liu, Q., Wang, X., Chen, T., Ye, X., Li, D., Jin, X., & Huang, Z. (2015). High-yield production of recombinant virus-like particles of enterovirus 71 in Pichia pastoris and their protective efficacy against oral viral challenge in mice. *Vaccine*, *33*(20), 2335–2341.

Zhao, H., Li, H.-Y., Han, J.-F., Deng, Y.-Q., Zhu, S.-Y., Li, X.-F., Yang, H.-Q., Li, Y.-X., Zhang, Y., Qin, E.-D., Chen, R., & Qin, C.-F. (2015). Novel recombinant chimeric virus-like particle is immunogenic and protective against both enterovirus 71 and coxsackievirus A16 in mice. *Scientific Reports*, *5*(1), 7878.

Zhou, Y., Li, J.-X., Jin, P.-F., Wang, Y.-X., & Zhu, F.-C. (2016). Enterovirus 71: a whole virion inactivated enterovirus 71 vaccine. *Expert Review of Vaccines*, *15*(7), 803–813.

Zhao, D., Sun, B., Sun, S., Fu, B., Liu, C., Liu, D., Chu, Y., Ma, Y., Bai, L., Wu, Y., Zhou, Y., Su, W., Hou, A., Cai, L., Xu, F., Kong, W., & Jiang, C. (2017). Characterization of human enterovirus71 virus-like particles used for vaccine antigens. *PLOS ONE*, *12*(7), e0181182.

Zhao, T., Zhang, Z., Zhang, Y., Feng, M., Fan, S., Wang, L., Liu, L., Wang, X., Wang, Q., Zhang, X., Wang, J., Liao, Y., He, Z., Lu, S., Yang, H., & Li, Q. (2017). Dynamic interaction of enterovirus

71 and dendritic cells in infected neonatal rhesus macaques. Frontiers in Cellular and Infection Microbiology, 7(MAY).

# Appendices

## Appendices (1)

## EVA71 alignment wt/#9

```
           10        20        30        40        50        60
wt     MGSQVSTQRSGSHENSNSATEGSTINYTTINYYKDSYAATAGKQSLKQDPDKFANPVKDV
       ::::::::::::::::::::::::::::::::::::::::::::::::::::::::::::
9      MGSQVSTQRSGSHENSNSATEGSTINYTTINYYKDSYAATAGKQSLKQDPDKFANPVKDV
           10        20        30        40        50        60

           70        80        90       100       110       120
wt     FTEMAAPLKSPSAEACGYSDRVAQLTIGNSTITTQEAANIIVGYGEWPSYCSDDDATAVD
       ::::::::::::::::::::::::::::::::::::::::::::::::::::::::::::
9      FTEMAAPLKSPSAEACGYSDRVAQLTIGNSTITTQEAANIIVGYGEWPSYCSDDDATAVD
           70        80        90       100       110       120

          130       140       150       160       170       180
wt     KPTRPDVSVNRFYTLDTKLWEKSSKGWYWKFPDVLTETGVFGQNAQFHYLYRSGFCIHVQ
       ::::::::::::::::::::::::::::::::::::::::::::::::::::::::::::
9      KPTRPDVSVNRFYTLDTKLWEKSSKGWYWKFPDVLTETGVFGQNAQFHYLYRSGFCIHVQ
          130       140       150       160       170       180

          190       200       210       220       230       240
wt     CNASKFHQGALLVAILPEYVIGTVAGGTGTEDSHPPYIQTQPGADGFELQHPYVLDAGIP
       ::::::::::::::::::::::::::::::::::::::::::::::::::::::::::::
9      CNASKFHQGALLVAILPEYVIGTVAGGTGTEDSHPPYIQTQPGADGFELQHPYVLDAGIP
          190       200       210       220       230       240

          250       260       270       280       290       300
wt     ISQLTVCPHQWINLRTNNCATIIVPYMNTLPFDSALNHCNFGLLVVPISPLDFDQGATPV
       ::::::::::::::::::::::::::::::::::::::::::::::::::::::::::::
9      ISQLTVCPHQWINLRTNNCATIIVPYMNTLPFDSALNHCNFGLLVVPISPLDFDQGATPV
          250       260       270       280       290       300

          310       320       330       340       350       360
wt     IPITITLAPMCSEFAGLRQAVTQGFPTELKPGTNQFLTTDDGVSAPILPNFHPTPCIHIP
       ::::::::::::::::::::::::::::::::::::::::::::::::::::::::::::
9      IPITITLAPMCSEFAGLRQAVTQGFPTELKPGTNQFLTTDDGVSAPILPNFHPTPCIHIP
          310       320       330       340       350       360

          370       380       390       400       410       420
wt     GEVRNLLELCQVETILEVNNVPTNATSLMERLRFPVSAQAGKGELCAVFRADPGRDGPWQ
       ::::::::::::::::::::::::::::::::::::::::::::::::::::::::::::
9      GEVRNLLELCQVETILEVNNVPTNATSLMERLRFPVSAQAGKGELCAVFRADPGRDGPWQ
          370       380       390       400       410       420

          430       440       450       460       470       480
wt     STMLGQLCGYYTQWSGSLEVTFMFTGSFMATGKMLIAYTPPGGPLPKDRATAMLGTHVIW
       ::::::::::::::::::::::::::::::::::::::::::::::::::::::::::::
9      STMLGQLCGYYTQWSGSLEVTFMFTGSFMATGKMLIAYTPPGGPLPKDRATAMLGTHVIW
          430       440       450       460       470       480
```

```
     480       490       500       510       520       530
wt     DFGLQSSVTLVIPWISNTHYRAHARDGVFDYYTTGLVSIWYQTNYVVPIGAPNTAYIIAL
       ::::::::::::::::::::::::::::::::::::::::::::::::::::::::::::
9      DFGLQSSVTLVIPWISNTHYRAHARDGVFDYYTTGLVSIWYQTNYVVPIGAPNTAYIIAL
              490       500       510       520       530       540

     540       550       560       570       580       590
wt     AAAQKNFTMKLCKDTSHILQTASIQGDRVADMIESSIGNSVSRALTQALPAPTGQNTQVS
       ::::::::::::::::.:::::::::::::::::::::::::::::::::::::::::::
9      AAAQKNFTMKLCKDTSHMLQTASIQGDRVADMIESSIGNSVSRALTQALPAPTGQNTQVS
              550       560       570       580       590       600

     600       610       620       630       640       650
wt     SHRLDTGEVPALQAAEIGASSNTSDESMIETRCVLNSHSTAETTLDSFFSRAGLVGEIDL
       ::::::::::::::::::::::::::::::::::::::::::::::::::::::::::::
9      SHRLDTGEVPALQAAEIGASSNTSDESMIETRCVLNSHSTAETTLDSFFSRAGLVGEIDL
              610       620       630       640       650       660

     660       670       680       690       700       710
wt     PLEGTTNPNGYANWDIDITGYAQMRRKVELFTYMRFDAEFTFVACTPTGQVVPQLLQYMF
       :::::::::::::::::::: ::::::::::::::::::::::::::::::::::::::::
9      PLEGTTNPNGYANWDIDITGCAQMRRKVELFTYMRFDAEFTFVACTPTGQVVPQLLQYMF
              670       680       690       700       710       720

     720       730       740       750       760       770
wt     VPPGAPKPESRESLAWQTATNPSVFVKLTDPPAQVSVPFMSPASAYQWFYDGYPTFGEHK
       :::::: ::::::::::::::::::::::::::::::::::::::::::::::::::::::
9      VPPGAPIPESRESLAWQTATNPSVFVKLTDPPAQVSVPFMSPASAYQWFYDGYPTFGEHK
              730       740       750       760       770       780

     780       790       800       810       820       830
wt     QEKDLEYGACPNNMMGTFSVRTVGSSKSKYPLVVRIYMRMKHVRAWIPRPMRNQNYLFKA
       :::::::::::::::::::::::::::::: ::::::::::::::::::::::::::::::
9      QEKDLEYGACPNNMMGTFSVRTVGSSKSKYALVVRIYMRMKHVRAWIPRPMRNQNYLFKA
              790       800       810       820       830       840

     840       850       860       870       880       890
wt     NPNYAGDSIKPTGTSRNAITTLGKFGQQSGAIYVGNFRVVNRHLATHNDWANLVWEDSSR
       ::::::::::::::::::::::::::::::::::::::::::::::::::::::::::::
9      NPNYAGDSIKPTGTSRNAITTLGKFGQQSGAIYVGNFRVVNRHLATHNDWANLVWEDSSR
              850       860       870       880       890       900

     900       910       920       930       940       950
wt     DLLVSSTTAQGCDTIARCNCQTGVYYCNSKRKHYPVSFSKPSLIYVEASEYYPARYQSHL
       ::::::::::::::::::::::::::::::::::::::::::::::::::::::::::::
9      DLLVSSTTAQGCDTIARCNCQTGVYYCNSKRKHYPVSFSKPSLIYVEASEYYPARYQSHL
              910       920       930       940       950       960
```

```
     960       970       980       990      1000      1010
wt     MLAAGHSEPGDCGGILRCQHGVVGIVSTGGNGLVGFADVRDLLWLDEEAMEQGVSDYIKG
       ::::::::::::::::::::::::::::::::::::::::::::::::::::::::::::
9      MLAAGHSEPGDCGGILRCQHGVVGIVSTGGNGLVGFADVRDLLWLDEEAMEQGVSDYIKG
              970       980       990      1000      1010      1020

    1020      1030      1040      1050      1060      1070
wt     LGDAFGTGFTDAVSREVEALRNHLIGSDGAVEKILKNLIKLISALVIVIRSDYDMVTLTA
       ::::::::::::::::::::::::::::::::::::::::::::::::::::::::::::
9      LGDAFGTGFTDAVSREVEALRNHLIGSDGAVEKILKNLIKLISALVIVIRSDYDMVTLTA
             1030      1040      1050      1060      1070      1080

    1080      1090      1100      1110      1120      1130
wt     TLALIGCHGSPWAWIKAKTASILGIPIAQKQSASWLKKFNDMASAAKGLEWISNKISKFI
       ::::::::::::::::::::::::::::::::::::::::::::::::::::::::::::
9      TLALIGCHGSPWAWIKAKTASILGIPIAQKQSASWLKKFNDMASAAKGLEWISNKISKFI
             1090      1100      1110      1120      1130      1140

    1140      1150      1160      1170      1180      1190
wt     DWLREKIVPAAKEKAEFLTNLKQLPLLENQITNLEQSAASQEDLEAMFGNVSYLAHFCRK
       ::::::::::::::::::::::::::::::::::::::::::::::::::::::::::::
9      DWLREKIVPAAKEKAEFLTNLKQLPLLENQITNLEQSAASQEDLEAMFGNVSYLAHFCRK
             1150      1160      1170      1180      1190      1200

    1200      1210      1220      1230      1240      1250
wt     FQPLYATEAKRVYVLEKRMNNYMQFKSKHRIEPVCLIIRGSPGTGKSLATGIIARAIADK
       ::::::::::::::::::::::::::::::::::::::::::::::::::::::::::::
9      FQPLYATEAKRVYVLEKRMNNYMQFKSKHRIEPVCLIIRGSPGTGKSLATGIIARAIADK
             1210      1220      1230      1240      1250      1260

    1260      1270      1280      1290      1300      1310
wt     YHSSVYSLPPDPDHFDGYKQQVVTVMDDLCQNPDGKDMSLFCQMVSTVDFIPPMASLEEK
       ::::::::::::::::::::::::::::::::::::::::::::::::::::::::::::
9      YHSSVYSLPPDPDHFDGYKQQVVTVMDDLCQNPDGKDMSLFCQMVSTVDFIPPMASLEEK
             1270      1280      1290      1300      1310      1320

    1320      1330      1340      1350      1360      1370
wt     GVSFTSKFVIASTNASNIIVPTVSDSDAIRRRFYMDCDIEVTDSYKTDLGRLDAGRAAKL
       ::::::::::::::::::::::::::::::::::::::::::::::::::::::::::::
9      GVSFTSKFVIASTNASNIIVPTVSDSDAIRRRFYMDCDIEVTDSYKTDLGRLDAGRAAKL
             1330      1340      1350      1360      1370      1380

    1380      1390      1400      1410      1420      1430
wt     CSENNTANFKRCSPLVCGKAIQLRDRKSKVRYSVDTVVSELIREYNSRSAIGNTIEALFQ
       ::::::::::::::::::::::::::::::::::::::::::::::::::::::::::::
9      CSENNTANFKRCSPLVCGKAIQLRDRKSKVRYSVDTVVSELIREYNSRSAIGNTIEALFQ
             1390      1400      1410      1420      1430      1440

    1440      1450      1460      1470      1480      1490
wt     GPPKFRPIRISFEEKPAPDAISDLLASVDSEEVRQYCREQGWIIPETPTNVERHLNRAVL
       ::::::::::.::::::::::::::::::::::::::::::::::::::::::::::::
9      GPPKFRPIRISLEEKPAPDAISDLLASVDSEEVRQYCREQGWIIPETPTNVERHLNRAVL
             1450      1460      1470      1480      1490      1500
```

```
    1500      1510      1520      1530      1540      1550
wt     VMQSIATVVAVVSLVYVIYKLFAGFQGAYSGAPKQVLKKPVLRTATVQGPSLDFALSLLR
       :::::.::::::::::::::::::::::::::::::::::::::::::::::::::::::
9      VMQSITTVVAVVSLVYVIYKLFAGFQGAYSGAPKQVLKKPVLRTATVQGPSLDFALSLLR
             1510      1520      1530      1540      1550      1560

    1560      1570      1580      1590      1600      1610
wt     RNIRQVQTDQGHFTMLGVRDRLAVLPRHSQPGKTIWVEHKLVNILDAAELVDEQGVNLEL
       ::::::::::::::::::::::::::::::::::::::::::::::::::::::::::::::
9      RNIRQVQTDQGHFTMLGVRDRLAVLPRHSQPGKTIWVEHKLVNILDAAELVDEQGVNLEL
             1570      1580      1590      1600      1610      1620

    1620      1630      1640      1650      1660      1670
wt     TLVTLDTNEKFRDITKFIPETISGASDATLVINTEHMPSMFVPVGDVVQYGFLNLSGKPT
       ::::::::::::::::::::::::::::::::::::::::::::::::::::::::::::::
9      TLVTLDTNEKFRDITKFIPETISGASDATLVINTEHMPSMFVPVGDVVQYGFLNLSGKPT
             1630      1640      1650      1660      1670      1680

    1680      1690      1700      1710      1720      1730
wt     HRTMMYNFPTKAGQCGGVVTSVGKIIGIHIGGNGRQGFCAGLKRSYFASEQGEIQWVKSN
       ::::::::::::::::::::::::::::::::::::::::::::::::::::::::::::::
9      HRTMMYNFPTKAGQCGGVVTSVGKIIGIHIGGNGRQGFCAGLKRSYFASEQGEIQWVKSN
             1690      1700      1710      1720      1730      1740

    1740      1750      1760      1770      1780      1790
wt     KETGRLNINGPTRTKLEPSVFHDVFEGNKEPAVLTSKDPRLEVDFEQALFSKYVGNVLHE
       ::::::::::::::::::::::::::::::::::::::::::::::::::::::::::::::
9      KETGRLNINGPTRTKLEPSVFHDVFEGNKEPAVLTSKDPRLEVDFEQALFSKYVGNVLHE
             1750      1760      1770      1780      1790      1800

    1800      1810      1820      1830      1840      1850
wt     PDEYVHQAALHYANQLKQLDINTKKMSMEEACYGTDNLEAIDLHTSAGYPYSALGIKKRD
       ::::::::::::::::::::::::::::::::::::::::::::::::::::::::::::::
9      PDEYVHQAALHYANQLKQLDINTKKMSMEEACYGTDNLEAIDLHTSAGYPYSALGIKKRD
             1810      1820      1830      1840      1850      1860

    1860      1870      1880      1890      1900      1910
wt     ILDPATKDVSKMKSYMDKYGLDLPYSTYVKDELRSLDKIKKGKSRLIEASSLNDSVYLRM
       ::::::::::::::::::::::::::::::::::::::::::::::::::::::::::::::
9      ILDPATKDVSKMKSYMDKYGLDLPYSTYVKDELRSLDKIKKGKSRLIEASSLNDSVYLRM
             1870      1880      1890      1900      1910      1920
```

```
    1920      1930      1940      1950      1960      1970
wt     TFGHLYEVFHANPGTVTGSAVGCNPDVFWSKLPILLPGSLFAFDYSGYDASLSPVWFRAL
       ::::::::::::::::::::::::::::::::::::::::::::::::::::::::::::
9      TFGHLYEVFHANPGTVTGSAVGCNPDVFWSKLPILLPGSLFAFDYSGYDASLSPVWFRAL
            1930      1940      1950      1960      1970      1980

    1980      1990      2000      2010      2020      2030
wt     EVVLREIGYSEEAVSLIEGINHTHHIYRNKTYCVLGGMPSGCSGTSIFNSMINNIIIRTL
       ::::::::::::::::::::::::::::::::::::::::::::::::::::::::::::
9      EVVLREIGYSEEAVSLIEGINHTHHIYRNKTYCVLGGMPSGCSGTSIFNSMINNIIIRTL
            1990      2000      2010      2020      2030      2040

    2040      2050      2060      2070      2080      2090
wt     LIKTFKGIDLDELNMVAYGDDVLASYPFPIDCLELAKTGKEYGLTMTPADKSPCFNEVTW
       ::::::::::::::::::::::::::::::::::::::::::::::::::::::::::::
9      LIKTFKGIDLDELNMVAYGDDVLASYPFPIDCLELAKTGKEYGLTMTPADKSPCFNEVTW
            2050      2060      2070      2080      2090      2100

    2100      2110      2120      2130      2140      2150
wt     ENATFLKRGFLPDHQFPFLIHPTMPMKEIHESIRWTKDARNTQDHVRSLCLLAWHNGKDE
       ::::::::::::::::::::::::::::::::::::::::::::::::::::::::::::
9      ENATFLKRGFLPDHQFPFLIHPTMPMKEIHESIRWTKDARNTQDHVRSLCLLAWHNGKDE
            2110      2120      2130      2140      2150      2160

    2160      2170      2180      2190
wt     YEKFVSTIRSVPVGKALAIPNFENLRRNWLELF
       ::::::::::::::::::::::::::::::::
9      YEKFVSTIRSVPVGKALAIPNFENLRRNWLELF
            2170      2180      2190
```

## Appendices (2)

## EVA71 alignment wt/#9x5

```
            10        20        30        40        50        60
wt      MGSQVSTQRSGSHENSNSATEGSTINYTTINYYKDSYAATAGKQSLKQDPDKFANPVKDV
        ::::::::::::::::::::::::::::::::::::::::::::::::::::::::::::
95      MGSQVSTQRSGSHENSNSATEGSTINYTTINYYKDSYAATAGKQSLKQDPDKFANPVKDV
            10        20        30        40        50        60

            70        80        90       100       110       120
wt      FTEMAAPLKSPSAEACGYSDRVAQLTIGNSTITTQEAANIIVGYGEWPSYCSDDDATAVD
        ::::::::::::::::::::::::::::::::::::::::::::::::::::::::::::
95      FTEMAAPLKSPSAEACGYSDRVAQLTIGNSTITTQEAANIIVGYGEWPSYCSDDDATAVD
            70        80        90       100       110       120

           130       140       150       160       170       180
wt      KPTRPDVSVNRFYTLDTKLFPDVLTETGVFGQNAQFHYLYRSGFCIHVQCNASKFHQGAL
        ::::::::::::::::::::::.::::::::::::::::::::::::::::::::::::
95      KPTRPDVSVNRFYTLDTKLFPDLLTETGVFGQNAQFHYLYRSGFCIHVQCNASKFHQGAL
           130       140       150       160       170       180

           190       200       210       220       230       240
wt      LVAILPEYVIGTVAGGTGTEDSHPPYIQTQPGADGFELQHPYVLDAGIPISQLTVCPHQW
        ::::::::::::::::::::::::::::::::::::::::::::::::::::::::::::
95      LVAILPEYVIGTVAGGTGTEDSHPPYIQTQPGADGFELQHPYVLDAGIPISQLTVCPHQW
           190       200       210       220       230       240

           250       260       270       280       290       300
wt      INLRTNNCATIIVPYMNTLPFDSALNHCNFGLLVVPISPLDFDQGATPVIPITITLAPMC
        ::::::::::::::::::::::::::::::::::::::::::::::::::::::::::::
95      INLRTNNCATIIVPYMNTLPFDSALNHCNFGLLVVPISPLDFDQGATPVIPITITLAPMC
           250       260       270       280       290       300

           310       320       330       340       350       360
wt      SEFAGLRQAVTQGFPTELKPGTNQFLTTDDGVSAPILPNFHPTPCIHIPGEVRNLLELCQ
        ::::::::::::::::::::::::::::::::::::::::::::::::::::::::::::
95      SEFAGLRQAVTQGFPTELKPGTNQFLTTDDGVSAPILPNFHPTPCIHIPGEVRNLLELCQ
           310       320       330       340       350       360

           370       380       390       400       410       420
wt      VETILEVNNVPTNATSLMERLRFPVSAQAGKGELCAVFRADPGRDGPWQSTMLGQLCGYY
        ::::::::::::::::::::::::::::::::::::::::::::::::::::::::::::
95      VETILEVNNVPTNATSLMERLRFPVSAQAGKGELCAVFRADPGRDGPWQSTMLGQLCGYY
           370       380       390       400       410       420

           430       440       450       460       470       480
wt      TQWSGSLEVTFMFTGSFMATGKMLIAYTPPGGPLPKDRATAMLGTHVIWDFGLQSSVTLV
        ::::::::::::::::::::::::::::::::::::::::::::::::::::::::::::
95      TQWSGSLEVTFMFTGSFMATGKMLIAYTPPGGPLPKDRATAMLGTHVIWDFGLQSSVTLV
           430       440       450       460       470       480

           490       500       510       520       530       540
wt      IPWISNTHYRAHARDGVFDYYTTGLVSIWYQTNYVVPIGAPNTAYIIALAAAQKNFTMKL
        ::::::::::::::::::::::::::::::::::::::::::::::::::::::::::::
95      IPWISNTHYRAHARDGVFDYYTTGLVSIWYQTNYVVPIGAPNTAYIIALAAAQKNFTMKL
           490       500       510       520       530       540
```

```
           550       560       570       580       590       600
wt     CKDTSHILQTASIQGDRVADMIESSIGNSVSRALTQALPAPTGQNTQVSSHRLDTGEVPA
       ::::::.::::::::::::::::::::::::::::::::::::::::::::::::::::
95     CKDTSHMLQTASIQGDRVADMIESSIGNSVSRALTQALPAPTGQNTQVSSHRLDTGEVPA
           550       560       570       580       590       600

           610       620       630       640       650       660
wt     LQAAEIGASSNTSDESMIETRCVLNSHSTAETTLDSFFSRAGLVGEIDLPLEGTTNPNGY
       ::::::::::::::::::::::::::::::::::::::::::::::::::::::::::::
95     LQAAEIGASSNTSDESMIETRCVLNSHSTAETTLDSFFSRAGLVGEIDLPLEGTTNPNGY
           610       620       630       640       650       660

           670       680       690       700       710       720
wt     ANWDIDITGYAQMRRKVELFTYMRFDAEFTFVACTPTGQVVPQLLQYMFVPPGAPKPESR
       ::::::::: :::::::::::::::::::::::::::::::::::::::::: ::::
95     ANWDIDITGCAQMRRKVELFTYMRFDAEFTFVACTPTGQVVPQLLQYMFVPPGAPIPESR
           670       680       690       700       710       720

           730       740       750       760       770       780
wt     ESLAWQTATNPSVFVKLTDPPAQVSVPFMSPASAYQWFYDGYPTFGEHKQEKDLEYGACP
       ::::::::::::::::::::::::::::::::::::::::::::::::::::::::::::
95     ESLAWQTATNPSVFVKLTDPPAQVSVPFMSPASAYQWFYDGYPTFGEHKQEKDLEYGACP
           730       740       750       760       770       780

           790       800       810       820       830       840
wt     NNMMGTFSVRTVGSSKSKYPLVVRIYMRMKHVRAWIPRPMRNQNYLFKANPNYAGDSIKP
       :::::::::::::::::: ::::::::::::::::::::::::::::::::::::::::
95     NNMMGTFSVRTVGSSKSKYALVVRIYMRMKHVRAWIPRPMRNQNYLFKANPNYAGDSIKP
           790       800       810       820       830       840

           850       860       870       880       890       900
wt     TGTSRNAITTLGKFGQQSGAIYVGNFRVVNRHLATHNDWANLVWEDSSRDLLVSSTTAQG
       ::::::::::::::::::::::::::::::::::::::::::::::::::::::::::::
95     TGTSRNAITTLGKFGQQSGAIYVGNFRVVNRHLATHNDWANLVWEDSSRDLLVSSTTAQG
           850       860       870       880       890       900

           910       920       930       940       950       960
wt     CDTIARCNCQTGVYYCNSKRKHYPVSFSKPSLIYVEASEYYPARYQSHLMLAAGHSEPGD
       ::::::::::::::::::::::::::::::::::::::::::::::::::::::::::::
95     CDTIARCNCQTGVYYCNSKRKHYPVSFSKPSLIYVEASEYYPARYQSHLMLAAGHSEPGD
           910       920       930       940       950       960

           970       980       990      1000      1010      1020
wt     CGGILRCQHGVVGIVSTGGNGLVGFADVRDLLWLDEEAMEQGVSDYIKGLGDAFGTGFTD
       ::::::::::::::::::::::::::::::::::::::::::::::::::::::::::::
95     CGGILRCQHGVVGIVSTGGNGLVGFADVRDLLWLDEEAMEQGVSDYIKGLGDAFGTGFTD
           970       980       990      1000      1010      1020

          1030      1040      1050      1060      1070      1080
wt     AVSREVEALRNHLIGSDGAVEKILKNLIKLISALVIVIRSDYDMVTLTATLALIGCHGSP
       ::::::::::::::::::::::::::::::::::::::::::::::::::::::::::::
95     AVSREVEALRNHLIGSDGAVEKILKNLIKLISALVIVIRSDYDMVTLTATLALIGCHGSP
          1030      1040      1050      1060      1070      1080

          1090      1100      1110      1120      1130      1140
wt     WAWIKAKTASILGIPIAQKQSASWLKKFNDMASAAKGLEWISNKISKFIDWLREKIVPAA
       ::::::::::::::::::::::::::::::::::::::::::::::::::::::::::::
95     WAWIKAKTASILGIPIAQKQSASWLKKFNDMASAAKGLEWISNKISKFIDWLREKIVPAA
          1090      1100      1110      1120      1130      1140
```

```
            1150      1160      1170      1180      1190      1200
wt      KEKAEFLTNLKQLPLLENQITNLEQSAASQEDLEAMFGNVSYLAHFCRKFQPLYATEAKR
        ::::::::::::::::::::::::::::::::::::::::::::::::::::::::::::
95      KEKAEFLTNLKQLPLLENQITNLEQSAASQEDLEAMFGNVSYLAHFCRKFQPLYATEAKR
            1150      1160      1170      1180      1190      1200

            1210      1220      1230      1240      1250      1260
wt      VYVLEKRMNNYMQFKSKHRIEPVCLIIRGSPGTGKSLATGIIARAIADKYHSSVYSLPPD
        ::::::::::::::::::::::::::::::::::::::::::::::::::::::::::::
95      VYVLEKRMNNYMQFKSKHRIEPVCLIIRGSPGTGKSLATGIIARAIADKYHSSVYSLPPD
            1210      1220      1230      1240      1250      1260

            1270      1280      1290      1300      1310      1320
wt      PDHFDGYKQQVVTVMDDLCQNPDGKDMSLFCQMVSTVDFIPPMASLEEKGVSFTSKFVIA
          ::::::::::::::::::::::::::::::::::::::::::::::::::::::::::::
95      DPHFDGYKQQVVTVMDDLCQNPDGKDMSLFCQMVSTVDFIPPMASLEEKGVSFTSKFVIA
            1270      1280      1290      1300      1310      1320

            1330      1340      1350      1360      1370      1380
wt      STNASNIIVPTVSDSDAIRRRFYMDCDIEVTDSYKTDLGRLDAGRAAKLCSENNTANFKR
        ::::::::::::::::::::::::::::::::::::::::::::::::::::::::::::
95      STNASNIIVPTVSDSDAIRRRFYMDCDIEVTDSYKTDLGRLDAGRAAKLCSENNTANFKR
            1330      1340      1350      1360      1370      1380

            1390      1400      1410      1420      1430      1440
wt      CSPLVCGKAIQLRDRKSKVRYSVDTVVSELIREYNSRSAIGNTIEALFQGPPKFRPIRIS
        ::::::::::::::::::::::::::::::::::::::::::::::::::::::::::::
95      CSPLVCGKAIQLRDRKSKVRYSVDTVVSELIREYNSRSAIGNTIEALFQGPPKFRPIRIS
            1390      1400      1410      1420      1430      1440

            1450      1460      1470      1480      1490      1500
wt      FEEKPAPDAISDLLASVDSEEVRQYCREQGWIIPETPTNVERHLNRAVLVMQSIATVVAV
        .::::::::::::::::::::::::::::::::::::::::::::::::::::::.:::::
95      LEEKPAPDAISDLLASVDSEEVRQYCREQGWIIPETPTNVERHLNRAVLVMQSITTVVAV
            1450      1460      1470      1480      1490      1500

            1510      1520      1530      1540      1550      1560
wt      VSLVYVIYKLFAGFQGAYSGAPKQVLKKPVLRTATVQGPSLDFALSLLRRNIRQVQTDQG
        ::::::::::::::::::::::::::::::::::::::::::::::::::::::::::::
95      VSLVYVIYKLFAGFQGAYSGAPKQVLKKPVLRTATVQGPSLDFALSLLRRNIRQVQTDQG
            1510      1520      1530      1540      1550      1560

            1570      1580      1590      1600      1610      1620
wt      HFTMLGVRDRLAVLPRHSQPGKTIWVEHKLVNILDAAELVDEQGVNLELTLVTLDTNEKF
        ::::::::::::::::::::::::::::::::::::::::::::::::::::::::::::
95      HFTMLGVRDRLAVLPRHSQPGKTIWVEHKLVNILDAAELVDEQGVNLELTLVTLDTNEKF
            1570      1580      1590      1600      1610      1620

            1630      1640      1650      1660      1670      1680
wt      RDITKFIPETISGASDATLVINTEHMPSMFVPVGDVVQYGFLNLSGKPTHRTMMYNFPTK
        ::::::::::::::::::::::::::::::::::::::::::::::::::::::::::::
95      RDITKFIPETISGASDATLVINTEHMPSMFVPVGDVVQYGFLNLSGKPTHRTMMYNFPTK
            1630      1640      1650      1660      1670      1680

            1690      1700      1710      1720      1730      1740
wt      AGQCGGVVTSVGKIIGIHIGGNGRQGFCAGLKRSYFASEQGEIQWVKSNKETGRLNINGP
        ::::::::::::::::::::::::::::::::::::::::::::::::::::::::::::
95      AGQCGGVVTSVGKIIGIHIGGNGRQGFCAGLKRSYFASEQGEIQWVKSNKETGRLNINGP
            1690      1700      1710      1720      1730      1740
```

```
            1750      1760      1770      1780      1790      1800
wt      TRTKLEPSVFHDVFEGNKEPAVLTSKDPRLEVDFEQALFSKYVGNVLHEPDEYVHQAALH
        ::::::::::::::::::::::::::::::::::::::::::::::::::::::::::::
95      TRTKLEPSVFHDVFEGNKEPAVLTSKDPRLEVDFEQALFSKYVGNVLHEPDEYVHQAALH
            1750      1760      1770      1780      1790      1800

            1810      1820      1830      1840      1850      1860
wt      YANQLKQLDINTKKMSMEEACYGTDNLEAIDLHTSAGYPYSALGIKKRDILDPATKDVSK
        ::::::::::::::::::::::::::::::::::::::::::::::::::::::::::::
95      YANQLKQLDINTKKMSMEEACYGTDNLEAIDLHTSAGYPYSALGIKKRDILDPATKDVSK
            1810      1820      1830      1840      1850      1860

            1870      1880      1890      1900      1910      1920
wt      MKSYMDKYGLDLPYSTYVKDELRSLDKIKKGKSRLIEASSLNDSVYLRMTFGHLYEVFHA
        ::::::::::::::::::::::::::::::::::::::::::::::::::::::::::::
95      MKSYMDKYGLDLPYSTYVKDELRSLDKIKKGKSRLIEASSLNDSVYLRMTFGHLYEVFHA
            1870      1880      1890      1900      1910      1920

            1930      1940      1950      1960      1970      1980
wt      NPGTVTGSAVGCNPDVFWSKLPILLPGSLFAFDYSGYDASLSPVWFRALEVVLREIGYSE
        ::::::::::::::::::::::::::::::::::::::::::::::::::::::::::::
95      NPGTVTGSAVGCNPDVFWSKLPILLPGSLFAFDYSGYDASLSPVWFRALEVVLREIGYSE
            1930      1940      1950      1960      1970      1980

            1990      2000      2010      2020      2030      2040
wt      EAVSLIEGINHTHHIYRNKTYCVLGGMPSGCSGTSIFNSMINNIIIRTLLIKTFKGIDLD
        ::::::::::::::::::::::::::::::::::::::::::::::::::::::::::::
95      EAVSLIEGINHTHHIYRNKTYCVLGGMPSGCSGTSIFNSMINNIIIRTLLIKTFKGIDLD
            1990      2000      2010      2020      2030      2040

            2050      2060      2070      2080      2090      2100
wt      ELNMVAYGDDVLASYPFPIDCLELAKTGKEYGLTMTPADKSPCFNEVTWENATFLKRGFL
        ::::::::::::::::::::::::::::::::::::::::::::::::::::::::::::
95      ELNMVAYGDDVLASYPFPIDCLELAKTGKEYGLTMTPADKSPCFNEVTWENATFLKRGFL
            2050      2060      2070      2080      2090      2100

            2110      2120      2130      2140      2150      2160
wt      PDHQFPFLIHPTMPMKEIHESIRWTKDARNTQDHVRSLCLLAWHNGKDEYEKFVSTIRSV
        ::::::::::::::::::::::::::::::::::::::::::::::::::::::::::::
95      PDHQFPFLIHPTMPMKEIHESIRWTKDARNTQDHVRSLCLLAWHNGKDEYEKFVSTIRSV
            2110      2120      2130      2140      2150      2160

            2170      2180
wt      PVGKALAIPNFENLRRNWLELF
        ::::::::::::::::::::::
95      PVGKALAIPNFENLRRNWLELF
            2170      2180
```